

Development of New Antibiotics

Based on Biotin Biology

Kwang Jun Lee

A thesis submitted in total fulfilment of the requirements for
the degree of Doctor of Philosophy



July 2019

School of Physical Sciences

Department of Chemistry

Table of Contents

Abstract.....	IV
Publications.....	VI
Declaration.....	VII
Acknowledgement	VIII
Abbreviations.....	IX

Chapter One

1.1 The need for new antibiotics	2
1.2 Biotin biology and biosynthesis	2
1.3 Biotin protein ligase (BPL)	3
1.3.1 Mechanism of BPL.....	5
1.3.2 Structural classes of BPL.....	6
1.3.3 BPL active site.....	7
1.4 SaBPL inhibitors - preliminary data.....	9
1.4.1 1,2,3-Triazole based analogues	9
1.4.2 Sulfonamide based analogues.....	11
1.5 Dethiobiotin synthase (DTBS)	12
1.5.1 Mechanism of DTBS	12
1.5.2 DTBS structure.....	13
1.5.3 DTBS active site.....	14
1.5.4 <i>Mtb</i> DTBS as an antituberculosis drug target.....	16
1.6 Research described in this thesis	17
1.7 References for Chapter One	18

Chapter Two

2.1 Introduction	26
2.2 Statement of authorship	27
2.3 Publication.....	30

Chapter Three

3.1	Introduction	49
3.2	Statement of authorship.	50
3.2	Publication.....	54

Chapter Four

4.1	Introduction	87
4.2	Design and synthesis of DAPA pocket binders.....	89
4.2.1	Docking	90
4.2.2	Synthesis of <i>trans</i> - 4.01	92
4.2.3	Synthesis of cyclopentylacetic acid analogues 4.03 – 4.08	98
4.3	DTBS binding affinity and antimicrobial activity of Cyclopentylacetic acid analogues	100
4.4	X-ray crystal structure of 4.03 – 4.06 and 4.10 bound to <i>Mtb</i> DTBS	102
4.5	Conclusion.....	105
4.6	References for Chapter Four	107

Chapter Five

5.1	Introduction	110
5.2	Design and synthesis of linked compounds	112
5.2.1	Cytidine building blocks for the synthesis of 5.03 – 5.05	114
5.2.2	Synthesis of triazole linked compound 5.03	117
5.2.3	Synthesis of amino acid linked compound 5.05	118
5.3	DTBS binding assay results	121
5.4	X-ray crystal structure of 5.03 and 5.05 bound to DTBS.....	123
5.5	Conclusion.....	125
5.6	References for Chapter Five.....	127

Chapter Six

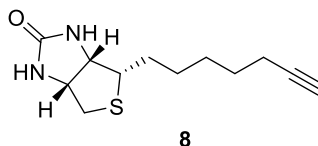
6.1	General methods.....	130
6.2	Experimental work as described in Chapter 2.....	130
6.3	Experimental work as described in Chapter 3.....	152
6.4	Experimental work as described in Chapter 4.....	161
6.5	Experimental work as described in Chapter 5.....	174
6.6	References for Chapter Six.....	189

Abstract

Biotin is an essential vitamin that is required for growth and pathogenicity of bacteria. Biotin protein ligase (BPL) catalyses the ordered reaction of biotin and ATP to give biotinyl-5'-AMP, which then activates a number of biotin dependent enzymes that are critical to cell survival. Dethiobiotin synthase (DTBS) is the sole enzyme responsible for catalysing a key step in biotin biosynthesis, namely the carboxylation of 7,8-diaminopelargonic acid (DAPA), closing the ureido ring to form dethiobiotin in a reaction requiring a nucleotide triphosphate. Research undertaken in this thesis highlights strategies to selectively inhibit *Staphylococcus aureus* biotin protein ligase (*Sa*BPL) using 1,2,3-triazole and sulfonamide isosteres to replace the phosphoroanhydride linker found in biotinyl-5'-AMP. In addition, this thesis discusses the design and development of inhibitors targeting *Mycobacterium tuberculosis* dethiobiotin synthase (*Mtb*DTBS).

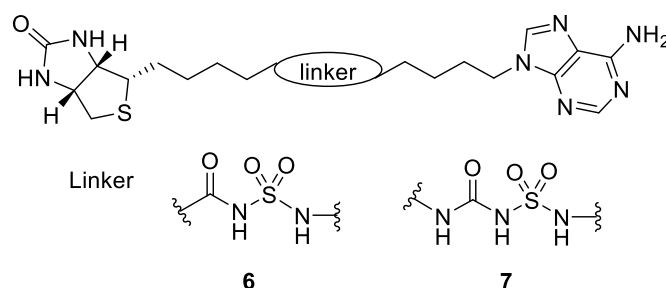
Chapter one describes the structure and catalytic mechanism of the target enzymes *Sa*BPL and *Mtb*DTBS. Preliminary studies on the utility of 1,2,3-triazole and sulfonamide as bioisosteres of the phosphoroanhydride linker of biotinyl-5'-AMP are also discussed.

Chapter two elaborates on the potent inhibitors with chemical modifications carried out at the C5 position of the triazole ring to generate 1,4,5-trisubstituted 1,2,3-triazoles. A class of 5-iodo 1,2,3-triazoles was synthesised from biotin acetylene **8** and azides using CuAAC. Subsequent halogen exchange reaction allowed conversion of iodide to fluoride. The halogenated triazoles exhibited significantly improved antibacterial activity against *S. aureus* over nonhalogenated counterparts.

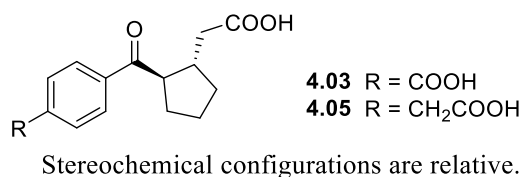


Chapter three describes the design, synthesis, and biological assay of sulfonamide analogues targeting *Sa*BPL assisted by computational chemistry. Acylsulfamide **6** and amino sulfonylurea **7** showed potent *in vitro* inhibitory activities ($K_i = 0.007 \pm 0.003$ and $0.065 \pm 0.03 \mu\text{M}$ respectively) and also antibacterial activity against *S. aureus* ATCC49775 with a minimum inhibitory concentration (MIC) of 0.25 and 4 $\mu\text{g/ml}$ respectively. Compound **7**

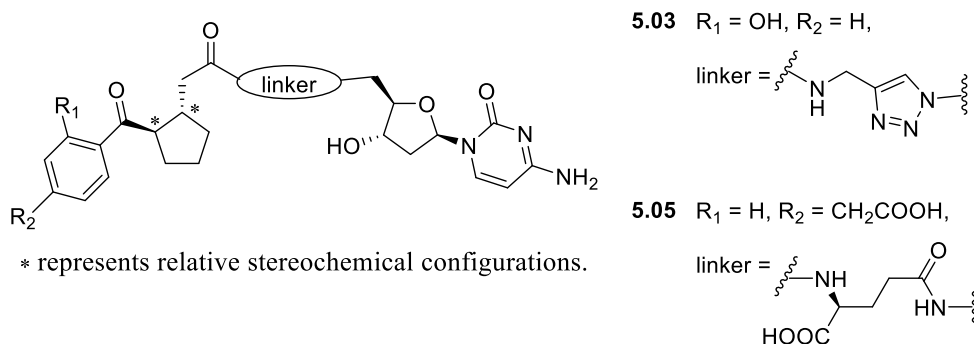
displayed a vastly improved pharmacokinetic profile compared to **6** presumably due to the enhanced metabolic stability of the sulfonamide linker moiety.



Chapter four focuses on the structure-guided chemical optimization of a hit compound targeting the DAPA binding site of *Mtb*DTBS using X-ray crystallography screening and docking experiments. Analogues **4.03** and **4.05** were shown to be potent toward *Mtb*DTBS ($K_D = 19 \pm 5$ and $17 \pm 1 \mu\text{M}$ respectively). The crystal structures of **4.03** and **4.05** bound to *Mtb*DTBS reveals that carboxylic acid groups attached to benzene ring form hydrogen bonds with residues Leu146 and Asn147 in the binding site as observed in DAPA carbamate **1.16**.



Chapter five describes the linking between the optimized DAPA pocket binder (discovered in Chapter four) and 2'-deoxycytidine **5.01** to create potent bi-substrate ligands for *Mtb*DTBS. Linked compounds **5.03** and **5.05** showed binding affinities toward *Mtb*DTBS ($K_D = 0.6 \pm 0.2$ and $0.7 \pm 0.2 \text{ mM}$ respectively). The linker moieties of **5.03** and **5.05** do not bind to the P-loop of the enzyme, with the crystallographic precipitant (sulfate or citrate) occupying this site.



Chapter six details the experimental procedures for compounds described in chapter 2 – 5.

Publications

Paparella, A. S.; Lee, K. J.; Hayes, A. J.; Feng, J. G.; Feng, Z. K.; Cini, D.; Deshmukh, S.; Booker, G. W.; Wilce, M. C. J.; Polyak, S. W.; Abell, A. D., Halogenation of Biotin Protein Ligase Inhibitors Improves Whole Cell Activity against *Staphylococcus aureus*. *ACS infectious diseases* **2018**, *4* (2), 175-184.

Lee, K. J.; Tieu, W.; Rodriguez, B. B.; Paparella, A. S.; Yu, J.; Hayes, A. J.; Feng, J. G.; Marshall, A. C.; Noll, B.; Milne, R.; Cini, D.; Wilce, M. C. J.; Booker, G. W.; Bruning, J. B.; Polyak, S. W.; Abell, A. D., Sulfonamide-based inhibitors of biotin protein ligase as new antibiotic leads. *Submitted to ACS Chemical Biology*.

Declaration

I certify that this work contains no material which has been accepted for the award of any other degree or diploma in my name, in any university or other tertiary institution and, to the best of my knowledge and belief, contains no material previously published or written by another person, except where due reference has been made in the text. In addition, I certify that no part of this work will, in the future, be used in a submission in my name, for any other degree or diploma in any university or other tertiary institution without the prior approval of the University of Adelaide and where applicable, any partner institution responsible for the joint-award of this degree.

I acknowledge that copyright of published works contained within this thesis resides with the copyright holder(s) of those works.

I also give permission for the digital version of my thesis to be made available on the web, via the University's digital research repository, the Library Search and also through web search engines, unless permission has been granted by the University to restrict access for a period of time.

I acknowledge the support I have received for my research through the provision of an Australian Government Research Training Program Scholarship.

.....

Kwang Jun Lee

23 / 7 / 19
.....

Date

Acknowledgement

Foremost, I would like to express my special gratitude to my supervisor, Professor Andrew Abell for his supervision and guidance. I am deeply grateful for his extensive knowledge, enormous support, enthusiastic view on research and tireless efforts in revising this thesis.

I would like to thank all the past and present members of the Abell group for creating a friendly and stimulating working atmosphere. I am grateful to the Post-docs (Beatiz Blanco Rodriguez and Thomas Avery) for having shared many experiences and thoughts with me throughout my candidature. My thanks and appreciations also go to Damian Stachura who have willingly helped me out with his abilities.

I would also like to express my gratitude to our collaborators in the BPL and DTBS projects. I would like to thank Andrew Hayes, Andrew Tompson, and Dr. Steven Polyak for performing enzyme and antimicrobial assays; Dani Cini and Professor Mathew Wilce for solving the invaluable X-ray crystallographic structures of inhibitors bound to *Sa*BPL.

Last but not least, thank you to my supportive family for the encouragement which helped me in completion of this thesis. My beloved wife, Geum who always by my side especially in difficult times, and my lovable children, Ruby and Suzy who served as my inspiration to pursue this undertaking.

Abbreviations

AaBPL	<i>A. aeolicus</i> biotin protein ligase
ABL	ATP binding loop
AcBPL	<i>A. calcoaceticus</i> biotin protein ligase
ACP	Acyl carrier protein
ACC	Acetyl CoA carboxylase
AcOH	Acetic acid
ADP	Adenosine diphosphate
AMP	Adenosine monophosphate
AMTOD	<i>S</i> -Adenosyl-2-oxo-4-thiomethylbutyrate
ATP	Adenosine triphosphate
AUC	Area under the curve
BAIB	Bis(acetoxy)iodobenzene
BBL	Biotin binding loop
BCCP	Biotin carboxyl carrier protein
Boc	<i>tert</i> -Butyloxycarbonyl
Boc-Glu-OBzl	Boc-L-glutamic acid 1-benzyl ester
BPL	Biotin protein ligase
BS	Biotin synthase
BSA	Bovine serum albumin
BzCl	Benzoyl chloride
BzOH	Benzoic acid
CaBPL	<i>C. albicans</i> biotin protein ligase
Cbz	Carbobenzyloxy
CDI	1,1'-Carbonyldiimidazole
CDP	Cytidine diphosphate
CDMT	2-Chloro-4,6-dimethoxy-1,3,5-triazine
COSY	Correlation spectroscopy
CTP	Cytidine triphosphate
¹³ C NMR	Carbon nuclear magnetic resonance
CSI	Chlorosulfonyl isocyanate

CuAAC	Copper(I)-catalysed azide alkyne cycloaddition
DAPA	7,8-Diaminopelargonic acid
DAPAS	7,8-Diaminopelargonic acid synthase
DBU	1,8-Diazabicyclo[5.4.0]undec-7-ene
dCDP	2'-Deoxycytidine diphosphate
DCM	Dichloromethane
dCTP	2'-Deoxycytidine triphosphate
DIPEA	N, N-Diisopropylethylamine
DMAP	Dimethylaminopyridine
DMF	Dimethylformamide
DMSO	Dimethyl sulfoxide
DMP	Dess-Martin periodinane
DNA	Deoxyribonucleic acid
5'-DOA	5'-Deoxyadenosine
DTBS	Dethiobiotin synthase
DTT	Dithiothreitol
<i>EcBPL</i>	<i>E. coli</i> biotin protein ligase
EDC	1-Ethyl-3-(3-dimethylaminopropyl)carbodiimide
EDTA	Ethylenediaminetetraacetic acid
EtOAc	Ethyl acetate
EtONa	Sodium ethoxide
EtOH	Ethanol
FTIR	Fourier transform infrared spectroscopy
¹⁹ F NMR	Fluorine nuclear magnetic resonance
GST	Glutathione S-transferase
¹ H NMR	Proton nuclear magnetic resonance
HATU	Hexafluorophosphate azabenzotriazole tetramethyl uranium
HEPES	4-(2-Hydroxyethyl)-1-piperazineethanesulfonic acid
HMBC	Heteronuclear multiple bond correlation spectroscopy
HOBt	Hydroxybenzotriazole
HPLC	High-performance liquid chromatography
HRMS	High resolution mass spectrometry
<i>HsBPL</i>	<i>Homo sapiens</i> biotin protein ligase

HSQC	Heteronuclear single quantum coherence spectroscopy
IC ₅₀	Half maximum inhibitory concentration
k_a	Association rate constant
KAPA	7-Keto-7-aminopelargonic acid
KAPAS	7-Keto-7-aminopelargonic acid synthase
k_d	Dissociation rate constant
K_D	Affinity constant
K_i	Inhibition constant
<i>Kp</i> BPL	<i>K. pneumoniae</i> biotin protein ligase
LC-MS	Liquid chromatography–mass spectrometry
LDA	Lithium diisopropylamide
MD	Molecular dynamics
MDR-TB	Multidrug-resistant tuberculosis
Me	Methyl group
MeCN	Acetonitrile
MIC	Minimum inhibitory concentration
MRSA	Methicillin-resistant <i>S. aureus</i>
MSSA	Methicillin-sensitive <i>S. aureus</i>
<i>Mtb</i> BPL	<i>M. tuberculosis</i> biotin protein ligase
<i>Mtb</i> DTBS	<i>M. tuberculosis</i> dethiobiotin synthase
NMM	<i>N</i> -methylmorpholine
NMO	<i>N</i> -methylmorpholin <i>N</i> -oxide
NMI	<i>N</i> -Iodomorpholine hydriodide
NMR	Nuclear magnetic resonance
NOESY	Nuclear Overhauser effect spectroscopy
NTP	Nucleoside triphosphate
PC	Pyruvate carboxylase
Pd/C	Palladium on carbon
PDC	Pyridinium dichromate
PEG	Polyethylene glycol
<i>Ph</i> BPL	<i>P. horikoshii</i> biotin protein ligase
P-loop	Phosphate binding loop
RMSD	Root-mean-square deviation of atomic positions

<i>Sa</i> BPL	<i>S. aureus</i> biotin protein ligase
SAM	<i>S</i> -Adenosyl- <i>L</i> -methionine
<i>Sa</i> PC90	90 amino acid biotin-acceptor domain from PC
SAR	Structure activity relationship
SPR	Surface plasma resonance
<i>t</i> -BuOH	<i>tert</i> -Butanol
TB	Tuberculosis
TBS	Tris-buffered saline
TCA	Tricarboxylic acid
TEA	Triethylamine
TEMPO	(2,2,6,6-Tetramethylpiperidin-1-yl)oxyl
TFA	Trifluoroacetic acid
THF	Tetrahydrofuran
TLC	Thin layer chromatography
TOF	Top of flight
Tris	2-Amino-2-hydroxymethylpropane-1,3-diol
Ts	4-Toluenesulfonyl group
Z-Asp-OMe	N-Cbz- <i>L</i> -aspartic acid α -methyl ester

Chapter One

1.1 The need for new antibiotics

There is an urgent need for novel classes of antimicrobials due to rapidly escalating incidence of bacterial resistance and the associated threat to human health. The Centers for Disease Control and Prevention (CDC) at the US Department of Health and Human Services has predicted over 2 million illnesses and 23,000 mortalities due to antibiotic resistance every year in the USA alone.¹ However, current antibacterial drug development pipelines have ‘dried up’ mainly due to the exit of major pharmaceutical companies from antibiotic research.² In addition, only five of 30 new antibiotics introduced worldwide between 2000 and 2015 were first-in-class.³ Large pharmaceutical companies remain reluctant to initiate or continue their antibiotic research programmes due to a low return on investment. Thus academic-led research on antimicrobial agents is crucial to overcome the rapid emergence of new drug-resistant strains and the declining rate of new antibiotic development. *Staphylococcus aureus* (*S. aureus*) is responsible for numerous diseases in humans from mild skin infection to fatal sepsis.⁴ In particular, methicillin-resistant *S. aureus* (MRSA) has become a major cause of life threatening infections. It is estimated that MRSA causes more than 80,000 invasive infections and 11,000 deaths each year in the United States.⁵ *Mycobacterium tuberculosis* (*M. tuberculosis*) is the principal pathogen for tuberculosis, one of the top ten causes of human mortality worldwide.⁶ There has been a significant rise in cases of multidrug-resistant tuberculosis (MDR-TB), with an estimated 458,000 new cases of MDR-TB in 2017 alone.⁶ One logical strategy to combat resistance is to discover new chemical classes affecting novel drug targets that are not subject to pre-existing resistance mechanisms. This thesis presents work on *S. aureus* biotin protein ligase (*SaBPL*) and *M. tuberculosis* dethiobiotin synthase (*MtbDTBS*) as novel targets for antibiotic research and the design of small molecule inhibitors thereof. These proteins play key roles in biotin biology and biosynthesis.

1.2 Biotin biology and biosynthesis

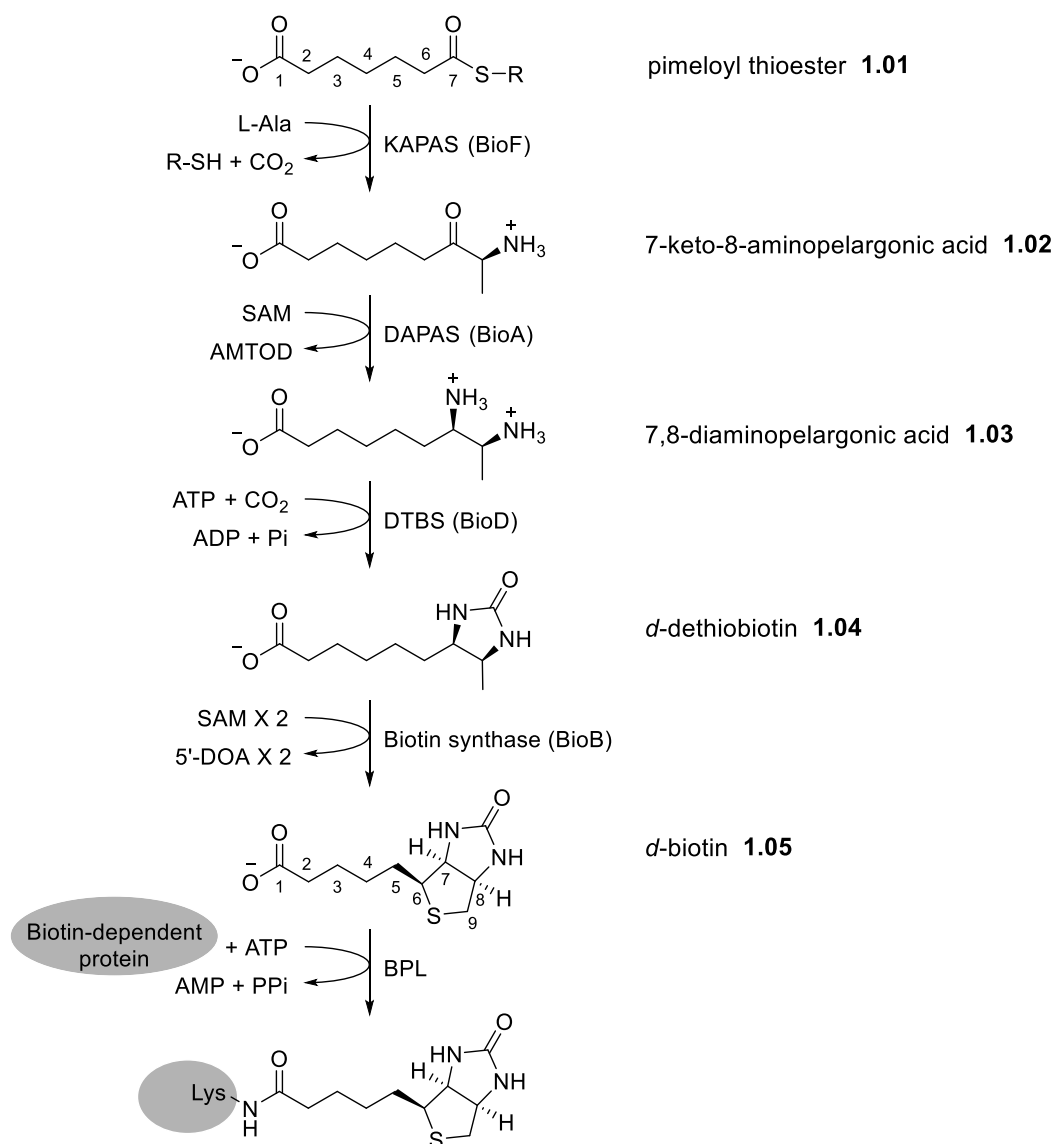
Biotin (also known as vitamin B7 or vitamin H) is an essential vitamin that is required for growth and pathogenicity of bacteria. Biotin serves as an indispensable cofactor for biotin-dependent enzymes that are involved in membrane lipid synthesis, gluconeogenesis and amino acid metabolism.⁷⁻¹¹ Two representative biotin-dependent enzymes, namely acetyl CoA carboxylase (ACC)¹² and pyruvate carboxylase (PC)¹³, play critical roles in bacteria. These enzymes are activated when ligated to biotin by biotin protein ligase (BPL). ACC

catalyses the carboxylation of acetyl-CoA to malonyl-CoA in fatty acid biosynthesis, which is essential for cell membrane biogenesis and maintenance.¹⁴ PC is a critical enzyme for the conversion of pyruvate to oxaloacetate in the TCA cycle which then plays a pivotal role in a number of key metabolic pathways including gluconeogenesis and amino acid biosynthesis.¹⁵ Even though biotin is essential for all living cells, only microbes, plants and some fungi are able to synthesise biotin *de novo*.¹⁶ Humans and other mammals, lack this biosynthetic pathway and thus must obtain biotin through exogenous sources, i.e. diet and/or from intestinal microflora.¹⁷

The biotin biosynthetic pathway can be readily divided into two stages, synthesis of a pimeloyl thioester precursor and assembly of the bicyclic rings. Scheme 1.1 shows the second stage of biotin biosynthetic pathway and the chemical structures of the synthetic intermediates involved.¹⁸ The steps leading to the synthesis of a pimeloyl thioester precursor **1.01** are variable among different biotin-producing organisms. Unlike the formation of the pimeloyl thioester precursor **1.01**, the final four reaction steps in the pathway that assemble the bicyclic rings of biotin **1.05**, are conserved in all biotin-producing organisms. The pimeloyl thioester **1.01** is a dedicated precursor of the second stage of the biosynthetic pathway and provides the majority of the biotin backbone carbon atoms. In a four-step pathway, a pimelate thioester **1.01** is firstly converted to 7-keto-7-aminopelargonic acid (KAPA) **1.02** and the pathway then proceeds through two more intermediates, 7,8-diaminopelargonic acid (DAPA) **1.03** and dethiobiotin (DTB) **1.04**, to form biotin **1.05** (Scheme 1.1). The enzymes of 7-keto-7-aminopelargonic acid synthase (KAPAS), 7,8-diaminopelargonic acid synthase (DAPAS), dethiobiotin synthase (DTBS) and biotin synthase (BS) are encoded by *bioF*, *bioA*, *bioD*, and *bioB* respectively.¹⁰

1.3 Biotin protein ligase (BPL)

BPL, a ubiquitous enzyme found in all organisms, is responsible for the post-translational attachment of biotin **1.05** onto the biotin domain of biotin-dependent enzymes (ACC and PC).¹⁹⁻²⁰ ACC and PC are highly related to bacteria survival and virulence, and as such BPL presents as a potential new antibacterial drug target. Moreover, genetic knockout studies using *S. aureus* deficient in the *bpl* gene prevent cell growth, indicating that there is no alternative pathway for the biotinylation of biotin-dependent proteins in bacteria.²¹⁻²²



Scheme 1.1. The second stage of biotin biosynthesis, the assembly of the bicyclic rings, consists of four reactions catalysed by KAPAS, DAPAS, DTBS and BS. The R group indicates either CoA or acyl carrier protein (ACP). Abbreviations: SAM, *S*-adenosyl-L-methionine; AMTOD, *S*-adenosyl-2-oxo-4-thiomethylbutyrate; 5'-DOA, 5'-deoxyadenosine. The figure is modified from Lin & Cronan.¹⁸

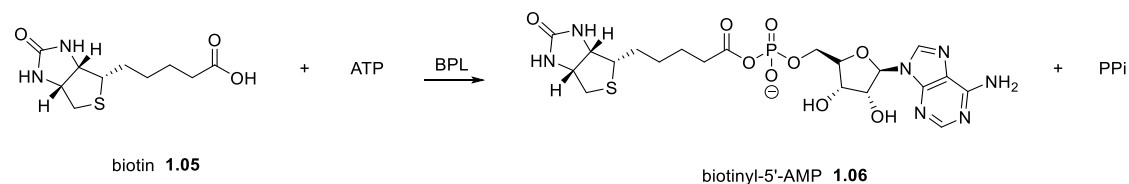
S. aureus BPL (*Sa*BPL) utilises biotin and also controls the uptake and biosynthesis of biotin in response to cellular demand.²³⁻²⁵ Without activated biotin-dependent enzymes, *Sa*BPL produces a homodimer that is responsive to DNA binding. The *Sa*BPL homodimer serves as a transcriptional repressor that regulates biotin biosynthesis and transport by binding specific DNA sequences present in the operator site of the biotin biosynthesis operon. Therefore, *Sa*BPL not only activates biotin-dependent enzymes including ACC and PC, but also functions as a transcriptional repressor of the biotin biosynthesis operon. *Sa*BPL is a

promising drug target due to its bifunctionality as it is less likely for *S. aureus* to develop target based resistance by reason of the intimate involvement with multiple metabolic pathways.²⁵

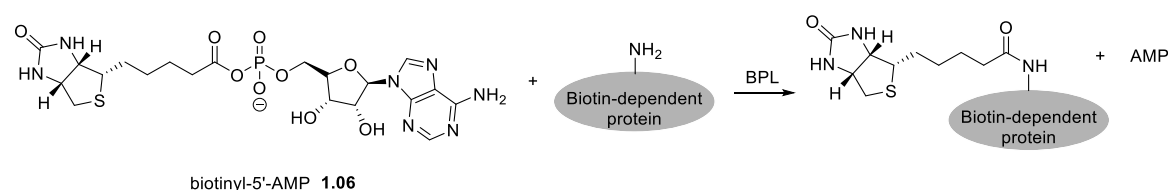
1.3.1 Mechanism of BPL

Protein biotinylation is achieved through a two-step ordered reaction that is catalysed by BPL in all organisms as shown in Scheme 1.2.^{20, 26} In the first step, biotin **1.05** reacts with ATP to form biotinyl-5'-AMP **1.06**, with the release of pyrophosphate (PPi). During this stage, biotin **1.05** binds to the biotin binding pocket in BPL and stimulates ordering of a biotin binding loop (BBL) within the enzyme (Figure 1.1). This conformational change in BPL generates the ATP binding pocket that allows subsequent binding of ATP. A condensation reaction between biotin and the α -phosphate of ATP then produces the reaction intermediate biotinyl-5'-AMP **1.06** to complete the first step. When the cellular demand for biotin **1.05** is low, the complex of BPL with biotinyl-5'-AMP **1.06** can dimerize and bind DNA without the second step of biotinylation. This then results in the concomitant repression of biotin biosynthesis. In the presence of a biotin-dependent enzyme (e.g. ACC or PC) requiring biotinylation, the BPL/**1.06** complex recognises and binds to a biotin carboxyl carrier protein (BCCP) domain present in the unliganded biotin-dependent enzyme (see Step 2 in Scheme 1.2). During this step, the ϵ -amino group of the target lysine residue present in BCCP domain reacts with the carbonyl group of **1.06**, resulting in the transfer of the biotin moiety onto the biotin domain to give biotinylated ACC or PC, with the release of AMP.

Step 1



Step 2



Scheme 1.2. The catalytic two-step reaction of biotinylation.

1.3.2 Structural classes of BPL

BPL can be divided into three divergent structural classes (Figure 1.2). Class I BPLs are composed solely of the conserved catalytic domain, which is required for protein biotinylation, and C-terminal domain. X-ray crystal structures of class I BPLs have been reported for *M. tuberculosis*²⁷, *Aquifex aeolicus*²⁸, and *Pyrococcus horikoshii*²⁰. Class II BPLs contain an additional N-terminal DNA binding domain, suggesting these class enzymes have both biotin ligase and transcriptional repressor activities. The X-ray crystal structures of bifunctional class II BPLs from *S. aureus*²⁹ and *Escherichia coli* (*E. coli*)²⁶ have been reported. Class III BPLs, such as those found in certain eukaryotes and mammals, have

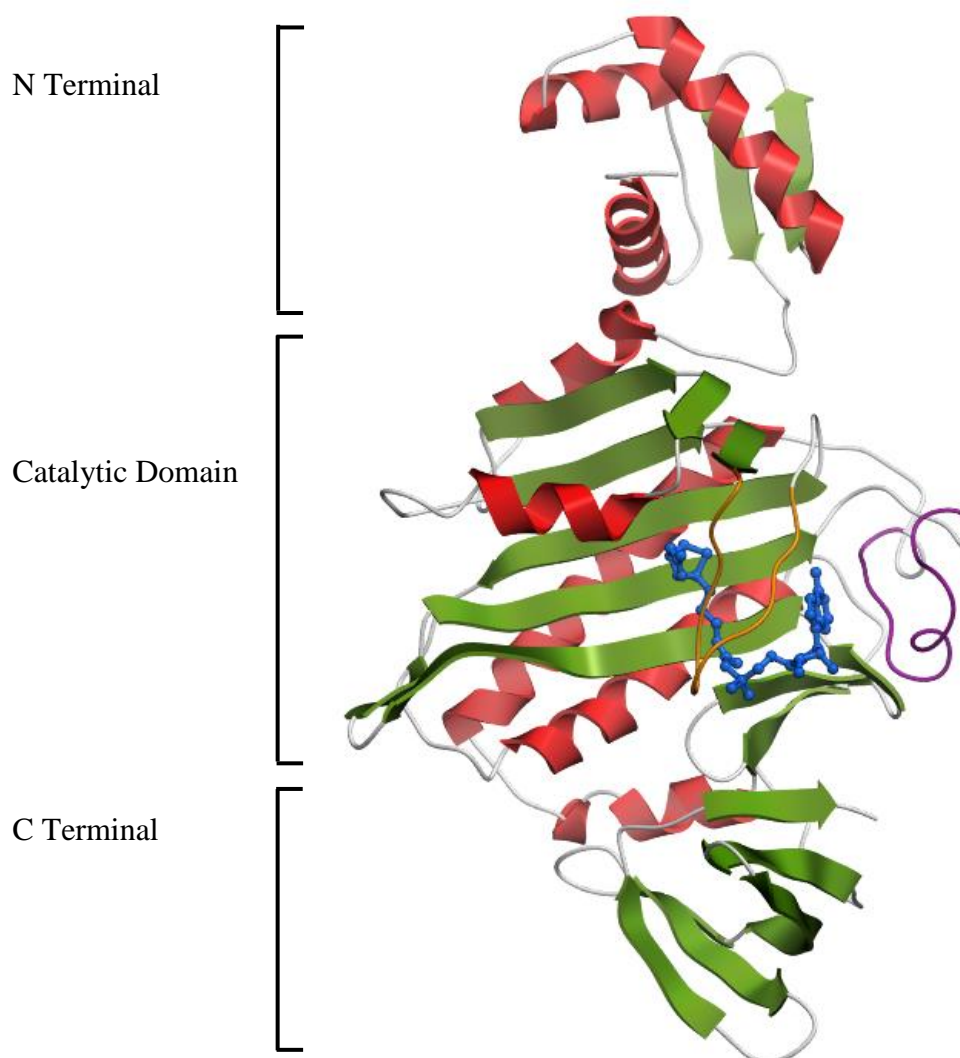


Figure 1.1. 3D depiction of SaBPL in complex with biotinyl-5'-AMP **1.06** (PDB: 3V8L). The β sheets are shown in green, α helices in red, biotin binding loop (BBL) in orange, ATP binding loop (ABL) in purple and biotinyl-5'-AMP **1.06** in blue.

a large N-terminal extension that bears no similarity to the DNA binding domain of class II BPLs.³⁰⁻³³ According to recent mutagenic and genetic studies, this extension contains a ‘proof reading’ activity to ensure that the correct enzymes are chosen for protein biotinylation.³⁰ All BPLs contain a conserved catalytic core through a disordered to ordered conformational change within the enzyme.³⁴ Comparison of the catalytic domains of liganded and unliganded *Sa*BPL shows two disordered binding loops, a biotin binding loop (BBL; highlighted in orange in Figure 1.1) and an ATP binding loop (ABL; highlighted in purple in Figure 1.1).³⁵ A closer examination of the active site is described below.

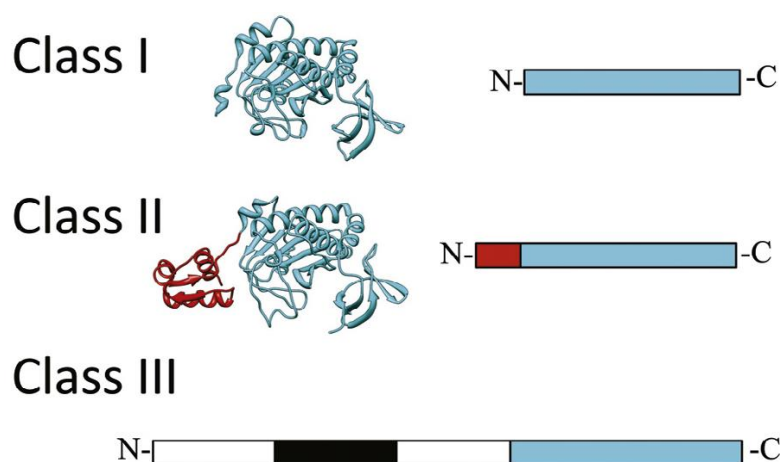


Figure 1.2. Schematic diagram of the three classes of BPL. The conserved catalytic region is depicted in blue, the DNA binding domain of class II enzymes in red and the proof reading domain in human BPL is boxed black. The figure is adapted from Satiaputra *et al.*³⁶

1.3.3 BPL active site

The active site of BPL is located in the catalytic domain, where synthesis of biotinyl-5'-AMP **1.06** and biotin transfer occur. The BPL active site consists of two major pockets including biotin binding pocket and ATP binding pocket. In the biotin pocket of *Sa*BPL, the oxygen on the ureido ring of biotin **1.05** forms multiple hydrogen bonds with the side chain of Ser93 and a backbone amide at Arg120, as depicted in Figure 1.3. The ureido NH also form hydrogen bonds with the backbone oxygen of Arg120 and the side chain of Gln116, respectively (Figure 1.3). These residues are highly conserved in BPLs across most species.³⁷ The valeric tail of biotin on the other hand is encased in a hydrophobic tunnel defined by induced fit binding of biotin in the first catalytic step of BPL.³⁸⁻³⁹ The hydrophobic tunnel is composed of Gly119, Gly210, Gly189, Leu192 and Ile209. Structural analysis with co-crystal structures of biotin **1.05** and biotinyl-5'-AMP **1.06** bound to BPLs reveals a high

degree of conservation in the biotin binding pocket of *Sa*BPL²⁹, *Ec*BPL (*E. coli*)²⁶, *Mtb*BPL (*M. tuberculosis*)⁴⁰, *Aa*BPL (*Aquifex aeolicus*)²⁸ and *Ph*BPL (*Pyrococcus horikoshii*)³⁹.

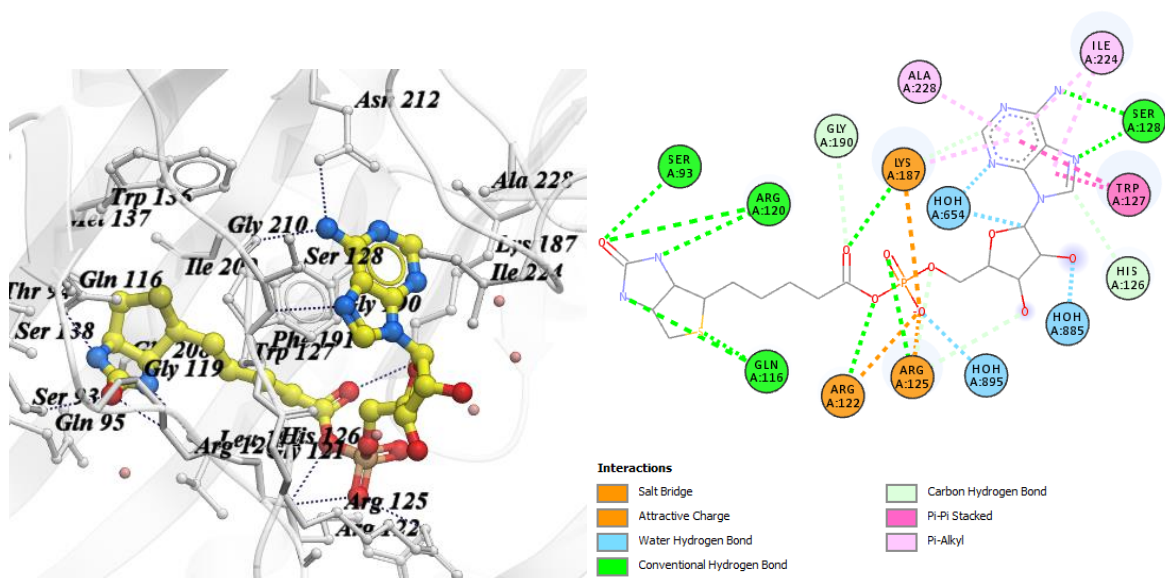


Figure 1.3. 3D depiction of reaction intermediate biotinyl-5'-AMP **1.06** bound to *Sa*BPL (PDB: 3V8L) (left). 2D interaction diagram of reaction intermediate biotinyl-5'-AMP **1.06** bound to *Sa*BPL (right).

The induced fit ordering of BBL orientates the side chain of Trp127 of *Sa*BPL such that it generates a binding surface for nucleotide binding in the ATP binding pocket. This binding is stabilised by a π - π stacking interaction between the adenine moiety of ATP and the indole ring of Trp127.^{37, 41} In the absence of biotin, Trp127 is not appropriately oriented, without π - π stacking interaction between the adenine moiety and the indole ring.²⁰ The adenine ring of ATP also forms hydrogen bonding interactions with Ser128 at the base of the ATP binding pocket. After ATP binding, the previously mentioned reaction (step 1 in Scheme 1.2) occurs to afford biotinyl-5'-AMP **1.06**.⁴² ATP binding loop (ABL) then turns to the ordered conformation to stabilise the reaction intermediate **1.06** by forming hydrophobic interactions with **1.06** through Ile224, and Ala228. Here, ABL is proposed to encapsulate the adenine moiety of **1.06**.

The phosphate binding domain of *Sa*BPL is situated between the ATP pocket and biotin pocket. The phosphoanhydride linker of biotinyl-5'-AMP **1.06** forms a number of hydrogen bonding interactions with the backbone of Arg122 and the side chains of Lys187 and Arg125.⁴² A defined feature on BBL is a highly conserved 'Gly-Arg-Gly-Arg-X' motif present in all BPLs. Of particular note is Arg122 (i.e. Gly-Arg-Gly-Arg¹²²-X) that plays a

central role in stabilising the active binding site via a complex network with water-mediated hydrogen bonds with the side chain of Asp180.^{37, 42}

1.4 SaBPL inhibitors - preliminary data

SaBPL is an attractive novel target for antibiotic development. Firstly, SaBPL is a sole enzyme that regulates biotinylation of ACC and PC of *S. aureus*.⁴³ Targeting SaBPL will consequently target metabolic pathways critical for survival and virulence as ACC and PC are responsible for these metabolic pathways including fatty acid biosynthesis. Secondly, SaBPL is the only enzyme in *S. aureus* that is involved in the biosynthesis and uptake of biotin in response to cellular demand. Thus, targeting SaBPL will target not only biotin utilisation but also the source of biotin.²³⁻²⁴ Thirdly, SaBPL is not the target of antibiotics currently in clinical use. Novel classes of antibiotics are critically needed to develop as bacterial resistance to one antibiotic often leads to resistance to similar types of antibiotics.

1.4.1 1,2,3-Triazole based analogues

Our group previously identified 1,2,3-triazole as an alternative bioisostere for the labile phosphoanhydride linker in biotinyl-5'-AMP **1.06**.⁴⁴ Importantly, most 1,2,3-triazole BPL inhibitors were highly selective for SaBPL over *Homo sapiens* BPL (HsBPL). There are a number of advantages in a triazole moiety over the natural phosphate linker of **1.06**. The 1,2,3-triazole moiety has two potential hydrogen bond acceptor sites and an ability to participate in π - π stacking interactions as shown in Figure 1.4. This motif is stable under acid/base hydrolysis, reductive and oxidative conditions, as well as typical physiological

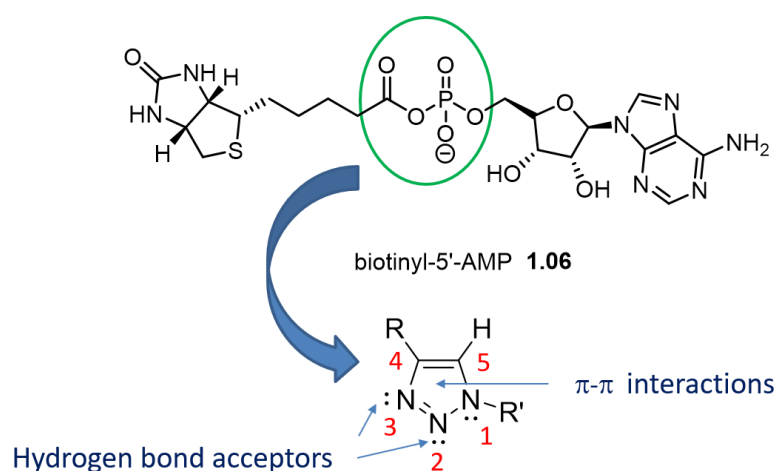


Figure 1.4. The assignment of 1,2,3-triazole with the potential intermolecular interaction sites.

conditions, and therefore resistant to metabolic degradation.⁴⁵ In addition, 1,2,3-triazole can be readily synthesised by copper(I)-catalysed azide alkyne cycloaddition (CuAAC).

A series of 1,4-disubstituted-1,2,3-triazole based analogues of **1.07** – **1.13** (see Figure 1.5) was synthesised and tested for inhibitory activity against *Sa*BPL.^{44, 46-48} The triazole **1.07** was found to be active against *Sa*BPL ($K_i = 1.17 \mu\text{M}$) but was effectively inactive against *Hs*BPL ($K_i > 33 \mu\text{M}$) *in vitro*, thereby providing the first example of a BPL inhibitor with high selectivity for *Sa*BPL over *Hs*BPL. In addition, the triazole **1.07** was not toxic against mammalian HepG2 cells in culture. The triazole analogue **1.08**, lacking the ribose group, proved to be more potent than **1.07** against *Sa*BPL with K_i of $0.66 \mu\text{M}$.^{44, 48} X-ray crystallography of *Sa*BPL in complex with **1.08** revealed that the triazole ring acts as an isostere of the phosphoanhydride group of biotinyl-5'-AMP **1.06** and adopts hydrogen bonds with Arg122 and Arg125.⁴⁴ Furthermore, the triazole **1.09**, with a 2-benzoxazolone moiety, was identified to be more potent than **1.08** against *Sa*BPL with a $K_i = 0.23 \pm 0.01 \mu\text{M}$ while exhibiting >1100 fold selectivity for *Sa*BPL compare to the human homologue.⁴⁴ This was an important finding as a 2-benzoxazolone group was identified as a isostere of the adenine moiety of **1.08** to target the ATP binding pocket. While this biotin triazole class exhibits *in vitro* potency and selectivity over the human homologue, it displays poor whole cell activity.⁴⁴ For example, **1.09** inhibited *S. aureus* growth by 60% at $8 \mu\text{g/mL}$, but did not completely reduce cell growth at the highest assayed concentration ($64 \mu\text{g/mL}$).^{44, 49} There were attempts to shorten and simplify the 1,4-disubstituted-1,2,3-triazole pharmacophore (**1.10** – **1.13**) to enhance antibacterial potency.⁴⁷ The 1-benzyl substituted 1,2,3-triazoles **1.10**, **1.11**, **1.12**, and **1.13** that lack the adenine group, or analogue thereof, had K_i values of 0.28, 0.39, 0.56, and $0.53 \mu\text{M}$, respectively. These derivatives inhibited the growth of *S.*

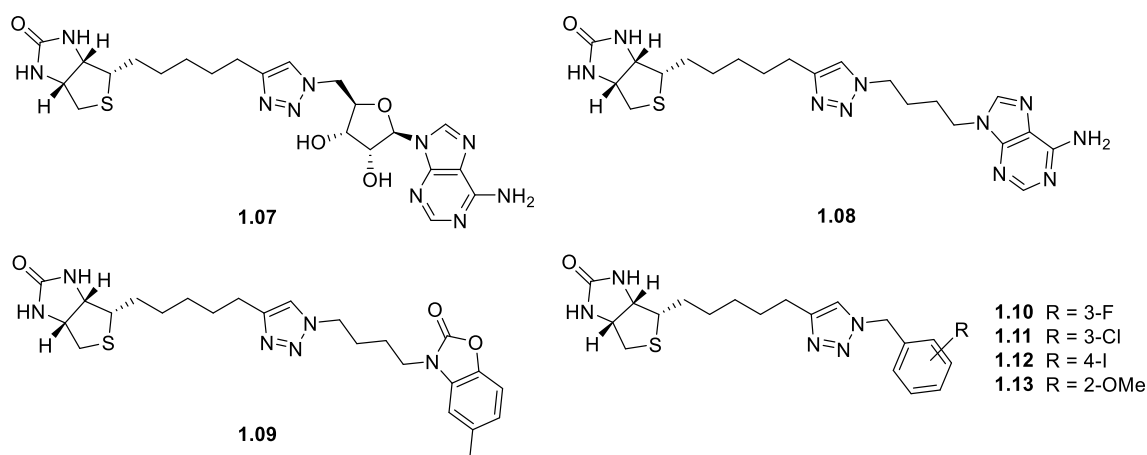


Figure 1.5. Representative 1,4-disubstituted-1,2,3-triazole BPL inhibitors.

aureus ATCC 49775 and displayed low cytotoxicity against mammalian HepG2 cells. The compounds **1.10** – **1.13** provide important new scaffolds for further chemical modification and activity optimization, specifically to interact with the adjacent adenylyl-binding site in the enzyme. Since these triazole BPL inhibitors did not show appropriate antibacterial profile to be preclinical candidates, an approach for improving the whole cell activity is required.

1.4.2 Sulfonamide based analogues

Brown and coworkers described a *N*-acyl sulfamate analogue **1.14** as a structure mimic of biotinyl-5'-AMP **1.06** (Figure 1.6).⁵⁰⁻⁵¹ This analogue is however reported to lack potency toward *Ec*BPL due to its structural instability and rapid decomposition.^{27,50} Duckworth *et al* reported a bisubstrate inhibitor of *Mtb*BPL termed Bio-AMS **1.15** which binds with a K_D of approximately 0.5 nM, more than 1700-fold more tightly than biotin.²⁷ This compound possesses potent and selective antimicrobial activity against the virulent *M. tuberculosis* strain H37Rv as well as a number of multi-drug resistant *M. tuberculosis* strains with minimum inhibitory concentrations (MICs) ranging from 0.16 to 0.625 μ M.²⁷ Interestingly, Bio-AMS **1.15** proved to be inactive against a panel of gram-positive bacteria (*E. faecalis* and *S. aureus*), gram-negative bacteria (*A. baumannii*, *E. coli*, *K. pneumoniae* and *P. aeruginosa*), and fungi (*C. neoformans*, and *C. albicans*). The X-ray crystal structure of Bio-AMS **1.15** bound to *Mtb*BPL revealed key hydrogen bonding interactions between the sulfamide oxygens of **1.15** and amino acid residues Arg69, Arg72, and Asn130 (as numbered in *Mtb*BPL). It is thought to be critical that the terminal amine of Lys138 interacts with the amide oxygen of the acylsulfamide linker of **1.15** through an electrostatic interaction because of the low pK_a of the central nitrogen atom of the linker. A sulfonamide linkage is a good candidate to achieve improved potency, solubility and drug-like property of *Sa*BPL inhibitors.

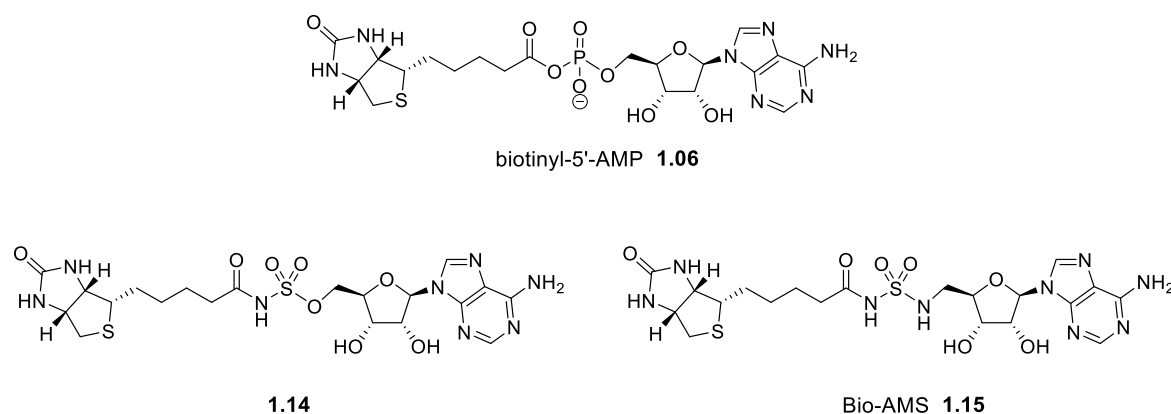
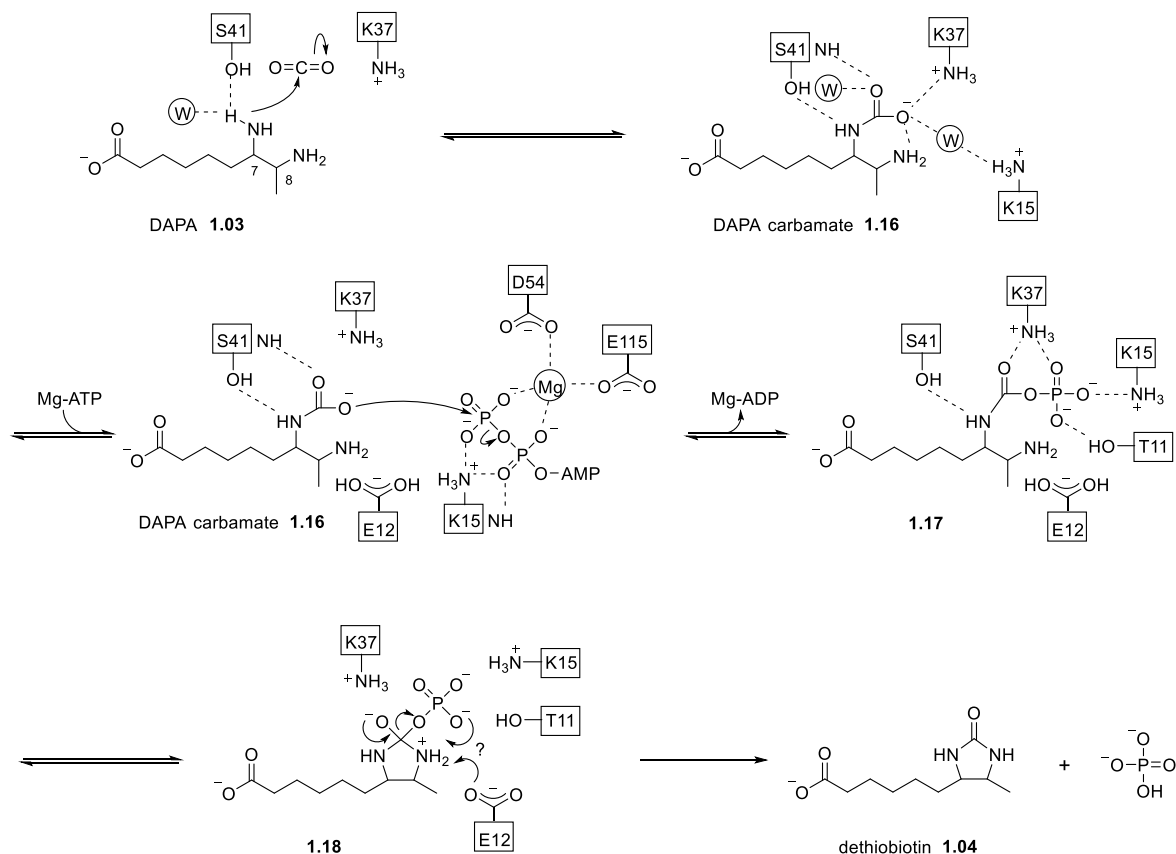


Figure 1.6. Reported sulfonamide BPL inhibitors **1.14** and **1.15**.

1.5 Dethiobiotin synthase (DTBS)

DTBS is the sole enzyme responsible for catalysing a key step in biotin biosynthesis, namely the carboxylation of 7,8-diaminopelargonic acid (DAPA) **1.03**, closing the ureido ring to form dethiobiotin **1.04** in a reaction requiring a nucleotide triphosphate (Scheme 1.1).



Scheme 1.3. The reaction scheme of DTBS, which catalyses the ATP-dependent insertion of CO_2 between the N7 and N8 nitrogen atoms of DAPA **1.03** to form the ureido ring, is modified from Huang *et al.*⁵²

1.5.1 Mechanism of DTBS

The carboxylation reaction catalysed by DTBS proceeds through three distinct steps (Scheme 1.3). In the first step, DAPA **1.03** reacts with CO_2 to form N7-DAPA carbamate **1.16**. This reaction is the regioselective with formation of carbamate at N7 of DAPA **1.03**, a highly coordinated event at the enzyme active site.⁵²⁻⁵³ During this stage, the N7 nitrogen is deprotonated and CO_2 is polarised by DTBS, facilitating a nucleophilic attack of the N7 nitrogen. The resulting carbamate intermediate **1.16** is partially buried in the enzyme shielding it from solvent and is further stabilised by a complex network with water-mediated hydrogen bonding and ionic interactions particularly involving the terminal amine groups of

Lys15 and Lys37 (Scheme 1.3).⁵² In the second step, DAPA carbamate **1.16** is converted to carbamic-phosphoric anhydride **1.17** by nucleophilic attack at the ATP γ -phosphate by the carbamate oxygen atom of the reaction intermediate **1.16**.⁵⁴ This event is thought to be facilitated by Lys37 which stabilises the resulting negatively charged carbonyl oxygen. In the final step, carbamic-phosphoric anhydride **1.17** is converted to dethiobiotin **1.04** by the closure of the ureido ring, with the release of inorganic phosphate. The proposed mechanism begins with nucleophilic attack at the carbamate carbon by N8 to form a tetrahedral intermediate **1.18** (Scheme 1.3).⁵² The carbon – oxygen bond is then cleaved to complete formation of the ureido ring and a proton from the N8 nitrogen is abstracted by possibly a Glu12 residue or a phosphate oxygen atom (Scheme 1.3).⁵²

1.5.2 DTBS structure

The structure of DTBS has been reported from *M. tuberculosis*, *E. coli*, *H. pylori* and *F. tularensis* either with or without ligands such as DAPA or ATP.^{52, 54-59} The active DTBS is a homodimer with a molecular mass of ~46 kDa and contains two active sites which are placed at the interface between the two subunits in anti-parallel directions 25 Å apart (Figure 1.7).⁵⁷ Each subunit folds into a single globular domain containing seven parallel β -sheets interconnected with α -helices. Each active site includes adjacent binding pockets for DAPA

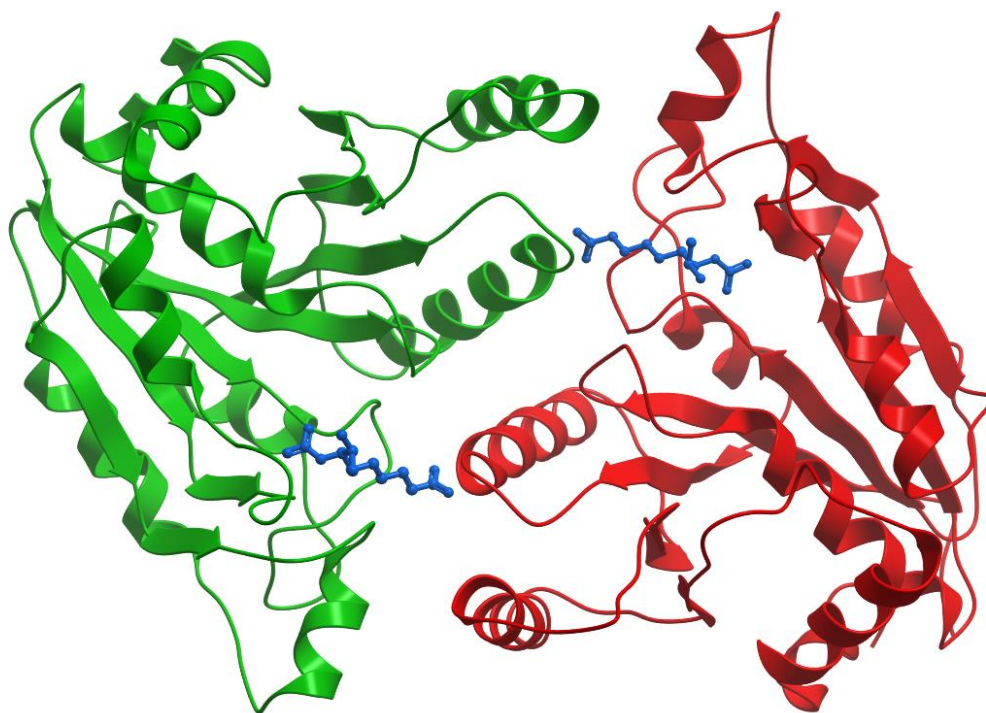


Figure 1.7. 3D depiction of *Mtb*DTBS with DAPA carbamate **1.16** bound (PDB: 3FMF). The chain A is shown in red, chain B in green, and DAPA carbamate **1.16** in blue.

and nucleotide substrates. The DAPA pocket is formed by amino acids from the two subunits. In particular, four amino acids, including Lys37, Thr41 from the first subunit and Leu146, Asn147 from the partner subunit (numbering in *M. tuberculosis* DTBS (*MtbDTBS*)), are involved in DAPA binding.⁵⁷ In contrast, the nucleotide pocket is situated exclusively in one subunit. Binding of ATP to *E. coli* DTBS is known to induce conformation changes of active site loop regions including the phosphate binding loop (P-loop).⁵² *MtbDTBS* includes the classical P-loop motif, Gly8-X-Gly10-X-Gly12-Val13-Gly14-Lys15-Thr16, which is crucial for binding to the α , β and γ phosphate groups of ATP.⁵⁸ While the overall fold is similar, the nucleotide binding pocket in *MtbDTBS* is different from that in DTBS from other species.

1.5.3 DTBS active site

The DTBS active site can be divided into three distinct pockets: the DAPA pocket, phosphate-binding loop (P-loop), and nucleoside pocket (Figure 1.8). The catalytically competent unit for DTBS is a dimer and amino acids from both subunits contribute to the tunnel-like DAPA binding site placed at the dimer interface. The DAPA alkyl chain extends along this tunnel, whereas the amine and carboxyl groups form hydrogen bonds with DTBS at either end. The P-loop accommodates the phosphate groups of nucleoside triphosphate (NTP) via electrostatic interactions. The nucleoside base is stabilised by hydrogen bonding interactions in the nucleoside pocket.⁶⁰ The DAPA and nucleotide binding sites are discrete

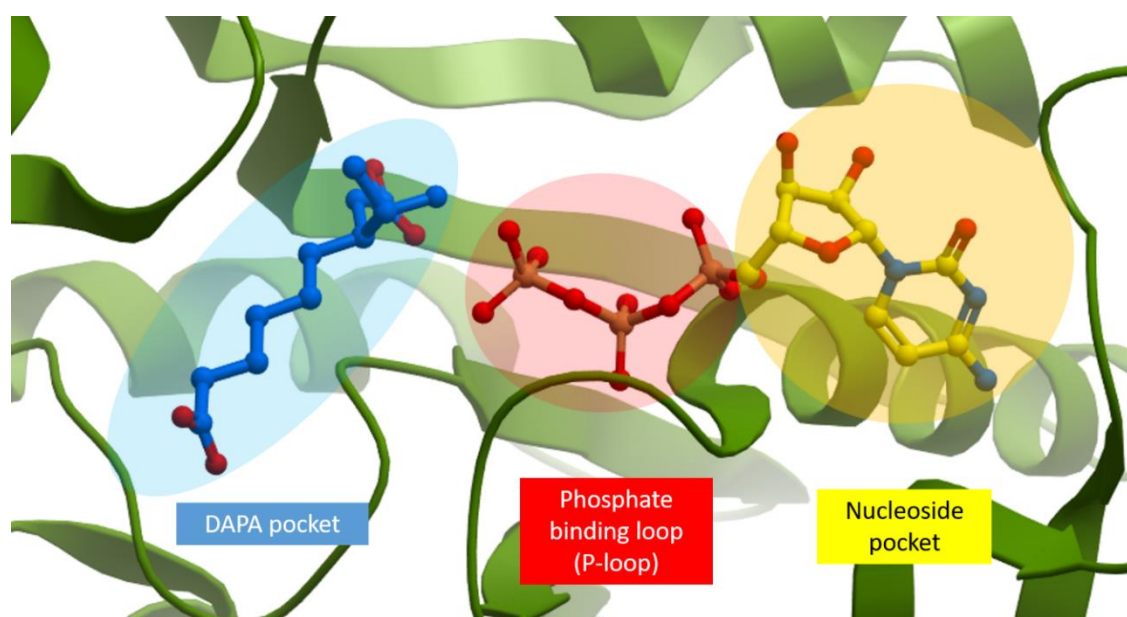


Figure 1.8. An overlay of DAPA carbamate **1.16** (blue) and CTP (yellow with phosphates in orange/red) bound to *MtbDTBS* (PDB: 3FMF and 4WOP, respectively).

and binding of one substrate is not required for binding of the other.⁶⁰ *Mtb*DTBS is not restricted to using ATP to generate dethiobiotin, with a range of different nucleotides allowing the reaction to proceed with similar rates.⁶⁰ In particular, DTBS has a significantly greater affinity for CTP ($K_D = 0.16 \mu\text{M}$) than ATP ($K_D = 75 \mu\text{M}$).⁶¹

In the DAPA pocket of *Mtb*DTBS, the carboxyl group of the carbamate in DAPA carbamate **1.16** occupies the position of the water molecule (W11) at the active site of the apo structure and the carboxy oxygen atoms are within hydrogen bond distance to the ϵ -amino groups of residues Lys37 (2.91 Å) and to the backbone amide nitrogen of Thr41 main-chain (2.84 Å) (Figure 1.9). The N7 atom of DAPA carbamate **1.16** forms a hydrogen bond with the hydroxyl group of Thr41 (2.86 Å). The long aliphatic chain of DAPA carbamate **1.16** spans the two subunits, making hydrophobic interactions with Ala73, Pro74, Gly111, and Val115. One of the C1-carboxy oxygen atoms coordinates with the backbone amide nitrogen of Leu146 (2.87 Å) and a neighbouring water molecule (2.31 Å), while the other of the C1-carboxy oxygen atoms interacts with the main-chain amide of Asn147 (2.81 Å) and with an ordered water molecule (2.99 Å).

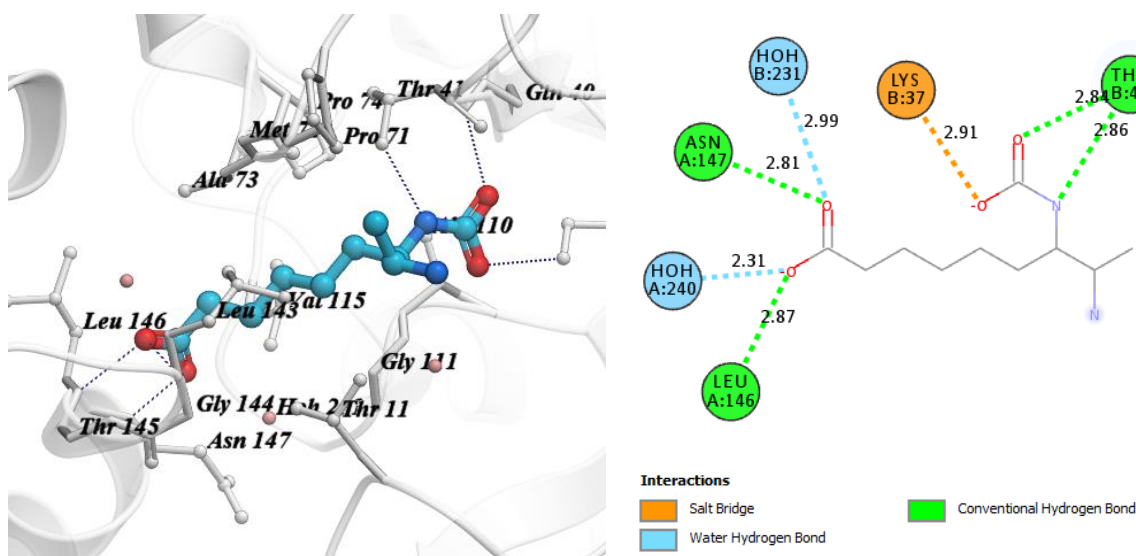


Figure 1.9. 3D depiction of reaction intermediate DAPA carbamate **1.16** bound to *Mtb*DTBS (PDB: 3FMF) (left). 2D interaction diagram of reaction intermediate DAPA carbamate **1.16** bound to *Mtb*DTBS (right).

The crystal structure of *Mtb*DTBS in complex with CTP reveals that hydrogen bonding interactions with the pyrimidine heterocycle occur exclusively through the peptide backbone of the enzyme, and not via side chains (Figure 1.10). Hydrogen bonding interactions are observed between the cytosine amine group and the backbone amide oxygens of Pro197

(2.94 Å) and Gly169 (2.85 Å), as well as between the cytosine N3 and the backbone amide NH of Ala200 (2.95 Å) (Figure 1.10). The pyrimidine heterocycle of CTP also forms a hydrophobic interaction with the side chains of Val17. The cytosine O2' coordinates with a neighbouring water molecule (2.94 Å).

The triphosphate moiety of CTP forms a network of intermolecular interactions with water molecules and amino acid residues of the P-loop. The backbone amides of Gly12, Val13, Gly14, Lys15, Thr16, and Val17 are involved in polar interactions with the triphosphate group. In particular, the β -phosphate of CTP coordinates with the P-loop through a network of hydrogen bonding interactions including the ϵ -amino groups of Lys15 and the hydroxyl group of Thr16 in addition to the backbone amides of Gly12, Val13, Gly14, Lys15, and Thr16. The α - and γ -phosphate moieties form comparatively fewer hydrogen bonding interactions with the P-loop than the β -phosphate.

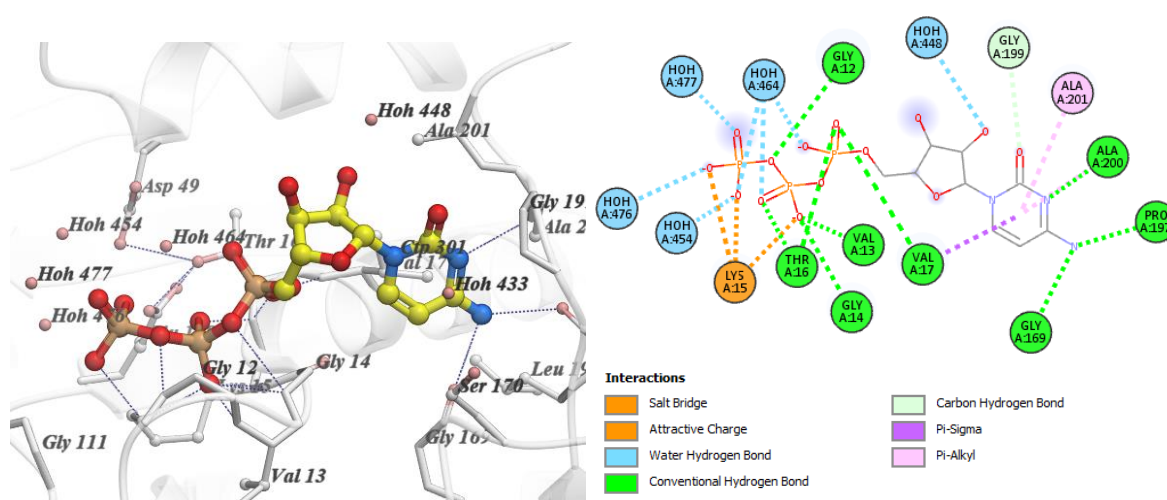


Figure 1.10. 3D depiction of CTP bound to *MtbDTBS* (PDB: 4WOP) (left). 2D interaction diagram of CTP bound to *MtbDTBS* (right).

1.5.4 *MtbDTBS* as an antituberculosis drug target

MtbDTBS appears to be a promising, untested target for antituberculosis drug development. Genetic knockout studies have demonstrated *MtbDTBS* is an essential enzyme for the growth and virulence of *M. tuberculosis*.⁶² Several structures of DTBS are available from many species such as *M. tuberculosis*, *E. coli*, *H. pylori*, and *F. tularensis*.^{52, 59} These crystal structures are powerful tools for the development of molecules that bind specifically to *MtbDTBS* and only inhibit *M. tuberculosis*. In addition, there are no human homologues to *MtbDTBS*, indicating that it is less likely that the inhibitor will have unintended side effects.

Despite the previous structural characterisation of *Mtb*DTBS, there are no published examples of inhibitors developed against this enzyme.

1.6 Research described in this thesis

This thesis describes the design of new classes of *Sa*BPL inhibitors that have improved antimicrobial activity and metabolic stability. This thesis also reports the design of novel *Mtb*DTBS binders based on the X-ray crystal structure of *Mtb*DTBS in complex with ligands.

Chapter 2 elaborates on the potent inhibitors **1.10** - **1.13** with chemical modifications carried out at the C5 position on the 1,2,3-triazole ring to increase antimicrobial activities towards *S. aureus*. Chapter 3 describes the design, synthesis, and biological assay of sulfonamide analogues targeting *Sa*BPL to improve metabolic stability, assisted by computational chemistry. Chapter 4 focuses on the structure guided chemical optimization of a hit compound targeting the DAPA binding site of *Mtb*DTBS using X-ray crystallography screening and docking experiments. Finally, chapter 5 describes the linking between the optimized DAPA pocket binder (discovered in Chapter 4) and 2'-deoxycytidine to produce potent bi-substrate ligands for *Mtb*DTBS.

1.7 References for Chapter One

1. Penchovsky, R.; Traykovska, M., Designing drugs that overcome antibacterial resistance: where do we stand and what should we do? *Expert Opinion on Drug Discovery* **2015**, *10* (6), 631-650.
2. Cooper, M. A.; Shlaes, D., Fix the antibiotics pipeline. *Nature* **2011**, *472* (7341), 32.
3. Butler, M. S.; Blaskovich, M. A. T.; Cooper, M. A., Antibiotics in the clinical pipeline at the end of 2015. *J. Antibiot.* **2017**, *70* (1), 3-24.
4. Yang, Y. C.; Hu, Z.; Shang, W. L.; Hu, Q. W.; Zhu, J. M.; Yang, J.; Peng, H. G.; Zhang, X. P.; Liu, H.; Cong, Y. G.; Li, S.; Hu, X. M.; Zhou, R. J.; Rao, X. C., Molecular and Phenotypic Characterization Revealed High Prevalence of Multidrug-Resistant Methicillin-Susceptible *Staphylococcus aureus* in Chongqing, Southwestern China. *Microb. Drug Resist.* **2017**, *23* (2), 241-246.
5. Dantes, R.; Mu, Y.; Belflower, R.; Aragon, D.; Dumyati, G.; Harrison, L. H.; Lessa, F. C.; Lynfield, R.; Nadle, J.; Petit, S.; Ray, S. M.; Schaffner, W.; Townes, J.; Fridkin, S.; Program-Active, E. I., National Burden of Invasive Methicillin-Resistant *Staphylococcus aureus* Infections, United States, 2011. *Jama Internal Medicine* **2013**, *173* (21), 1970-1978.
6. World Health Organization. *Global tuberculosis report 2018*; World Health Organization: Geneva, 2018.
7. Eisenreich, W.; Dandekar, T.; Heesemann, J.; Goebel, W., Carbon metabolism of intracellular bacterial pathogens and possible links to virulence. *Nature Reviews Microbiology* **2010**, *8* (6), 401-412.
8. Gago, G.; Diacovich, L.; Arabolaza, A.; Tsai, S. C.; Gramajo, H., Fatty acid biosynthesis in actinomycetes. *FEMS Microbiol. Rev.* **2011**, *35* (3), 475-497.
9. Park, S. W.; Klotzsche, M.; Wilson, D. J.; Boshoff, H. I.; Eoh, H.; Manjunatha, U.; Blumenthal, A.; Rhee, K.; Barry, C. E.; Aldrich, C. C.; Ehrt, S.; Schnappinger, D., Evaluating the Sensitivity of *Mycobacterium tuberculosis* to Biotin Deprivation Using Regulated Gene Expression. *PLoS Path.* **2011**, *7* (9).
10. Salaemae, W.; Azhar, A.; Booker, G. W.; Polyak, S. W., Biotin biosynthesis in *Mycobacterium tuberculosis*: physiology, biochemistry and molecular intervention. *Protein & Cell* **2011**, *2* (9), 691-695.

11. Takayama, K.; Wang, C.; Besra, G. S., Pathway to synthesis and processing of mycolic acids in *Mycobacterium tuberculosis*. *Clin. Microbiol. Rev.* **2005**, *18* (1), 81-+.
12. Nenortas, E.; Beckett, D., Purification and Characterization of Intact and Truncated Forms of the *Escherichia coli* Biotin Carboxyl Carrier Subunit of Acetyl-CoA Carboxylase. *Journal of Biological Chemistry* **1996**, *271* (13), 7559-7567.
13. Paul V, A., The structure and the mechanism of action of pyruvate carboxylase. *The International Journal of Biochemistry & Cell Biology* **1995**, *27* (3), 231-249.
14. Bloch, K.; Vance, D., Control Mechanisms in the Synthesis of Saturated Fatty Acids. *Annual Review of Biochemistry* **1977**, *46* (1), 263-298.
15. Wallace, J. C.; Jitrapakdee, S.; Chapman-Smith, A., Pyruvate carboxylase. *The International Journal of Biochemistry & Cell Biology* **1998**, *30* (1), 1-5.
16. Roje, S., Vitamin B biosynthesis in plants. *Phytochemistry* **2007**, *68* (14), 1904-1921.
17. Zempleni, J.; Wijeratne, S. S. K.; Hassan, Y. I., Biotin. *BioFactors* **2009**, *35* (1), 36-46.
18. Lin, S.; Cronan, J. E., Closing in on complete pathways of biotin biosynthesis. *Mol. Biosyst.* **2011**, *7* (6), 1811-1821.
19. Samols, D.; Thornton, C. G.; Murtif, V. L.; Kumar, G. K.; Haase, F. C.; Wood, H. G., Evolutionary conservation among biotin enzymes. *Journal of Biological Chemistry* **1988**, *263* (14), 6461-6464.
20. Bagautdinov, B.; Kuroishi, C.; Sugahara, M.; Kunishima, N., Crystal structures of biotin protein ligase from *Pyrococcus horikoshii* OT3 and its complexes: structural basis of biotin activation. *Journal of Molecular Biology* **2005**, *353* (2), 322-333.
21. Payne, D. J.; Gwynn, M. N.; Holmes, D. J.; Pompliano, D. L., Drugs for bad bugs: confronting the challenges of antibacterial discovery. *Nature Reviews Drug Discovery* **2007**, *6* (1), 29-40.
22. Forsyth, R.; Haselbeck, R. J.; Ohlsen, K. L.; Yamamoto, R. T.; Xu, H.; Trawick, J. D.; Wall, D.; Wang, L.; Brown - Driver, V.; Froelich, J. M., A genome - wide strategy for the identification of essential genes in *Staphylococcus aureus*. *Molecular Microbiology* **2002**, *43* (6), 1387-1400.
23. Abbott, J.; Beckett, D., Cooperative binding of the *Escherichia coli* repressor of biotin biosynthesis to the biotin operator sequence. *Biochemistry* **1993**, *32* (37), 9649-9656.

24. Rodionov, D. A.; Mironov, A. A.; Gelfand, M. S., Conservation of the Biotin Regulon and the BirA Regulatory Signal in Eubacteria and Archaea. *Genome Research* **2002**, *12* (10), 1507-1516.
25. Beckett, D., Biotin sensing at the molecular level. *The Journal of Nutrition* **2009**, *139* (1), 167-170.
26. Wood, Z. A.; Weaver, L. H.; Brown, P. H.; Beckett, D.; Matthews, B. W., Co-repressor Induced Order and Biotin Repressor Dimerization: A Case for Divergent Followed by Convergent Evolution. *Journal of Molecular Biology* **2006**, *357* (2), 509-523.
27. Duckworth, B. P.; Geders, T. W.; Tiwari, D.; Boshoff, H. I.; Sibbald, P. A.; Barry, C. E., 3rd; Schnappinger, D.; Finzel, B. C.; Aldrich, C. C., Bisubstrate adenylation inhibitors of biotin protein ligase from *Mycobacterium tuberculosis*. *Chemistry & Biology* **2011**, *18* (11), 1432-41.
28. Tron, C. M.; McNae, I. W.; Nutley, M.; Clarke, D. J.; Cooper, A.; Walkinshaw, M. D.; Baxter, R. L.; Campopiano, D. J., Structural and functional studies of the biotin protein ligase from *Aquifex aeolicus* reveal a critical role for a conserved residue in target specificity. *Journal of Molecular Biology* **2009**, *387* (1), 129-146.
29. Pardini, N. R.; Yap, M. Y.; Polyak, S. W.; Cowieson, N. P.; Abell, A.; Booker, G. W.; Wallace, J. C.; Wilce, J. A.; Wilce, M. C., Structural characterization of *Staphylococcus aureus* biotin protein ligase and interaction partners: an antibiotic target. *Protein Science* **2013**, *22* (6), 762-773.
30. Mayende, L.; Swift, R. D.; Bailey, L. M.; da Costa, T. P. S.; Wallace, J. C.; Booker, G. W.; Polyak, S. W., A novel molecular mechanism to explain biotin-unresponsive holocarboxylase synthetase deficiency. *Journal of Molecular Medicine-Jmm* **2012**, *90* (1), 81-88.
31. Polyak, S. W.; Chapman-Smith, A.; Brautigan, P. J.; Wallace, J. C., Biotin Protein Ligase from *Saccharomyces cerevisiae* THE N-TERMINAL DOMAIN IS REQUIRED FOR COMPLETE ACTIVITY. *Journal of Biological Chemistry* **1999**, *274* (46), 32847-32854.
32. Pardini, N. R.; Bailey, L. M.; Booker, G. W.; Wilce, M. C.; Wallace, J. C.; Polyak, S. W., Biotin protein ligase from *Candida albicans*: expression, purification and development of a novel assay. *Archives of Biochemistry and Biophysics* **2008**, *479* (2), 163-169.

33. Campeau, E.; Gravel, R. A., Expression in Escherichia coli of N-and C-terminally Deleted Human Holocarboxylase Synthetase INFLUENCE OF THE N-TERMINUS ON BIOTINYLATION AND IDENTIFICATION OF A MINIMUM FUNCTIONAL PROTEIN. *Journal of Biological Chemistry* **2001**, 276 (15), 12310-12316.
34. Feng, J.; Paparella, A. S.; Booker, G. W.; Polyak, S. W.; Abell, A. D., Biotin Protein Ligase Is a Target for New Antibacterials. *Antibiotics (Basel)* **2016**, 5 (3).
35. Pardini, N. R.; Yap, M. Y.; Polyak, S. W.; Cowieson, N. P.; Abell, A.; Booker, G. W.; Wallace, J. C.; Wilce, J. A.; Wilce, M. C. J., Structural characterization of Staphylococcus aureus biotin protein ligase and interaction partners: An antibiotic target. *Protein Sci.* **2013**, 22 (6), 762-773.
36. Satiaputra, J.; Shearwin, K. E.; Booker, G. W.; Polyak, S. W., Mechanisms of biotin-regulated gene expression in microbes. *Synthetic and Systems Biotechnology* **2016**, 1 (1), 17-24.
37. Kwon, K.; Beckett, D., Function of a conserved sequence motif in biotin holoenzyme synthetases. *Protein Science* **2000**, 9 (08), 1530-1539.
38. Chapman-Smith, A.; Cronan Jr, J. E., In vivo enzymatic protein biotinylation. *Biomolecular Engineering* **1999**, 16 (1-4), 119-125.
39. Bagautdinov, B.; Matsuura, Y.; Bagautdinova, S.; Kunishima, N., Protein biotinylation visualized by a complex structure of biotin protein ligase with a substrate. *Journal of Biological Chemistry* **2008**, 283 (21), 14739-14750.
40. Purushothaman, S.; Gupta, G.; Srivastava, R.; Ramu, V. G.; Surolia, A., Ligand Specificity of Group I Biotin Protein Ligase of *Mycobacterium tuberculosis*. *PLoS ONE* **2008**, 3 (5), e2320.
41. Naganathan, S.; Beckett, D., Nucleation of an Allosteric Response via Ligand-induced Loop Folding. *Journal of Molecular Biology* **2007**, 373 (1), 96-111.
42. Soares da Costa, T. P.; Tieu, W.; Yap, M. Y.; Zvarec, O.; Bell, J. M.; Turnidge, J. D.; Wallace, J. C.; Booker, G. W.; Wilce, M. C.; Abell, A. D., Biotin analogues with antibacterial activity are potent inhibitors of biotin protein ligase. *ACS Medicinal Chemistry Letters* **2012**, 3 (6), 509-514.
43. Rozwarski, D. A.; Vilchèze, C.; Sugantino, M.; Bittman, R.; Sacchettini, J. C., Crystal Structure of the Mycobacterium tuberculosis Enoyl-ACP Reductase, InhA, in

- Complex with NAD⁺ and a C16 Fatty Acyl Substrate. *Journal of Biological Chemistry* **1999**, 274 (22), 15582-15589.
44. Soares da Costa, T. P.; Tieu, W.; Yap, M. Y.; Pardini, N. R.; Polyak, S. W.; Sejer Pedersen, D.; Morona, R.; Turnidge, J. D.; Wallace, J. C.; Wilce, M. C.; Booker, G. W.; Abell, A. D., Selective inhibition of biotin protein ligase from *Staphylococcus aureus*. *J. Biol. Chem.* **2012**, 287 (21), 17823-32.
45. Rostovtsev, V. V.; Green, L. G.; Fokin, V. V.; Sharpless, K. B., A stepwise Huisgen cycloaddition process: copper (I) - catalyzed regioselective “ligation” of azides and terminal alkynes. *Angewandte Chemie* **2002**, 114 (14), 2708-2711.
46. Tieu, W.; Polyak, S. W.; Paparella, A. S.; Yap, M. Y.; Soares da Costa, T. P.; Ng, B.; Wang, G.; Lumb, R.; Bell, J. M.; Turnidge, J. D.; Wilce, M. C.; Booker, G. W.; Abell, A. D., Improved Synthesis of Biotinyl-5'-AMP: Implications for Antibacterial Discovery. *ACS Med. Chem. Lett.* **2015**, 6 (2), 216-20.
47. Feng, J.; Paparella, A. S.; Tieu, W.; Heim, D.; Clark, S.; Hayes, A.; Booker, G. W.; Polyak, S. W.; Abell, A. D., New Series of BPL Inhibitors To Probe the Ribose-Binding Pocket of *Staphylococcus aureus* Biotin Protein Ligase. *ACS Med. Chem. Lett.* **2016**, 7 (12), 1068-1072.
48. Tieu, W.; da Costa, T. P. S.; Yap, M. Y.; Keeling, K. L.; Wilce, M. C. J.; Wallace, J. C.; Booker, G. W.; Polyak, S. W.; Abell, A. D., Optimising in situ click chemistry: the screening and identification of biotin protein ligase inhibitors. *Chem. Sci.* **2013**, 4 (9), 3533-3537.
49. Tieu, W.; Jarrad, A. M.; Paparella, A. S.; Keeling, K. A.; Soares da Costa, T. P.; Wallace, J. C.; Booker, G. W.; Polyak, S. W.; Abell, A. D., Heterocyclic acyl-phosphate bioisostere-based inhibitors of *Staphylococcus aureus* biotin protein ligase. *Bioorg. Med. Chem. Lett.* **2014**, 24 (19), 4689-93.
50. Brown, P. H.; Cronan, J. E.; Grøtli, M.; Beckett, D., The Biotin Repressor: Modulation of Allostery by Corepressor Analogs. *Journal of Molecular Biology* **2004**, 337 (4), 857-869.
51. Brown, P. H.; Beckett, D., Use of Binding Enthalpy To Drive an Allosteric Transition†. *Biochemistry* **2005**, 44 (8), 3112-3121.
52. Huang, W. J.; Jia, J.; Gibson, K. J.; Taylor, W. S.; Rendina, A. R.; Schneider, G.; Lindqvist, Y., Mechanism of an Atp-Dependent Carboxylase, Dethiobiotin

- Synthetase, Based on Crystallographic Studies of Complexes with Substrates and a Reaction Intermediate. *Biochemistry* **1995**, *34* (35), 10985-10995.
53. Gibson, K. J.; Lorimer, G. H.; Rendina, A. R.; Taylor, W. S.; Cohen, G.; Gatenby, A. A.; Payne, W. G.; Roe, D. C.; Lockett, B. A.; Nudelman, A.; Marcovici, D.; Nachum, A.; Wexler, B. A.; Marsilii, E. L.; Turner, I. M.; Howe, L. D.; Kalbach, C. E.; Chi, H. J., Dethiobiotin Synthetase - the Carbonylation of 7,8-Diaminononanoic Acid Proceeds Regiospecifically Via the N7-Carbamate. *Biochemistry* **1995**, *34* (35), 10976-10984.
54. Kack, H.; Gibson, K. J.; Lindqvist, Y.; Schneider, G., Snapshot of a phosphorylated substrate intermediate by kinetic crystallography. *Proc. Natl. Acad. Sci. U. S. A.* **1998**, *95* (10), 5495-500.
55. Alexeev, D.; Baxter, R. L.; Sawyer, L., Mechanistic Implications and Family Relationships from the Structure of Dethiobiotin Synthetase. *Structure* **1994**, *2* (11), 1061-1072.
56. Huang, W. J.; Lindqvist, Y.; Schneider, G.; Gibson, K. J.; Flint, D.; Lorimer, G., Crystal-Structure of an Atp-Dependent Carboxylase, Dethiobiotin Synthetase, at 1.65-Angstrom Resolution. *Structure* **1994**, *2* (5), 407-414.
57. Sandalova, T.; Schneider, G.; Kack, H.; Lindqvist, Y., Structure of dethiobiotin synthetase at 0.97 angstrom resolution. *Acta Crystallogr., Sect. D: Biol. Crystallogr.* **1999**, *55*, 610-624.
58. Dey, S.; Lane, J. M.; Lee, R. E.; Rubin, E. J.; Sacchettini, J. C., Structural Characterization of the Mycobacterium tuberculosis Biotin Biosynthesis Enzymes 7,8-Diaminopelargonic Acid Synthase and Dethiobiotin Synthetase. *Biochemistry* **2010**, *49* (31), 6746-6760.
59. Porebski, P. J.; Klimecka, M.; Chruszcz, M.; Nicholls, R. A.; Murzyn, K.; Cuff, M. E.; Xu, X. H.; Cymborowski, M.; Murshudov, G. N.; Savchenko, A.; Edwards, A.; Minor, W., Structural characterization of Helicobacter pylori dethiobiotin synthetase reveals differences between family members. *FEBS J.* **2012**, *279* (6), 1093-1105.
60. Salaemae, W.; Yap, M. Y.; Wegener, K. L.; Booker, G. W.; Wilce, M. C. J.; Polyak, S. W., Nucleotide triphosphate promiscuity in *Mycobacterium tuberculosis* dethiobiotin synthetase. *Tuberculosis* **2015**, *95* (3), 259-266.

-
61. Thompson, A. P.; Salaemae, W.; Pederick, J. L.; Abell, A. D.; Booker, G. W.; Bruning, J. B.; Wegener, K. L.; Polyak, S. W., Mycobacterium tuberculosis Dethiobiotin Synthetase Facilitates Nucleoside Triphosphate Promiscuity through Alternate Binding Modes. *Acs Catalysis* **2018**, *8* (11), 10774-10783.
 62. Betts, J. C.; Lukey, P. T.; Robb, L. C.; McAdam, R. A.; Duncan, K., Evaluation of a nutrient starvation model of Mycobacterium tuberculosis persistence by gene and protein expression profiling. *Mol. Microbiol.* **2002**, *43* (3), 717-731.

Chapter Two

2.1 Introduction

As discussed in chapter one, biotin protein ligase (BPL) is the sole enzyme responsible for the activation of biotin-dependent enzymes (ACC and PC) through protein biotinylation. BPL catalyses protein biotinylation using a two-step ordered reaction requiring biotin **1.05** and ATP to produce an adenylated reaction intermediate, biotinyl-5'-AMP **1.06**. The BPL active site consists of two major pockets including biotin binding pocket and ATP binding pocket. The reaction intermediate **1.06** adopts a tight V shape geometry to allow binding to the biotin and ATP pockets.

Replacement of the labile phosphoanhydride linker in biotinyl-5'-AMP **1.06** with a non-hydrolysable 1,4-disubstituted-1,2,3-triazole heterocycle has led to the development of potent BPL inhibitors with excellent selectivity over the human isozyme. However, antibacterial activity is not sufficient to determine a minimal inhibitory concentration (MIC). This chapter discusses chemical modifications carried out at the C5 position on the 1,2,3-triazole linker to increase antimicrobial activities against *S. aureus*.

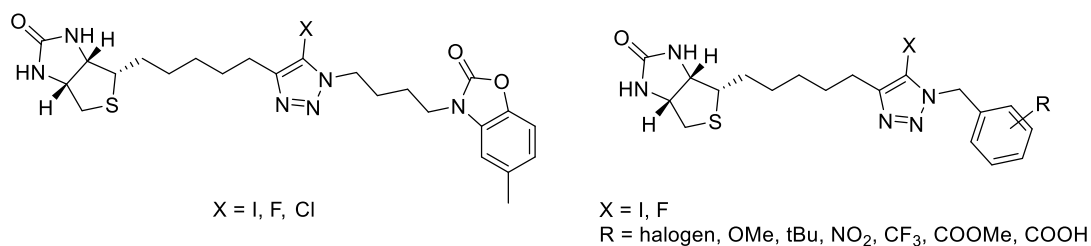


Figure 2.1. Chemical structures of BPL inhibitors in Chapter 2.

Statement of Authorship

Title of Paper	Halogenation of Biotin Protein Ligase Inhibitors Improves Whole Cell Activity against <i>Staphylococcus aureus</i>		
Publication Status	<input checked="" type="checkbox"/> Published	<input type="checkbox"/> Accepted for Publication	
	<input type="checkbox"/> Submitted for Publication	<input type="checkbox"/> Unpublished and Unsubmitted work written in manuscript style	
Publication Details	Paparella, A. S.; Lee, K. J.; Hayes, A. J.; Feng, J. G.; Feng, Z. K.; Cini, D.; Deshmukh, S.; Booker, G. W.; Wilce, M. C. J.; Polyak, S. W.; Abell, A. D., Halogenation of Biotin Protein Ligase Inhibitors Improves Whole Cell Activity against <i>Staphylococcus aureus</i> . <i>ACS infectious diseases</i> 2018, 4 (2), 175-184.		

Principal Author

Name of Principal Author (Candidate)	Kwang Jun Lee		
Contribution to the Paper	Performed synthesis and characterisation of analogues, analysis of data, provided advanced draft of manuscript and subsequent revisions.		
Overall percentage (%)	40%		
Certification:	This paper reports on original research I conducted during the period of my Higher Degree by Research candidature and is not subject to any obligations or contractual agreements with a third party that would constrain its inclusion in this thesis. I am the primary author of this paper.		
Signature		Date	5/7/2019

Co-Author Contributions

By signing the Statement of Authorship, each author certifies that:

- i. the candidate's stated contribution to the publication is accurate (as detailed above);
- ii. permission is granted for the candidate to include the publication in the thesis; and
- iii. the sum of all co-author contributions is equal to 100% less the candidate's stated contribution.

Name of Co-Author	Ashleigh S. Paparella		
Contribution to the Paper	Performed <i>in vitro</i> biochemical assays, surface plasmon experiments and analysis of assay results, co-author of the manuscript.		
Signature		Date	7/1/19

Name of Co-Author	Andrew J. Hayes		
Contribution to the Paper	Performed <i>in vitro</i> biochemical assays, cytotoxicity assays, antibacterial susceptibility assays and analysis of assay results, co-author of the manuscript.		
Signature		Date	01/07/2019

Name of Co-Author	Jiage Feng		
Contribution to the Paper	Performed synthesis and characterisation of compounds 4a-d.		
Signature		Date	2019. 7. 1

Name of Co-Author	Zikai Feng		
Contribution to the Paper	Performed <i>in vitro</i> biochemical assays and analysis of assay results.		
Signature		Date	26/7/2019

Name of Co-Author	Danielle Cini		
Contribution to the Paper	Performed crystallographic experiments including structure solving and interpretation.		
Signature		Date	11/7/19

Name of Co-Author	Sonali Deshmukh		
Contribution to the Paper	Performed <i>in vitro</i> biochemical assays and analysis of assay results.		
Signature		Date	26/7/2019

Name of Co-Author	Grant W. Booker		
Contribution to the Paper	Supervised the biological aspects of the project and revised manuscript.		
Signature		Date	1/7/2019,

Name of Co-Author	Matthew C. J. Wilce		
Contribution to the Paper	Supervised crystallographic experiments and revised manuscript.		
Signature		Date	03/07/2019

Name of Co-Author	Steven W. Polyak		
Contribution to the Paper	Worked closely with the principle authors to write the manuscript and supervised the biological testing. A corresponding author.		
Signature		Date	28/6/2019.

Name of Co-Author	Andrew D. Abell		
Contribution to the Paper	Supervised the medicinal chemistry of the project and revised manuscript. A corresponding author.		
Signature		Date	26/7/2019

Halogenation of Biotin Protein Ligase Inhibitors Improves Whole Cell Activity against *Staphylococcus aureus*

Ashleigh S. Paparella,^{†,||,¶} Kwang Jun Lee,^{‡,||} Andrew J. Hayes,^{†,||} Jiage Feng,^{‡,#} Zikai Feng,[†] Danielle Cini,[§] Sonali Deshmukh,[†] Grant W. Booker,[†] Matthew C. J. Wilce,[§] Steven W. Polyak,^{*,‡,¶} and Andrew D. Abell^{*,‡,¶,||}

[†]Department of Molecular and Cellular Biology, University of Adelaide, North Tce, Adelaide, South Australia 5005, Australia

[‡]Department of Chemistry, University of Adelaide, North Tce, Adelaide, South Australia 5005, Australia

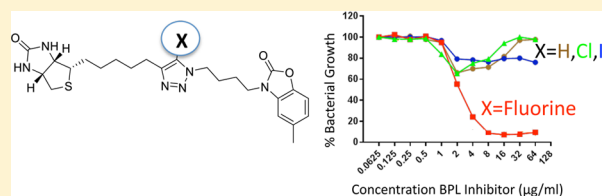
[§]School of Biomedical Science, Monash University, Wellington Road, Clayton, Victoria 3800, Australia

[#]Centre for Nanoscale BioPhotonics (CNBP), University of Adelaide, North Tce, Adelaide, South Australia 5005, Australia

Supporting Information

ABSTRACT: We report the synthesis and evaluation of 5-halogenated-1,2,3-triazoles as inhibitors of biotin protein ligase from *Staphylococcus aureus*. The halogenated compounds exhibit significantly improved antibacterial activity over their nonhalogenated counterparts. Importantly, the 5-fluoro-1,2,3-triazole compound **4c** displays antibacterial activity against *S. aureus* ATCC49775 with a minimum inhibitory concentration (MIC) of 8 $\mu\text{g}/\text{mL}$.

KEYWORDS: antibiotic, *Staphylococcus aureus*, enzyme inhibitor, biotin protein ligase



There is an urgent need for new therapeutics to combat antibiotic resistant bacteria.¹ Target based approaches to antibiotic discovery have been somewhat limited by poor translation of compounds with potent *in vitro* activity into bioactives with whole cell antibacterial activity.^{2–4} This is often due to an inability of compounds to permeate into the cell and access intracellular drug targets. One approach to improve whole cell activity is through halogenation of compounds that are otherwise cell impermeable.^{5,6} For example, fluoroquinolones display ~ 100 -fold improved whole cell potency compared to their protoanalogues.^{7,8} Other clinically relevant antibiotics that possess a halogen include chloramphenicol, chlortetracycline, and the glycopeptides vancomycin and teicoplanin. Fluorination presents as a particularly attractive modification to improve binding affinity, membrane permeability, and metabolic stability,⁹ with 20% of available drugs being fluorinated.¹⁰

Biotin protein ligase (BPL) is a promising drug target that has been the subject of antibiotic drug discovery programs by several groups.^{2,11–19} BPL serves as the sole enzyme responsible for the biotinylation, and subsequent activation, of biotin-dependent enzymes. The clinically important bacterial pathogen *Staphylococcus aureus* possesses two such biotin-dependent enzymes, namely, acetyl-CoA carboxylase and pyruvate carboxylase, which catalyze key reactions in the important metabolic pathways of fatty acid biosynthesis and gluconeogenesis, respectively.²⁰ BPL catalyzes protein biotinylation through ligation of biotin **1** and ATP to form biotinyl-5'-AMP, **2** (see Figure 1). Replacement of the labile phosphoanhydride linker in **2** with more stable bioisosteres has

produced inhibitors of BPL from bacterial pathogens such as *S. aureus*,^{16,17} *Mycobacterium tuberculosis*,^{18,19} and *Escherichia coli*.²¹ This work has recently been reviewed.^{20,22} However, there are precious few examples of BPL inhibitors with whole cell antistaphylococcal activity. The archetypal BPL inhibitor biotinol-5'-AMP (see **3**, Figure 2) is known to reduce the growth of *S. aureus* and *M. tuberculosis* with minimal inhibitory concentrations (MICs) of 2 and 2.5 $\mu\text{g}/\text{mL}$, respectively,¹⁷ thereby providing *in vitro* proof of concept that pharmacological inhibition of BPL is a strategy for new antibacterials. Recently, we reported 1,4-disubstituted-1,2,3-triazoles as novel BPL inhibitors that selectively target BPL from *S. aureus* over the human homologue.^{11,12,15} While this biotin triazole class exhibits *in vitro* potency and selectivity over the human homologue, it displays poor whole cell activity.¹¹ For example, **4a** (see Figure 3) only reduces the growth of *S. aureus* ATCC 49775 by 60% of nontreated controls at 8 $\mu\text{g}/\text{mL}$,¹¹ a level significantly below that required in a preclinical candidate. Attempts to improve antibacterial potency by shortening and simplifying the 1,4-disubstituted-1,2,3-triazole pharmacophore (see **5a–k**, **5m**, **5o**, Figure 3)¹² have had modest success. Here, we present halogenation of C5 on the 1,2,3-triazole of **4a** and **5a–o** as a route toward improved antistaphylococcal activity. The mechanism of action for the most potent antibacterials was demonstrated to be consistent with the inhibition of BPL through microbiological, biochemical, and structural studies.

Received: August 23, 2017

Published: November 13, 2017

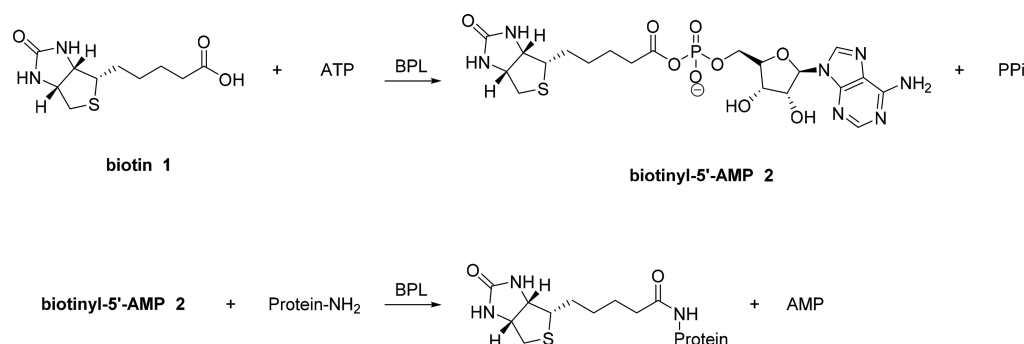


Figure 1. Reaction mechanism of biotin protein ligase.

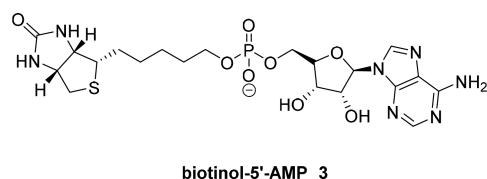


Figure 2. Chemical structure of biotinol-5'-AMP.

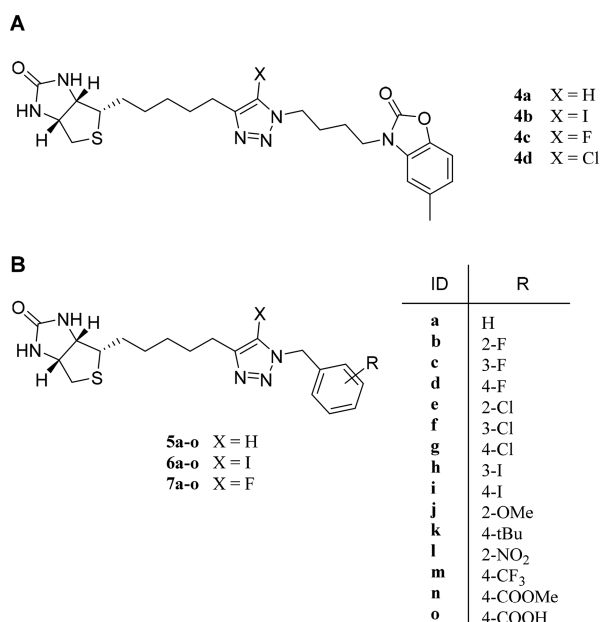


Figure 3. Chemical structure of BPL inhibitors. (A) Benzoxazolone triazole series. (B) Benzyl triazole series.

RESULTS AND DISCUSSION

Series 1: Compounds 4a–d (Figure 3A). The synthesis of the 1,4-disubstituted-1,2,3-triazole 4a¹¹ and the 1,4,5-trisubstituted-1,2,3-triazoles 4b–d was carried out as summarized in Scheme 1. Biotin acetylene 8¹¹ was first reacted with CuI and *N*-iodomorpholine to give biotin 1-iodoacetylene 10. Biotin 1-iodoacetylene 10 was then reacted with azide 9¹¹ in the presence of CuI as a catalyst and TEA as an amine ligand to afford 5-iodo-1,2,3-triazole 4b in 36% yield.²³ Iodinated 4b was subsequently converted to fluorinated 4c and chlorinated 4d by halogen exchange reaction based on optimized conditions reported by Worrell et al.²⁴ In particular, iodide 4b was treated with 5 equiv of either potassium fluoride or potassium chloride in a MeCN/H₂O (1:1) mixture in a microwave reactor, at 180

°C, to give 5-fluoro-1,2,3-triazole 4c and 5-chloro-1,2,3-triazole 4d in 89% and 80% yields, respectively.

Fluorination of Compound 4a Improved Whole Cell Activity without Cytotoxic Effects. The antibacterial potency of 4a–d was determined against *S. aureus* clinical isolate ATCC 49775 (Figure 4A).¹⁴ The optical density of bacterial cultures treated for 24 h with varying concentrations of 4a–d was measured spectrophotometrically at 620 nm. As previously reported,¹¹ parent compound 4a only reduced the optical density of the culture by ~40% of the nontreated control. This low level of activity is below the response required to determine an MIC (i.e., >90% inhibited growth). In contrast, 5-fluoro analogue 4c was bioactive against *S. aureus* and inhibited growth of the bacteria with an MIC of 8 μg/mL (16 μM). This represents the first example of a 1,2,3-triazole with potent antibacterial activity. Interestingly, the selection of halogen is critical with 5-iodo (4b) and the 5-chloro (4d) analogues having the same poor antistaphylococcal activity as parent derivative 4a. The mechanism of antibacterial action for 4c was determined to be due to the inhibition of BPL by performing antibacterial susceptibility assays with *S. aureus* RN4220 engineered to recombinantly overproduce the BPL target.¹² A concomitant decrease in whole cell activity is expected upon overexpression of a drug target, should the mechanism of action be directly through that target.^{12,18} This was first verified using the archetypical BPL inhibitor biotinol-5'-AMP 3, where an 8-fold increase in the MIC was observed as a result of BPL overexpression in *S. aureus* RN4220 (Figure S1). Consistent with 4c binding directly to the BPL target, overexpression of the enzyme significantly reduced the antibacterial potency of the compound (Figure 4B). Finally, cytotoxicity assays were performed with HepG2 liver cells on inhibitors 4b–d. No cytotoxicity was measured at the highest concentration tested (approximately 80 μM) (Table 1) demonstrating that inhibitors 4a–d have the same high therapeutic index of other reported biotin substituted 1,2,3-triazoles.^{11,12} Together, these results support the hypothesis that halogenation of BPL inhibitors can improve whole cell bioactivity against *S. aureus* without adverse *in vitro* cytotoxicity.

Antibacterial Activity Was Not a Result of Increased Inhibitory Activity in Compound 4c. The improved whole cell activity observed for 5-fluoro 4c over the nonhalogenated protoanalogue 4a was not the result of strengthened interactions between the inhibitor and BPL. This was established through *in vitro* binding and enzyme assays (Table 1). Surface plasmon resonance (SPR) studies on 4a–d with SaBPL immobilized onto a sensor chip^{11,14} revealed rapid association and dissociation rates that were unable to be quantified (Figure S2). Accordingly, the equilibrium dissocia-

Scheme 1. Synthesis of Benzoxazolone Triazole Series

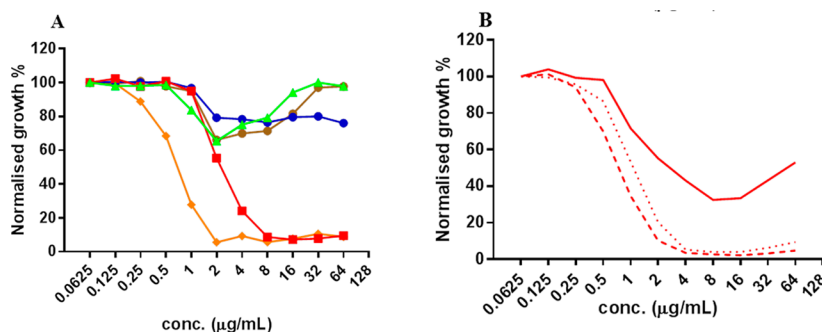
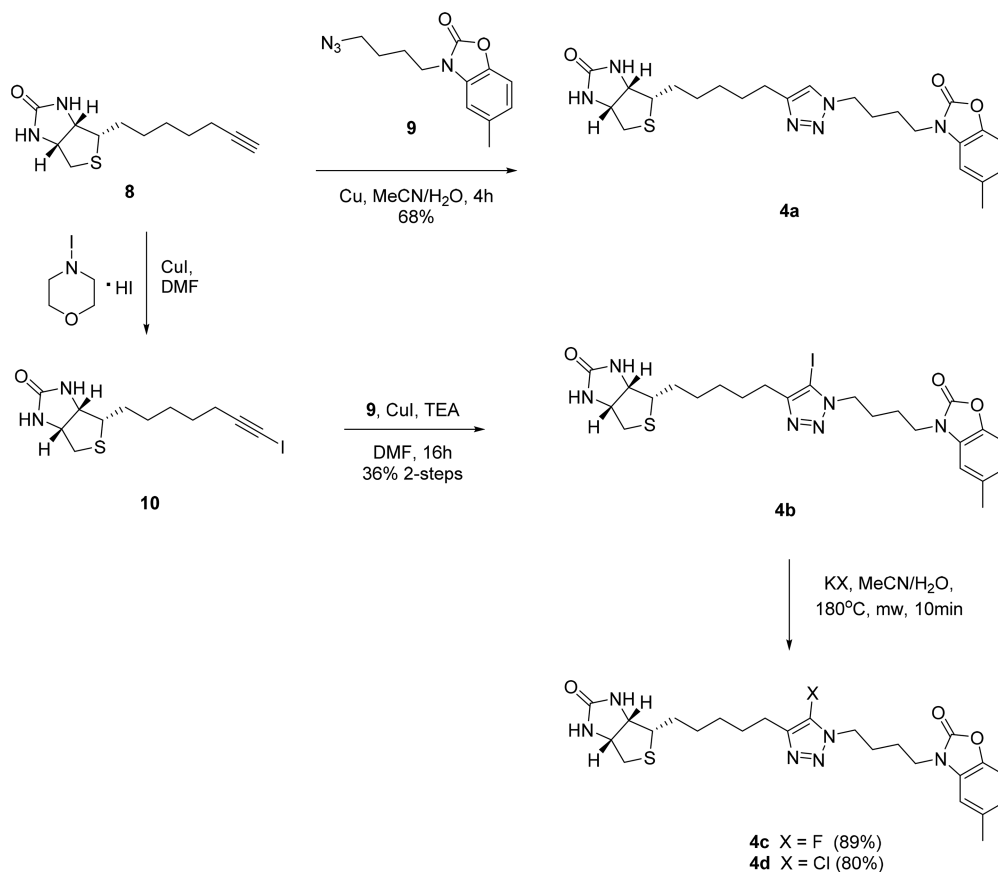


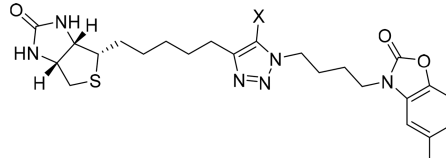
Figure 4. Inhibition of *S. aureus* growth *in vitro*. (A) Compounds 3 (orange), 4a (brown), 4b (blue), 4c (red), and 4d (green) were tested against *S. aureus* strain ATCC 49775. (B) Compound 4c was tested for antibacterial susceptibility against *S. aureus* RN4220 in the presence and absence of overexpressed SaBPL. *S. aureus* RN4220 harboring the SaBPL expression plasmid pCN51-BPL (solid line), the parent vector pCN51 (dashed line), or no plasmid (dotted line) are shown.

tion constants (K_D) were measured using a steady state affinity model. No significant differences in affinity were measured between 4a ($K_D = 8.4 \mu\text{M}$) and the halogenated analogues 4b–d (Table 1). The indistinguishable and fast dissociation rates observed for all inhibitors also ruled out increased occupancy of 4c on the BPL target (a function of slow dissociation kinetics) as a possible mechanism for increased whole cell potency. Similarly, biochemical analysis using an *in vitro* protein biotinylation assay demonstrated 4a–d were equipotent as BPL inhibitors. The enzymatic incorporation of radiolabeled biotin onto an acceptor protein (the 90 amino acid biotin-acceptor domain from pyruvate carboxylase (SaPC90)) was assayed using recombinant BPLs from *S. aureus* and *Homo sapiens*. Inhibition of BPL activity was then measured in the

presence of varying concentrations of inhibitors 4a–d. The biochemical assays demonstrated similar activities for parent 4a ($K_i = 0.23 \mu\text{M}$) and the halogenated derivatives 4b–d against SaBPL (Table 1). All compounds tested were inactive against human BPL ($K_i > 10 \mu\text{M}$) highlighting that halogenation does not adversely affect selective binding to the bacterial enzyme over the human homologue. Together, the SPR binding and biochemical assays demonstrate that the fluorination, as in 4c, plays no additional role in the inhibitor binding to BPL.

A crystal structure of 4c in complex with SaBPL was determined to define its mechanism of binding (Figure 5). The resulting data was compared to the published structures of SaBPL in complex with biotin 1, biotinyl-5'-AMP 2, and the parent compound 4a (PDB 3 V7S)¹¹ (Figure 5A). Both 4a and

Table 1. Binding Affinities Derived from SPR Analysis, Inhibition, and Cytotoxic Data for Compounds 4a–d



ID	X	K_D SaBPL (μM)	K_i SaBPL (μM) ^a	K_i HsBPL (μM)	MIC ATCC49775 (μM)	Cytotox HepG2 ($\mu\text{g}/\text{mL}$)
4a	H	8.4 ± 1.0	0.23 ± 0.01	>10	>100	>80
4b	I	3.8 ± 1.5	0.41 ± 0.02	>10	>100	>80
4c	F	7.1 ± 3.4	0.42 ± 0.05	>10	16	>80
4d	Cl	10.1 ± 1.8	0.9 ± 0.11	>10	>100	>80

^aInhibition constants (K_i) for the competitive inhibitors of biotin were derived from IC_{50} values using the K_M for biotin, as previously described.²⁵

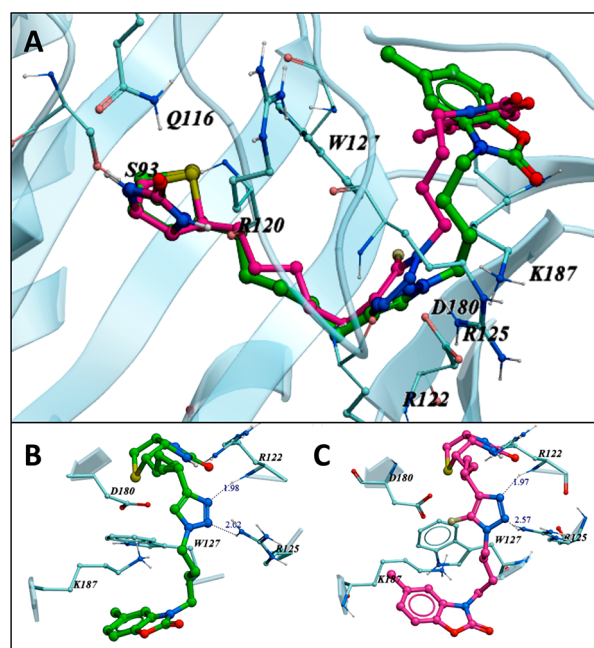


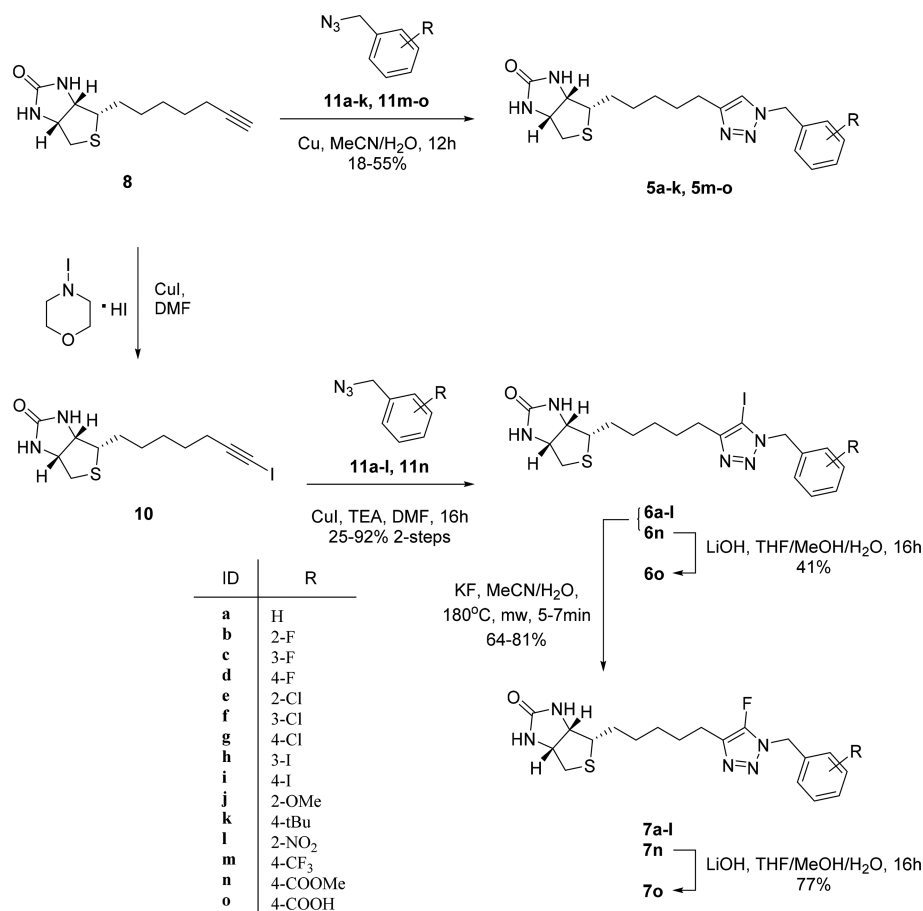
Figure 5. Comparison of cocrystal structures. (A) 4a (green) and 4c (magenta) were superimposed to reveal the different binding pose of the benzoxazolone ring. (B) Binding pocket of SaBPL in complex with 4a (PDB 3V7S). (C) Binding pocket of SaBPL in complex with 4c. Amino acids that encompass the triazole-binding site are shown. Dashed lines represent hydrogen bonds.

4c adopted similar binding modes with the biotinyl and benzoxazolone moieties occupying the biotin and nucleotide pockets, as expected. Consistent with our earlier *in vitro* assay results, the fluorine of 4c does not directly contribute any new bonding interactions with SaBPL compared with 4a. Previous crystallography studies on SaBPL in complex with 1 and 2 have established that conformational changes accompany ligand binding and these are necessary for inhibitor binding. The same conformational changes were observed for both 4a and 4c. In particular, residues T177–K131 undergo a disordered to ordered transition when in complex with biotin.^{11,26} This feature, known as the biotin-binding loop, encases the active site to prevent ligand dissociation and positions the side chain of W127 in the active site such that it can participate in a π – π stacking interaction with the adenyl group of ATP. Both 4a and 4c induced these same disordered-to-ordered conformational changes resulting in ordering of the biotin-binding loop. Hydrogen bonding between the triazole heterocycle and amino acids in the biotin-binding loop are apparent in both structures,

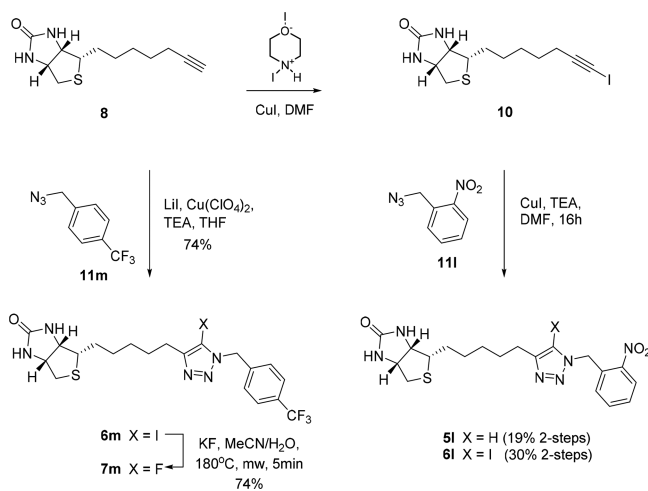
namely, between triazole N2 and the side chain of R125 and triazole N3 with R122 (Figure 5B,C). Further interactions were observed between the triazole and side chains of D180 and K187. The main differences between the 4a and 4c structures were apparent with the side chain of W127. For SaBPL in complex with 4a, the indole ring of W127 adopted the same conformation as observed in the costructure with biotin 1 and biotinyl-5'-AMP 2 that facilitates ATP binding. In the cocomplex with 4a, the conformation of the indole side chain defines a T-shaped π interaction with the triazole heterocycle. However, for 4c, the side chain of W127 was tilted, thereby disrupting the protein–triazole interaction. This was offset by a new T-shaped π interaction between W127 and the benzoxazolone group (Figure S3). The volume and area of the binding pocket of SaBPL were also increased as 5-fluoro triazole 4c was bound into the binding site of the enzyme (Table S1). These data suggest an induced fit model of ligand binding occurs involving the biotin-binding loop, and the BPL active site has enough flexibility to accommodate the C5 halogen-substituted biotinyl 1,2,3-triazole inhibitors.

Series 2: Compounds 5a–o, 6a–o, and 7a–o (Figure 3B). A second series (6a–o, 7a–o) was investigated to determine if the improved whole cell activity of 5-fluoro triazole 4c could be replicated in the truncated benzyl-biotin triazole BPL inhibitors.¹² The synthesis of 1-benzyl-5-*proto*-1,2,3-triazoles 5a–o,¹² 1-benzyl-5-iodo-1,2,3-triazoles 6a–o, and 1-benzyl-5-fluoro-1,2,3-triazoles 7a–o was accomplished as outlined in Schemes 2 and 3. Biotin 1-iodoacetylene 10 was reacted with benzyl azides 11a–l and 11n to yield 5-iodo-1,2,3-triazoles 6a–l according to the procedure described for the synthesis of compound 4b (Scheme 2). This two-step reaction required preformation and isolation of 1-iodoacetylene 10, and in some instances, the 5-*proto* triazole was obtained as a side product. For example, 5-*proto* triazole compound 5l was isolated as a side product along with 5-iodo triazole compound 6l after the two-step reaction (Scheme 3). Acetylene 8¹¹ was treated with LiI, Cu(ClO₄)₂, and TEA in THF to give 1-iodo acetylene 10 *in situ* to which 4-trifluoromethylbenzyl azide was added to give 5-iodo-1,2,3-triazole 6m to improve the synthetic method (Scheme 3). The 5-fluoro-1,2,3-triazoles 7a–n were prepared as per 4c (Scheme 1). MeCN/H₂O (1:1) was added to a mixture of potassium fluoride and 5-iodo-1,2,3-triazoles 6a–n, and the solution was reacted in a microwave for 5 min to give the corresponding 5-fluoro-triazoles 7a–n in 64–81% yields. Carboxylic acids 6o and 7o were prepared by hydrolysis using LiOH from the corresponding methyl esters 6n and 7n (Scheme 2).

Scheme 2. Synthesis of Benzyl Triazole Series



Scheme 3. Synthesis of Compounds 5l, 6l, 6m, and 7m



X-ray Structure of 5o in Complex with SaBPL. The truncated benzyl-biotin triazole BPL inhibitors 5a–o were designed for improved bioactivity with simpler structures than 4a–d. *In silico* docking experiments supported a model where the functionalized benzyl groups 11a–o, appended onto the biotin-triazole pharmacophore (Figure 2B), bound within the ribose-binding site of SaBPL.¹² The ribose-binding pocket provides multiple sites for hydrogen bonding interactions, specifically through the side chains of K187 and R227 as well as the peptide backbone atoms from R122, H126, and S125

(Figure 6A).²⁶ A crystal structure of SaBPL in complex with 5o was solved to define its mechanism of binding of the inhibitor (Figure 6B). Electron density was observed for amino acids T177–K131 in the biotin-binding loop, consistent with the inhibitor inducing the same disordered to ordered transition described earlier. The biotinyl moiety of 5o occupied the biotin pocket of SaBPL as expected, thus placing the inhibitor in the active site of the enzyme. Hydrogen bonding interactions between the N2 and N3 of the triazole and the side chains of R125 and R122, respectively, in the biotin-binding loop further stabilized the interaction. A comparison between the crystal structures of SaBPL in complex with biotinyl-5'-AMP 2²⁶ and 5o clearly demonstrated a common binding site for the ribosyl of 2 and the benzoic acid of 5o. Noteworthy was the absence of hydrogen bonds between the carboxylate of 5o and BPL target, implying that the affinity for the enzyme–ligand interaction is driven primarily by the biotinyl and 1,2,3-triazole moieties. Together, the X-ray and docking studies suggest that the functionalized benzyl moieties for 5a–o, 6a–o, and 7a–o can be accommodated in the ribose pocket of SaBPL.

Bioassays of 5a–o, 6a–o, and 7a–o. The antistaphylococcal potency of 5a–o, 6a–o, and 7a–o was measured using antibacterial susceptibility assays upon *S. aureus* RN4220. *S. aureus* RN4220 was employed for microbiological analysis as our earlier experiments with 4a–d revealed this strain to be more sensitive to BPL inhibitors than *S. aureus* ATCC 49775. This was exemplified with the archetypical BPL inhibitor biotinyl-5-AMP 3 that was 32-fold more active against RN4220 than ATCC 49775. In this series, 15 analogues halogenated at

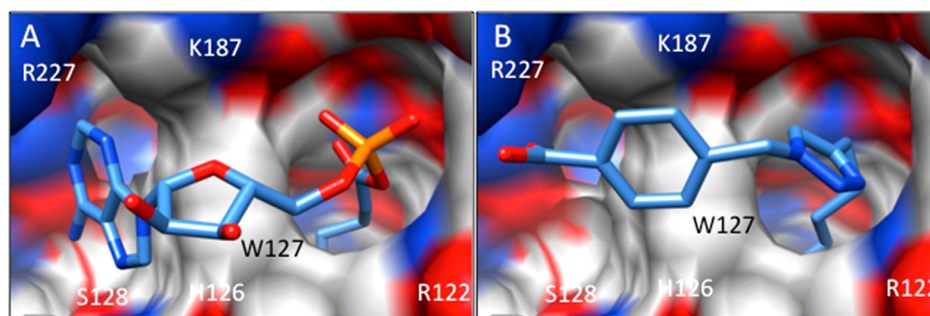


Figure 6. Comparison of crystal structures. Crystal structures of SaBPL in complex with (Figure 6A) the reaction intermediate biotinyl-5'-AMP 2 [PDB 3RIR]²⁶ and (Figure 6B) benzyl biotin triazole inhibitor **5o**. Amino acids that encompass the ribosyl moiety of **2** are shown. The ribosyl group of **2** and benzoic acid of **5o** both occupy a common binding site.

C5 on the 1,2,3-triazole were more potent antistaphylococcal agents than their nonhalogenated counterparts (Table 2). There was no clear preference for the selection of 5-halogen, with nine iodo (**6a**, **6b**, **6f–h**, **6j–m**) and six fluoro (**7a**, **7e**, **7f**, **7h**, **7j**, **7m**) compounds having improved whole cell activity over their prototypical parent. The most potent antibacterials (MIC of 4 $\mu\text{g}/\text{mL}$) in the series were all appended with a halogenated benzyl moiety. Both 5-iodo **6h** and 5-fluoro **7h** contain a 3-iodo benzyl, with 5-iodo **6f** and 5-iodo **6m** having 3-chloro and 4-CF₃ substitutions, respectively.

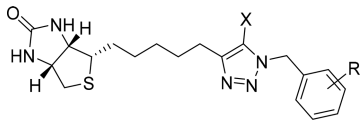
The MIC values obtained from the microbiological analysis were then compared with inhibition constants (K_i) obtained from *in vitro* protein biotinylation assays to investigate correlations between whole cell activity and *in vitro* inhibition of SaBPL (Table 2, Figure S4). For **6a–o** and **7a–o**, a modified BPL enzyme assay was developed as radiolabeled biotin could not be sourced commercially. Protein biotinylation was performed essentially as previously described except a GST tagged biotin domain (GST-SaPC90) was employed as the biotin acceptor protein. Biotinylated protein was captured on white 96-well plates coated with anti-GST antibody and quantitated using Europium-conjugated streptavidin and time-resolved fluorescence. This eliminated the need for costly radiolabeled biotin, while retaining the ability to accurately characterize inhibitory potency. In support, both assays gave comparable K_i values for the archetypical BPL inhibitor **3** (Table S2). Concomitant improvements of both *in vitro* inhibition and whole cell bioactivity due to halogenation of C5 on the 1,2,3-triazole were observed with five examples in this series, namely, **6/7b**, **6/7e**, **6/7h**, **6/7l**, and **6m**. In each case, the nonhalogenated parent compounds were inactive in both the biochemical ($K_i > 10 \mu\text{M}$) and microbiological (MIC $> 64 \mu\text{g}/\text{mL}$) testing but halogenation greatly improved potency in both assays. Three of the most potent antistaphylococcal compounds described above (**6h**, **7h**, and **6m**) belong in this category, where improved biochemical activity translated to increased microbiological potency. In contrast, 5-iodo analogues **6f**, **6g**, **6j**, and **6k** showed increased whole cell activity despite only modest changes in biochemical potency due to 5-halogenation. This was exemplified by the potent antibacterial **6g** (K_i 0.65 μM , MIC 16 $\mu\text{g}/\text{mL}$), where 5-iodination reduced the K_i by only 1.7-fold (**5g** 1.1 μM) but greatly improved antistaphylococci activity (**5g** inactive vs *S. aureus* RN4220). Importantly, all compounds in this series with antibacterial activity also inhibited BPL *in vitro*, and there were no examples where reduced whole cell activity was observed as a result of halogenation. This was consistent with their antibacterial mechanism of action being through the

inhibition of BPL. Furthermore, we confirmed that the antimicrobial activity was indeed due to the inhibition of SaBPL. Inhibitors **6f**, **7h**, and **7f** were reassayed for antistaphylococcal activity using the BPL overexpression strain of *S. aureus* described earlier. The growth of bacteria in culture media containing 32 $\mu\text{g}/\text{mL}$ of inhibitor was monitored over 20 h. Growth was observed for those bacteria harboring the SaBPL overexpression plasmid pCNS1-BPL, consistent with these compounds engaging the BPL target inside the bacteria (Figure 7). In contrast, *S. aureus* devoid of the plasmid was highly sensitive to all three compounds and failed to grow. Together, these data demonstrate that C5-halogenation of a 1,2,3-triazole is a valid approach for improving whole cell antibacterial activity of biotin-triazole BPL inhibitors.

CONCLUSION

Here, we employed halogenation as an approach for improving the whole cell activity of two series of BPL inhibitors. Both series contain a common biotin 1,2,3-triazole pharmacophore prepared by Huisgen cycloaddition using biotin triazole **8** and an appropriate azide functionalized partner. Our previous work has identified 1,2,3-triazole benzoxalone **4a** and the benzyl substituted 1,2,3-triazoles **5a–o** as inhibitors of BPL from the clinically important bacteria *S. aureus* but with poor antibacterial activity. The first proof of concept data demonstrating that halogenation of C5 of the 1,2,3-triazole could improve whole cell potency was obtained with the 5-fluoro analogue **4c** upon the clinical isolate *S. aureus* ATCC 49775 (MIC 8 $\mu\text{g}/\text{mL}$). Biochemical assays and biophysical binding analysis with SPR demonstrated that fluorinated triazole **4c** had no effect upon the interaction between enzyme and inhibitor compared with the nonhalogenated parent **4a**. The SPR data also argued against a role for the fluorine for increasing the occupancy of the inhibitor on the BPL target (a function of a slow dissociation rate) as indistinguishable fast on and off rates were observed for **4a–d**. We extended the halogenation study to the benzyl biotin-triazoles series of BPL inhibitors and identified **6f**, **7h**, and **7f** as potent antibacterials with confirmed mechanism of action through the inhibition of SaBPL. We propose increased cellular uptake leading to higher intracellular concentrations of inhibitor as the most likely mechanism for the observed improvements in whole cell activity observed here. In support, fluorination of drugs has been shown to enhance free energy of partitioning and improve passive diffusion across lipid membranes.^{5,6} As understanding compound entry into bacteria is one of the more challenging aspects for antibiotic discovery,^{2–4} a better understanding of

Table 2. Biochemical and Antistaphylococcal Properties of Compounds 5a–o, 6a–o, and 7a–o



ID	R	X	K_i SaBPL (μM)	MIC <i>S. aureus</i> RN4220 ($\mu\text{g/mL}$)
5a	H	H	N/D	>64 (>172)
6a		I	2.86 \pm 0.13	16 (32)
7a		F	2.50 \pm 0.13	64 (164)
5b	2-F	H	>10	>64 (>164)
6b		I	0.67 \pm 0.09	16 (31)
7b		F	1.32 \pm 0.26	>64 (>157)
5c	3-F	H	0.28 \pm 0.02	>64 (>164)
6c		I	0.54 \pm 0.08	>64 (>124)
7c		F	1.77 \pm 0.15	>64 (>157)
5d	4-F	H	0.6 \pm 0.1	>64 (>164)
6d		I	3.86 \pm 0.17	>64 (>124)
7d		F	4.16 \pm 0.29	>64 (>157)
5e	2-Cl	H	>10	>64 (>157)
6e		I	0.39 \pm 0.03	>64 (>120)
7e		F	1.15 \pm 0.07	8 (18)
5f	3-Cl	H	0.39 \pm 0.04	16 (39)
6f		I	0.48 \pm 0.03	4 (7)
7f		F	1.40 \pm 0.05	8 (18)
5g	4-Cl	H	1.1 \pm 0.07	>64 (>144)
6g		I	0.65 \pm 0.06	16 (30)
7g		F	3.26 \pm 0.13	>64 (>150)
5h	3-I	H	>10	>64 (128)
6h		I	0.38 \pm 0.01	4 (6)
7h		F	0.86 \pm 0.06	4 (7)
5i	4-I	H	0.56 \pm 0.06	>64 (>128)
6i		I	0.43 \pm 0.07	>64 (>102)
7i		F	1.02 \pm 0.25	>64 (>124)
5j	2-OMe	H	0.53 \pm 0.05	>64 (>159)
6j		I	0.80 \pm 0.03	16 (30)
7j		F	0.55 \pm 0.04	32 (76)
5k	4-tBu	H	1.22 \pm 0.07	>64 (>149)
6k		I	0.66 \pm 0.11	8 (14)
7k		F	0.73 \pm 0.05	>64 (>143)
5l	2-NO ₂	H	>10	>64 (>153)
6l		I	0.80 \pm 0.06	8 (14)
7l		F	0.78 \pm 0.07	>64 (>147)
5m	4-CF ₃	H	>10	>64 (>145)
6m		I	2.75 \pm 0.20	4 (7)
7m		F	N/D	8 (17)
5n	4-COOMe	H	N/D	>64 (>149)
6n		I	1.54 \pm 0.08	>64 (>113)
7n		F	>10	>64 (>140)
5o	4-COOH	H	0.67 \pm 0.06	>64 (>154)
6o		I	0.23 \pm 0.07	>64 (>118)
7o		F	>10	>64 (>148)

the mechanisms of membrane permeation can drive the development of new antibiotics. Structure activity relationship studies that specifically address compound uptake into bacteria, such as those as detailed here, are required to achieve this objective.

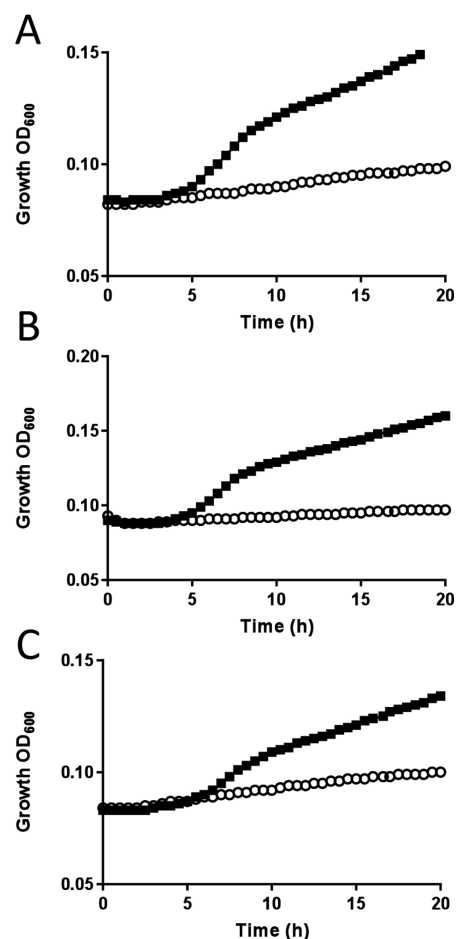


Figure 7. Mechanism of action studies. Growth curves for *S. aureus* RN4220 harboring the plasmid pCNS1 (open circles, negative control) or pCNS1-BPL (solid boxes, for recombinant BPL over-expression) are shown. Growth media contained 32 $\mu\text{g/mL}$ of (A) 6f, (B) 7h, or (C) 7f.

METHODS

Recombinant Protein Production and Assay. The cloning and purification of recombinant BPL from *Staphylococcus aureus* and *Homo sapiens* have been previously described.^{13,27} The inhibitory activity of compounds 4a–d and 5a–o was determined by measuring BPL activity in the presence of varying concentrations of compound. Quantification of BPL catalyzed ³H-biotin incorporation into the biotin domain substrate was performed as previously described.¹² Briefly, a reaction mixture was prepared containing 50 mM Tris HCl, pH 8.0, 3 mM ATP, 4.94 μM biotin, 0.06 μM ³H-biotin (American Radiolabeled Chemicals), 5.5 mM MgCl₂, 100 mM KCl, 0.1 μM DTT, and 10 μM biotin domain of *S. aureus* pyruvate carboxylase (SaPC90). All compounds were dissolved in DMSO and then diluted into the reaction buffer to give a final concentration of 4% DMSO. BPL reaction was initiated by the addition of enzyme to give final concentrations of 6.25 nM for SaBPL and 140 nM for HsBPL. After 10 min at 37 °C, 90 μL of stop buffer (110 mM EDTA and 50 mM Tris HCl, pH 8.0) was added to terminate the reaction and a 100 μL aliquot of the reaction mixture was added to the wells of 96-well HTS multiscreen plate containing an Immobilon-P (Merck Millipore) membrane that had been pretreated with 50 μL of 70% ethanol and 400 μL of Milli-Q H₂O, followed by 200 μL of

TBS. Quantitation of protein-bound radiolabeled biotin was determined by liquid scintillation counting. Compounds **6a–o** and **7a–o** were assayed essentially as described above with the following modifications. The assay medium contained 5 μM biotin (i.e., no ^3H biotin), and the SaPC90 was replaced with 25 μM SaPC90 fused to GST. The reaction was terminated with 80 μL of stop buffer, and three 20 μL aliquots were added to each well of a white Lumitrac-600 96-well plate (Greiner) that had been precoated with a polyclonal anti-GST antibody (Sigma-Aldrich, 50 μL per well, 1:40 000 dilution) at 4 $^\circ\text{C}$ overnight, followed by blocking for 2 h (200 μL per well) with 1% BSA in TBS at 37 $^\circ\text{C}$ and incubated at 37 $^\circ\text{C}$ for 1 h. The plate was then washed 5 times (200 μL per well) with TBS containing 0.1% Tween-20. Europium labeled streptavidin (PerkinElmer) was diluted to 0.1 $\mu\text{g}/\text{mL}$ in TBS containing 0.1% Tween-20. The streptavidin probe (50 μL per well) was incubated for 30 min at 37 $^\circ\text{C}$ followed by washing 5 times with TBS containing 0.1% Tween-20 followed by another 5 washes in sterile water. Enhancement solution (PerkinElmer, 50 μL) was added to each well and incubated for 10 min before reading the plate using a PerkinElmer Victor X5 multilabel reader (time-resolved fluorescence settings, 340 nm excitation, and 612 nm emission).²⁸

The IC_{50} value of each compound was determined from a dose–response curve by varying the concentration of inhibitor under the same enzyme concentration. The data was analyzed with GraphPad prism (version 6) using a nonlinear fit of \log_{10} [inhibitor] vs normalized response. The K_i , the absolute inhibition constant for a compound, was determined using eq 1:²⁵

$$K_i = \frac{\text{IC}_{50}}{1 + \frac{[S]}{K_M}} \quad (1)$$

where $[S]$ is the substrate concentration ($[\text{biotin}] = 5 \mu\text{M}$) and K_M is the affinity of the enzyme for biotin (*S. aureus* BPL = 1 μM ¹¹ and *H. sapiens* BPL = 1 μM ²⁹).

Surface Plasmon Resonance. SPR was performed using a Biacore S200 instrument (GE healthcare).^{11,14} *S. aureus* BPL was immobilized on a CMS sensor chip by standard amine coupling chemistry. The carboxymethyl groups on the chip were activated by the addition *N*-ethyl-*N*-(3-diethylamino-propyl) carbodiimide and *N*-hydroxysuccinimide. BPL (120 $\mu\text{g}/\text{mL}$) in 10 mM sodium acetate buffer (pH 5.8) was coupled onto the surface, and 50 mM Tris, pH 8.0, was injected to block any unreacted sites. Typically, 7000 resonance units of BPL were immobilized on the sensor chip. One channel was left blank which was subtracted from the sample channel to allow analysis methods to distinguish between actual and nonspecific binding. Experiments were conducted at 25 $^\circ\text{C}$ with a running buffer containing 10 mM HEPES, pH 7.4, 150 mM NaCl, 0.005% surfactant P20, and 5% (v/v) DMSO. For compounds that were poorly water-soluble, samples were initially dissolved in DMSO and diluted in running buffer so that the final concentration of DMSO was 5%. To correct for variations in DMSO concentration during the preparation of these compounds, a solvent correction curve was included in the analysis by preparing a series of test solutions between 4.5% and 5.8% DMSO. Binding experiments were performed by injecting the analyte solutions into the instrument across the sensor surface of all flow cells at a flow rate of 30 $\mu\text{L}/\text{min}$ with a contact time of 120 s followed by a dissociation time of 300 s. Zero concentration samples were used as blanks. The time-

dependent binding curves of all flow cells were monitored simultaneously. The results of compounds **4a–d** showed fast on and off rates outside the range of kinetic quantification, so K_D values were determined by transforming time-dependent binding curves into an affinity-steady state 1:1 model using Biacore S200 evaluation software (GE healthcare).

Antibacterial Activity Evaluation. Antibacterial activity was determined by a microdilution broth method as recommended by the CLSI (Clinical and Laboratory Standards Institute, Document M07-A8, 2009, Wayne, PA) using cation-adjusted Mueller-Hinton broth (Trek Diagnostics Systems, U.K.). Compounds were dissolved in DMSO. Serial 2-fold dilutions of each compound were made using DMSO as the diluent. Trays were inoculated with 5×10^4 CFU of each strain in a volume of 100 μL (final concentration of DMSO was 3.2% (v/v)) and incubated at 35 $^\circ\text{C}$ for 16–20 h. Growth of the bacterium was quantified by measuring the absorbance at 620 nm.

X-ray Crystallography. To prepare SaBPL-4c and SaBPL-5o crystals, 1 mg/mL apo SaBPL, 790 μM of the respective inhibitor, 4% (v/v) DMSO, 50 mM Tris-HCl, pH 7.5, 50 mM NaCl, 1 mM DTT, and 5% (v/v) glycerol were incubated overnight at 4 $^\circ\text{C}$. The incubation was filtered through a 0.2 μm Nanosep MF centrifugal device (Pall Corp.), and protein was concentrated to 5 mg/mL. Crystals were prepared at 4 $^\circ\text{C}$ using the hanging drop vapor diffusion method, with a 500 μL reservoir comprised of 12% (w/v) PEG 8000, 100 mM Tris-HCl, pH 7.5, and 10% (v/v) glycerol.¹¹ To prepare the hanging drop, 0.8 μL of reservoir solution was mixed with 1 μL of protein solution and 0.2 μL of microseeds of SaBPL in complex with a known inhibitor. A single crystal was looped and cryoprotected with reservoir solution containing saturated sucrose, prior to flash freezing with liquid nitrogen. X-ray diffraction data were collected at the Australian Synchrotron MX2Micro Crystallography beamline, using an ADSC Quantum 315r Detector for SaBPL-4c and an Eiger 16 M Detector for SaBPL-5o. The diffraction data were integrated using XDS,³⁰ and the intensities were merged and scaled using Aimless³¹ in the CCP4 program suite.³² MOLREP³³ was used to perform molecular replacement, using a single protein chain from PDB 3 V7R¹¹ as a search model. PDB and cif files for **4c** and **5o** were generated using eLBOW³⁴ in PHENIX.³⁵ Refinement was performed in PHENIX³⁵ and REFMAC,³⁶ and manual model building was undertaken in COOT.³⁷ Statistics for the data and refinement are reported in Table S3. All structures were deposited in the Protein Databank (accession codes 6AQQ for SaBPL-4c and 6APW for SaBPL-5o).

Docking Studies. Docking experiments were performed using ICM software version 3.8–5 (Molsoft L.L.C., San Diego, CA, USA). Proteins for docking were retrieved from RCSB protein data bank 3V7S¹¹ and SaBPL-4c. Then, formal charges were assigned; protonation states of histidines were adjusted, and hydrogens, histidine, glutamine, and asparagine were optimized using the protein preparation procedure implemented in ICM.³⁸ The original bound ligand and all water molecules were removed from the binding site before docking. The binding site was defined as the cavity delimited by residues with at least one nonhydrogen atom within a 4.0 Å cutoff radius from the ligand **4a** or **4c**. The pocket was represented by 0.5 Å grid maps accounting for hydrogen bonding, hydrophobic, van der Waals, and electrostatic interactions. The molecules were

flexibly docked into the rigid binding site and scored based on the ICM scoring function.

■ ASSOCIATED CONTENT

Supporting Information

The Supporting Information is available free of charge on the ACS Publications website at DOI: 10.1021/acsinfecdis.7b00134.

Supplementary figures and tables, synthesis, compound characterization, crystallographic data tables, and NMR spectra for chemical compounds (PDF)

■ AUTHOR INFORMATION

Corresponding Authors

*E-mail: steven.polyak@adelaide.edu.au. Phone +61883136042 (S.W.P.).

*E-mail: andrew.abell@adelaide.edu.au. Phone +6183135652 (A.D.A.).

ORCID

Steven W. Polyak: 0000-0002-8458-5194

Andrew D. Abell: 0000-0002-0604-2629

Present Address

[¶]A.S.P.: Albert Einstein College of Medicine, 1300 Morris Park Avenue, Bronx, New York 10461, United States of America.

Author Contributions

[¶]A.S.P., K.J.L., and A.J.H. all contributed equally. G.W.B., M.C.J.W., S.W.P., and A.D.A. conceived the study. A.S.P., K.J.L., A.J.H., J.F., Z.F., D.C., and S.D. performed the experiments and analyzed the data. A.S.P., K.J.L., A.J.H., S.W.P., and A.D.A. wrote the paper with input from all authors.

Notes

The authors declare no competing financial interest.

■ ACKNOWLEDGMENTS

This work was supported by the National Health and Medical Research Council of Australia (application APP1068885). We are grateful to the Wallace and Carthew families for their financial support of this work.

■ ABBREVIATIONS

BPL, biotin protein ligase; SaBPL, *Staphylococcus aureus* biotin protein ligase; SaPC90, 90 amino acid biotin-acceptor domain from pyruvate carboxylase; SPR, surface plasmon resonance

■ REFERENCES

- (1) Butler, M. S., Blaskovich, M. A., and Cooper, M. A. (2017) Antibiotics in the clinical pipeline at the end of 2015. *J. Antibiot.* 70, 3–24.
- (2) Payne, D. J., Gwynn, M. N., Holmes, D. J., and Pompliano, D. L. (2007) Drugs for bad bugs: confronting the challenges of antibacterial discovery. *Nat. Rev. Drug Discovery* 6 (1), 29–40.
- (3) Tommasi, R., Brown, D. G., Walkup, G. K., Manchester, J. I., and Miller, A. A. (2015) ESKAPEing the labyrinth of antibacterial discovery. *Nat. Rev. Drug Discovery* 14 (8), 529–42.
- (4) Brown, E. D., and Wright, G. D. (2016) Antibacterial drug discovery in the resistance era. *Nature* 529 (7586), 336–43.
- (5) Gillis, E. P., Eastman, K. J., Hill, M. D., Donnelly, D. J., and Meanwell, N. A. (2015) Applications of fluorine in medicinal chemistry. *J. Med. Chem.* 58 (21), 8315–59.
- (6) Gerebtzoff, G., Li-Blatter, X., Fischer, H., Frenz, A., and Seelig, A. (2004) Halogenation of drugs enhances membrane binding and permeation. *ChemBioChem* 5 (5), 676–84.

- (7) Brighty, K. E., and Gootz, T. D. (1997) The chemistry and biological profile of trovafloxacin. *J. Antimicrob. Chemother.* 39 (Suppl 2), 1–14.
- (8) Domagala, J. M. (1994) Structure-activity and structure-side-effect relationships for the quinolone antibacterials. *J. Antimicrob. Chemother.* 33 (4), 685–706.
- (9) Hagemann, W. K. (2008) The many roles of fluorine in medicinal chemistry. *J. Med. Chem.* 51 (15), 4359–69.
- (10) Purser, S., Moore, P. R., Swallow, S., and Gouverneur, V. (2008) Fluorine in medicinal chemistry. *Chem. Soc. Rev.* 37 (2), 320–30.
- (11) Soares da Costa, T. P., Tieu, W., Yap, M. Y., Pendini, N. R., Polyak, S. W., Pedersen, D. S., Morona, R., Turnidge, J. D., Wallace, J. C., Wilce, M. C. J., Booker, G. W., and Abell, A. D. (2012) Selective inhibition of Biotin Protein Ligase from *Staphylococcus aureus*. *J. Biol. Chem.* 287 (21), 17823–17832.
- (12) Feng, J., Paparella, A. S., Tieu, W., Heim, D., Clark, S., Hayes, A., Booker, G. W., Polyak, S. W., and Abell, A. D. (2016) New series of BPL inhibitors to probe the ribose-binding pocket of *Staphylococcus aureus* Biotin protein ligase. *ACS Med. Chem. Lett.* 7 (12), 1068–1072.
- (13) Pendini, N. R., Polyak, S. W., Booker, G. W., Wallace, J. C., and Wilce, M. C. J. (2008) Purification, crystallization and preliminary crystallographic analysis of biotin protein ligase from *Staphylococcus aureus*. *Acta Crystallogr., Sect. F: Struct. Biol. Cryst. Commun.* 64, 520–523.
- (14) Soares da Costa, T. P., Tieu, W., Yap, M. Y., Zvarec, O., Bell, J. M., Turnidge, J. D., Wallace, J. C., Booker, G. W., Wilce, M. C. J., Abell, A. D., and Polyak, S. W. (2012) Biotin analogues with antibacterial activity are potent inhibitors of biotin protein ligase. *ACS Med. Chem. Lett.* 3 (6), 509–514.
- (15) Tieu, W., Soares da Costa, T. P., Yap, M. Y., Keeling, K. L., Wilce, M. C. J., Wallace, J. C., Booker, G. W., Polyak, S. W., and Abell, A. D. (2013) Optimising *in situ* click chemistry: the screening and identification of biotin protein ligase inhibitors. *Chem. Sci.* 4 (9), 3533–3537.
- (16) Tieu, W., Jarrad, A. M., Paparella, A. S., Keeling, K. A., Soares da Costa, T. P., Wallace, J. C., Booker, G. W., Polyak, S. W., and Abell, A. D. (2014) Heterocyclic acyl-phosphate bioisostere-based inhibitors of *Staphylococcus aureus* biotin protein ligase. *Bioorg. Med. Chem. Lett.* 24 (19), 4689–4693.
- (17) Tieu, W., Polyak, S. W., Paparella, A. S., Yap, M. Y., Soares da Costa, T. P., Ng, B., Wang, G., Lumb, R., Bell, J. M., Turnidge, J. D., Wilce, M. C. J., Booker, G. W., and Abell, A. D. (2015) Improved synthesis of biotinol-5'-AMP: Implications for antibacterial discovery. *ACS Med. Chem. Lett.* 6 (2), 216–220.
- (18) Duckworth, B. P., Geders, T. W., Tiwari, D., Boshoff, H. I., Sibbald, P. A., Barry, C. E., Schnappinger, D., Finzel, B. C., and Aldrich, C. C. (2011) Bisubstrate adenylation inhibitors of Biotin protein ligase from *Mycobacterium tuberculosis*. *Chem. Biol.* 18 (11), 1432–1441.
- (19) Bockman, M. R., Kalinda, A. S., Petrelli, R., De la Mora-Rey, T., Tiwari, D., Liu, F., Dawadi, S., Nandakumar, M., Rhee, K. Y., Schnappinger, D., et al. (2015) Targeting *Mycobacterium tuberculosis* biotin protein ligase (MtBPL) with nucleoside-based bisubstrate adenylation inhibitors. *J. Med. Chem.* 58 (18), 7349–7369.
- (20) Paparella, A. S., Soares da Costa, T. P., Yap, M. Y., Tieu, W., Wilce, M. C. J., Booker, G. W., Abell, A. D., and Polyak, S. W. (2014) Structure guided design of Biotin protein ligase inhibitors for antibiotic discovery. *Curr. Top. Med. Chem.* 14 (1), 4–20.
- (21) Brown, P. H., Cronan, J. E., Gröthli, M., and Beckett, D. (2004) The biotin repressor: modulation of allostery by corepressor analogs. *J. Mol. Biol.* 337 (4), 857–69.
- (22) Feng, J., Paparella, A. S., Booker, G. W., Polyak, S. W., and Abell, A. D. (2016) Biotin protein ligase is a target for new antibacterials. *Antibiotics (Basel, Switz.)* 5 (3), 26.
- (23) Hein, J. E., Tripp, J. C., Krasnova, L. B., Sharpless, K. B., and Fokin, V. V. (2009) Copper(I)-catalyzed cycloaddition of organic azides and 1-iodoalkynes. *Angew. Chem., Int. Ed.* 48 (43), 8018–8021.
- (24) Worrell, B. T., Hein, J. E., and Fokin, V. V. (2012) Halogen exchange (HalEx) reaction of 5-iodo-1,2,3-triazoles: synthesis and

applications of 5-fluorotriazoles. *Angew. Chem., Int. Ed.* 51 (47), 11791–11794.

(25) Cheng, Y., and Prusoff, W. H. (1973) Relationship between the inhibition constant (KI) and the concentration of inhibitor which causes 50% inhibition (IC50) of an enzymatic reaction. *Biochem. Pharmacol.* 22 (23), 3099–3108.

(26) Pendini, N. R., Yap, M. Y., Polyak, S. W., Cowieson, N. P., Abell, A., Booker, G. W., Wallace, J. C., Wilce, J. A., and Wilce, M. C. J. (2013) Structural characterization of *Staphylococcus aureus* biotin protein ligase and interaction partners: An antibiotic target. *Protein Sci.* 22 (6), 762–773.

(27) Mayende, L., Swift, R. D., Bailey, L. M., Soares da Costa, T. P., Wallace, J. C., Booker, G. W., and Polyak, S. W. (2012) A novel molecular mechanism to explain biotin-unresponsive holocarboxylase synthetase deficiency. *J. Mol. Med.* 90 (1), 81–88.

(28) Ng, B., Polyak, S. W., Bird, D., Bailey, L., Wallace, J. C., and Booker, G. W. (2008) Escherichia coli biotin protein ligase: Characterization and development of a high-throughput assay. *Anal. Biochem.* 376 (1), 131–136.

(29) Bailey, L. M., Ivanov, R. A., Jitrapakdee, S., Wilson, C. J., Wallace, J. C., and Polyak, S. W. (2008) Reduced half-life of holocarboxylase synthetase from patients with severe multiple carboxylase deficiency. *Hum. Mutat.* 29 (6), E47–57.

(30) Kabsch, W. (2010) Xds. *Acta Crystallogr., Sect. D: Biol. Crystallogr.* 66 (Pt 2), 125–132.

(31) Evans, P. R., and Murshudov, G. N. (2013) How good are my data and what is the resolution? *Acta Crystallogr., Sect. D: Biol. Crystallogr.* 69 (Pt 7), 1204–1214.

(32) Collaborative Computational Project (1994) The CCP4 suite: programs for protein crystallography. *Acta Crystallogr., Sect. D: Biol. Crystallogr.* 50 (Pt 5), 760–763.

(33) Vagin, A., and Teplyakov, A. (1997) MOLREP: an automated program for molecular replacement. *J. Appl. Crystallogr.* 30, 1022–1025.

(34) Moriarty, N. W., Grosse-Kunstleve, R. W., and Adams, P. D. (2009) Electronic ligand builder and optimization workbench (eLBOW): a tool for ligand coordinate and restraint generation. *Acta Crystallogr., Sect. D: Biol. Crystallogr.* 65 (Pt 10), 1074–1080.

(35) Adams, P. D., Afonine, P. V., Bunkoczi, G., Chen, V. B., Davis, I. W., Echols, N., Headd, J. J., Hung, L. W., Kapral, G. J., Grosse-Kunstleve, R. W., McCoy, A. J., Moriarty, N. W., Oeffner, R., Read, R. J., Richardson, D. C., Richardson, J. S., Terwilliger, T. C., and Zwart, P. H. (2010) PHENIX: a comprehensive Python-based system for macromolecular structure solution. *Acta Crystallogr., Sect. D: Biol. Crystallogr.* 66 (Pt 2), 213–221.

(36) Murshudov, G. N., Vagin, A. A., and Dodson, E. J. (1997) Refinement of macromolecular structures by the maximum-likelihood method. *Acta Crystallogr., Sect. D: Biol. Crystallogr.* 53 (Pt 3), 240–255.

(37) Emsley, P., Lohkamp, B., Scott, W. G., and Cowtan, K. (2010) Features and development of Coot. *Acta Crystallogr., Sect. D: Biol. Crystallogr.* 66 (Pt 4), 486–501.

(38) Neves, M. A. C., Totrov, M., and Abagyan, R. (2012) Docking and scoring with ICM: the benchmarking results and strategies for improvement. *J. Comput.-Aided Mol. Des.* 26 (6), 675–686.

SUPPORTING INFORMATION

Halogenation of biotin protein ligase inhibitors improve whole cell activity against *Staphylococcus aureus*

Ashleigh S. Paparella,^{†+} Kwang Jun Lee,^{‡+} Andrew J. Hayes,^{†+} Jiage Feng,^{‡#} Zikai Feng,[†] Danielle Cini,[§]
Grant W. Booker,[†] Matthew C. J. Wilce,[§] Steven W. Polyak^{†*} and Andrew D. Abell^{‡#*}

[†] Department of Molecular and Cellular Biology, University of Adelaide, South Australia 5005, Australia

[‡] Department of Chemistry, University of Adelaide, Adelaide, South Australia 5005, Australia

[§] School of Biomedical Science, Monash University, Victoria 3800, Australia

[#] Centre for Nanoscale BioPhotonics (CNBP), University of Adelaide, Adelaide, South Australia 5005,
Australia

⁺ = These authors contributed equally

^{*} = Corresponding author

FIGURE S1.....	2
FIGURE S2.....	3
FIGURE S3.....	4
FIGURE S4.....	5
TABLE S1.....	6
TABLE S2.....	6
TABLE S3.....	7

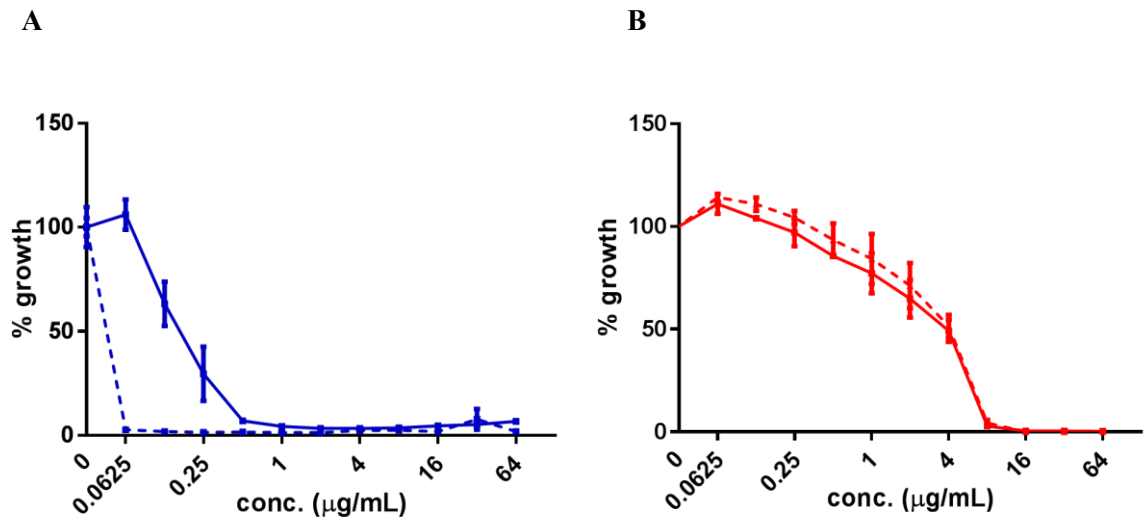


Figure S1.

Mechanism of action studies. *S. aureus* RN4220 + pCN51-NcoI control (dashed line) and pCN51-BPL overexpression (solid line) vectors susceptibility to (A) archetypical BPL inhibitor biotinol-5'-AMP 3 and (B) non BPL targeting antibiotic amoxicillin. Assays were performed in triplicate and normalised to no compound control.

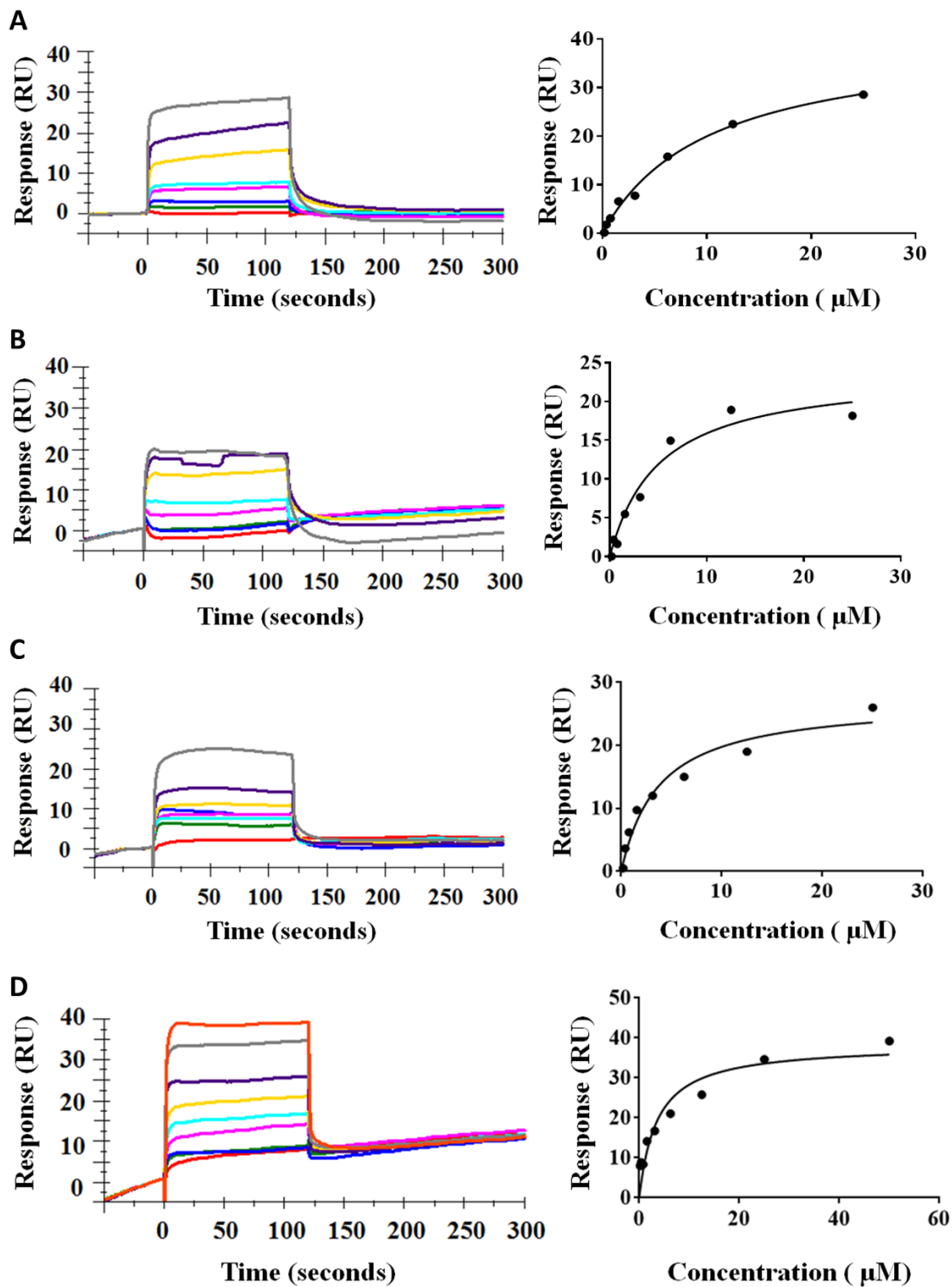


Figure S2.

SPR sensograms (left) and binding isotherms for compounds **4a-d** binding to SaBPL. SPR sensogram and concentration vs response plots are shown for (A) **4a**, (B) **4b**, (C) **4c** and (D) **4d**. Concentrations of compounds used were: 0.2 μM (red), 0.4 μM (green), 0.8 μM (blue), 1.6 μM (magenta), 3.1 μM (cyan), 6.3 μM (yellow), 12.5 μM (purple), 25 μM (grey) and 50 μM (orange).

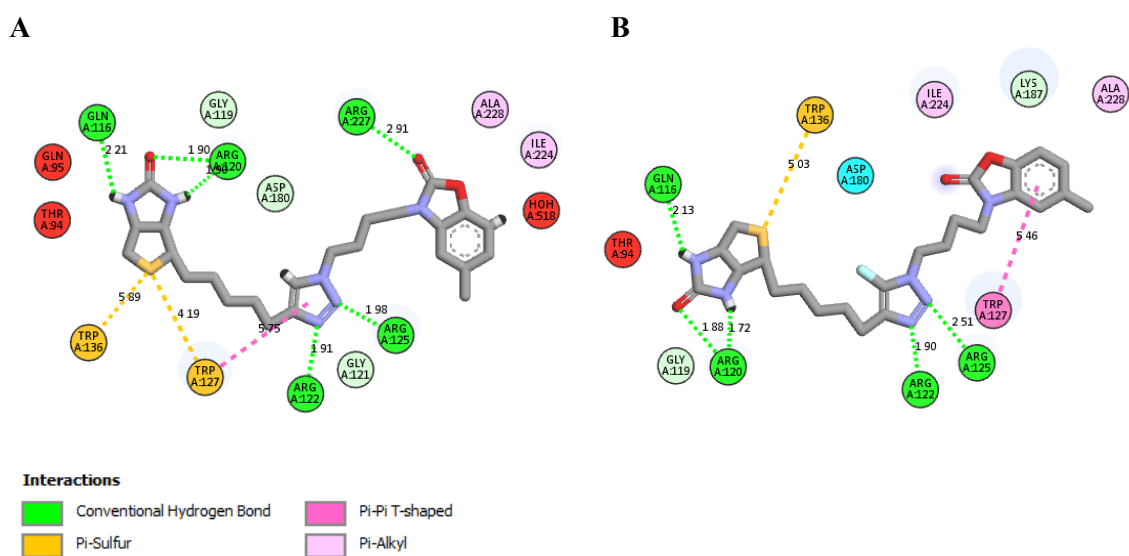


Figure S3.

(A) 2D interaction diagram of **4a** and *SaBPL*. (B) 2D interaction diagram of **4c** and *SaBPL*. 2D interaction diagrams were viewed using Discovery Studio Visualizer (Dassault Systèmes BIOVIA, Discovery Studio Modeling Environment, Release 4.5, San Diego: Dassault Systèmes, 2015).

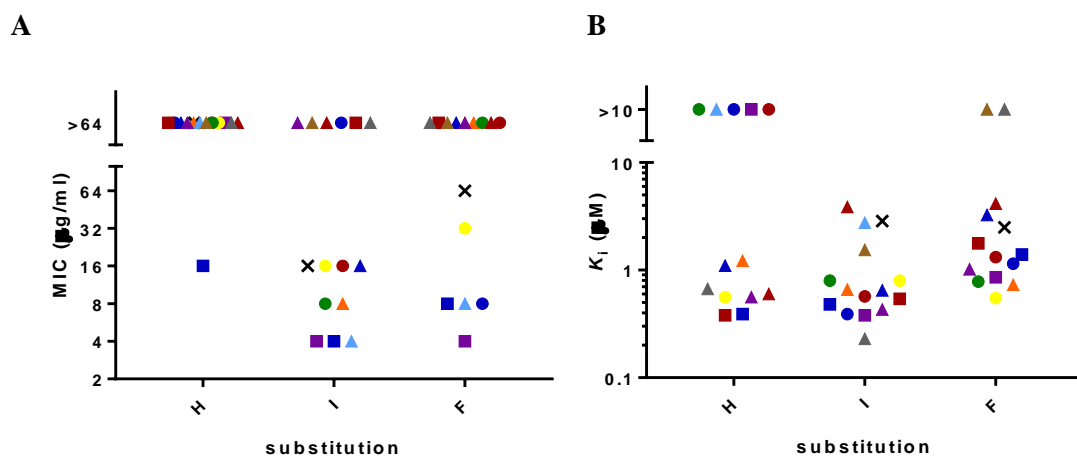


Figure S4.

Biological activities of benzyl-biotin 1,2,3 triazole series. Graphically demonstrated are the (A) MIC against *S. aureus* RN4220 and (B) K_i for *S. aureus* BPL for the benzyl-biotin 1,2,3 triazole series (5a-o) and halogenated analogues 5-iodo (6a-o) and 5-fluoro (7a-o). Benzyl substitutions shown are H **a** (×), 2-F **b** (●), 3-F **c** (■), 4-F **d** (▲), 2-Cl **e** (●), 3-Cl **f** (■), 4-Cl **g** (▲), 3-I **h** (■), 4I **i** (▲), 2-OMe **j** (●), 4-tBu **k** (▲), 2-NO₂ **l** (●), 4-CF₃ **m** (▲), 4-COOMe **n** (▲) and 4-COOH **o** (▲).

Table S1.

Comparison of binding pockets. The volume and area of binding pocket of **4c**-SaBPL was increased in order to accommodate 5-fluoro triazole **4c**. The icmPocketFinder macro was used to measure the properties of the binding site at SaPBL.

ID	Volume (Å ³)	Area(Å ²)	Hydrophobicity	Buriedness
SaBPL- 4a (PBD 3V7S)	679.9	635.2	0.5932	0.8844
SaBPL- 4c	800.6	706.9	0.5645	0.8758

Table S2.

Comparison of K_i values as determined by enzyme assay with radiolabelled biotin compared to assay utilising GST fusion of SaPC90 for antibody capture and detection with Eu-streptavidin conjugate.

Compound	K _i radiolabelled biotin (μM)	K _i GST-fusion (μM)
3	0.016 ± 0.01	0.004 ± 0.001

Table S3.Data collection and Refinement Statistics for *SaBPL* in complex with inhibitors

Data collection ^a	<i>SaBPL-4c</i>	<i>SaBPL-5o</i>
Wavelength (Å)	0.9537	0.95374
Resolution range (Å)	39.67 - 2.397 (2.482 - 2.397)	46.76 - 2.614 (2.708 - 2.614)
Space group	P 42 21 2	P 42 21 2
Unit cell <i>a, b, c</i> (Å)	94.241, 94.241, 131.192	94.454 94.454 130.978
α, β, γ (°)	90, 90, 90	90,90,90
Total reflections	84981 (8264)	488740 (46053)
Unique reflections	22814 (2233)	18559 (1788)
Multiplicity	3.7 (3.7)	26.3 (25.8)
Completeness (%)	95.52 (95.26)	99.79 (98.51)
Mean I/sigma(I)	13.86 (1.07)	38.43 (4.37)
Wilson B-factor	57.05	67.66
R-merge	0.06603 (1.2)	0.06458 (0.849)
R-pim	0.038 (0.79)	0.01277 (0.1675)
CC1/2	0.999 (0.454)	1 (0.948)
CC*	1 (0.79)	1 (0.987)
R-work (%)	20.77 (37.00)	0.1937 (0.2859)
R-free (%)	25.40 (42.72)	0.2280 (0.3401)
Number of non-hydrogen atoms	2680	2649
macromolecules	2613	2613
ligands	35	29
water	32	7
Protein residues	322	322
RMS(bonds)	0.007	0.003
RMS(angles)	0.94	0.60
Ramachandran favored (%)	98	96.56
Ramachandran allowed (%)	2.7	3.44
Ramachandran outliers (%)	0.3	0.00

Rotamer outliers (%)	0.0	0.00
Clashscore	8.42	5.18
Average B-factor	66.60	75.17
macromolecules	66.500	75.24
ligands	78.00	70.70
solvent	64.80	68.64

^aDiffraction data were collected from one crystal
Values given in parentheses are for the high resolution shell

Chapter Three

3.1 Introduction

Chapter 2 described the design and development of 5-halogenated-1,2,3-triazoles that target *Sa*BPL with improved antimicrobial activity. An investigation of diverse sulfonamide moieties is considered in this chapter to develop potent BPL inhibitors, given limitations of 1,2,3-triazoles (e.g. lack of antimicrobial activity and solubility). This chapter describes the design, synthesis, and biological assay of sulfonamide analogues targeting *Sa*BPL to improve inhibitory activity, antimicrobial activity, and metabolic stability.

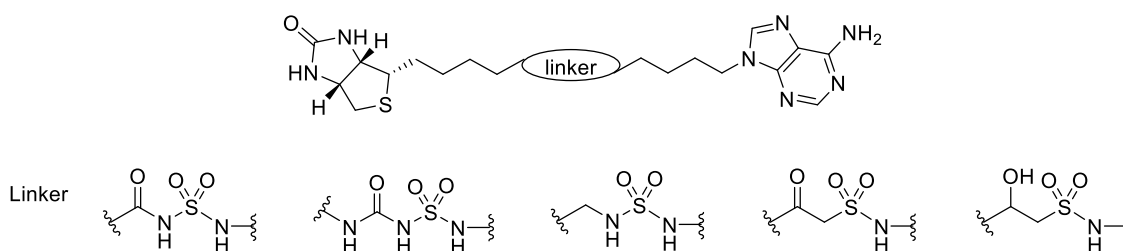


Figure 3.1. Chemical structures of BPL inhibitors in Chapter 3.

Statement of Authorship

Title of Paper	Sulfonamide-based inhibitors of biotin protein ligase as new antibiotic leads
Publication Status	<input type="checkbox"/> Published <input type="checkbox"/> Accepted for Publication <input checked="" type="checkbox"/> Submitted for Publication <input type="checkbox"/> Unpublished and Unsubmitted work written in manuscript style
Publication Details	Authors: Kwang Jun Lee, William Tieu, Beatriz Blanco Rodriguez, Ashleigh S. Paparella, Jingxian Yu, Andrew J. Hayes, Jiage Feng, Andrew C. Marshall, Benjamin Noll, Robert Milne, Danielle Cini, Matthew C. J. Wilce, Grant W. Booker, John B. Bruning, Steven W. Polyak, and Andrew D. Abell The manuscript was submitted to ACS Chemical Biology.

Principal Author

Name of Principal Author (Candidate)	Kwang Jun Lee		
Contribution to the Paper	Performed synthesis and characterisation of analogues, analysis of data, provided advanced draft of manuscript and subsequent revisions.		
Overall percentage (%)	70%		
Certification:	This paper reports on original research I conducted during the period of my Higher Degree by Research candidature and is not subject to any obligations or contractual agreements with a third party that would constrain its inclusion in this thesis. I am the primary author of this paper.		
Signature		Date	5/7/2019

Co-Author Contributions

By signing the Statement of Authorship, each author certifies that:

- the candidate's stated contribution to the publication is accurate (as detailed above);
- permission is granted for the candidate to include the publication in the thesis; and
- the sum of all co-author contributions is equal to 100% less the candidate's stated contribution.

Name of Co-Author	William Tieu		
Contribution to the Paper	Performed synthesis and characterisation of compounds 6.		
Signature		Date	1/7/19

Name of Co-Author	Beatriz Blanco Rodriguez		
Contribution to the Paper	Performed synthesis and characterisation of compounds 6.		
Signature		Date	01/07/19

Name of Co-Author	Ashleigh S. Paparella		
Contribution to the Paper	Performed <i>in vitro</i> biochemical assays and analysis of assay results.		
Signature		Date	7/1/19

Name of Co-Author	Jingxian Yu		
Contribution to the Paper	Performed molecular dynamics simulations and binding energy calculations.		
Signature		Date	1/7/2019

Name of Co-Author	Andrew J. Hayes		
Contribution to the Paper	Performed <i>in vitro</i> biochemical assays, antibacterial susceptibility assays and analysis of assay results.		
Signature		Date	01/07/2019

Name of Co-Author	Jiage Feng		
Contribution to the Paper	Performed synthesis and characterisation of compounds 6.		
Signature		Date	2019. 7. 1

Name of Co-Author	Andrew C. Marshall		
Contribution to the Paper	Performed crystallographic experiments of compound 7 including structure solving and interpretation.		
Signature		Date	1/7/2019

Name of Co-Author	Benjamin Noll		
Contribution to the Paper	Performed pharmacokinetic studies and whole blood stability tests.		
Signature		Date	8/7/19

Name of Co-Author	Robert Milne		
Contribution to the Paper	Supervised pharmacokinetic studies and revised manuscript.		
Signature		Date	11 JUL 2019

Name of Co-Author	Danielle Cini		
Contribution to the Paper	Performed crystallographic experiments of compound 6 including structure solving and interpretation.		
Signature		Date	11/7/19

Name of Co-Author	Matthew C. J. Wilce		
Contribution to the Paper	Supervised crystallographic experiments of compound 6 and revised manuscript.		
Signature		Date	03/07/2019

Name of Co-Author	Grant W. Booker		
Contribution to the Paper	Supervised the biological aspects of the project and revised manuscript.		
Signature		Date	1/7/2019.

Name of Co-Author	John B. Bruning		
Contribution to the Paper	Supervised crystallographic experiments of compound 7, helped with data processing and interpretation and revised manuscript.		
Signature		Date	1/7/2019

Name of Co-Author	Steven W. Polyak		
Contribution to the Paper	Supervised the biological testing and revised manuscript.		
Signature		Date	28/6/2019.

Name of Co-Author	Andrew D. Abell		
Contribution to the Paper	Worked closely with the principle author to write the manuscript and supervised the medicinal chemistry of the project and revised manuscript. A corresponding author.		
Signature		Date	2/7/2019

Sulfonamide-based inhibitors of biotin protein ligase as new antibiotic leads

Kwang Jun Lee,^{†#} William Tieu,[†] Beatriz Blanco Rodriguez,[†] Ashleigh S. Paparella,[‡] Jingxian Yu,^{†#} Andrew J. Hayes,[‡] Jiage Feng,[†] Andrew C. Marshall,[‡] Benjamin Noll,[¶] Robert Milne,[¶] Danielle Cini,[§] Matthew C. J. Wilce,[§] Grant W. Booker,[‡] John B. Bruning,^{||} Steven W. Polyak,[‡] and Andrew D. Abell^{†##}

[†] Department of Chemistry, School of Physical Sciences, University of Adelaide, Adelaide, South Australia 5005, Australia

[‡] Department of Molecular and Cellular Biology, School of Biological Sciences, University of Adelaide, South Australia 5005, Australia

[¶] School of Pharmacy & Medical Sciences, University of South Australia, Adelaide, South Australia 5000, Australia

[§] Department of Biochemistry, School of Biomedical Science, Monash University, Victoria 3800, Australia

[#] Centre for Nanoscale BioPhotonics (CNBP), University of Adelaide, Adelaide, South Australia 5005, Australia

^{||} Institute of Photonics and Advanced Sensing (IPAS), School of Biological Sciences, University of Adelaide, South Australia 5005, Australia

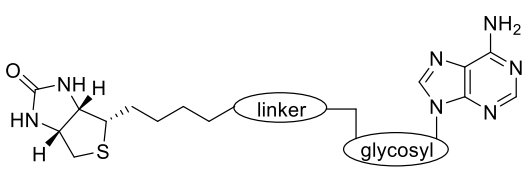
ABSTRACT

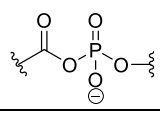
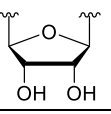
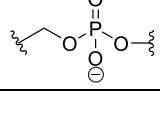
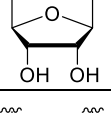
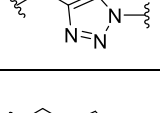
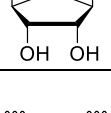
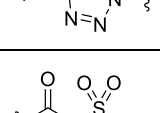
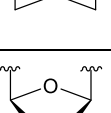
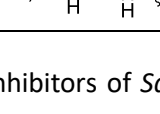
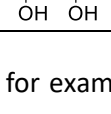
Here we report the design, synthesis, and evaluation of a series of sulfonamide-based inhibitors with activity against SaBPL. Compounds **6** and **7** showed potent *in vitro* inhibitory activities ($K_i = 0.007 \pm 0.003$ and 0.065 ± 0.03 μM respectively) and also antibacterial activity against *S. aureus* ATCC49775 with a minimum inhibitory concentration (MIC) of 0.25 and 4 $\mu\text{g}/\text{ml}$ respectively. Additionally, the bimolecular interactions between the BPL and the inhibitors **6** and **7** were defined by X-ray crystallography and molecular dynamics (MD) simulations. The high acidity of sulfonamide linker of **6** and **7** likely contributes to the enhanced *in vitro* inhibitory activities compared to **8–10** via strong interactions with Lys187 in the active site of SaBPL. Binding free energy estimation using computational methods suggest deprotonated **6** and **7** to be the best binders, which is consistent with enzyme assay results. Compound **6** was unstable in whole blood leading to poor pharmacokinetics. Importantly, **7** has a vastly improved pharmacokinetic profile compared to **6** presumably due to the enhanced metabolic stability of the sulfonamide linker moiety.

Biotin protein ligase (BPL) is a promising target for antibiotic development, with inhibitors showing efficacy against clinically important bacterial pathogens such as *Staphylococcus aureus* (*S. aureus*)¹ and *Mycobacterium tuberculosis* (*M. tuberculosis*).^{2, 3} It plays a key role in the viability of bacteria catalyzing reaction of biotin and ATP to give biotinyl-5'-AMP **1**, which then biotinylates and activates key biotin-dependent enzymes.^{4, 5} *S. aureus* expresses two such biotin-dependent enzymes, namely acetyl CoA carboxylase (ACC) and pyruvate carboxylase (PC), that play critical roles in the important metabolic pathways of fatty acid biosynthesis and gluconeogenesis respectively.⁶ *S. aureus* BPL (*SaBPL*) also functions as a transcriptional repressor that controls the uptake and biosynthesis of biotin.⁷⁻⁹ All this presents BPL as an attractive target for the generation of new antibiotics.

Inhibitors of BPL are typically generated by replacing the labile phosphoanhydride of biotinyl-5'-AMP **1** with more stable bioisosteres, see **Table 1**. For example, biotinyl-5'-AMP **2**, which lacks the labile carbonyl group of biotinyl-5'-AMP **1**, is a potent inhibitor of *SaBPL* ($K_i = 0.03 \mu\text{M}$) with whole cell activity against *S. aureus*, including methicillin resistant *S. aureus* (MRSA).^{10, 11} However, **2** also inhibits

Table 1. Biotinyl-5'-AMP **1** and reported BPL inhibitors **2 – 5**.



compound	linker	glycosyl
biotinyl-5'-AMP 1		
biotinyl-5'-AMP 2		
3		
4		
Bio-AMS 5		

the human BPL homologue and hence lacks the selectivity necessary for antibiotic development.

The molecular basis of inhibitor binding has been defined by structural studies to assist chemical optimization of preclinical candidates with enhanced binding potency and selectivity.

In particular, the crystal structure of *SaBPL* in complex with biotinyl-5'-AMP **2** reveals an extended water mediated network of hydrogen bonds between the phosphodiester linkage of **2** and amino acid residues Arg122, Arg125 and Lys187.¹⁰ The binding interaction with Lys187 is particularly important as this amino acid plays an essential role in the synthesis of the reaction intermediate **1** and, consequently, protein biotinylation.^{12, 13} This hydrogen bonding network is central to binding and likely contributes to the high affinity of **2** toward *SaBPL*. Our group has also reported biotin

triazoles as potent inhibitors of *SaBPL*, for example **3** ($K_i = 1.17 \mu\text{M}$) and **4** ($K_i = 0.66 \mu\text{M}$) as direct analogues of **2**.^{10, 14} The triazole ring of these derivatives acts as an isostere of the phosphodiester group of **2** and adopts hydrogen bonds with Arg122 and Arg125 based on its X-ray structure in complex

with SaBPL.¹⁰ Mutagenesis studies confirm a key hydrogen-bonding interaction between the triazole heterocycle and Arg125 (an asparagine in the human homologue) that defines selective binding.¹⁰ The biotin triazole structure is an important pharmacophore for the development of improved BPL inhibitors with enhanced whole cell activity against *S. aureus*.^{10, 15, 16}

Duckworth *et al* reported a series of acylsulfamide analogues of biotinyl-5'-AMP **1** (e.g. Bio-AMS **5**) that target *M. tuberculosis* BPL (*Mtb*BPL) with a K_D of approximately 0.5 nM, more than 1700-fold more tightly than biotin.^{17, 18} This compound possesses potent and selective antimicrobial activity against *M. tuberculosis* including multi-drug resistant and extensively drug resistant strains, with a minimum inhibitory concentration (MIC) ranging from 0.16 to 0.625 μ M. Interestingly, Bio-AMS **5** proved to be inactive against a panel of gram-positive (*E. faecalis* and *S. aureus*) and gram-negative bacteria (*A. baumannii*, *E. coli*, *K. pneumoniae* and *P. aeruginosa*), as well as fungi (*C. neoformans*, and *C. albicans*).¹⁷ An X-ray structure of Bio-AMS **5** bound to *Mtb*BPL reveals key hydrogen bonds between the sulfamide oxygens of **5** and amino acid residues Arg69, Arg72, and Asn130 (the equivalent of Arg122, Arg125 and Asn179 in SaBPL, respectively).¹⁷ Critically, the side chain aminium ion of Lys138 (the equivalent of Lys187 in SaBPL) also interacts with the carbonyl oxygen of the acylsulfamide through an electrostatic interaction, where the acidic central NH of the acylsulfamide linker would be expected to be deprotonated to enhance delocalization and hence interaction.¹⁷ We propose that this strong electrostatic interaction contributes to the potent inhibition of BPL given the important role Lys138 in catalysis.¹³

Clinical development of bio-AMS **5** has been limited by instability of its acylsulfamide linkage, which degrades to biotin and sulfamoylamino adenosine *in vivo* through the mechanism depicted in **Figure S1**.^{19, 20} This results in rapid elimination of Bio-AMS **5** from mice and, hence, limited bioavailability.^{19, 20} *M. tuberculosis* has also been shown to develop spontaneous resistance to Bio-AMS **5** through the overexpression of Rv3406, a type II alkylsulfatase capable of sulfate scavenging for metabolic and biosynthetic purposes.²⁰ Some work has been reported to circumvent this Rv3406-mediated chemical inactivation by modifying the component nucleoside.¹⁹ Interestingly, *S. aureus* does not possess an equivalent sulfatase so is likely to be highly susceptible to inhibition by sulfonamide-based BPL inhibitors. Triazole-based inhibitors offer an advantage of improved stability, but to date they somewhat lack the antimicrobial potency and solubility required for further development as antibiotics.

Here we describe the synthesis and evaluation of a panel of novel BPL inhibitors, acylsulfamide **6**, amino sulfonylurea **7** and related isosteres **8** – **10** as shown **Figure 1**. These compounds were designed to improve metabolic stability relative to **5** and also to target SaBPL with enhanced potency, selectivity and/or drug-like properties compared to biotinyl-5'-AMP **2** and the biotin-triazoles. The acylsulfamide

6 is based on earlier 1,2,3-triazole analogues **3** and **4**, where the 1,2,3-triazole is replaced with an acylsulfamide as found in **5**. We anticipated that removal of the ribose moiety of Bio-AMS **5** would increase potency against *Sa*BPL, where this group is known in the triazole series to be superfluous for binding to the enzyme.^{10, 14} Amino sulfonylurea **7** (and also **8** – **10**) were specifically designed to improve the metabolic stability of the problematic acylsulfamide linker of Bio-AMS **5** and also acylsulfamide **6** (see above for discussion), while maintaining key interactions with the BPL active site. In addition, while Lys187 of *Sa*BPL is believed to be critical for protein biotinylation, it does not interact with the 1,2,3-triazole ring of biotin triazole **4**.¹⁴ Compounds **6** – **10** thus allow the relative importance of this key residue to *Sa*BPL binding to be elucidated with an ensuing opportunity for the ongoing development of more potent inhibitors of *Sa*BPL.

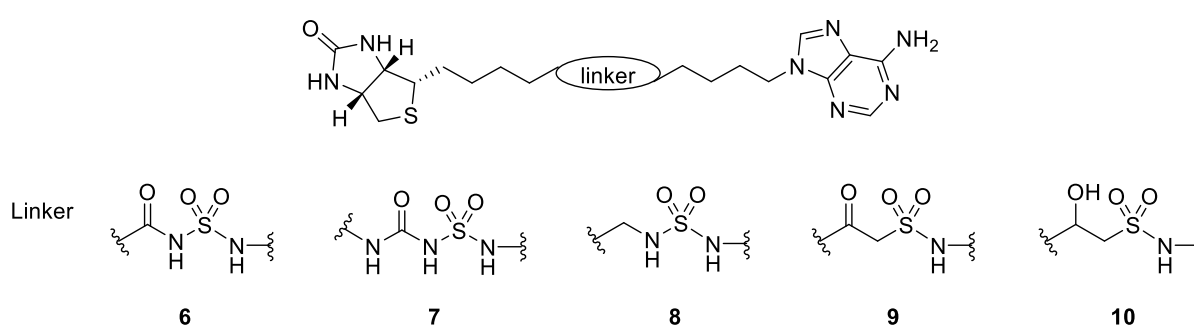


Figure 1. Proposed sulfonamide analogues **6** – **10**

RESULTS AND DISCUSSION

Inhibitory and antimicrobial activities

Derivatives **6** – **10**, prepared as described in supporting information, were evaluated for inhibitory activity and selectivity against BPLs from *S. aureus* and *Homo sapiens* using an *in vitro* protein biotinylation assay,¹⁶ with results summarized in **Table 2**. Acylsulfamide **6**, which lacks the ribose of **5**, was the most potent inhibitor of *Sa*BPL ($K_i = 0.007 \pm 0.003 \mu\text{M}$) and is devoid of activity against *Homo sapiens* BPL (*Hs*BPL) at the highest concentrations tested ($K_i > 5 \mu\text{M}$). This compound is in fact the most potent inhibitor of *Sa*BPL reported to date and confirms our earlier observation in the triazole series^{10, 14} that activity does not require the ribose group of biotinol-5'-AMP **2**. Importantly, the acylsulfamide **6** also demonstrated whole cell activity against *S. aureus* (discussed further below). Amino sulfonylurea **7** was also a potent inhibitor of *Sa*BPL (K_i of $0.065 \pm 0.03 \mu\text{M}$) and only 9-fold less potent than acylsulfamide **6**. However, removal of the acylsulfamide carbonyl group of **6**, as in alkylsulfamide **8**, results in approximately 300-fold decrease in potency against *Sa*BPL with $K_i = 2.34 \pm 0.19 \mu\text{M}$. Interestingly, β -ketosulfonamide **9** and β -hydroxysulfonamide **10** were inactive against *Sa*BPL ($K_i > 5 \mu\text{M}$). The acidity of the central NH of derivatives **6** and **7** likely contributes to binding and

hence potency towards *Sa*BPL, where the less acidic analogues **8**, **9**, and **10** all show poor or no inhibitory activities. The resulting increased anion character of the linkers of **6** and **7** would be expected to enhance electrostatic interaction with Lys187. This is supported by pK_a values of these linkers, with **6** and **7** having calculated values of 4.15 and 4.26 respectively (**Figure S2**). Derivatives **8**, **9**, and **10** were all significantly less active and have higher predicted pK_a 's > 9.6 (**Figure S2**).

Antimicrobial activity of sulfonamide analogues **6** – **10** was measured against the *S. aureus* clinical isolate ATCC 49775 and also the well characterised strain RN4220, using a broth microdilution assay and the results are shown in **Table 2**. Acylsulfamide **6** proved to be a particularly potent antibacterial against both *S. aureus* strains, with MIC values of 0.125 and 0.25 $\mu\text{g}/\text{mL}$ respectively. This compares to the most potent reported biotin-1,2,3 triazole, which only inhibits growth of *S. aureus* ATCC 49775 by 80% with a MIC of 8 $\mu\text{g}/\text{mL}$.¹⁶ The antibacterial activity of **6** was particularly noteworthy, with ribose-containing bio-AMS **5** reported to be inactive against *S. aureus*.¹⁷ This finding suggests that replacement of the ribose moiety of **5** with an alkyl linker (**6**) significantly improves whole cell activity against *S. aureus*. The alkylsulfamide **8** showed antibacterial activity against *S. aureus* RN4220 with a MIC of 16 $\mu\text{g}/\text{mL}$, but it was inactive against the clinical isolate (ATCC 49775, MIC > 64 $\mu\text{g}/\text{mL}$). Amino sulfonylurea **7** was also active against *S. aureus* RN4220 (MIC 1 $\mu\text{g}/\text{mL}$) and ATCC 49775 (4 $\mu\text{g}/\text{mL}$), albeit with reduced potency compared with **6**. As expected, *Sa*BPL inactive β -ketosulfonamide **9** and β -hydroxysulfonamide **10** were inactive against *S. aureus* RN4220. Together the biochemical and microbiological data demonstrates a clear and strong correlation between antimicrobial activity and inhibitory activity against *Sa*BPL.

Table 2. K_i (μM) values of sulfonamide analogues **6** – **10** against *Sa*BPL and *Hs*BPL and antimicrobial activity against *S. aureus* strains MIC ATCC 49775 and MIC RN4220.

Compound	K_i <i>Sa</i> BPL (μM)	K_i <i>Hs</i> BPL (μM)	MIC ATCC 49775 ($\mu\text{g}/\text{mL}$)	MIC RN4220 ($\mu\text{g}/\text{mL}$)
6	0.007 ± 0.003	>5	0.25	0.125
7	0.065 ± 0.03	N/D	4	1
8	2.34 ± 0.19	N/D	>64	16
9	>5	N/D	N/D	>64
10	>5	N/D	N/D	>64

Structural studies

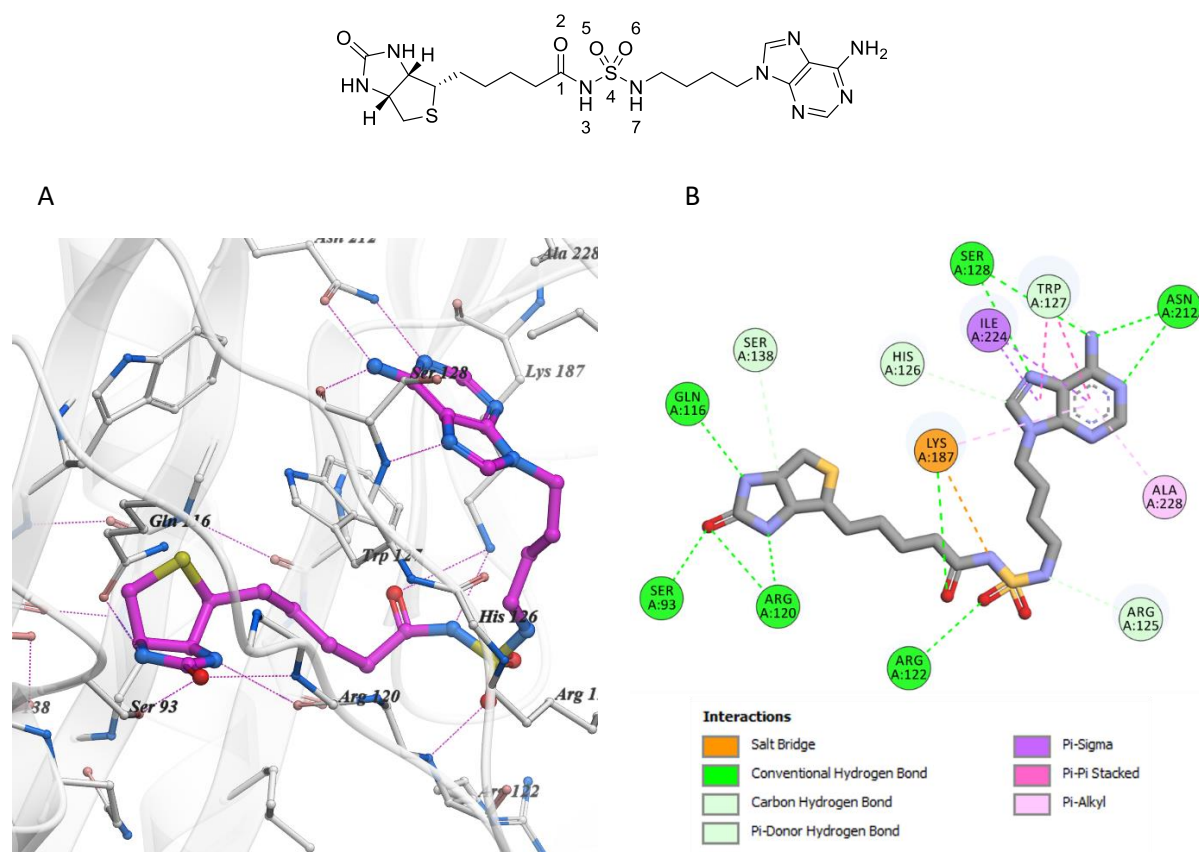
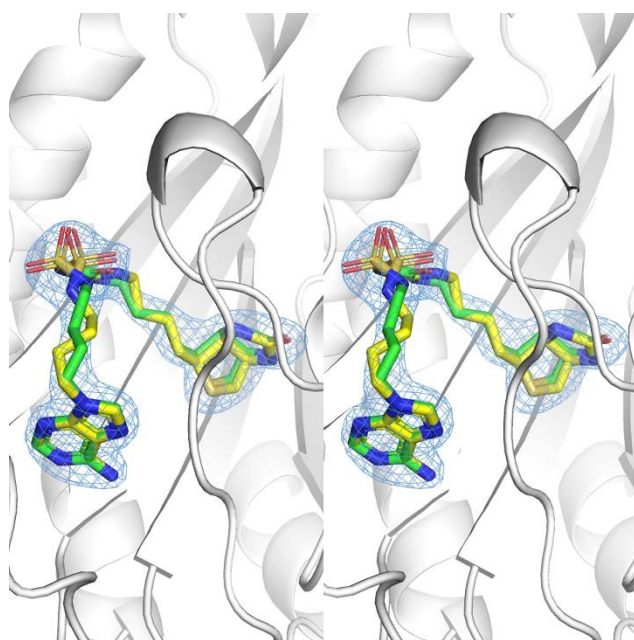


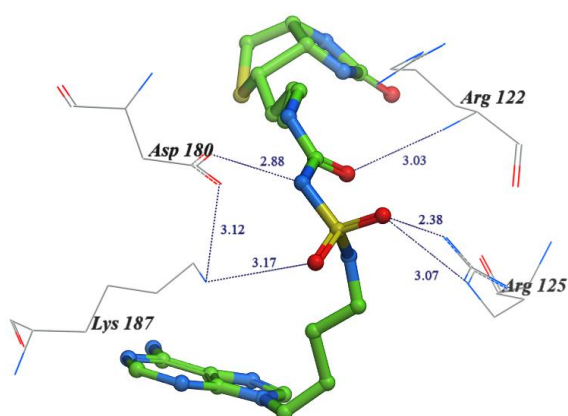
Figure 2. (A) A 3D depiction of acylsulfamide **6** bound to SaBPL with hydrogen bonds shown in purple. (B) 2D depiction of acylsulfamide **6** bound to SaBPL with interactions shown in dashes.

Crystal structures of SaBPL in complex with acylsulfamide **6** and amino sulfonylurea **7** were solved (at 2.39 and 2.00 Å, respectively) in order to define and compare the molecular details of binding (see **Table S1** for data collection and refinement statistics). Acylsulfamide **6** adopts a ‘U-shape’ conformation when bound to SaBPL, with the biotinyl and adenine groups occupying the biotin and nucleoside pockets respectively as per biotinyl-5'-AMP **2** and 1,2,3-triazole **4**²¹ (shown in **Figure 2**). The adenine group of **6** forms hydrogen bonds with Asn212 and Ser128, while the biotin urea forms hydrogen bonds with Arg120, Ser93 and Gln116. The same hydrogen bonding interactions are apparent in the reported crystal structures of biotinyl-5'-AMP **2** and 1,2,3-triazole **4** bound to SaBPL.²¹ The acylsulfamide isostere of **6** interacts with amino acid residues in the phosphate binding domain of SaBPL, specifically Arg122, Arg125, and Lys187. N3 of the acylsulfamide linker of **6** is likely deprotonated, where this isostere has a calculated pK_a of 4.15 (**Figure S2**). The resulting anion is delocalized over N3 and O2 of the acylsulfamide linker, to facilitate interaction with the side chain amine of Lys187. The backbone nitrogen atom of Arg122 forms a hydrogen bond with one sulfamide oxygen O5 of the acylsulfamide linker of **6**.

A



B



C

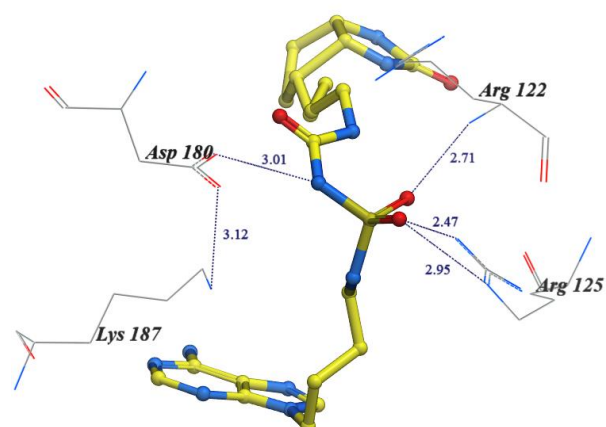


Figure 3. (A) A multiconformer model of amino sulfonylurea **7** bound to SaBPL with a major conformer shown in green sticks (coloured by element) and a minor conformer shown in yellow sticks (coloured by element). Displayed in blue mesh is a $2F_o-F_c$ composite omit map contoured at 2σ . Image is depicted in wall eye stereo. (B) 3D depiction of a major conformer of amino sulfonylurea **7** (green) looking down into the phosphate binding pocket of SaBPL. (C) 3D depiction of a minor conformer of amino sulfonylurea **7** (yellow) looking down into the phosphate binding pocket of SaBPL. Hydrogen bonds are depicted by blue dashes with distances shown therein.

Interestingly, the electron density observed in the structure of amino sulfonylurea **7** bound to SaBPL suggests a multiple conformer model, see **Figure 3A**. Both conformers adopt the hydrogen bonds observed between the biotin heterocycle/adenine ring of **6** and amino acid residues of SaBPL. A single conformation of Arg125 was apparent, but the two ligand conformations show distinct hydrogen

bonding patterns. The two conformers differ in positioning of the central isostere in the active site. The central nitrogen atom of the linker of the major conformer of amino sulfonylurea **7** forms a hydrogen bond with the carboxylate of Asp180 (**Figure 3B**). The side chain amine of Lys187 then forms a hydrogen bonding network with one sulfamide oxygen and the carboxylate of Asp180. The backbone nitrogen atom of Arg122 forms hydrogen bonds with the urea oxygen of the amino sulfonylurea linker, while the guanidium group of Arg125 forms hydrogen bonds with one of the sulfamide oxygens of **7**. The amino sulfonylurea carbonyl groups of both conformers point in opposite directions. As a consequence, one of the sulfamide oxygens in the minor conformer forms a hydrogen bond with the backbone nitrogen atom of Arg122 (**Figure 3C**). The side chain amine of Lys187 forms a hydrogen bond with one sulfamide oxygen in the linker of the major conformer of **7**, but not for the minor conformer. Interaction between Lys187 and the linker moiety likely contributes to the potent inhibition of BPL, as Lys187 of *Sa*BPL is believed to be critical for protein biotinylation. The acylsulfamide linker of **6** interacts with Lys187, while only the major binding conformer of **7** forms a hydrogen bond with Lys187. This limited interaction with Lys187 in **7** supports the reduced potency of **7** ($K_i = 0.065 \pm 0.03 \mu\text{M}$) compared to **6** ($K_i = 0.007 \pm 0.003 \mu\text{M}$).

Molecular dynamics (MD) simulations of acylsulfamide **6** and amino sulfonylurea **7** in the binding pocket of *Sa*BPL were carried out using the Sander algorithm as implemented in Amber 16 package as described in supporting information, in order to gain further insight into the binding of both protonated and deprotonated forms to *Sa*BPL. Although the acylsulfamide linker of **6** is likely deprotonated as discussed above, both protonated and deprotonated forms were considered to define how this feature might influence the binding conformation. The co-crystal structure of acylsulfamide **6** bound to *Sa*BPL was first superimposed with the time-averaged conformations of both deprotonated and protonated **6** obtained by MD simulations (**Figure S3**). Deprotonated **6** is clearly a better binder, with the time-averaged conformation of deprotonated and protonated **6** giving root-mean-square deviation (RMSD) values of 0.62 and 1.13 Å, respectively. The early crystal structure, shown in **Figure 2**, thus likely contains deprotonated **6**. The major and minor conformers of amino sulfonylurea **7**, found in the X-ray structure *Sa*BPL, were superimposed with time-averaged conformation of deprotonated and protonated **7** similarly obtained by MD simulations (**Figure S4**). The major binding conformer gave RMSD values of 1.02 and 0.86 Å for time-averaged conformations of deprotonated and protonated **7**, respectively. In comparison, the minor binding conformer gave RMSD values of 0.78 and 0.98 Å, respectively. This suggests that the major and minor conformers in crystal structure of **7** bound to *Sa*BPL may correspond to the protonated and deprotonated forms respectively.

MD simulations of inactive analogues **8** – **10** bound to *Sα*BPL were also conducted to gain some insight into the binding affinity of the extended series of sulfonamide analogues. Binding free energies of **6** – **10** were estimated from MD simulation results, as summarized in **Table S2**, using quantum mechanics/molecular mechanics generalized Born surface area (QM/MM-GBSA) methods. Deprotonated **6** and **7** were predicted to have enhanced binding affinities compared to protonated **6** and **7** as well as **8** – **10**. In support, free energies for deprotonated **6** and **7** were calculated to be -73.75 and -81.27 kcal/mol respectively, while values for protonated **6** and **7**, and **8** – **10** were all estimated to be higher than -71.28 kcal/mol. The relatively low estimated binding energies for deprotonated **6** and **7** are consistent with their enhanced potency, see **Table 2**.

Pharmacokinetic studies

The acylsulfamide **6** was administered into mice in order to define its pharmacokinetic profile. In particular, thirty mice were administered an intravenous bolus dose of **6** and samples of blood collected at regular intervals post administration and blood concentrations were measured by LC-MS, see **Figure 4**. Pharmacokinetic parameters were then calculated after fitting a two-compartmental model of disposition to the profile of concentrations versus time. Values for the areas under concentrations in blood-time curves (AUC) and clearance were determined to be 17300 (\pm 1740, S.E.) ng·min/mL and 1210 (\pm 154, S.E.) mL/min·kg, respectively. The latter value reflects the efficiency with which the compound is cleared irreversibly from circulating blood and this far exceeds the summed flow of blood to the two major eliminating organs, i.e. the liver (blood flow of 90 mL/min·kg) and kidney (blood flow of 65 mL/min·kg).²² Thus, hepatic and renal mechanisms do not account for the high clearance of acylsulfamide **6**, suggesting an additional route of the irreversible elimination of **6** from circulating blood.

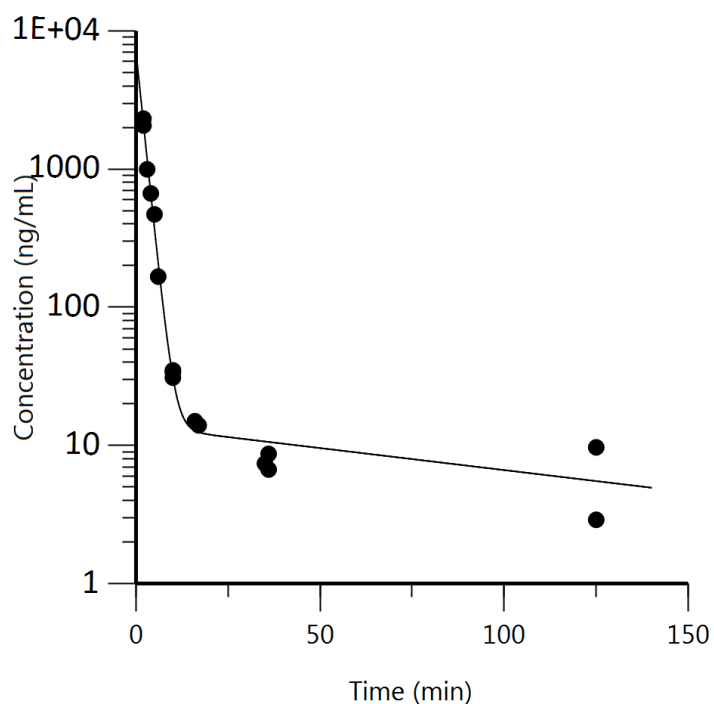


Figure 4. Concentrations of acylsulfamide **6** in blood after administration of an intravenous dose (16.6 mg/kg) to mice.

The fate of acylsulfamide **6** in blood was thus investigated *in vitro* by incubating **6** in drug-free rat whole blood and the resulting peak response ratios are shown in **Figure S5**. It is clear that acylsulfamide **6** decomposes rapidly in blood, with approximately 50% lost after 3 h of incubation. This rapid degradation likely accounts for the high clearance observed after an intravenous dose of acylsulfamide **6** in mice. Full mass scans of samples taken at 0, 3 and 71 h identified a m/z of 512.1863 at 0 h and 3 h (**Figure S6A**), which corresponds to acylsulfamide **6** (**Figure 5**). Interestingly, a potential decomposition product was also observed at 3 h and 71 h ($m/z = 286.1081$) (**Figure S6B**), the mass of which is consistent with adenine sulfamide (**Figure 5**). This suggests that acylsulfamide **6** is quickly eliminated in rodent whole blood partially by the hydrolysis event (**Figure 5**).

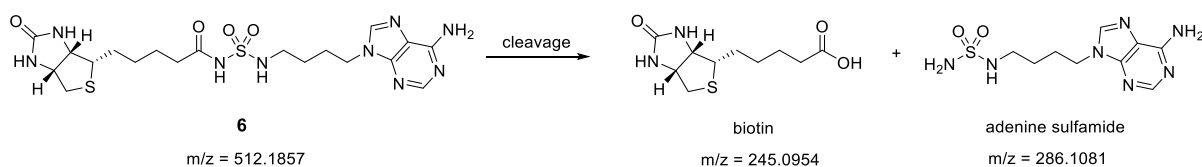
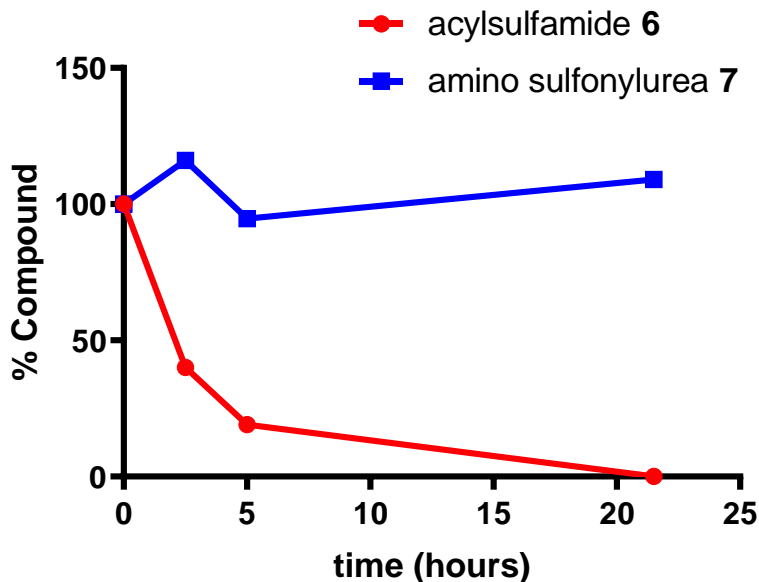


Figure 5. Putative degradation pathway of acylsulfamide **6**.

The stability study in blood was repeated with amino sulfonylurea **7**, with comparative data for **6** and **7** shown in **Figure 6A**. Importantly, amino sulfonylurea **7** was dramatically more stable in whole blood, with most of the compound remaining at 21.5 h (**Figure 6A**). This contrast acylsulfamide **6** which rapidly degrades after a few hours, with complete degradation over the same 21.5 h timeframe (**Figure 6A**). The amino sulfonylurea linker of **7** is clearly more stable than the acylsulfamide linker of **6** in blood resulting in a significantly longer residence time. Given the evidence of enhanced metabolic stability, amino sulfonylurea **7** was administered into mice in order to determine its pharmacokinetic profile. Nine mice were administered an intravenous bolus dose of **7** and three samples of blood were collected from each mouse. Concentrations of **7** in plasma were measured by LC-MS and a two-compartmental model was fitted over time (**Figure 6B**). Clearance of **7** in plasma was estimated at $91.7 (\pm 7.9)$ mL/min·kg. Considering a hematocrit value of 0.4, blood clearance is equal to about $1.66 \times$ plasma clearance.²³ Clearance of **7** in plasma thus equates to an approximate value of 152 mL/min·kg in blood. The estimated clearance of **7** in blood is much lower than the value for **6** (1210 mL/min·kg), and commensurates with its greater residence in plasma.

A



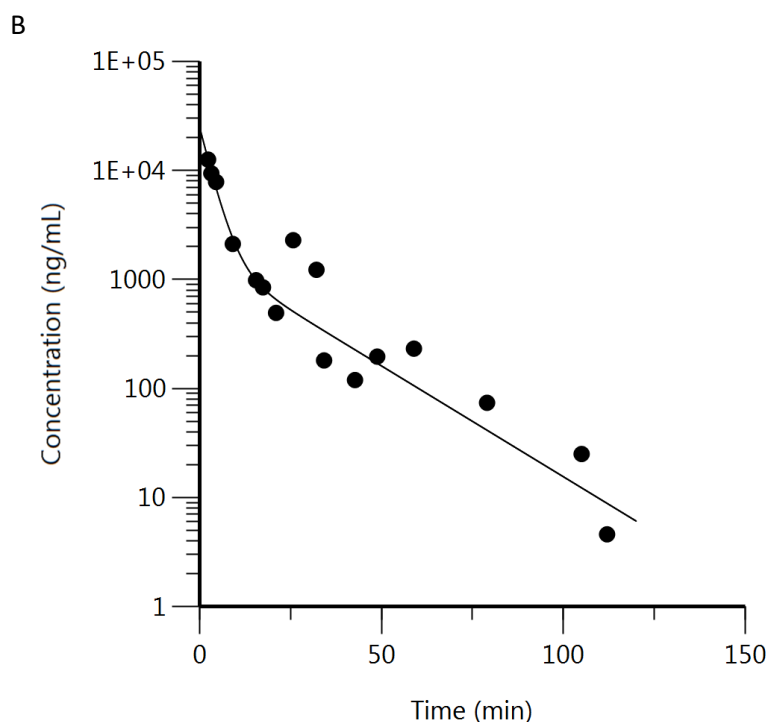


Figure 6. (A) Comparison of the stability of acylsulfamide **6** and amino sulfonylurea **7** in drug-free rat blood. The mass spectrometer responses were converted to a percentage of the response at 0 h. (B) Concentrations of amino sulfonylurea **7** in plasma after administration of an intravenous dose (10 mg/kg) to mice.

Conclusion

Acylsulfonamide **6** was synthesized and shown to be highly potent against *SaBPL* ($K_i = 0.007 \pm 0.003$ μM) and, critically, it displays excellent antibacterial activity against *S. aureus* with MIC = 0.25 $\mu\text{g/ml}$. Crystallographic analysis and computational studies on the acylsulfamide **6** reveal the importance of the central nitrogen, with the associated NH being deprotonated. The anion then binds to the side chain of Lys187 in the active site of *SaBPL*, to account for the high inhibitory activity of **6** towards the enzyme. However, acylsulfonamide **6** was unstable in whole blood leading to rapid clearance. The poor pharmacokinetics observed for **6** is likely to impact its clinical utility with agents that show slower clearance rates more likely to demonstrate efficacy in treating bacterial infections. Sulfonamide analogues **7-10** were also prepared and assayed against *SaBPL* with a view to improving metabolic stability over acylsulfamide **6**. Whilst sulfonamide analogues **8-10** were devoid of biochemical and microbiological activity, amino sulfonylurea **7** showed potent *in vitro* inhibitory activity ($K_i = 0.065 \pm 0.03$ μM) and also antibacterial activity against *S. aureus* (MIC = 4 $\mu\text{g/ml}$). Critically, amino sulfonylurea **7** had a vastly improved pharmacokinetic profile compared to acylsulfamide **6**, presumably due to the enhanced stability of the amino sulfonylurea linker in blood. These combined studies validate the amino sulfonylurea **7** as an important inhibitor of *SaBPL* suitable for further pre-clinical developed.

METHODS

Enzyme inhibition assays

The inhibitory activity of compounds was determined by measuring *S. aureus* BPL activity in the presence of varying concentrations of compound as previously described.¹⁶ The inhibition constant (K_i) was analysed with GraphPad prism (version 6) by fitting the data to the Morrison equation.

Antibacterial susceptibility assays

Antimicrobial activity of the compounds was determined by a broth microdilution method as recommended by the Clinical and Laboratory Standards Institute (Document M07-A8, 2009, Wayne, PA) with cation-adjusted Mueller-Hinton broth (Trek Diagnostics Systems). Compounds were dissolved using DMSO. Serial 2-fold dilutions of each compound were made using DMSO as the diluent. Trays were inoculated with 5×10^4 colony-forming units of *S. aureus* ATCC 49775 in a volume of 100 μ L (final concentration of DMSO was 3.2% (v/v)) and incubated at 35 °C for 16–20 h. Growth of the bacterium was quantitated by measuring the absorbance at 620 nm.

X-Ray Crystallography

Crystallization of SaBPL with 6 and 7. SaBPL was prepared for co-crystallization with **6** and **7** using the method described by Paparella *et al.*²⁴ Crystals were grown by hanging drop vapour diffusion with 2 μ L drops composed of equal volumes of protein sample and reservoir solution. Crystals grew as square rods to a maximum size of $400 \times 200 \times 200 \mu$ m in approximately 2 weeks at 4°C with 14% PEG 8000, 0.1 M Tris pH 8.5, 10% glycerol as the reservoir solution.

Data collection. A single crystal was flash frozen in liquid nitrogen using reservoir solution supplemented with 16% glycerol as cryoprotectant. X-ray diffraction data were collected at 100 K using an energy of 13000 eV on the MX1 beamline at the Australian Synchrotron²⁵. 360 frames were collected with 1° oscillations.

Data processing and refinement. Data were integrated using XDS²⁶ and scaled and merged using Aimless²⁷. Molecular replacement using phaserMR²⁸ with 6APW as the search model was used to derive initial phases. Two conformations of the compound **7** were visible in initial electron $F_o - F_c$ density maps as well as composite omit maps generated later in refinement. Each conformation of ligand **7** was occupancy refined. Model refinement was performed by iterations of manual rebuilding in Coot²⁹ and automated refinement using phenix.refine³⁰, where anisotropic B-factor refinement was restricted to automatically defined translation-liberation-screw (TLS) groups³¹. Statistics for the data and refinement are reported in **Table S1**. All structures were deposited in the Protein Databank (accession codes 6ORU for SaBPL-**6** and 6NDL for SaBPL-**7**).

Pharmacokinetic study of acylsulfamide 6

Thirty swiss mice, weighing 20-30g, were administered an intravenous bolus dose of acylsulfamide **6** (16.6 mg/kg, as a dispersion of 5.3 mg/mL in PEG400). Samples of blood (approximately 1 mL) collected from the mice while under anaesthesia via cardiac puncture at 2, 5, 10, 15 and 30 min, and 1, 2, 4, 7 and 24 h after the dose and transferred to heparinised 1.5 mL polypropylene tubes; they were stored at -20°C. The next day, the samples were thawed and the concentrations of acylsulfamide **6** in blood measured by liquid chromatography-mass spectrometry.

To 10 µL of blood, 10 µL of either acylsulfamide **6** working solution (drug-free blood for the calibration standards) or water (unknown samples of blood) was added, followed by 50 µL internal standard solution (100 ng/mL a biotin analogue in water) and 50 µL 2.8% (w/v) ZnSO₄ solution. The mixture was vortexed briefly, and 50 µL cold methanol added, vortex-mixed for 10 s and centrifuged at high speed for 10 min. Ten µL was injected into the LC-MS system.

A Shimadzu Nexera HPLC system (Shimadzu Oceania, Rydalmere, NSW) was used to pump the mobile phase through a Kinetex column (C18 2.6µm 50 x 3.0 mm; Phenomenex Australia, Lane Cove, NSW) at a flow of 0.4 mL/min. Mobile phase A (MPA) was 5% acetonitrile and 0.1% formic acid in water and mobile phase B (MPB) was 95% acetonitrile and 0.1% formic acid. The mobile phase was run as a gradient using the following timetable: 0.2-5.0 min 0-25% MPB; 5.0-6.0 min 25-100% MPB; 6.0-7.0 min 100% MPB. Acylsulfamide **6** and the internal standard were detected using a Triple-TOF 5600 (Sciex, Mt.Waverley, Vic) following the mass transitions m/z 512.2 → 269.1 (acylsulfamide **6**) and 427.2 → 227.1 (internal standard). Peak ratios were obtained from known concentrations of acylsulfamide **6** and internal standard and were used to construct a seven-point calibration curve spanning from 3.5 ng/mL to 3500 ng/mL. Two-compartmental model was fitted over time (Phoenix 64 WinNonLin 6.4, Certara, Princeton, NJ, USA).

Stability of acylsulfamide 6 in whole blood

Acylsulfamide **6** was incubated in drug-free rat blood at concentrations of 1 (low) and 10 (high) µg/mL, and samples of blood taken at 0, 15 min and 3 and 24 h. The samples were processed and subjected to liquid chromatography-mass spectrometry as described above.

Stability of acylsulfamide 6 and amino sulfonylurea 7 in whole blood

Fresh whole rat blood (490 µL) in separate tubes was spiked with 10 µL 0.5 mg/mL of either acylsulfamide **6** or amino sulfonylurea **7** (dissolved in methanol/water 50/50). Samples were mixed well and incubated at 22 °C for up to 21.5 h. Blood was then extracted for LC/MS by protein precipitation (10 µL blood + 100µL 1.4% ZnSO₄ + 50µL methanol).

Pharmacokinetic study of amino sulfonylurea 7

Nine, male Balb/C mice weighing 22.7 ± 0.6 g (mean \pm SD) were administered a bolus dose of amino sulfonylurea **7** (10 mg/kg, 4.5 mg/mL in 10/90 DMSO/ 0.9% sodium chloride) via the tail vein. Three samples of blood (two from alternate cheek veins and a final one from cardiac puncture under anaesthesia) were collected from each mouse into polypropylene tubes containing 100 U of heparin. Collection of the twenty-seven samples were timed so that they were spread from 2 min to 5 h. Samples were centrifuged, and plasma harvested for storage at -20°C pending analysis. The concentrations of amino sulfonylurea **7** in plasma were measured by LC-MS/MS. Plasma (20 μL drug-free rat plasma or the unknown samples of plasma plus 10 μL 50/50 methanol/water; 20 μL drug-free plasma plus 10 μL calibrator working solution in 50/50 methanol/water; 20 μL drug-free plasma plus 10 μL quality control working solution in 50/50 methanol/water) were mixed with 10 μL of internal standard solution (2 $\mu\text{g}/\text{mL}$ of β -ketosulfonamide **9** in 50/50 methanol/water) and then with 20 μL of 2.8% (w/v) ZnSO_4 solution and 100 μL methanol, vortex-mixed for 10 s then centrifuged at high speed for 10 min. The supernatant (5 μL) was eluted through a Phenomenex Kinetex column (5 μm C18, 3 x 50 mm; Phenomenex, Australia, Lane Cove, NSW) under conditions identical to those described for acylsulfamide **6**. The mass transitions m/z 527.2 \rightarrow 312.1 (amino sulfonylurea **7**); m/z 511.2 \rightarrow 207.1 (internal standard) were monitored. Peak area ratios of the signal responses of amino sulfonylurea **7** and internal standard were used to construct a linear calibration curve spanning from 3.5 to 10,000 ng/mL with a weighting of $1/x$, using MultiQuant 3.0.1 software. If the volume of the unknown plasma sample was less than 20 μL , the remaining volume was supplemented with drug-free plasma and an appropriate correction made. For samples with a measured concentration exceeding 10,000 ng/mL, the supernatant was diluted ten-times with drug-plasma supernatant. Quality controls were prepared at concentrations of 15,400 and 4,000 ng/mL. Measured concentrations of these controls, including the highest diluted ten-times, were within 15% of their nominal values. Two-compartmental model was fitted over time (Phoenix 64 WinNonLin 6.4, Certara, Princeton, NJ, USA).

ASSOCIATED CONTENT

Supporting information contains: supplementary figures and tables, computation methods, synthesis, compound characterization, NMR spectra for chemical compounds (PDF).

AUTHOR INFORMATION

Corresponding authors

* (A.D.A) Email: andrew.abell@adelaide.edu.au. Phone +6183135652

ORCID

Andrew D. Abell 0000-0002-0604-2629

Author Contributions

GWB, MCJW, SWP and ADA conceived the study. KJL, WT, BBR, ASP, JY, AJH, JF, ACM, BN, RM and DC performed the experiments and analyzed the data. KJL and ADA wrote the paper with input from all authors.

Notes

The authors declare no competing financial interests

ACKNOWLEDGMENT

The computational aspects of this work were supported by an award under the National Computational Merit Allocation Scheme (NCMAS) for JY on the National Computing Infrastructure (NCI) National Facility at the Australian National University. The studies were also supported by NHMRC and the Australian Research Council (ARC). SWP is supported by the National Health and Medical Research Council (GN1147538).

REFERENCES

1. Paparella, A. S., Soares da Costa, T. P., Yap, M. Y., Tieu, W., Wilce, M. C., Booker, G. W., Abell, A. D., and Polyak, S. W. (2014) Structure guided design of biotin protein ligase inhibitors for antibiotic discovery, *Curr. Top. Med. Chem.* *14*, 4-20.
2. Duckworth, B. P., Nelson, K. M., and Aldrich, C. C. (2012) Adenylating enzymes in *Mycobacterium tuberculosis* as drug targets, *Curr. Top. Med. Chem.* *12*, 766.
3. Duckworth, B. P., Geders, T. W., Tiwari, D., Boshoff, H. I., Sibbald, P. A., Barry, C. E., 3rd, Schnappinger, D., Finzel, B. C., and Aldrich, C. C. (2011) Bisubstrate adenylation inhibitors of biotin protein ligase from *Mycobacterium tuberculosis*, *Chem. Biol.* *18*, 1432-1441.
4. Samols, D., Thornton, C. G., Murtif, V. L., Kumar, G. K., Haase, F. C., and Wood, H. G. (1988) Evolutionary conservation among biotin enzymes, *Journal of Biological Chemistry* *263*, 6461-6464.
5. Bagautdinov, B., Kuroishi, C., Sugahara, M., and Kunishima, N. (2005) Crystal structures of biotin protein ligase from *Pyrococcus horikoshii* OT3 and its complexes: structural basis of biotin activation, *Journal of Molecular Biology* *353*, 322-333.

6. Paparella, A. S., da Costa, T. P. S., Yap, M. Y., Tieu, W., Wilce, M. C. J., Booker, G. W., Abell, A. D., and Polyak, S. W. (2014) Structure Guided Design of Biotin Protein Ligase Inhibitors for Antibiotic Discovery, *Curr Top Med Chem* 14, 4-20.
7. Abbott, J., and Beckett, D. (1993) Cooperative binding of the Escherichia coli repressor of biotin biosynthesis to the biotin operator sequence, *Biochemistry* 32, 9649-9656.
8. Rodionov, D. A., Mironov, A. A., and Gelfand, M. S. (2002) Conservation of the Biotin Regulon and the BirA Regulatory Signal in Eubacteria and Archaea, *Genome Research* 12, 1507-1516.
9. Beckett, D. (2009) Biotin sensing at the molecular level, *The Journal of Nutrition* 139, 167-170.
10. da Costa, T. P. S., Tieu, W., Yap, M. Y., Pendini, N. R., Polyak, S. W., Pedersen, D. S., Morona, R., Turnidge, J. D., Wallace, J. C., Wilce, M. C. J., Booker, G. W., and Abell, A. D. (2012) Selective inhibition of Biotin Protein Ligase from Staphylococcus aureus, *J Biol Chem* 287, 17823-17832.
11. Tieu, W., Polyak, S. W., Paparella, A. S., Yap, M. Y., Soares da Costa, T. P., Ng, B., Wang, G., Lumb, R., Bell, J. M., Turnidge, J. D., Wilce, M. C., Booker, G. W., and Abell, A. D. (2015) Improved Synthesis of Biotinol-5'-AMP: Implications for Antibacterial Discovery, *Acs Med Chem Lett* 6, 216-220.
12. Bagautdinov, B., Matsuura, Y., Bagautdinova, S., and Kunishima, N. (2008) Protein biotinylation visualized by a complex structure of biotin protein ligase with a substrate, *J Biol Chem* 283, 14739-14750.
13. Ma, Q. J., Akhter, Y., Wilmanns, M., and Ehebauer, M. T. (2014) Active site conformational changes upon reaction intermediate biotinyl-5'-AMP binding in biotin protein ligase from Mycobacterium tuberculosis, *Protein Science* 23, 932-939.
14. Tieu, W., da Costa, T. P. S., Yap, M. Y., Keeling, K. L., Wilce, M. C. J., Wallace, J. C., Booker, G. W., Polyak, S. W., and Abell, A. D. (2013) Optimising in situ click chemistry: the screening and identification of biotin protein ligase inhibitors, *Chem Sci* 4, 3533-3537.
15. Feng, J., Paparella, A. S., Tieu, W., Heim, D., Clark, S., Hayes, A., Booker, G. W., Polyak, S. W., and Abell, A. D. (2016) New Series of BPL Inhibitors To Probe the Ribose-Binding Pocket of Staphylococcus aureus Biotin Protein Ligase, *Acs Med Chem Lett* 7, 1068-1072.
16. Paparella, A. S., Lee, K. J., Hayes, A. J., Feng, J. G., Feng, Z. K., Cini, D., Deshmukh, S., Booker, G. W., Wilce, M. C. J., Polyak, S. W., and Abell, A. D. (2018) Halogenation of Biotin Protein Ligase Inhibitors Improves Whole Cell Activity against Staphylococcus aureus, *ACS infectious diseases* 4, 175-184.
17. Duckworth, B. P., Geders, T. W., Tiwari, D., Boshoff, H. I., Sibbald, P. A., Barry, C. E., Schnappinger, D., Finzel, B. C., and Aldrich, C. C. (2011) Bisubstrate Adenylation Inhibitors of Biotin Protein Ligase from Mycobacterium tuberculosis, *Chem Biol* 18, 1432-1441.
18. Bockman, M. R., Kalinda, A. S., Petrelli, R., De la Mora-Rey, T., Tiwari, D., Liu, F., Dawadi, S., Nandakumar, M., Rhee, K. Y., Schnappinger, D., Finzel, B. C., and Aldrich, C. C. (2015) Targeting Mycobacterium tuberculosis Biotin Protein Ligase (MtBPL) with Nucleoside-Based Bisubstrate Adenylation Inhibitors, *J Med Chem* 58, 7349-7369.
19. Bockman, M. R., Engelhart, C. A., Dawadi, S., Larson, P., Tiwari, D., Ferguson, D. M., Schnappinger, D., and Aldrich, C. C. (2018) Avoiding Antibiotic Inactivation in Mycobacterium tuberculosis by Rv3406 through Strategic Nucleoside Modification, *ACS infectious diseases* 4, 1102-1113.
20. Tiwari, D., Park, S. W., Essawy, M. M., Dawadi, S., Mason, A., Nandakumar, M., Zimmerman, M., Mina, M., Ho, H. P., Engelhart, C. A., Ioerger, T., Sacchettini, J. C., Rhee, K., Ehrt, S., Aldrich, C. C., Dartois, V., and Schnappinger, D. (2018) Targeting protein biotinylation enhances tuberculosis chemotherapy, *Sci Transl Med* 10.
21. Soares da Costa, T. P., Tieu, W., Yap, M. Y., Zvarec, O., Bell, J. M., Turnidge, J. D., Wallace, J. C., Booker, G. W., Wilce, M. C., and Abell, A. D. (2012) Biotin analogues with antibacterial activity are potent inhibitors of biotin protein ligase, *ACS Medicinal Chemistry Letters* 3, 509-514.
22. Davies, B., and Morris, T. (1993) Physiological-Parameters in Laboratory-Animals and Humans, *Pharmaceut Res* 10, 1093-1095.
23. Toutain, P. L., and Bousquet-Melou, A. (2004) Plasma clearance, *J Vet Pharmacol Ther* 27, 415-425.

24. Paparella, A. S., Lee, K. J., Hayes, A. J., Feng, J., Feng, Z., Cini, D., Deshmukh, S., Booker, G. W., Wilce, M. C. J., Polyak, S. W., and Abell, A. D. (2018) Halogenation of Biotin Protein Ligase Inhibitors Improves Whole Cell Activity against *Staphylococcus aureus*, *ACS infectious diseases* 4, 175-184.
25. McPhillips, T. M., McPhillips, S. E., Chiu, H. J., Cohen, A. E., Deacon, A. M., Ellis, P. J., Garman, E., Gonzalez, A., Sauter, N. K., Phizackerley, R. P., Soltis, S. M., and Kuhn, P. (2002) Blu-Ice and the Distributed Control System: software for data acquisition and instrument control at macromolecular crystallography beamlines, *Journal of Synchrotron Radiation* 9, 401-406.
26. Kabsch, W. (2010) Xds, *Acta Crystallogr D Biol Crystallogr* 66, 125-132.
27. Evans, P. R., and Murshudov, G. N. (2013) How good are my data and what is the resolution?, *Acta Crystallogr D Biol Crystallogr* 69, 1204-1214.
28. McCoy, A. J., Grosse-Kunstleve, R. W., Adams, P. D., Winn, M. D., Storoni, L. C., and Read, R. J. (2007) Phaser crystallographic software, *J Appl Crystallogr* 40, 658-674.
29. Emsley, P., Lohkamp, B., Scott, W. G., and Cowtan, K. (2010) Features and development of Coot, *Acta Crystallographica Section D-Biological Crystallography* 66, 486-501.
30. Afonine, P. V., Grosse-Kunstleve, R. W., Echols, N., Headd, J. J., Moriarty, N. W., Mustyakimov, M., Terwilliger, T. C., Urzhumtsev, A., Zwart, P. H., and Adams, P. D. (2012) Towards automated crystallographic structure refinement with phenix.refine, *Acta Crystallogr. D Biol. Crystallogr.* 68, 352-367.
31. Winn, M. D., Isupov, M. N., and Murshudov, G. N. (2001) Use of TLS parameters to model anisotropic displacements in macromolecular refinement, *Acta Crystallogr. D Biol. Crystallogr.* 57, 122-133.

SUPPORTING INFORMATION

Sulfonamide-based inhibitors of biotin protein ligase as new antibiotic leads

Kwang Jun Lee,^{†#} William Tieu,[†] Beatriz Blanco Rodriguez,[†] Ashleigh S. Paparella,[‡] Jingxian Yu,^{†#}
Andrew J. Hayes,[‡] Jiage Feng,[†] Andrew C. Marshall,[‡] Ben Noll,[¶] Robert Milne,[¶] Danielle Cini,[§]
Matthew C. J. Wilce,[§] Grant W. Booker,[‡] John B. Bruning,^{||} Steven W. Polyak,[‡] and Andrew D. Abell^{†#}

[†] Department of Chemistry, School of Physical Sciences, University of Adelaide, Adelaide, South Australia 5005, Australia

[‡] Department of Molecular and Cellular Biology, School of Biological Sciences, University of Adelaide, South Australia 5005, Australia

[¶] School of Pharmacy & Medical Sciences, University of South Australia, Adelaide, South Australia 5000, Australia

[§] Department of Biochemistry, School of Biomedical Science, Monash University, Victoria 3800, Australia

[#] Centre for Nanoscale BioPhotonics (CNBP), University of Adelaide, Adelaide, South Australia 5005, Australia

^{||} Institute of Photonics and Advanced Sensing (IPAS), School of Biological Sciences, University of Adelaide, South Australia 5005, Australia

FIGURE S1	2
FIGURE S2	2
FIGURE S3	3
FIGURE S4	4
FIGURE S5	5
FIGURE S6	6
TABLE S1	7
TABLE S2	8
HYBRID QM/MM MOLECULAR DYNAMICS SIMULATIONS	9
QM/MM-GBSA BINDING FREE ENERGY CALCULATIONS	10
CHEMISTRY	11
REFERENCES	14

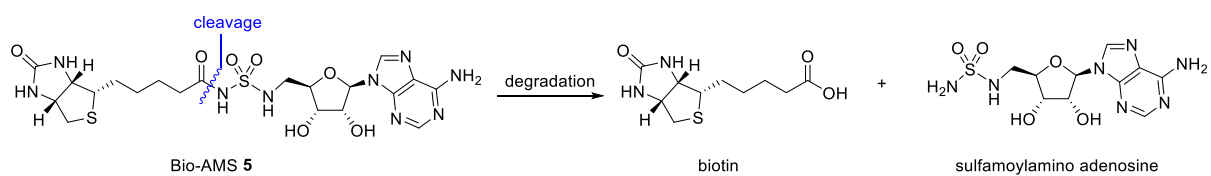


Figure S1. Major metabolites of Bio-AMS 5 in mice.

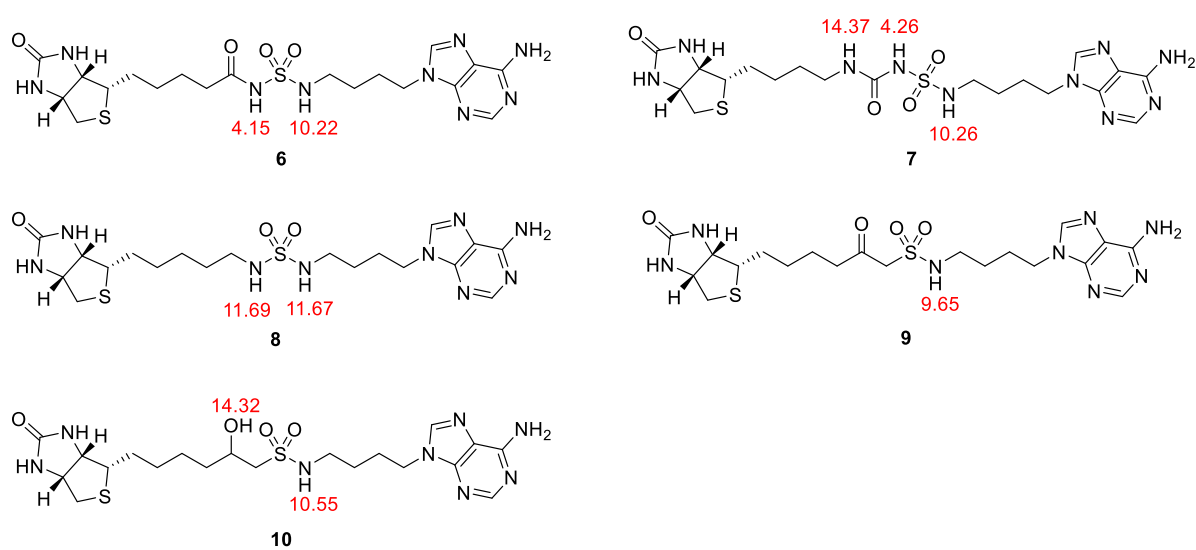
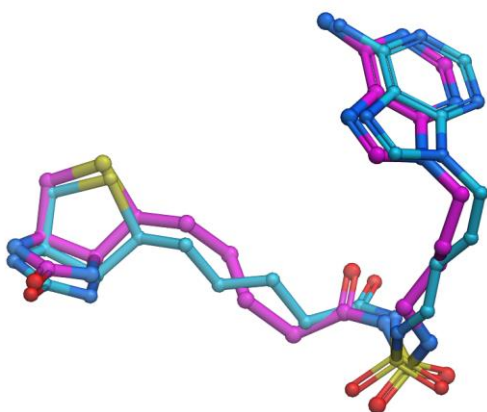


Figure S2. pK_a prediction of sulfonamide linkage of analogues 6 - 10 using Marvin from ChemAxon.¹

¹ MarvinSketch, version 18.19.0; ChemAxon: Budapest, 2018

A



B

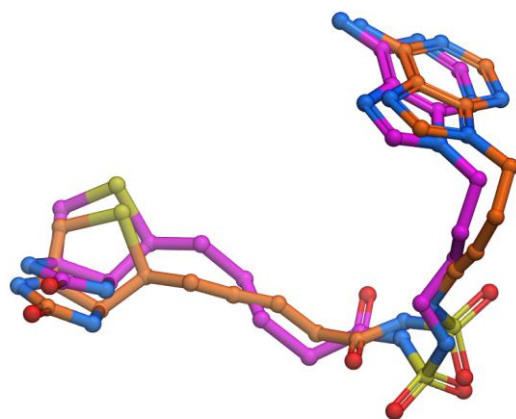


Figure S3. (A) Superposition of the time-averaged conformation of deprotonated form of **6** (cyan) with the cocrystal structure of **6** bound to SaBPL (magenta) - (RMSD - 0.62 Å). (B) Superposition of the time-averaged conformation of protonated form of **6** (orange) with the cocrystal structure of **6** bound to SaBPL (magenta) - (RMSD - 1.13 Å).

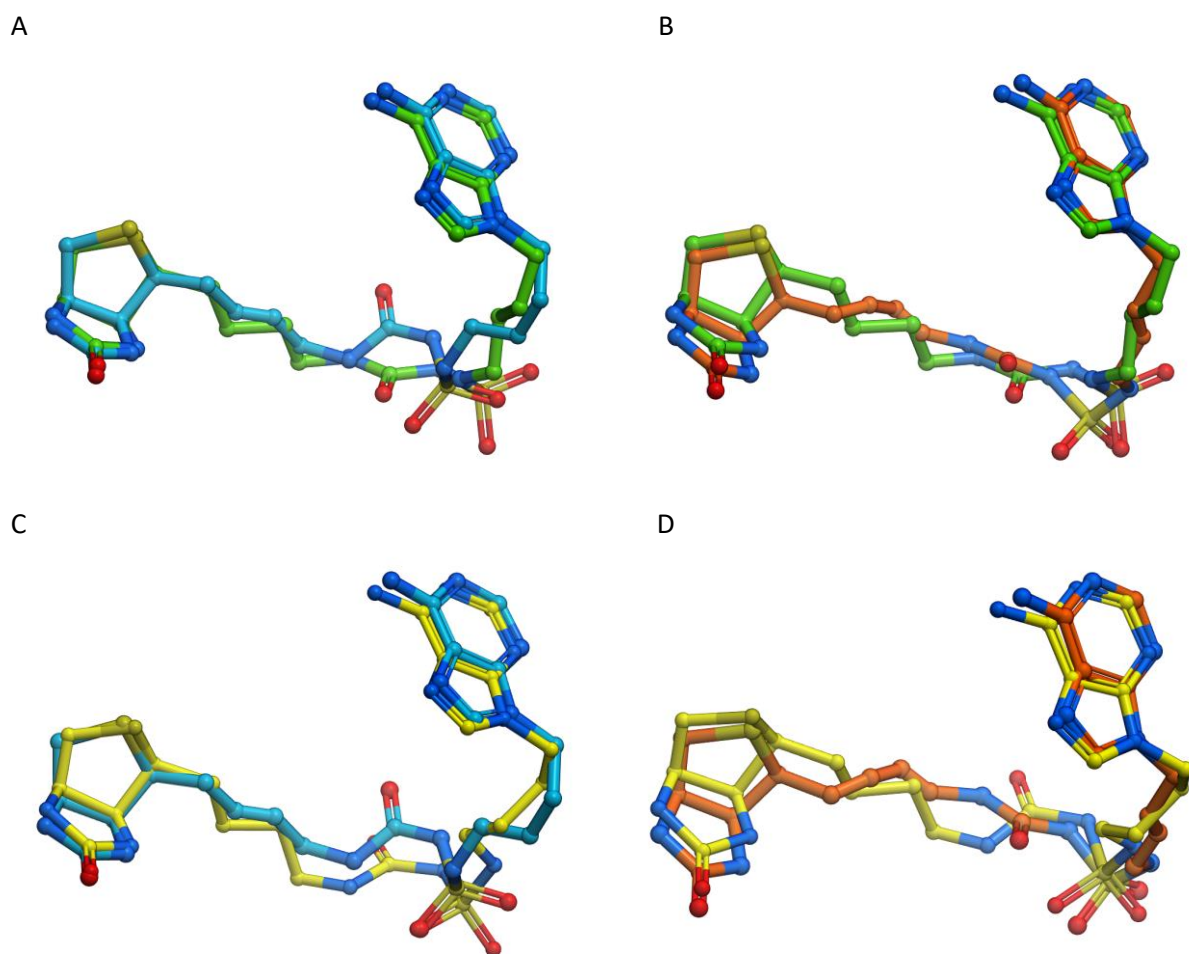


Figure S4. (A) Superposition of the time-averaged conformation of deprotonated form of **7** (cyan) with the major conformer of **7** bound to *SaBPL* (green) - (RMSD - 1.02 Å). (B) Superposition of the time-averaged conformation of protonated form of **7** (orange) with the major conformer of **7** bound to *SaBPL* (green) - (RMSD - 0.86 Å). (C) Superposition of the time-averaged conformation of deprotonated form of **7** (cyan) with the minor conformer of **7** bound to *SaBPL* (yellow) - (RMSD - 0.78 Å). (D) Superposition of the time-averaged conformation of protonated form of **7** (orange) with the minor conformer of **7** bound to *SaBPL* (yellow) - (RMSD - 0.98 Å).

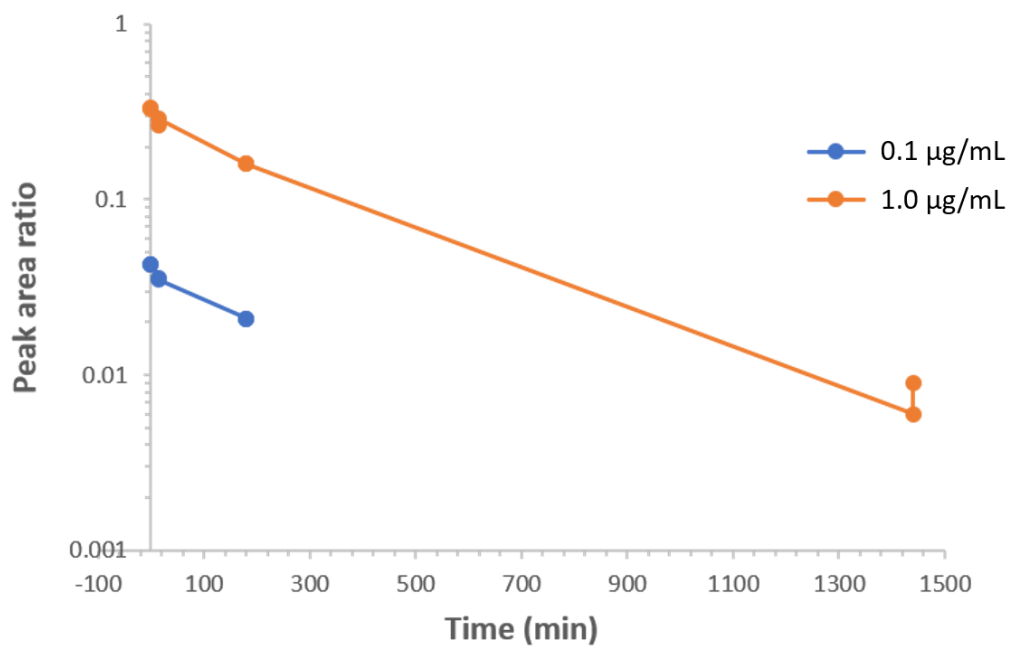
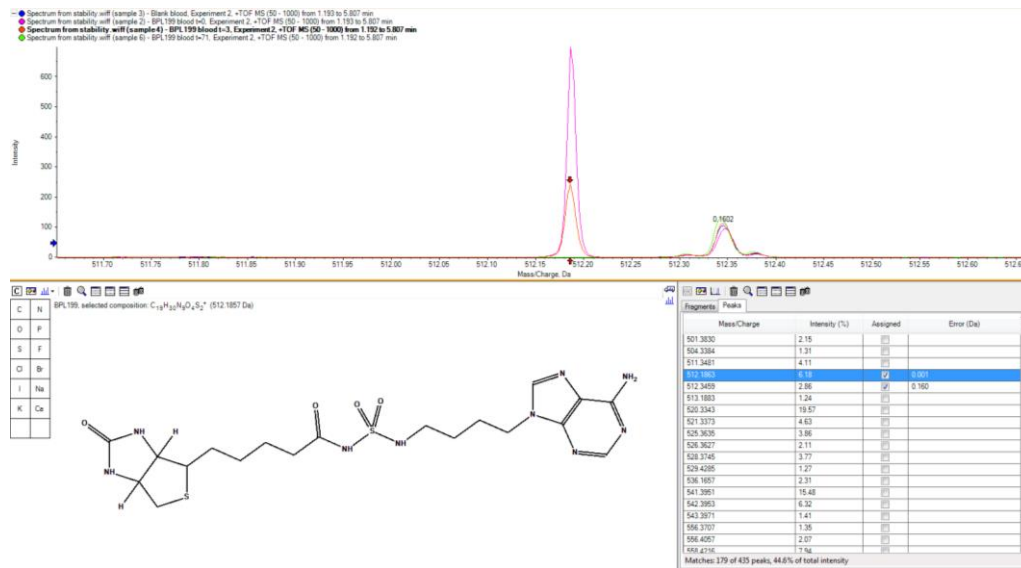


Figure S5. Change in the ratio of the peak responses to acylsulfamide **6** to internal standard against incubation time in blood.

A



B

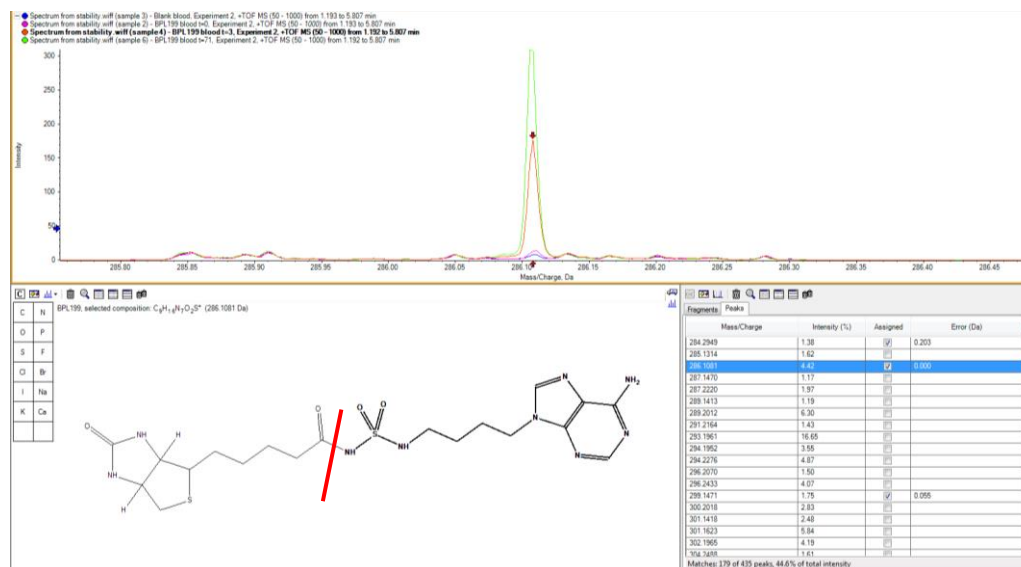


Figure S6. Peak responses for acylsulfamide **6** (A) and its decomposition product (B) at time 0 (purple lines), 3 h (red) and 71 h (green) from the commencement of the incubation of acylsulfamide **6** in rat blood. The solid red line indicates the proposed site for cleavage of acylsulfamide **6**.

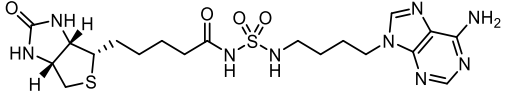
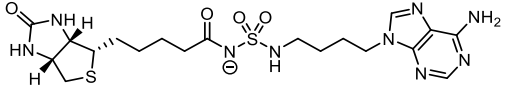
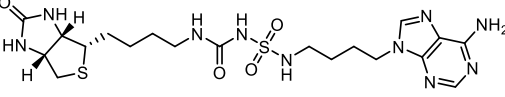
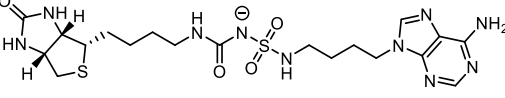
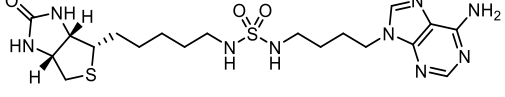
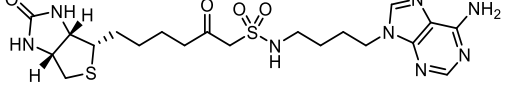
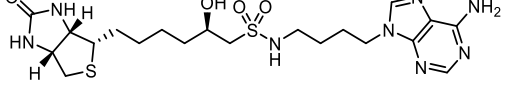
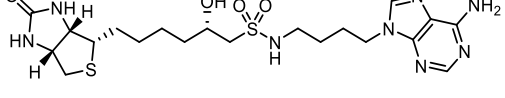
Table S1. Data collection and refinement statistics (molecular replacement).

	<i>Sa</i> BPL + 6 (PDB: 6ORU)	<i>Sa</i> BPL + 7 (PDB: 6NDL)
Data collection^a	MX1 Beamline Australian Synchrotron	MX1 Beamline Australian Synchrotron
Space group	<i>P</i> 4 ₂ 2 ₁ 2	<i>P</i> 4 ₂ 2 ₁ 2
Cell dimensions		
<i>a</i> , <i>b</i> , <i>c</i> (Å)	92.5, 92.5, 129.0	94.0, 94.0, 131.0
α , β , γ (°)	90.0, 90.0, 90.0	90.0, 90.0, 90.0
Wavelength (Å)	0.95	0.95
Resolution (Å)	45.93 - 2.392 (2.478 - 2.392) ^b	46.66 – 2.00 (2.05 – 2.00) ^b
<i>R</i> _{merge}	0.02762 (0.4816)	0.129 (6.729)
<i>CC</i> (1/2)	0.997 (0.959)	1.000 (0.204)
<i>I</i> / σ <i>I</i>	15.65 (1.49)	16.1 (0.7)
Completeness (%)	99.94 (99.96)	100.0 (100.0)
Redundancy	2.0 (2.0)	28.4 (29.5)
Refinement		
Resolution (Å)	45.93 - 2.39	46.66 – 2.00
No. reflections	22803	40340
<i>R</i> _{work} / <i>R</i> _{free}	0.2069/0.2607 (0.3157/0.3536)	0.1693 (0.3650) / 0.2193 (0.3705)
No. atoms		
Protein	2610	2622
Ligand	34	35
Glycerol	-	36
Water	43	347
Average <i>B</i> -factors (Å ²)		
Protein	78.80	67.2
Ligand	95.80	51.9
Glycerol	-	101.7
Water	58.70	78.7
RMS deviations		
Bond lengths (Å)	0.017	0.007
Bond angles (°)	1.56	0.870

^a Diffraction data were collected from one crystal for each structure.

^b Values in parentheses are for highest-resolution shell.

Table S2. QM/MM-GBSA binding free energy calculations.

Compound	Structure	$\Delta G_{\text{QM/MM-GBSA}}$ (kcal/mol)
Protonated 6		-68.59
Deprotonated 6		-73.57
Protonated 7		-62.80
Deprotonated 7		-81.27
8		-71.28
9		-69.01
<i>R</i> form of 10		-65.46
<i>S</i> form of 10		-70.10

HYBRID QM/MM MOLECULAR DYNAMICS SIMULATIONS

Molecular dynamics simulations were performed for the protein-ligand complexes using the Sander algorithm as implemented in Amber 16 package,¹ with the ligand molecule treated by the semi-empirical PM6-DH+ method while the protein (*Sa*BPL) by the Amber ff14SB force fields.

Structure preparation. Initial geometry for the complex of *Sa*BPL with **6** was taken from the X-ray crystallographic data revealed in this study. The complexes with other ligands were constructed by modifying the ligand molecule in the *Sa*BPL-**6** crystal structure (PDB code: 6ORU), as these ligands are structurally analogous to **6**. In case of deprotonated **6** and **7**, the involved proton was removed. Charge and spin multiplicity were manually specified for each ligand and their deprotonated state. The LEaP program from Antechamber tools (AmberTools 17) was used to prepare the parameter/topology (.top) and input coordinate (.crd) files. The net charge of each protein-ligand complex was neutralized by adding Na⁺ ions at positions of high negative electron potential around the complex. The system was immersed in a truncated octahedral box of pre-equilibrated TIP3P water molecules, ensuring that no atoms in the protein-ligand complex were closer than 12 Å to any of the sides of the water box. The solvent molecules and counter-ions were firstly minimized for 6000 steps (involving 1000 of the steepest decent steps and 5000 of conjugate gradient steps) to remove any bad steric contacts with the complexes, whereby the protein and ligand were position-restrained using a force constant of 100 kcal·mol⁻¹·Å⁻². This was followed by additional 6000-step energy minimization without any restriction.

Heating and production phases. MD simulation was carried out for the heating phase, under a constant volume periodic boundary condition with an initial temperature of 0 K, allowing to heat up to 300 K over 40 ps. The final production simulation was carried out under an NVT ensemble condition. The following settings were activated throughout the heating and production phases: The Langevin dynamics was used to control the temperature using a collision frequency of 1.0 ps⁻¹ and 0.5 ps coupling time constant. The SHAKE algorithm was used to constrain bonds involving hydrogen, allowing time step of 2 fs, for a total of 2500000 steps (5 ns). The default particle mesh Ewald (PME) method was employed to compute the long range electrostatic interactions using a 1.0 Å grid space and a fourth-order spline for interpolation. The non-bonded cutoff value was set to 10 Å in the QM and MM regions. In the production runs, the MD trajectory was written for every 50 steps, resulting in 50000 frames for subsequent time-averaged structures and QM/MM-GBSA analyses.

Time-averaged structures. Time-averaged structures were calculated from 40000 trajectory frames (final 4 ns) of the production phase using the Cptraj program in AmberTools 17, with the water molecules and counter-ions stripped.

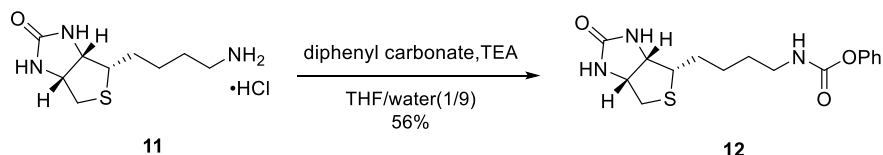
QM/MM-GBSA BINDING FREE ENERGY CALCULATIONS

The binding free energies of ligands to SaBPL were calculated using MMPBSA.py² in AmberTools 17. For each complex, we calculated the ΔG_{bind} values for the 200 snapshots of the MD trajectory (one snapshot for each 20 ps during the last 4 ns of the stable trajectory) and the final ΔG_{bind} value was the average of the calculated ΔG_{bind} values for these snapshots. Specifically, the python utility ante-MMPBSA.py was used to prepare the complex, protein and ligand topology files from the topology file of the solvated complex, by setting radii=mbondi2 and stripping water molecules (and counterions). The default MM-GBSA parameters α , β , and γ have the values of 1.0, 0.8, and 4.85 respectively. The ligand was treated as the QM region using the semi-empirical PM6-DH+ Hamiltonian theory. As only one MD simulation for each complex was performed, this method is less computationally demanding and leads to an increase of convergence due to cancellation of errors, conformational restraints imposed by the complex geometry, and reduction of noise arising from flexible remote regions relative to the binding site.³

CHEMISTRY

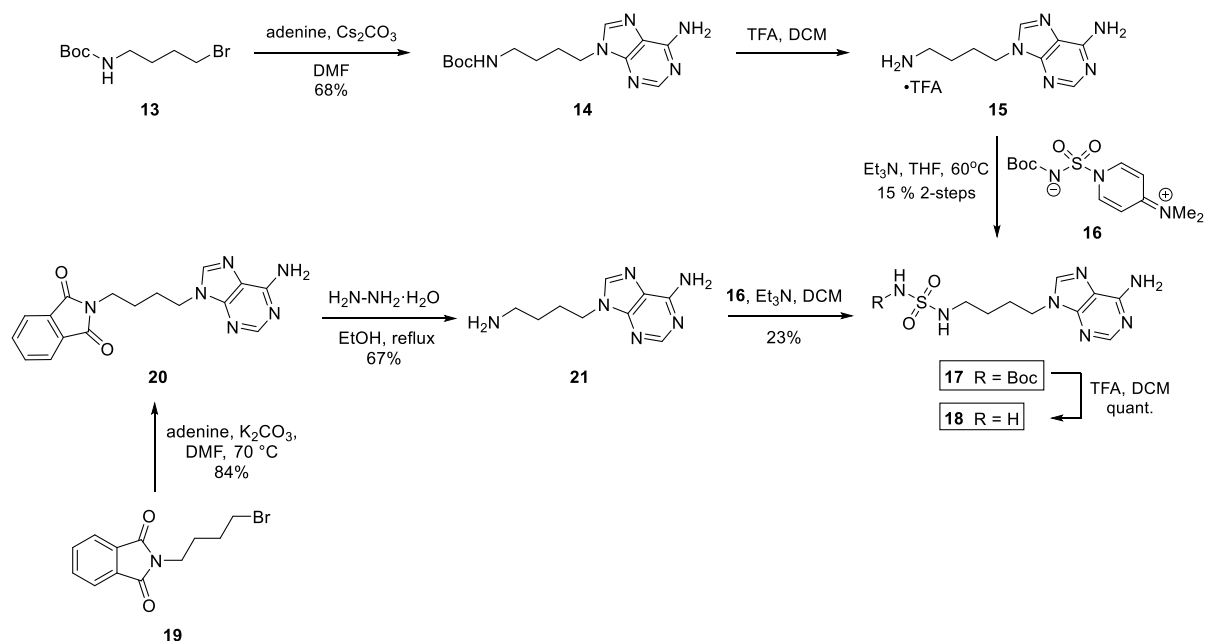
Synthesis

The preparation of **6-8** required preparation of the key intermediates **12**, **17**, **18**, and **25** as outlined in **Schemes S1 – S3**. Biotin carbamate **12**, required for the preparation of amino sulfonylurea **7**, was prepared as shown in **Scheme S1**. In particular, biotin amine **11**⁴ was converted into biotin carbamate **12** on reaction with diphenyl carbonate



Scheme S1. Synthesis of biotin carbamate **12**

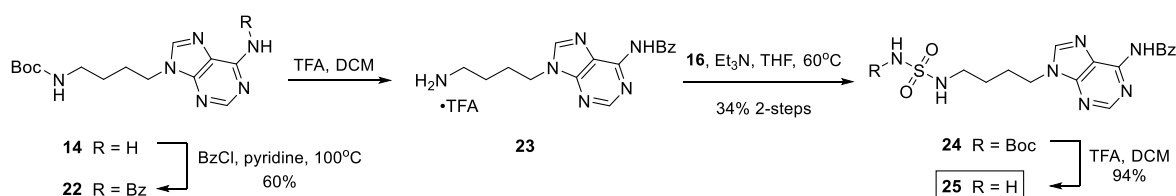
Adenine sulfamides **17** and **18** required for the synthesis of alkylsulfamide **8** and acylsulfamide **6** respectively were prepared as shown in **Scheme S2**. Adenine was alkylated on reaction with caesium carbonate and Boc-protected amino bromide **13**⁵ to give Boc-protected adenine amine **14** in 68% yield. Treatment with TFA in DCM gave the amine salt **15**, which was then reacted with **16**⁶ in THF to give Boc-protected sulfamide **17**. The key starting material **17** could also be prepared via adenine phthalimide **20** in a superior overall yield of 13% as shown in **Scheme S2**. In particular, Adenine was reacted with N-(4-bromobutyl)phthalimide **19** in the presence of K₂CO₃ to give adenine phthalimide **20** in 84% yield. Treatment with hydrazine in ethanol gave adenine amine **21**, which was converted



Scheme S2. Synthesis of adenine sulfamide building blocks **17** and **18**

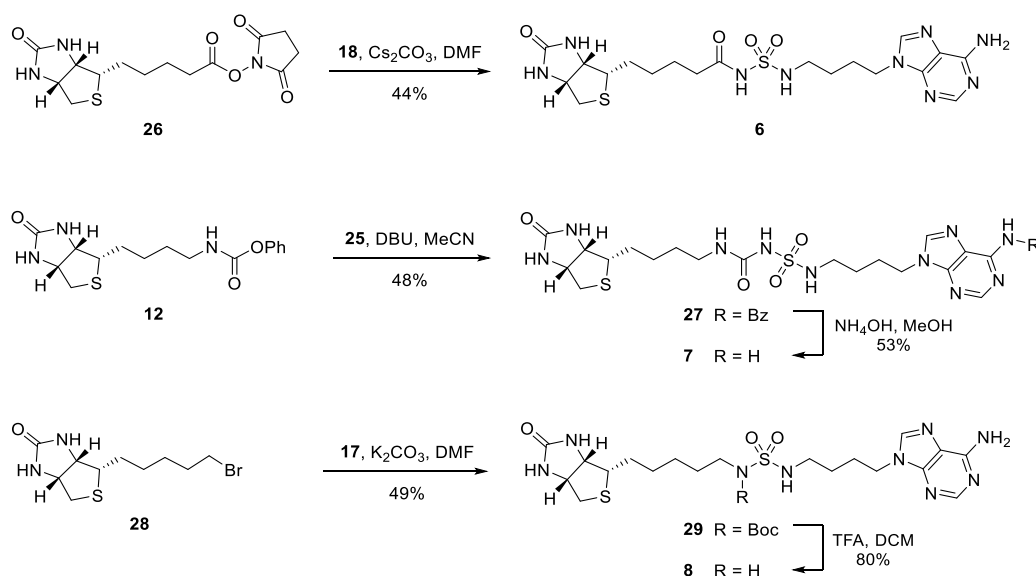
into Boc-protected adenine sulfamide **17** on reaction with **16**⁶ in DCM. Removal of the Boc protecting group from **17**, on reaction with 10% TFA in DCM, gave the desired adenine sulfamide **18** as shown.

Adenine sulfamides **25** required for the synthesis of amino sulfonylurea **7** was prepared as shown in **Scheme S3**. Boc-protected adenine amine **14** was reacted with benzoyl chloride, in the presence of pyridine, to give **22**. This was then treated with TFA in DCM to give adenine amine salt **23**, which was reacted with **16**⁶ in THF to give sulfamide **24** as per the preparation of **17**, see **Scheme S2**. Removal of the Boc group, on reaction with TFA in DCM, then gave the key benzoyl-protected adenine sulfamide **25**.



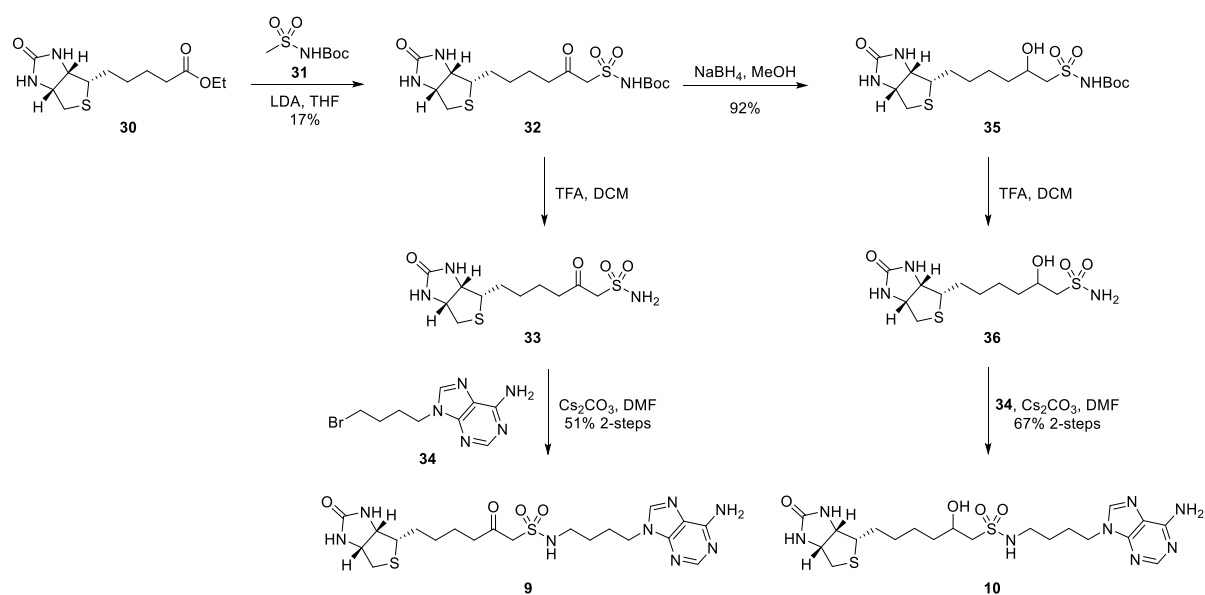
Scheme S3. Synthesis of adenine sulfamide building block **25**

Acylsulfamide **6**, amino sulfonylurea **7**, and alkylsulfamide **8** were next prepared as outlined in **Scheme S4**. In particular, D-(+)-biotin *N*-hydroxysuccinimide ester (Biotin-NHS) **26**⁷ was reacted with adenine sulfamide **18**, in the presence of Cs₂CO₃, to give acylsulfamide **6** in 44% yield. Biotin carbamate **12** was coupled to benzoyl-protected adenine sulfamide **25**, in the presence of DBU, to give benzoyl-protected amino sulfonylurea **27**, the benzoyl group of which was removed on treatment with NH₄OH in MeOH to give amino sulfonylurea **7**. Biotin bromide **28**⁴ was reacted with boc-protected adenine sulfamide **17** in the presence of K₂CO₃ in DMF to give boc-protected alkylsulfamide **29**, which was then treated with TFA in DCM to give alkylsulfamide **8**.



Scheme S4. Synthesis of acylsulfamide **6**, amino sulfonylurea **7**, and alkylsulfamide **8**

The final derivatives, β -ketosulfonamide **9** and β -hydroxysulfonamide **10**, were prepared as summarised in **Scheme S5**. Biotin ester **30**⁸ was coupled to sulphonamide **31**⁹ in the presence of LDA to give *N*-boc- β -ketosulfonamide **32**. Reaction with TFA in DCM then gave the biotin β -ketosulfonamide **33**, which was alkylated with adenine bromide **34**,¹⁰ in the presence of Cs₂CO₃, in DMF to give β -ketosulfonamide **9**. *N*-Boc- β -ketosulfonamide **32** was also reduced with NaBH₄ to give **35**, the boc group of which was removed on treatment with TFA in DCM to give the biotin β -hydroxysulfonamide **36**. Treatment with **34** in the presence of Cs₂CO₃ gave β -hydroxysulfonamide **10** as per the synthesis of β -ketosulfonamide **9**.



Scheme S5. Synthesis of β -ketosulfonamide **9** and β -hydroxysulfonamide **10**

REFERENCES

1. Gotz, A. W., Clark, M. A., and Walker, R. C. (2014) An Extensible Interface for QM/MM Molecular Dynamics Simulations with AMBER, *Journal of Computational Chemistry* 35, 95-108.
2. Miller, B. R., McGee, T. D., Swails, J. M., Homeyer, N., Gohlke, H., and Roitberg, A. E. (2012) MMPBSA.py: An Efficient Program for End-State Free Energy Calculations, *Journal of Chemical Theory and Computation* 8, 3314-3321.
3. Dubey, K. D., Tiwari, R. K., and Ojha, R. P. (2013) Recent Advances in Protein-Ligand Interactions: Molecular Dynamics Simulations and Binding Free Energy, *Current Computer-Aided Drug Design* 9, 518-531.
4. Soares da Costa, T. P., Tieu, W., Yap, M. Y., Zvarec, O., Bell, J. M., Turnidge, J. D., Wallace, J. C., Booker, G. W., Wilce, M. C., Abell, A. D., and Polyak, S. W. (2012) Biotin analogues with antibacterial activity are potent inhibitors of biotin protein ligase, *Acs Med Chem Lett* 3, 509-514.
5. Simonin, J., Vernekar, S. K. V., Thompson, A. J., Hothersall, J. D., Connolly, C. N., Lummis, S. C. R., and Lochner, M. (2012) High-affinity fluorescent ligands for the 5-HT3 receptor, *Bioorg Med Chem Lett* 22, 1151-1155.
6. Winum, J. Y., Toupet, L., Barragan, V., Dewynter, G., and Montero, J. L. (2001) N-(tert-butoxycarbonyl)-N-[4-(dimethylazaniumylidene)-1,4-dihydropyridin-1-ylsulfonyl] azanide: A new sulfamoylating agent. Structure and reactivity toward amines (vol 3, pg 2243, 2001), *Org Lett* 3, 2939-2939.
7. Muhammad, N., Sadia, N., Zhu, C. C., Luo, C., Guo, Z. J., and Wang, X. Y. (2017) Biotin-tagged platinum(IV) complexes as targeted cytostatic agents against breast cancer cells, *Chem Commun* 53, 9971-9974.
8. Goswami, S., and Dey, S. (2006) Directed molecular recognition: design and synthesis of neutral receptors for biotin to bind both its functional groups, *J Org Chem* 71, 7280-7287.
9. Neustadt, B. R. (1994) Facile Preparation of N-(Sulfonyl)Carbamates, *Tetrahedron Lett* 35, 379-380.
10. Tieu, W., da Costa, T. P. S., Yap, M. Y., Keeling, K. L., Wilce, M. C. J., Wallace, J. C., Booker, G. W., Polyak, S. W., and Abell, A. D. (2013) Optimising in situ click chemistry: the screening and identification of biotin protein ligase inhibitors, *Chem Sci* 4, 3533-3537.

Chapter Four

4.1 Introduction

As discussed in chapter one, dethiobiotin synthetase (DTBS) is an enzyme responsible for catalysing a key step in biotin biosynthesis, the conversion of 7,8-diaminopelargonic acid (DAPA) **1.03** to dethiobiotin **1.04**. The DTBS active site consists of three distinct pockets: the DAPA pocket, phosphate-binding loop (P-loop), and nucleoside pocket.

Collaborators at the Department of Molecular and Biomedical Science, University of Adelaide carried out virtual screening in order to identify potential DTBS inhibitors. In particular, twenty-six hits (11 cytidine analogues and 15 ZINC fragments) were predicted to have lower binding energy than CTP by *in silico* screening. Surface plasmon resonance (SPR) binding experiments were carried out on the twenty-six virtual hits to identify 4 cytidine analogues and 7 fragment hits as weak affinity binders. Interestingly, X-ray crystallography identified cyclopentylacetic acid **4.01** as a fragment binding to DAPA binding sites of *Mtb*DTBS (Figure 4.1). Each of the four possible diastereomers (*RS/SR/RR/SS*) of **4.01** were modelled into the crystal structure to see which most closely matched the observed electron density of co-crystal structure of **4.01** with *Mtb*DTBS. *RS trans* isomer exhibited the highest occupancy after refinement (*RS*: 0.51, *SR*: 0.13, *RR*: 0.32, *SS*: 0.34) and the most preferable real-space refinement statistics. It was however impossible to distinguish the stereochemistry of **4.01** with confidence due to the minimal structural differences observed between stereoisomers.

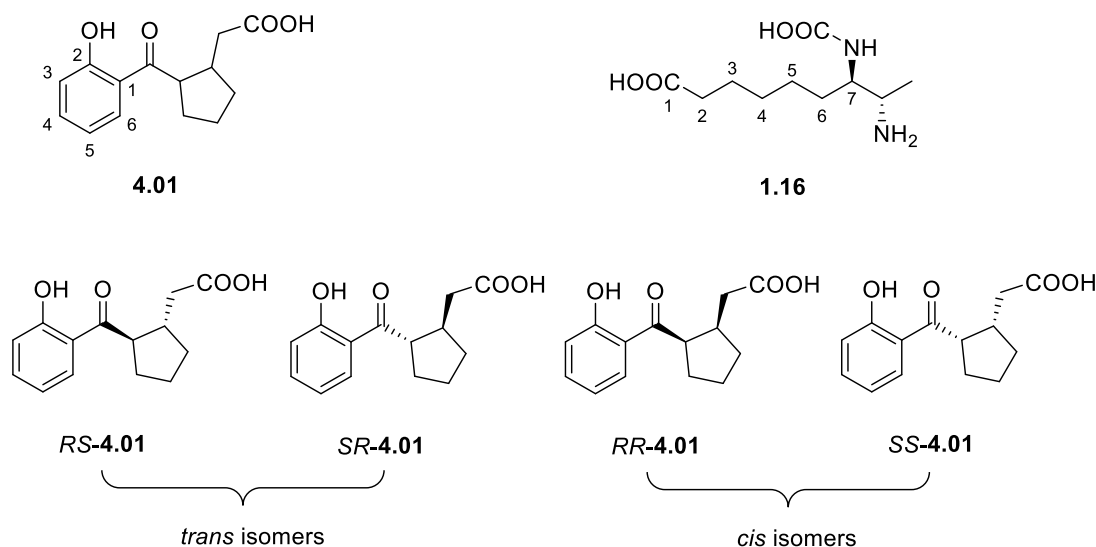
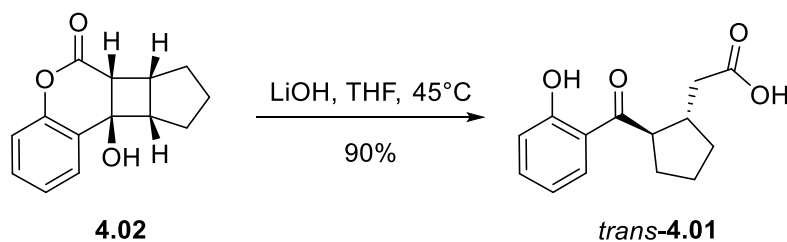


Figure 4.1. Structures of the fragment **4.01** and DAPA carbamate **1.16** binding to *Mtb*DTBS.



Scheme 4.1. Induced degradation of **4.02** to *trans*-**4.01**. Stereochemical configurations are relative.

The *trans* isomers of **4.01** were prepared by Birgit Gaiser (Department of Chemistry, University of Adelaide) as shown in Scheme 4.1. Compound **4.02** was treated with lithium hydroxide in THF/H₂O at 45°C to give *trans*-**4.01**. The *cis*-**4.01** was not isolated under these basic hydrolysis conditions. Binding affinity and X-ray crystallography experiments were then carried out to reveal that *trans*-**4.01** binds predominantly within the DAPA binding pocket of *Mtb*DTBS with $K_D = 3.4 \pm 0.4$ mM (Figure 4.2). The absolute stereochemistry of *trans*-**4.01** could not be definitively identified by crystallography. Consequently, the *SR* and *RS* compounds were simultaneously modelled into ligand bound *Mtb*DTBS. The carboxyl group of *trans*-**4.01** occupies a similar region to the γ -phosphate of CTP, forming interactions observed in its structure bound to *Mtb*DTBS, for example hydrogen bonding to the side chain of Thr11 (2.36 – 2.71Å), Lys15 (2.96 – 3.45Å), amide backbone of Gly111 (3.02 – 3.21Å), and a water molecule. The disubstituted cyclopentane

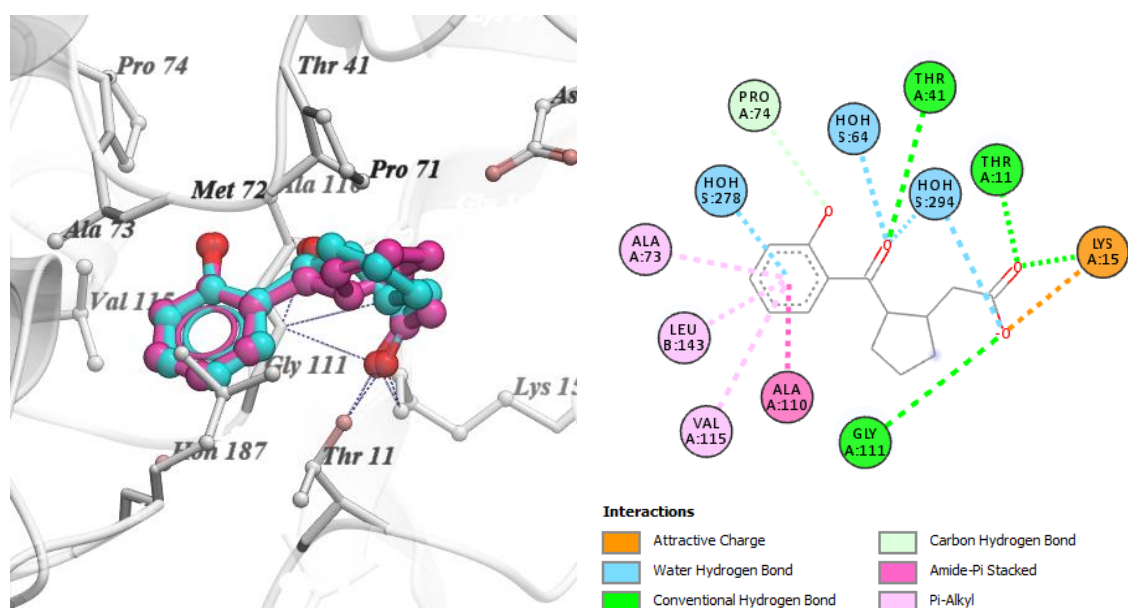


Figure 4.2. 3D depiction of racemic *trans*-**4.01** (*RS*: magenta, *SR*: cyan) bound to *Mtb*DTBS (PDB: 6NMZ) with hydrogen bonds shown in blue dashes (left). 2D interaction diagram of *trans*-**4.01** bound to *Mtb*DTBS with interactions shown in dashes (right).

ring of *trans*-**4.01** overlaps with the amine terminus of DAPA carbamate **1.16**, whilst the aromatic ring lies in the hydrophobic tunnel normally home to the alkyl chain of DAPA carbamate **1.16**. This observation suggests that the DAPA pocket can accommodate larger, more complex structures than a simple alkyl chain.

4.2 Design and synthesis of DAPA pocket binders

The design of DAPA pocket binders, shown in Figure 4.3 and discussed in this chapter, was based on the co-crystal structure of *trans*-**4.01** bound to *Mtb*DTBS. A single *RS*-isomer of *trans*-**4.01** in the co-crystal structure was chosen to simplify the analysis. An overlay of *RS*-**4.01** with DAPA carbamate **1.16** bound to *Mtb*DTBS indicates that C4 on the benzene ring of *RS*-**4.01** superimposes well with C3 of alkyl chain of DAPA carbamate **1.16** (Figure 4.1 and 4.4). This suggests that appending carboxyl or carboxymethyl groups at C4 position on the aromatic ring of *RS*-**4.01** would mimic the interactions made between the DAPA carboxyl group and residues Gly144, Leu146 and Asn147 of the adjacent *Mtb*DTBS subunit, see structures **4.03** and **4.05**.

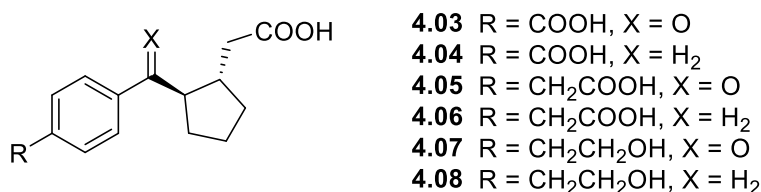


Figure 4.3. Proposed cyclopentylacetic acid analogues **4.03** – **4.08**. Stereochemical configuration is relative.

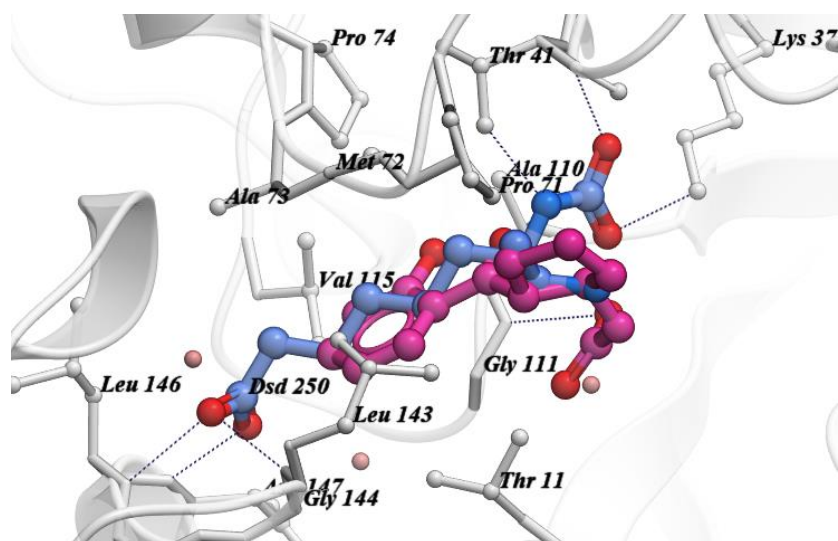


Figure 4.4. Overlay of DAPA carbamate **1.16** (blue)¹ and *RS*-**4.01** (magenta) binding to *Mtb*DTBS with hydrogen bonds shown in blue dashes.

The proposed cyclopentylacetic acid analogues **4.03** – **4.08** were docked with the X-ray crystal structure of *Mtb*DTBS in complex with *trans*-**4.01** by ICM software version 3.8-7, and results are discussed below in section 4.2.1, in order to predict and visualise the binding modes of these analogues. Key features of proposed cyclopentylacetic acid analogues **4.03** – **4.08** are summarised below.

1. None of the proposed compounds (**4.03** – **4.08**) contains the *o*-phenol group of *RS*-**4.01**. This group does not seem to be important for binding to *Mtb*DTBS as no strong interaction is found between the residues of the binding pocket and the *o*-phenol group.
2. Cyclopentylacetic acids **4.03**, **4.05**, and **4.07** contain *p*-carboxyl, *p*-carboxymethyl, or *p*-hydroxyethyl group respectively on the benzene ring. This is to explore potential hydrogen bonds between these functional groups and Leu146 and/or Asn147 of the binding pocket. An overlay of *RS*-**4.01** and DAPA carbamate **1.16** bound to *Mtb*DTBS, as shown in Figure 4.4, suggests introducing these substitution groups to increase the binding affinity toward *Mtb*DTBS.
3. Compounds **4.04**, **4.06**, and **4.08** lack the ketone functionality of compounds **4.03**, **4.05**, and **4.07**. This allows to probe the importance of this group in the DAPA binding site.

4.2.1 Docking

Structures **4.03** – **4.08** (*RS* isomer) and the bound ligand *RS*-**4.01** of the protein *Mtb*DTBS were docked using ICM software version 3.8-7 (Molsoft L.L.C., San Diego, CA, USA) in order to examine whether appended functional groups at C4 position on the aromatic ring of *RS*-**4.01** are able to interact with Gly144, Leu146 and Asn147, and also if appending these functional groups alters the entire binding conformation. Proteins for docking were retrieved from *Mtb*DTBS in complex with *trans*-**4.01** (PDB: 6NMZ). Formal charges were assigned, protonation states of histidines were adjusted, and hydrogens, histidine, glutamine, and asparagine were optimized using the protein preparation procedure implemented in ICM.² The original bound ligand *trans*-**4.01** and all water molecules were removed from the binding site before docking. The binding site was defined as the cavity enclosed by residues with at least one non-hydrogen atom within a 4.0 Å cut-off radius from the ligand *trans*-**4.01**. The pocket was represented by 0.5 Å grid maps accounting for hydrogen bonding, hydrophobic, van der Waals, and electrostatic interactions. All molecules were flexibly docked into the rigid binding site and scored based on the ICM scoring function.

The docking protocol was first validated by removing bound ligand (*trans*-**4.01**, Figure 4.2 left) from its co-crystal structure with *Mtb*DTBS, followed by redocking into the vacated enzyme. A low value of root-mean-square deviation of atomic positions (RMSD) is a good indicator of appropriate docking accuracy and values below 2 Å are generally considered acceptable. The RMSD value of the top-scoring pose in this study was 0.35 Å. As shown in Figure 4.5, the predicted binding conformation of *RS*-**4.01** (yellow) superimposes well with the obtained ligand from the X-ray crystallography (magenta), suggesting that these docking parameters are amenable to docking studies of the proposed cyclopentylacetic acid analogues **4.03** – **4.08**.

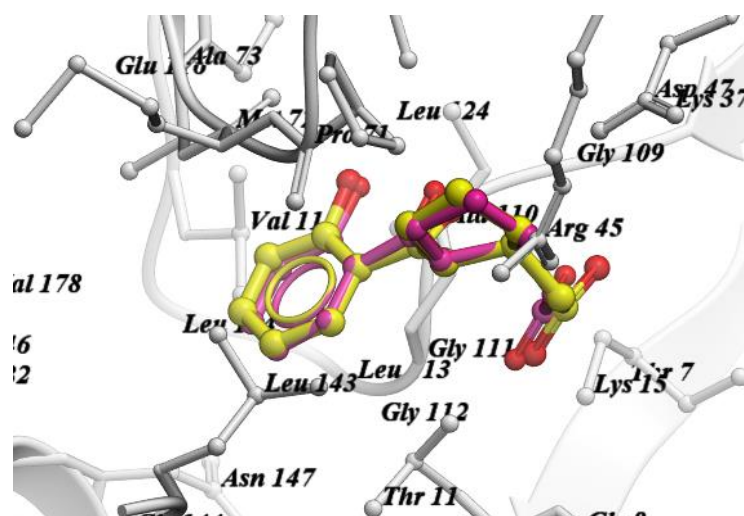


Figure 4.5. A superimposed image of the predicted binding conformation of *RS*-**4.01** (yellow) with the original bound ligand (magenta).

Final docked conformations were ranked by ICM scoring function and the conformation with the highest ranking was selected to compare and overlay with the original bound ligand *RS*-**4.01**. The overlaid images for compounds **4.03** – **4.08** (*RS* isomer) are listed in Figure 4.6. All docked structures adopt essentially the same geometrical orientation as was observed with the original ligand *RS*-**4.01** bound to *Mtb*DTBS, suggesting that the cyclopentylacetic acid analogues **4.03** – **4.08** can bind to DAPA binding pockets. In particular, *p*-carboxyl, *p*-carboxymethyl, and *p*-hydroxyethyl on the benzene ring of all docked compounds occupied the binding region of carboxylic acid group of DAPA carbamate **1.16**. This then maximizes binding interactions with Leu146 and/or Asn147. Thus, the proposed analogues **4.03** – **4.08** were expected to have more binding interactions with *Mtb*DTBS than *trans*-**4.01**, suggesting that these proposed analogues may possess improved binding affinities over *trans*-**4.01**.

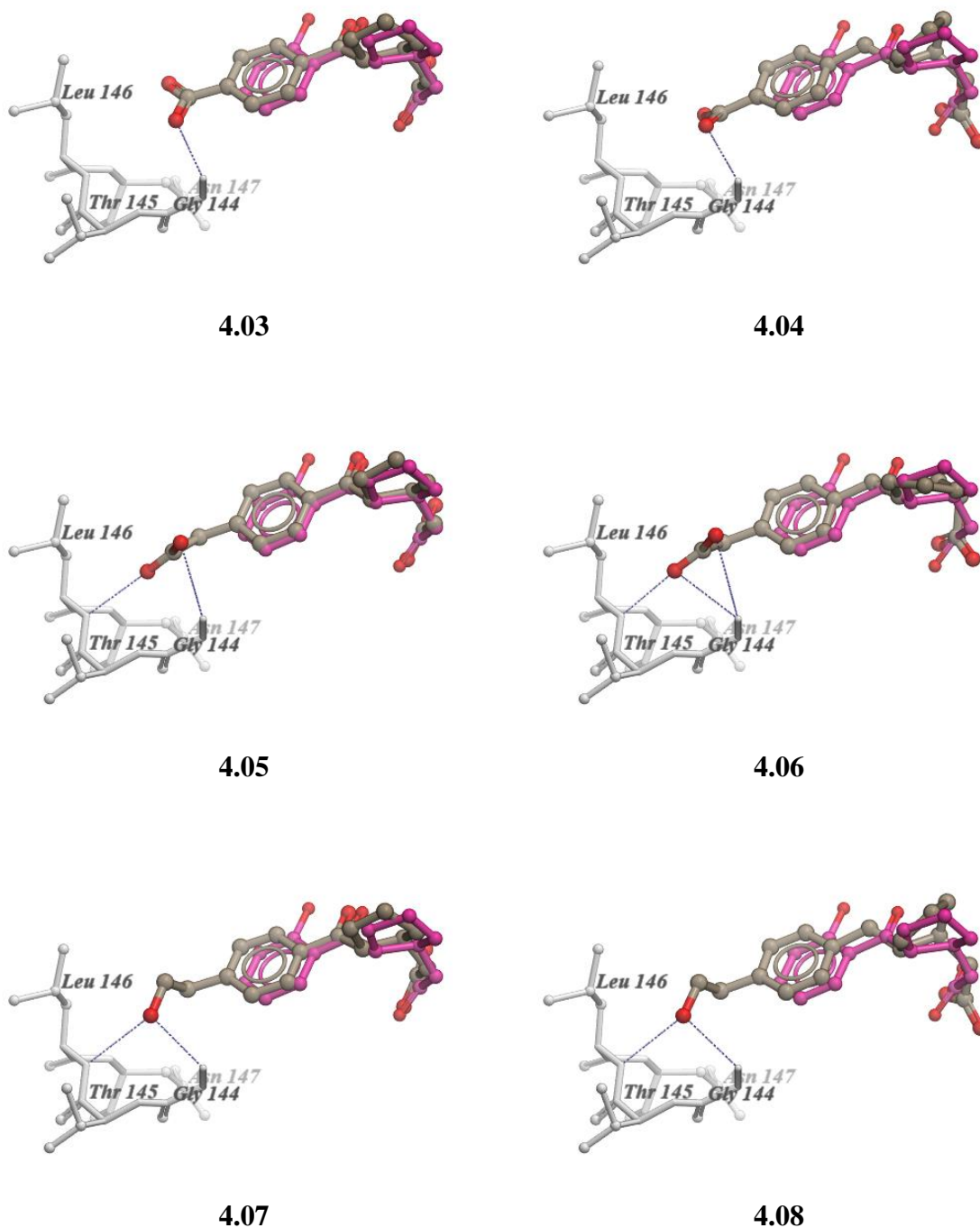


Figure 4.6. Superimposed images of the proposed cyclopentylacetic acid analogues **4.03** – **4.08** (*RS* isomer, grey) with the original bound ligand *RS*-**4.01** (magenta). Hydrogen bonds are depicted by blue dashes.

4.2.2 Synthesis of *trans*-**4.01**

The *trans*-**4.01** compounds were prepared from **4.02** as shown in Scheme 4.1. However, this synthetic method is not only inefficient, but is also inapplicable to the synthesis of the proposed compounds **4.03** - **4.08** since each derivative requires a variant of **4.02** as starting materials. An alternative and more widely applicable approach to *trans*-**4.01** was therefore

investigated. This new synthetic strategy toward *trans*-**4.01** was based on the retrosynthetic analysis outlined in Figure 4.7. Tentatively, the target compound *trans*-**4.01** could be obtained from 2-bromoanisole **4.13** and cyclopent-1-enecarbaldehyde **4.14** via an organometallic addition reaction to generate the corresponding alcohol **4.12**. Subsequent conversion of the hydroxyl group to the corresponding ketone, as shown in **4.11**, would enable introduction of the required malonic acid moiety via Michael addition. Both *cis* and *trans* isomers could be synthesised to allow separation and isolation of the *trans* isomer (**4.10**). Dicarboxylic acid **4.10** could further be decarboxylated to the corresponding monocarboxylic acid **4.09**. Finally, *trans*-**4.01** could be obtained by *O*-demethylation.

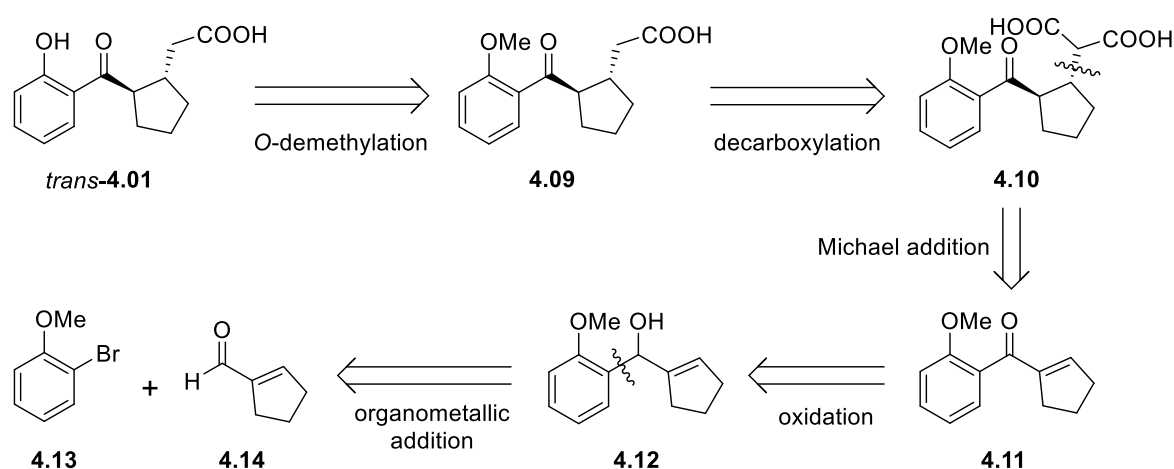
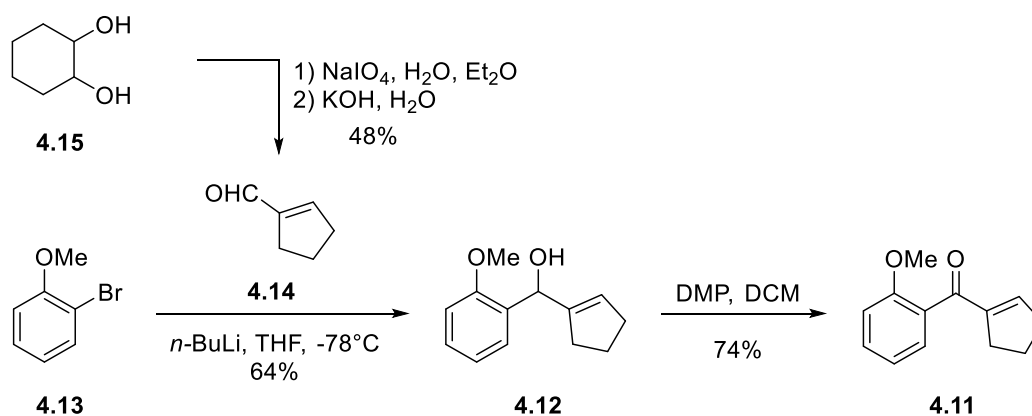


Figure 4.7. Retrosynthetic analysis. Stereochemical configurations are relative.

Aryl vinyl ketone 4.11

The synthesis of the key aryl vinyl ketone **4.11** is depicted in Scheme 4.2.

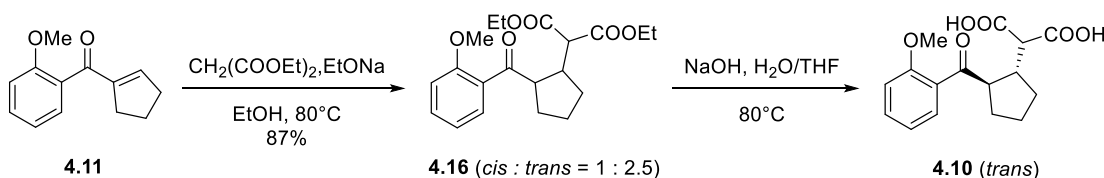


Scheme 4.2. Synthesis of aryl vinyl ketone **4.11**.

1,2-Cyclohexanediol **4.15** was first treated with sodium periodate, followed by 20% aqueous potassium hydroxide, to give cyclopent-1-enecarbaldehyde **4.14** in 48% yield.³ Treatment of 2-bromoanisole **4.13** with *n*-BuLi followed by addition of aldehyde **4.14**, in THF at -78°C , gave alcohol **4.12** in 64% yield after purification by flash chromatography. Subsequent oxidation of the alcohol **4.12** using Dess-Martin periodinane (DMP) gave ketone **4.11** in 74% yield.

Dicarboxylic acid **4.10**

Dicarboxylic acid **4.10** was synthesised from the unsaturated ketone **4.11**, with the malonate group introduced by Michael addition followed by basic ester hydrolysis (Scheme 4.3).



Scheme 4.3. Synthesis of dicarboxylic acid **4.10**.

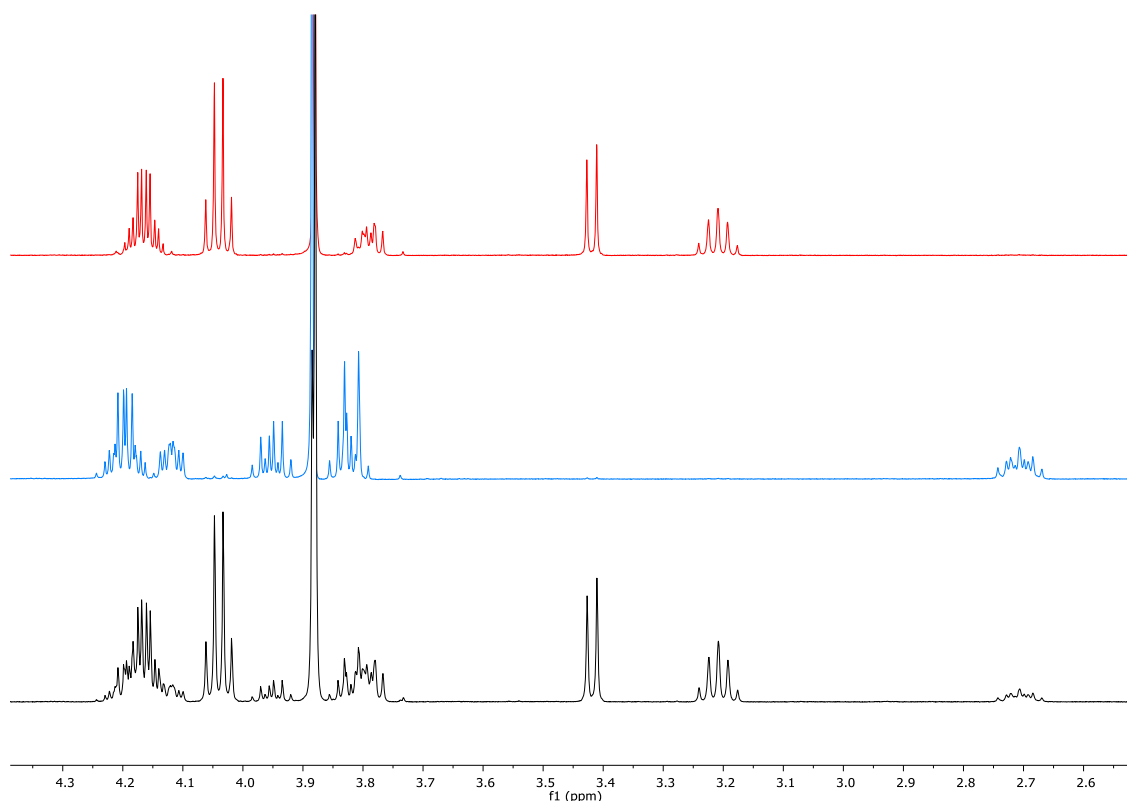


Figure 4.8. ^1H proton NMR of the whole Michael adduct **4.16** (black), *cis* form of **4.16** (blue), and *trans* form of **4.16** (red).

Unsaturated ketone **4.11** was treated with ethyl malonate in the presence of a catalytic amount of sodium ethoxide to give the Michael adduct **4.16** in 87% yield. This sample was found to be a mixture of *cis* and *trans* isomers based on ^1H NMR analysis which revealed two singlet methoxy peaks and four triplet malonate CH_3 peaks. The mixture was separated by silica gel chromatography to give the two isomers of **4.16** which were analysed by ^1H NMR to reveal single diastereoisomers (Figure 4.8).

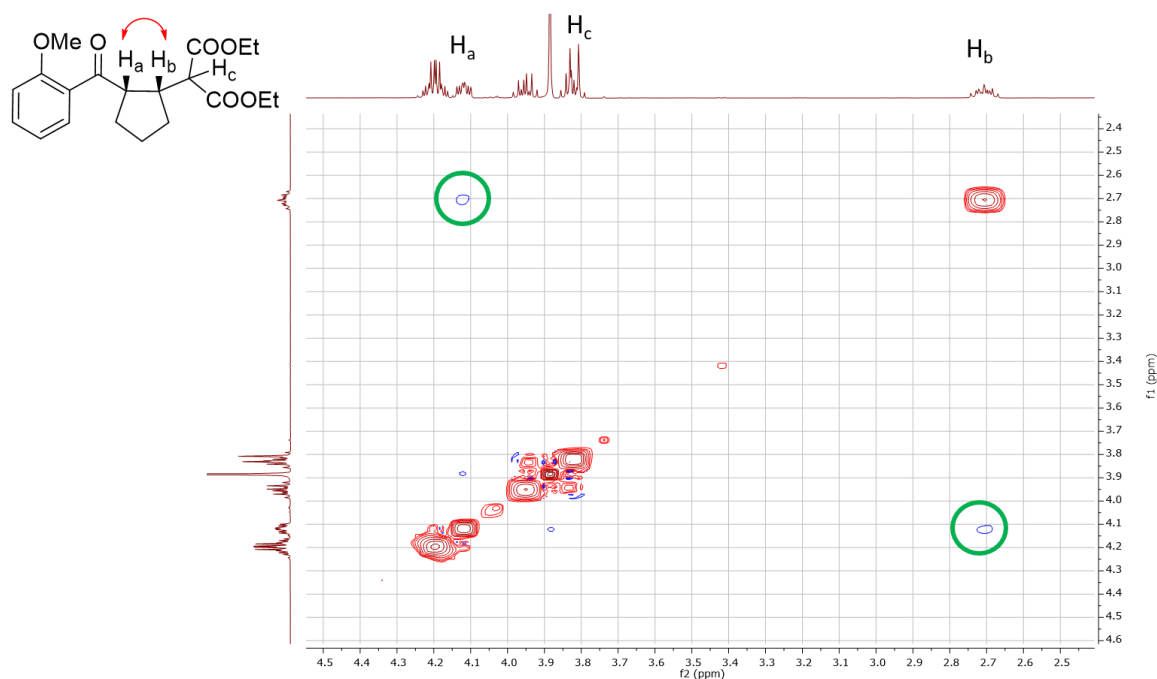
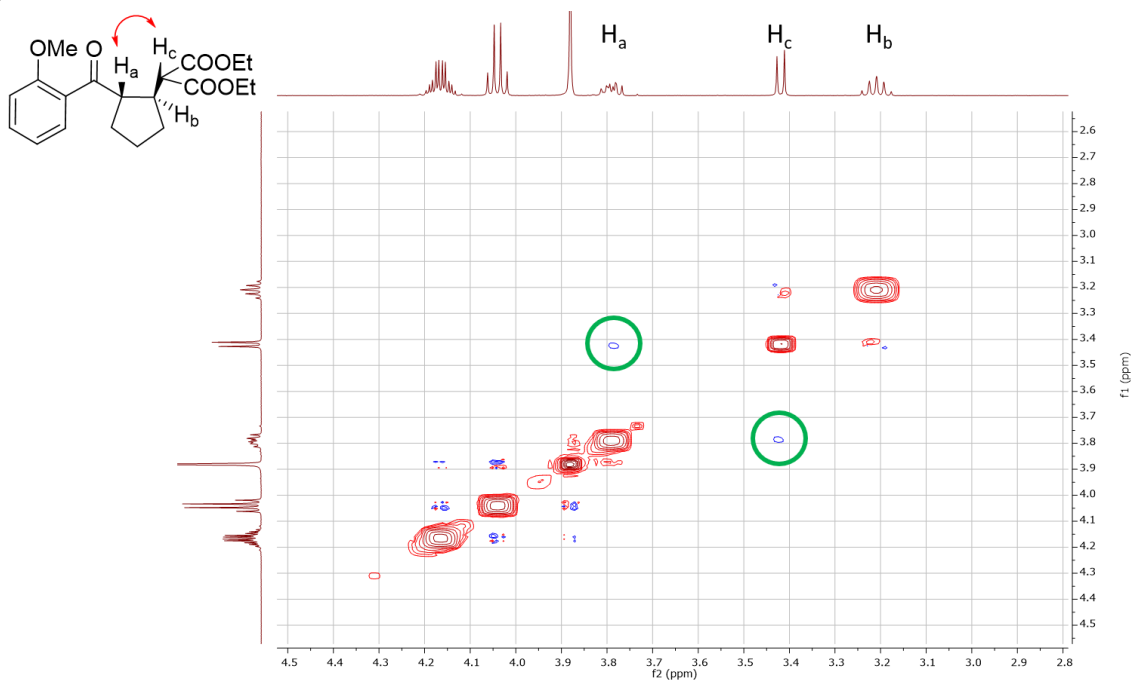
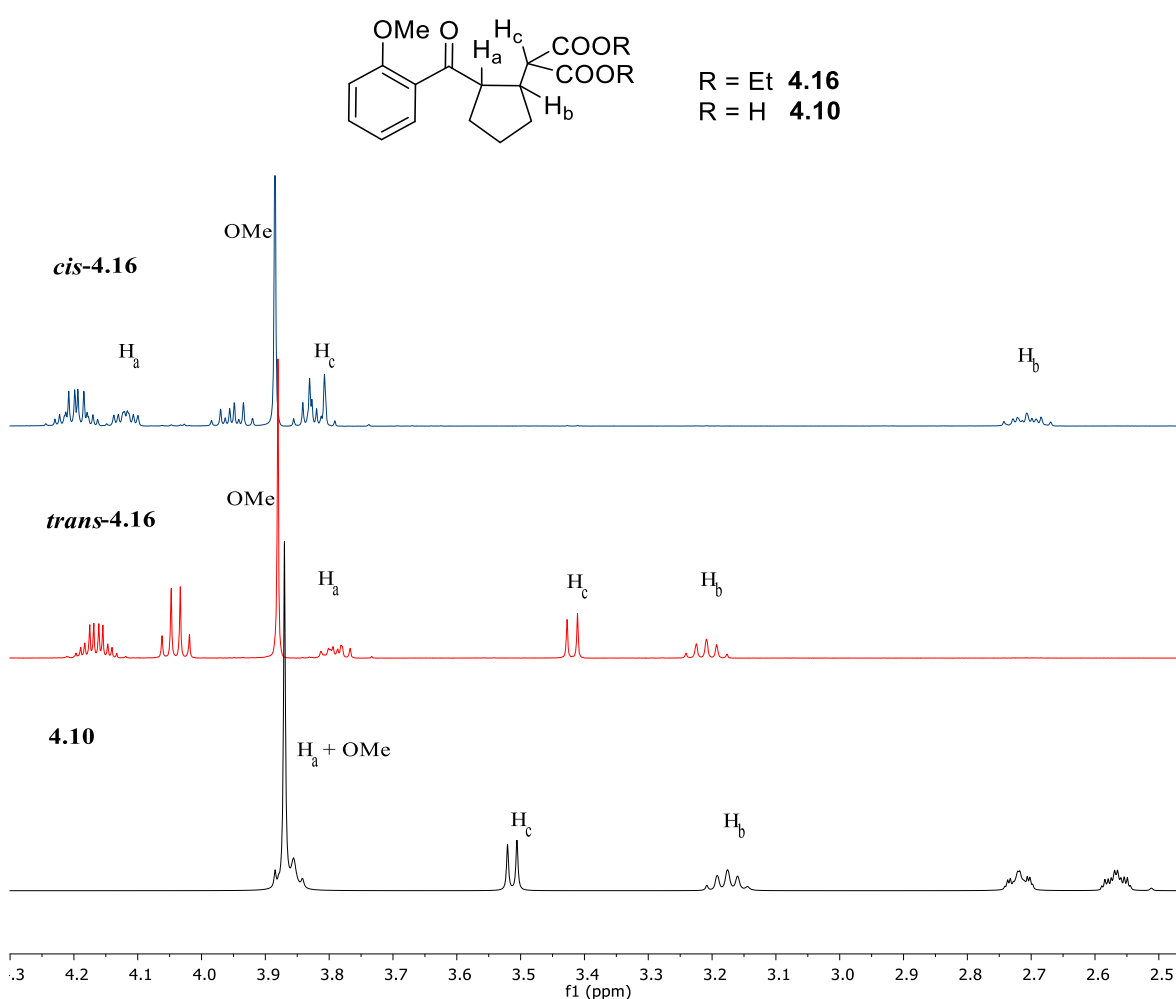
A**B**

Figure 4.9. (A) NOESY spectrum of *cis*-**4.16**. (B) NOESY spectrum of *trans*-**4.16**.

The relative stereochemistry of each isomer of **4.16** was determined with the aid of NOESY spectroscopy (Figure 4.9). The *cis* isomer showed a clear correlation between the resonances for H_a and H_b on the cyclopentane ring at 4.12 and 2.71 ppm respectively (Figure 4.9A). In comparison, the *trans* isomer showed a correlation between the ketone α -proton (H_a) and the malonate α -proton (H_c) (Figure 4.9B). Notably, the ketone α -proton (H_a) and the malonate α -proton (H_c) of the *cis* isomer were significantly downfield compared to the *trans* isomer (δ_{H_a} = 4.12 and 3.79 ppm; δ_{H_c} = 3.82 and 3.42 ppm for *cis* and *trans* respectively), see Figure 4.9 and Table 4.1.

Table 4.1. ¹H NMR data of *cis*-**4.16**, *trans*-**4.16**, and **4.10**.

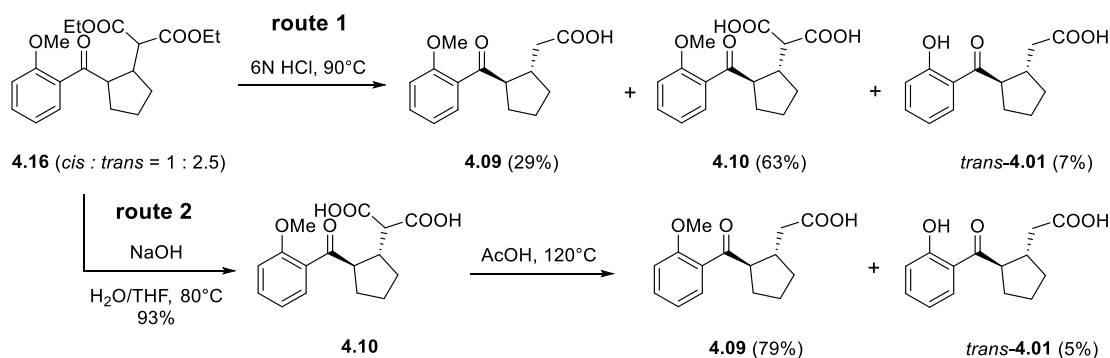


compound	δ_{H_a} (ppm)	δ_{H_b} (ppm)	δ_{H_c} (ppm)	$J_{H_bH_c}$ (Hz)	$\delta_{H_a} - \delta_{H_b}$ (ppm)	$\delta_{H_a} - \delta_{H_c}$ (ppm)	$\delta_{H_c} - \delta_{H_b}$ (ppm)
<i>cis</i> - 4.16	4.12	2.71	3.82	11.6	1.41	0.30	1.11
<i>trans</i> - 4.16	3.79	3.21	3.42	8.2	0.58	0.37	0.21
4.10	3.87	3.18	3.51	7.4	0.69	0.36	0.33

Separate samples of *cis*-**4.16** and *trans*-**4.16** were hydrolysed with an excess of NaOH to give a single common dicarboxylic acid, assigned as **4.10**. The relative configuration of H_a and H_b of **4.10** was assigned *trans* on the basis of its ¹H NMR data compared to the ¹H NMR data of *cis*-**4.16** and *trans*-**4.16** (see Table 4.1). Chemical shifts of H_a and H_b for **4.10** (3.87 and 3.18 ppm respectively) were similar with the values for *trans*-**4.16** ($\delta_{H_a} = 3.79$ and $\delta_{H_b} = 3.21$) compare to the values for *cis*-**4.16** ($\delta_{H_a} = 4.12$ and $\delta_{H_b} = 2.71$). In particular, the difference in chemical shifts of H_a and H_b ($\delta_{H_a} - \delta_{H_b}$) in **4.10** (0.69 ppm) more closely resembled a value for *trans*-**4.16** (0.58 ppm) rather than *cis*-**4.16** (1.41 ppm). In addition, the observed coupling constant between H_b and H_c ($J_{H_bH_c} = 7.4$ Hz) in **4.10** matches well with that of *trans*-**4.16** ($J_{H_bH_c} = 8.2$ Hz) compared to that of *cis*-**4.16** ($J_{H_bH_c} = 11.6$ Hz). These results support an assignment of a *trans* relative configuration of H_a and H_b for **4.10**. Both *cis*-**4.16** and *trans*-**4.16** give rise to *trans*-dicarboxylic acid **4.10** under these basic hydrolysis conditions, likely due to deprotonation α to the ketone. Dicarboxylic acid **4.10** did not give the NOE correlations observed for **4.16**.

Monocarboxylic acid 4.09

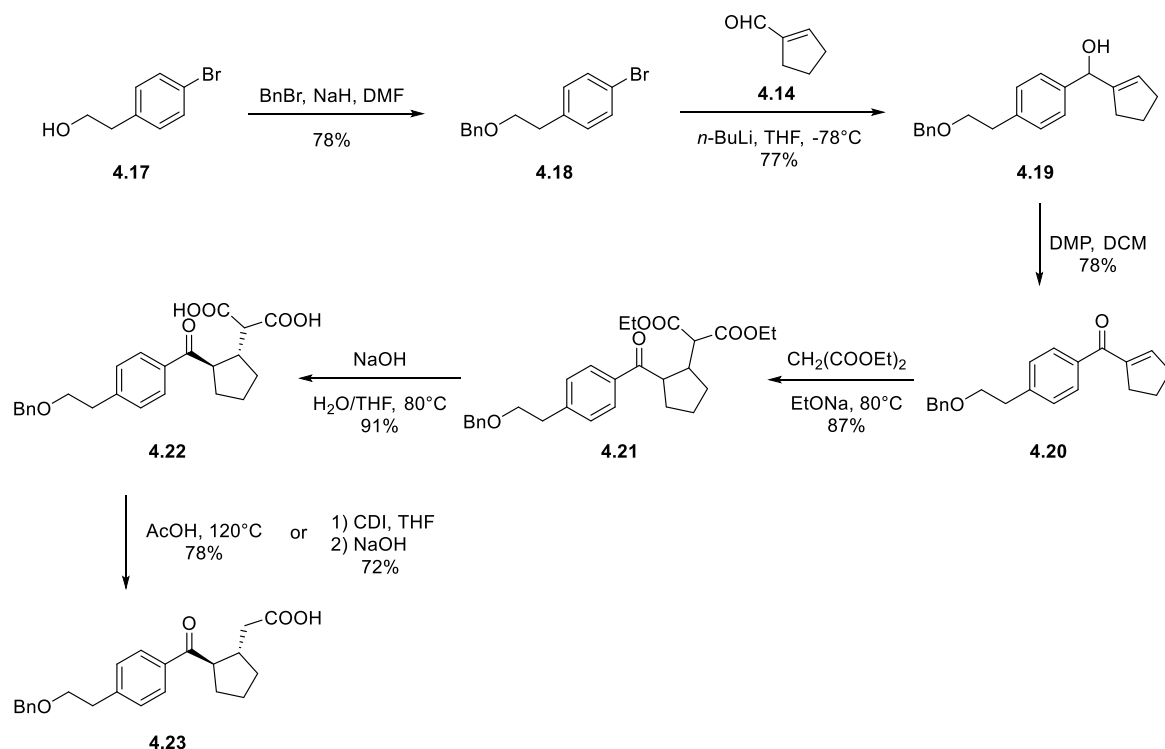
Two methods were attempted for the synthesis of monocarboxylic acid **4.09** as summarised in Scheme 4.3. Treatment of ketodiester **4.16** with aqueous 6N hydrogen chloride at 90°C for 2 days gave monocarboxylic acid **4.09** in a modest yield of 29%, with formation of dicarboxylic acid **4.10** and carboxylic acid *trans*-**4.01** as by-products (route 1). An alternative two-step method (route 2) was thus investigated. The stereoisomer mixture **4.16** (*cis:trans* = 1:2.5) was first hydrolysed with sodium hydroxide to give *trans*-dicarboxylic acid **4.10** in 93% yield without flash column purification. The dicarboxylic acid **4.10** was then heated in acetic acid to give the monocarboxylic acid **4.09** in 79% yield. Decarboxylation in acetic acid at 120°C gave *O*-demethylated *trans*-**4.01** also in an isolated yield of 5%.



Scheme 4.3. Synthesis of monocarboxylic acid **4.09** and *trans*-**4.01**. Stereochemical configurations are relative.

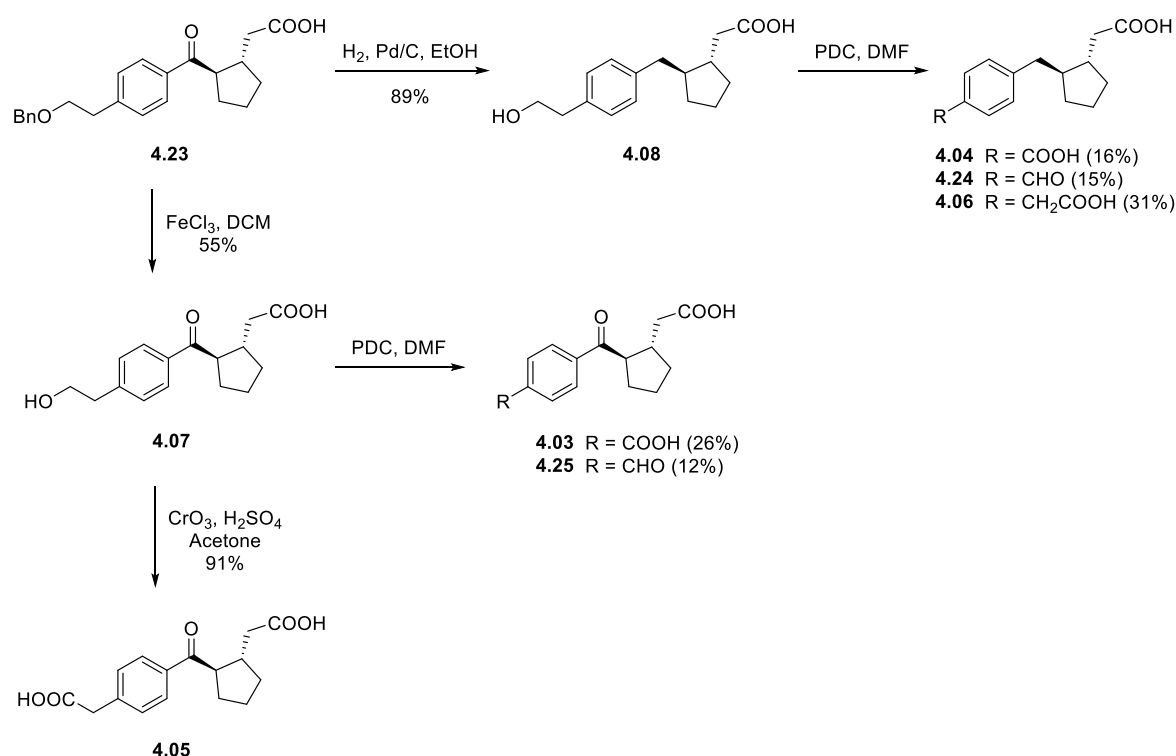
4.2.3 Synthesis of cyclopentylacetic acid analogues 4.03 – 4.08

The synthetic method used for the preparation of monocarboxylic acid **4.09** was next applied to preparation of cyclopentylacetic acid analogues **4.03** – **4.08**. The synthesis of benzyl-protected monocarboxylic acid **4.23**, a key intermediate for the preparation of **4.03** – **4.08**, is depicted in Scheme 4.4. Hydroxy bromobenzene **4.17** was treated with benzyl bromide, in the presence of sodium hydride in DMF, to give *O*-benzyl protected bromobenzene **4.18** in 78% yield. Treatment of bromobenzene **4.18** with *n*-BuLi followed by addition of aldehyde **4.14**, in THF at -78°C , gave alcohol **4.19** in 77% yield. This alcohol was oxidised using Dess-Martin periodinane (DMP) to give ketone **4.20** in 78% yield. Treatment of ketone **4.20** with ethyl malonate in the presence of a catalytic amount of sodium ethoxide then gave diester **4.21** (*cis* and *trans* mixture) in 87% yield. Subsequent hydrolysis of diester **4.21**, using sodium hydroxide at 80°C , gave dicarboxylic acid **4.22** (*trans* form) in 91% yield after trituration with hexane. The dicarboxylic acid **4.22** was then refluxed in acetic acid to give monocarboxylic acid **4.23** in 78% yield. Alternatively, the monocarboxylic acid **4.23** was prepared from **4.22** by decarboxylation using 1,1'-carbonyldiimidazole (CDI) at ambient temperature based on optimised conditions reported by Lafrance et al.⁴ CDI-mediated decarboxylation is milder than decarboxylation by heating in acetic acid, but both reactions gave a similar yield of **4.23** (72% vs 78%).



Scheme 4.4. Synthesis of benzyl-protected monocarboxylic acid **4.23**. Stereochemical configurations are relative.

The preparation of cyclopentylacetic acid analogues **4.03** – **4.08** is shown in Scheme 4.5. *O*-Benzyl protected compound **4.23** was reduced to alcohol **4.08** in 89% yield by catalytic hydrogenation in the presence of 10% palladium carbon (Pd/C). Subsequent oxidation of alcohol **4.08**, using pyridinium dichromate (PDC) in DMF, gave carboxyl benzene **4.04**, formyl benzene **4.24**, and carboxymethyl benzene **4.06**. Carboxymethyl benzene **4.06** was the only expected product under the PDC/DMF oxidation, but compounds **4.24** and **4.04** were also isolated from this reaction. This suggests that one carbon of the hydroxyethyl group in **4.08** is cleaved to produce **4.04** and **4.24** under these reaction conditions. A similar observation is reported.⁵ Exact reasons for this remain unclear, but likely involves benzylic oxidation. Selective removal of the *O*-benzyl protecting group of **4.23** in the presence of an aryl ketone moiety was achieved on reaction with ferric chloride in DCM to give alcohol **4.07** in 55% yield. Subsequent oxidation of **4.07** using PDC in DMF gave formyl benzene **4.25** and carboxyl benzene **4.03** as per the synthesis of **4.04** and **4.24**. Presumably **4.05** was also produced under these conditions, but the reaction mixture proved too complex to isolate **4.05**. Oxidation of the alcohol **4.07** using Jones reagent however gave carboxymethyl benzene **4.05** in 91% yield.

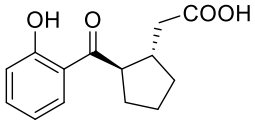
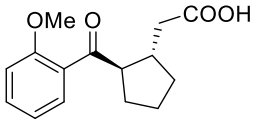
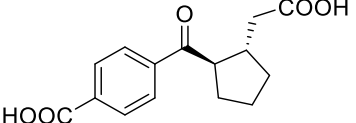
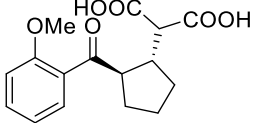
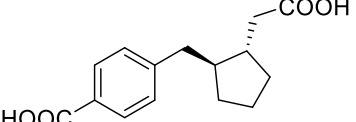
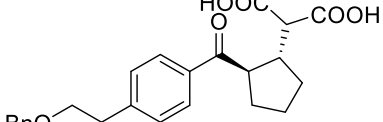
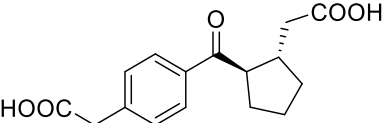
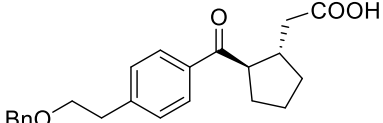
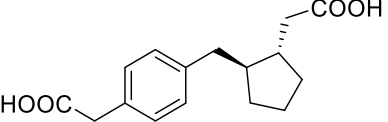
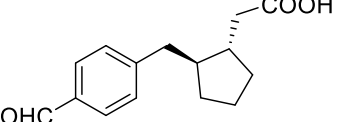
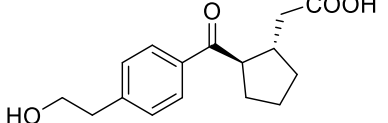
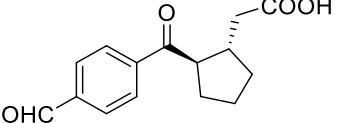
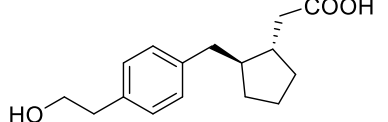


Scheme 4.5. Synthesis of cyclopentylacetic acid analogues **4.03** – **4.08**. Stereochemical configurations are relative.

4.3 DTBS binding affinity and antimicrobial activity of Cyclopentylacetic acid analogues

Cyclopentylacetic acid analogues **4.03** – **4.10** and **4.22** – **4.25** were assayed against *Mtb*DTBS by Surface Plasma Resonance (SPR) and the results are shown in Table 4.2. The assay was performed by collaborators at The Department of Molecular and Biomedical Science, University of Adelaide.

Table 4.2. Binding affinities of analogues **4.03** – **4.10**, **4.22** – **4.25** and parent compound *trans*-**4.01** towards *Mtb*DTBS. Stereochemical configurations are relative.

Compound	K_D (μM)	Compound	K_D (μM)
 <i>trans</i> - 4.01	3400 ± 400	 4.09	3400 ± 1300
 4.03	19 ± 5	 4.10	46 ± 2
 4.04	39 ± 2	 4.22	> 250
 4.05	17 ± 1	 4.23	> 250
 4.06	56 ± 8	 4.24	$> 1 \times 10^3$
 4.07	$> 1 \times 10^3$	 4.25	$> 1 \times 10^3$
 4.08	$> 1 \times 10^3$		

Replacing the phenol group of *trans*-**4.01** with a methoxy group, as in **4.09**, did not noticeably affect binding affinity ($K_D = 3.4 \pm 1.3$ mM), suggesting that the phenol group of *trans*-**4.01** does not play an important role in binding to *Mtb*DTBS. Interestingly, compound **4.10**, an intermediate in the synthesis of **4.09** with a malonic acid group, showed 74-fold improved binding affinity ($K_D = 46 \pm 2$ μ M) compared to **4.09**. The X-ray crystal structure of **4.10** bound to *Mtb*DTBS was solved and this is discussed in Section 4.4. Carboxybenzoyl compound **4.03** ($K_D = 19 \pm 5$ μ M) and carboxymethylbenzoyl compound **4.05** ($K_D = 17 \pm 1$ μ M) displayed more than 100-fold improved binding affinities towards *Mtb*DTBS compared to the parent compound *trans*-**4.01** ($K_D = 3.4$ mM). These results support the importance of the interaction site of DAPA carboxyl group in *Mtb*DTBS. Compounds lacking the ketone of **4.03** and **4.05**, i.e. **4.04** and **4.06**, have at least a 2-fold decrease in binding affinity toward *Mtb*DTBS with $K_D = 39 \pm 2$ and 56 ± 8 μ M respectively, suggesting the importance of this group in the DAPA binding site. Alcohol analogues **4.07** and **4.08** and the aldehyde analogues **4.24** and **4.25** were all inactive toward *Mtb*DTBS ($K_D > 1$ mM). The limited binding observed for analogues **4.07**, **4.08**, **4.24**, and **4.25** suggests that introducing alcohol and aldehyde groups at *p*-position on benzene ring provides limited scope for improving binding affinity. *O*-Benzyl protected compounds **4.22** and **4.23** showed limited binding affinities toward *Mtb*DTBS with $K_D > 0.25$ mM. This likely reflects the large size of the benzyl group or perhaps absence of the carboxyl group and associated hydrogen bonds.

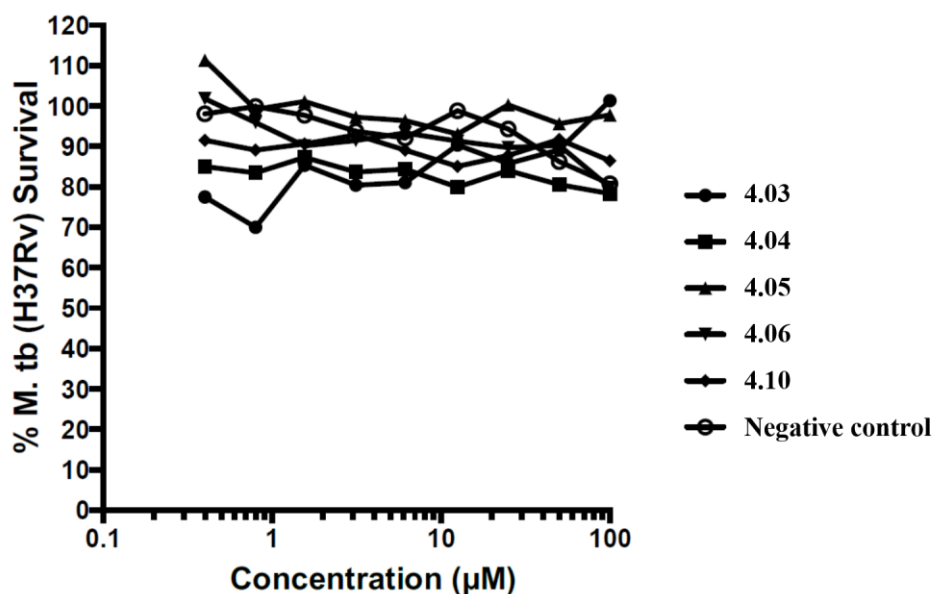


Figure 4.10. Antitubercular activity test of cyclopentylacetic acid analogues **4.03** – **4.06** and **4.10** against *M. tuberculosis* strain H37Rv.

Selected compounds **4.03** – **4.06** and **4.10** were tested for antimicrobial activity against *M. tuberculosis* and results are shown in Figure 4.10. These studies were performed by a collaborator Gayathri Nagalingam (Laboratory of A/Prof Jamie Triccas, Department of Infectious Diseases and Immunology, University of Sydney). Growth of *M. tuberculosis* in a biotin depleted media was measured in the presence of a range of compound concentrations. None of cyclopentylacetic acid analogues **4.03** – **4.06** or **4.10** inhibited growth of *M. tuberculosis* strain H37Rv at concentrations up to 100 μM . A carboxylic acid residue in a compound can cause limited passive diffusion across biological membranes.⁶⁻⁷ Based on this, it is perhaps not surprising that analogues **4.03** – **4.06** and **4.10** were inactive with likely limited permeability through the mycobacterial cell wall. The cell wall of *M. tuberculosis* consists mostly of mycolic acids, strong hydrophobic molecules which are thought to be a significant determinant of virulence.⁸⁻⁹ Mycolic acids are also thought to play key roles in the low cell permeability of *M. tuberculosis* by drugs, especially those that are hydrophilic. Small and hydrophilic TB drugs including isoniazid, ethambutol and pyrazinamide are thought to cross the mycobacterial cell wall through membrane bound porin proteins, which exhibit low rates of uptake.^{8, 10}

It is likely that compounds with higher binding affinity toward *Mtb*DTBS will be required to show significant antitubercular activity. Considering the carboxyl group of *trans*-**4.01** occupies a similar region to the γ -phosphate of CTP, these compounds would likely compete with nucleoside triphosphates for binding to *Mtb*DTBS. Since CTP exhibits a high binding with $K_D = 0.16 \pm 0.01 \mu\text{M}$,¹¹ CTP would likely outcompete cyclopentylacetic acid analogues **4.03** – **4.06** and **4.10** for binding to *Mtb*DTBS.

4.4 X-ray crystal structure of **4.03 – **4.06** and **4.10** bound to *Mtb*DTBS**

Crystal structures of cyclopentylacetic acid analogues **4.03** – **4.06** and **4.10** bound to *Mtb*DTBS were solved by collaborators at the Department of Molecular and Biomedical Science, University of Adelaide as depicted in Figure 4.11 – 4.13. *RS* isomers were modelled only as the inclusion of both isomers did not correlate with the crystallographic data. This manifested in either an occupancy refinement of less than 0.1 or negative peaks in the electron density map.

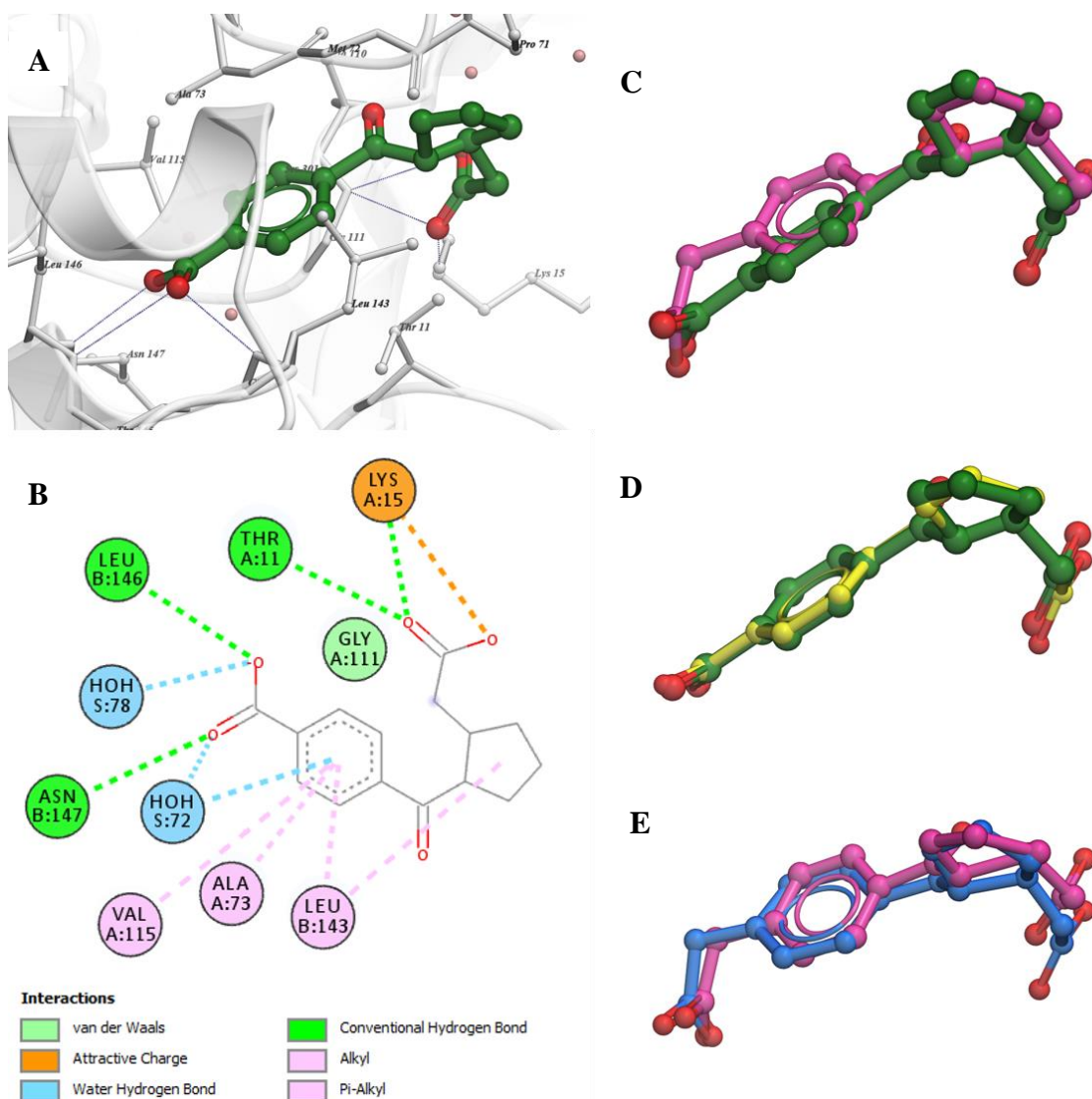


Figure 4.11. (A) 3D depiction of compound **4.03** (green) bound to *Mtb*DTBS (PDB: 6NU6) with hydrogen bonds shown in blue dashes. (B) 2D interaction diagram of compound **4.03** bound to *Mtb*DTBS with interactions shown in dashes. (C) An overlay of **4.03** (green) and **4.05** (magenta) bound to *Mtb*DTBS. (D) An overlay of **4.03** (green) and **4.04** (yellow) bound to *Mtb*DTBS. (E) An overlay of **4.05** (magenta) and **4.06** (blue) bound to *Mtb*DTBS.

The crystal structure of **4.03** bound to *Mtb*DTBS confirms that its benzoic acid moiety forms hydrogen bonds with residues Leu146 and Asn147 of the binding site as observed between the carboxyl group of **1.16** and the same residues (Figure 4.11A and B). The same interactions are evident within the crystal structures of **4.04** – **4.06** bound to *Mtb*DTBS. Compounds **4.03** and **4.05** have similar binding conformations, however the binding pose of **4.05** is slightly shifted to accommodate the longer carboxymethyl moiety (Figure 4.11C). The co-crystal structures of **4.04** and **4.06** bound to *Mtb*DTBS reveal that removal

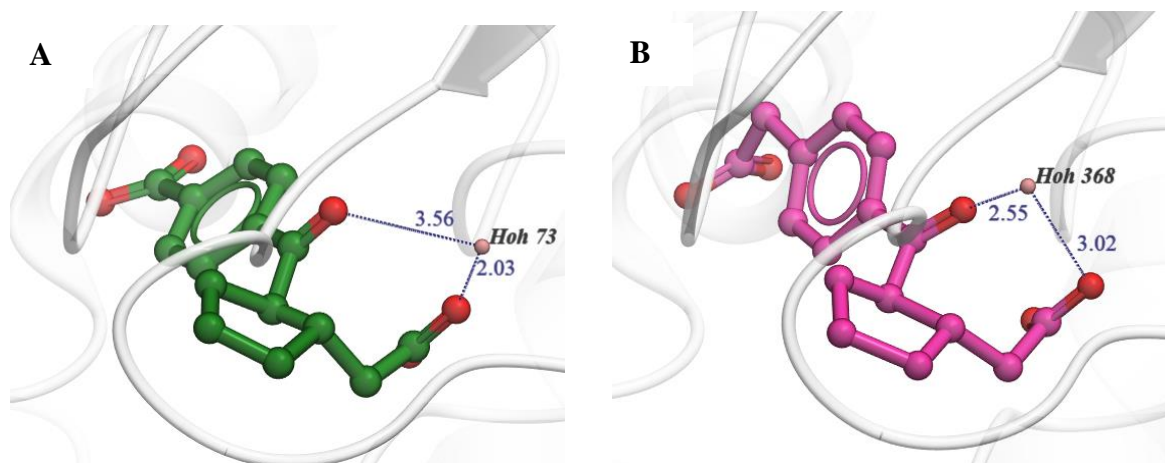


Figure 4.12. Close up of the ketone group. (A) 3D depiction of **4.03** (green) bound to *Mtb*DTBS (PDB: 6NU6). (B) 3D depiction of **4.05** (magenta) bound to *Mtb*DTBS (PDB: 6NVC). Hydrogen bonds are depicted by blue dashes with distances shown therein.

of the ketone group of **4.03** and **4.05** does not alter the binding pose (Figure 4.11C and D). The ketone group of **4.03** forms a hydrogen bond to a neighbouring water molecule (3.56 Å) that coordinates with the carboxyl group on cyclopentane ring of the compound (2.03 Å), as show in Figure 4.12A. The crystal structure of **4.05** bound to *Mtb*DTBS reveals an ordered water molecule interacts with the ketone and carboxyl group on cyclopentane ring of the compound (2.55 Å and 3.02 Å, respectively) (Figure 4.12B). These water-mediated interactions support the improved binding affinities of **4.03** and **4.05** compared to **4.04** and **4.06** respectively, see Table 4.2.

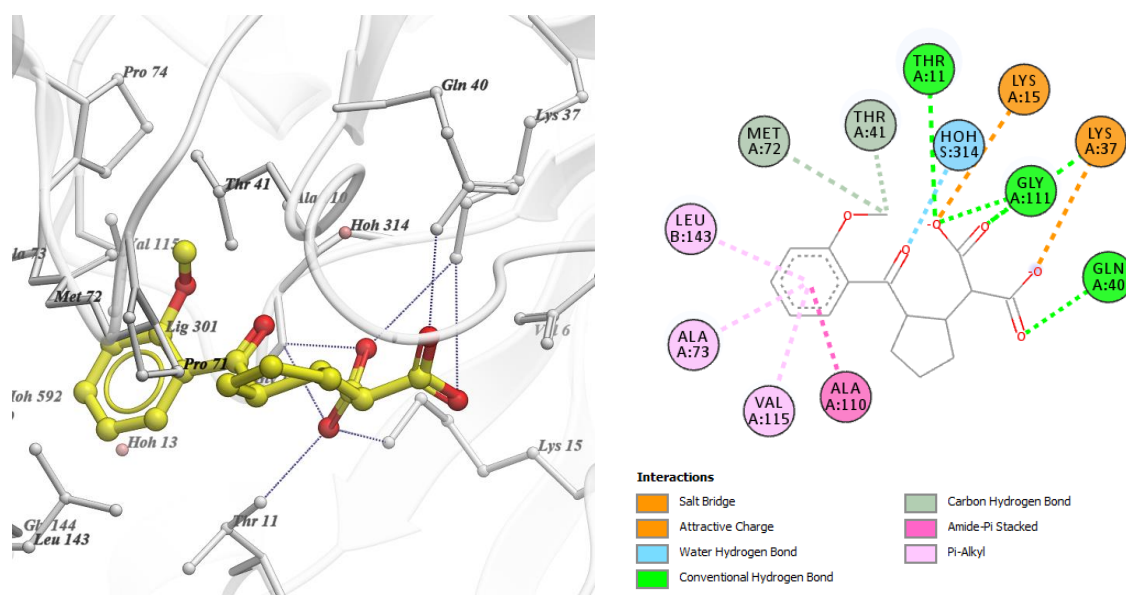


Figure 4.13. 3D depiction of compound **4.10** (yellow) bound to *Mtb*DTBS (PDB: 6NWG) with hydrogen bonds shown in blue dashes (left). 2D interaction diagram of compound **4.10** bound to *Mtb*DTBS with interactions shown in dashes (right).

The crystal structure of **4.10** bound to *Mtb*DTBS reveals that **4.10** retains all the hydrogen bonds between *trans*-**4.01** and amino acid residues of the binding site, but with hydrogen bonding/electrostatic interaction of the additional carboxyl group with the side chains of Lys37 and Asn40 (Figure 4.13). These additional interactions support the observed improved binding affinity of **4.10** compared to **4.09**, see Table 4.2. In particular, Lys37 is involved in stabilising the phosphorylated DAPA **1.17**, indicating that this additional carboxyl group acts as a bioisostere of the phosphoryl group of the reaction intermediate **1.17** (Figure 4.14).

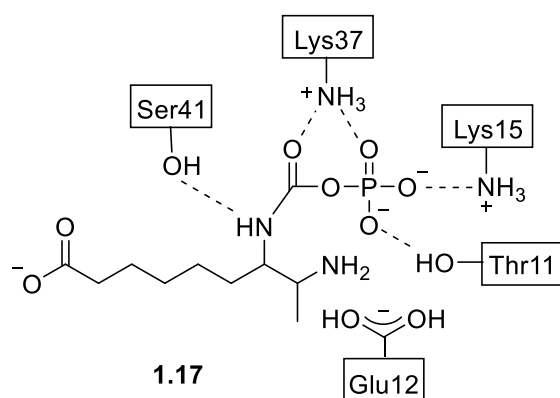


Figure 4.14. Schematic view of the interactions of the phosphorylated DAPA **1.17** with enzymic residues at the active site of *E. coli* DTBS.

4.5 Conclusion

A library of cyclopentylacetic acid analogues **4.03** – **4.10** and **4.22** – **4.25**, with varying *p*-substitution groups on benzene ring, were synthesised and assayed for binding affinity toward *Mtb*DTBS (see Table 4.2). Analogues **4.03** and **4.05**, with carboxylic acid group attached to the *para* position of benzene ring, were shown to be potent toward *Mtb*DTBS ($K_D = 19 \pm 5$ and 17 ± 1 μM respectively). Crystallographic analysis reveals the carboxylic acid groups of **4.03** and **4.05** form hydrogen bonds with residues Leu146 and Asn147 in the binding site as observed in DAPA carbamate **1.16**. Analogues **4.04** and **4.06**, which lack the ketone functionality of compounds **4.03** and **4.05**, were at least 2-fold less potent toward *Mtb*DTBS. Attachment of different C4 functional groups (see Figure 4.1 for numbering) including hydroxyl (**4.07** and **4.08**), formyl (**4.24** and **4.25**), and benzylether (**4.22** and **4.23**) resulted in loss of potency against *Mtb*DTBS ($K_D > 250$ μM). Interestingly, analogue **4.10**, with two carboxyl groups, was 74-fold more potent than **4.09** (see Table 4.2). The crystal structure of **4.10** bound to *Mtb*DTBS confirms that this

additional carboxyl group forms hydrogen bonds with Lys37 and Asn40 of the enzyme. None of cyclopentylacetic acid analogues **4.03** – **4.06** or **4.10** showed antibacterial activity against clinically significant strains of *M. tuberculosis*.

Future compound development would involve combining the malonate substituent of **4.10** with the carboxy or carboxymethyl substituents present in **4.03** and **4.05** in order to increase affinity for *Mt*DTBS (Figure 4.15A). Replacing the carboxylic acid groups of **4.03** and **4.05** with bioisosteres such as tetrazole, acylsulfonamide and oxazolidinedione could increase binding affinity and permeability through the mycobacterial cell and consequently show antituberculosis activity (Figure 4.15B). Acyclic analogues as well as other ring systems such as THF and cyclopropane could be investigated given their enhanced metabolic stability, solubility and ease of synthesis (Figure 4.15C).

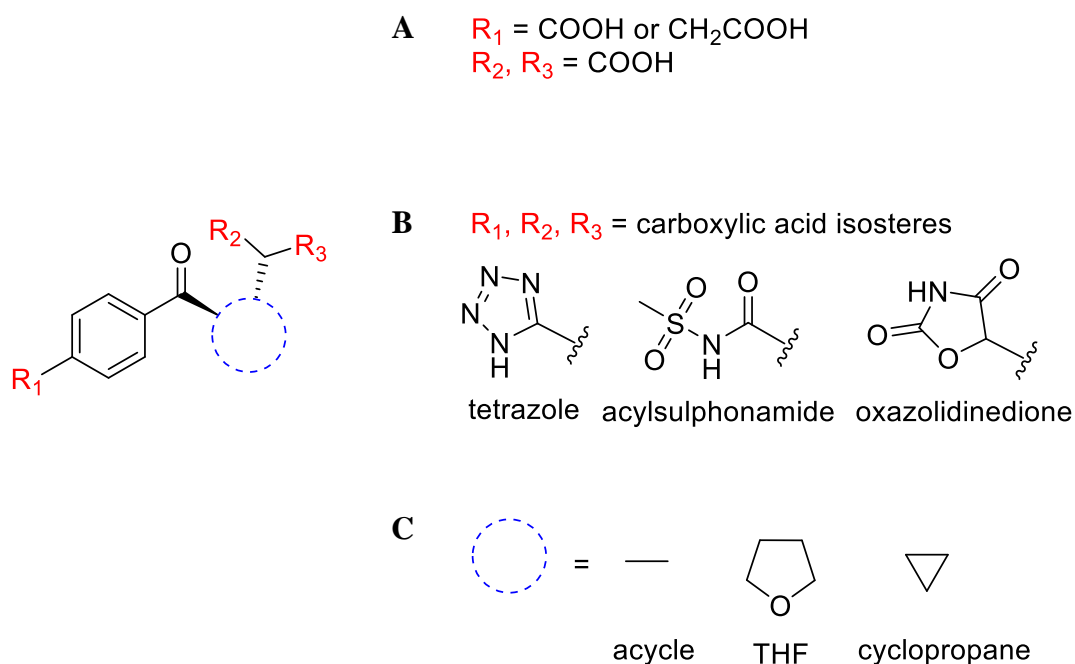


Figure 4.15. Future compound development targeting DAPA binding site.

4.6 References for Chapter Four

1. Dey, S.; Lane, J. M.; Lee, R. E.; Rubin, E. J.; Sacchettini, J. C., Structural Characterization of the Mycobacterium tuberculosis Biotin Biosynthesis Enzymes 7,8-Diaminopelargonic Acid Synthase and Dethiobiotin Synthetase. *Biochemistry* **2010**, *49* (31), 6746-6760.
2. Neves, M. A.; Totrov, M.; Abagyan, R., Docking and scoring with ICM: the benchmarking results and strategies for improvement. *J Comput Aided Mol Des* **2012**, *26* (6), 675-86.
3. Meyers, M. J.; Arhancet, G. B.; Hockerman, S. L.; Chen, X. Y.; Long, S. A.; Mahoney, M. W.; Rico, J. R.; Garland, D. J.; Blinn, J. R.; Collins, J. T.; Yang, S. T.; Huang, H. C.; McGee, K. F.; Wendling, J. M.; Dietz, J. D.; Payne, M. A.; Homer, B. L.; Heron, M. I.; Reitz, D. B.; Hu, X. A., Discovery of (3S,3aR)-2-(3-Chloro-4-cyanophenyl)-3-cyclopentyl-3,3a,4,5-tetrahydro-2H-benzo[g]indazole-7-carboxylic Acid (PF-3882845), an Orally Efficacious Mineralocorticoid Receptor (MR) Antagonist for Hypertension and Nephropathy. *J. Med. Chem.* **2010**, *53* (16), 5979-6002.
4. Lafrance, D.; Bowles, P.; Leeman, K.; Rafka, R., Mild Decarboxylative Activation of Malonic Acid Derivatives by 1,1'-Carbonyldiimidazole. *Org. Lett.* **2011**, *13* (9), 2322-2325.
5. Fernandes, R. A.; Kumar, P., PCC-mediated novel oxidation reactions of homobenzylic and homoallylic alcohols. *Tetrahedron Lett.* **2003**, *44* (6), 1275-1278.
6. Ballatore, C.; Huryn, D. M.; Smith, A. B., Carboxylic Acid (Bio)Isosteres in Drug Design. *Chemmedchem* **2013**, *8* (3), 385-395.
7. Lassalas, P.; Gay, B.; Lasfargeas, C.; James, M. J.; Tran, V.; Vijayendran, K. G.; Brunden, K. R.; Kozlowski, M. C.; Thomas, C. J.; Smith, A. B.; Huryn, D. M.; Ballatore, C., Structure Property Relationships of Carboxylic Acid Isosteres. *J. Med. Chem.* **2016**, *59* (7), 3183-3203.
8. Lambert, P. A., Cellular impermeability and uptake of biocides and antibiotics in Gram-positive bacteria and mycobacteria. *J. Appl. Microbiol.* **2002**, *92*, 46s-54s.

-
9. Takayama, K.; Wang, C.; Besra, G. S., Pathway to synthesis and processing of mycolic acids in *Mycobacterium tuberculosis*. *Clin. Microbiol. Rev.* **2005**, *18* (1), 81-+.
 10. Masi, M.; Refregiers, M.; Pos, K. M.; Pages, J. M., Mechanisms of envelope permeability and antibiotic influx and efflux in Gram-negative bacteria. *Nature Microbiology* **2017**, *2* (3).
 11. Thompson, A. P.; Salaemae, W.; Pederick, J. L.; Abell, A. D.; Booker, G. W.; Bruning, J. B.; Wegener, K. L.; Polyak, S. W., *Mycobacterium tuberculosis* Dethiobiotin Synthetase Facilitates Nucleoside Triphosphate Promiscuity through Alternate Binding Modes. *Acs Catalysis* **2018**, *8* (11), 10774-10783.

Chapter Five

5.1 Introduction

The DTBS active site can be divided into three distinct pockets, particularly the DAPA pocket, phosphate-binding loop (P-loop), and nucleoside pocket as discussed in Chapter 1. Based on this structural information, Chapter 4 described the design and development of cyclopentylacetic acid analogues **4.03** – **4.10** and **4.22** – **4.25** that target the DAPA pocket of *Mtb*DTBS. An investigation of the nucleoside pocket is considered here to develop potent DTBS inhibitors, where the DAPA pocket alone is too small to allow the development of new antibiotics.

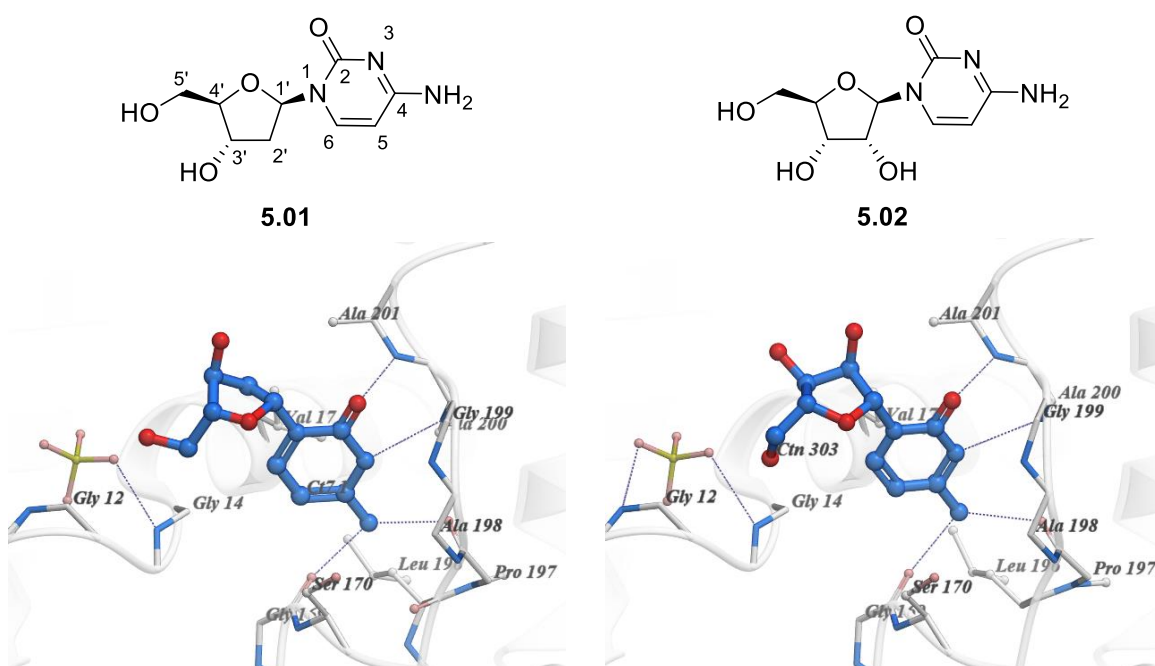


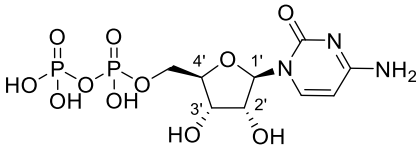
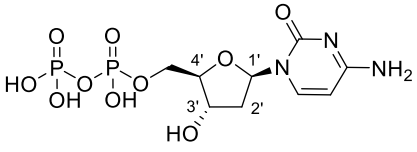
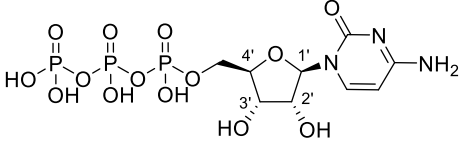
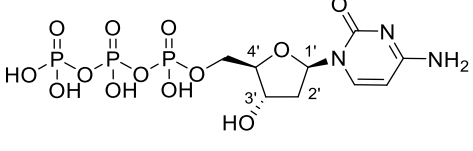
Figure 5.1. 3D depiction of 2'-deoxycytidine **5.01** bound to *Mtb*DTBS (PDB: 6NKA) (left). 3D depiction of cytidine **5.02** bound to *Mtb*DTBS (PDB: 6CVU)¹ (right).

Commercially available nucleoside analogues including cytidine, guanosine, adenine, uridine and cytidine derivatives were subjected to crystallographic screening against *Mtb*DTBS. Of those tested, 2'-deoxycytidine **5.01** and cytidine **5.02** were found to bind the nucleoside binding site of *Mtb*DTBS (Figure 5.1). Compound **5.01** lacks the 2' hydroxyl group of the ribose ring of cytidine **5.02**. The nucleoside binding site of *Mtb*DTBS thus appears able to accommodate substituents at the 2' position of ribose ring as depicted in Figure 5.1. The cytosine NH₂ of **5.01** forms hydrogen bonds with the backbone carbonyl groups of Pro197 and Gly169, while the cytosine N3 of **5.01** forms hydrogen bonds with the backbone amide nitrogen of Ala200. The same hydrogen bonding interactions are apparent in the crystal structures of **5.02** bound to *Mtb*DTBS as shown in Figure 5.1.

Hydrophobic interactions are also apparent between cytosine C4 and C5 of both **5.01** and **5.02**, and the side chain of Val17. The 2' position of the ribose ring of **5.01** and **5.02** are proximal to the hydrophobic sidechains of Ala201 and Val17 in the binding site, suggesting **5.01** would be a better binder than **5.02**, which contains 2' OH of ribose ring.

The binding affinities of 2'-deoxycytidine **5.01** and cytidine **5.02** against *Mtb*DTBS were determined by Surface Plasma Resonance (SPR) to be $K_D > 1$ mM, too weak to probe the effect of the 2' position of ribose ring on binding. However, 2'-deoxycytidine diphosphate (dCDP; $K_D = 120$ nM) bound to *Mtb*DTBS approximately 3-fold tighter than CDP ($K_D = 450$ nM)¹, while 2'-deoxycytidine triphosphate (dCTP; $K_D = 47$ nM) bound with approximately 3-fold higher affinity than CTP ($K_D = 160$ nM)¹ (Table 5.1). Binding kinetics values including association (k_a) and dissociation (k_d) constants for CTP, CDP, dCDP and dCTP demonstrate that the 2' hydroxy group of ribose ring leads to a slower association and faster dissociation. In addition, X-ray crystallographic analysis revealed binding modes of dCDP and dCTP are identical to binding poses of CDP and CTP respectively (Figure 5.2). These results support the notion that 2'-deoxycytidine **5.01** would be a better binder for the nucleoside binding site than cytidine **5.02**.

Table 5.1. Affinity (K_D), association (k_a), and dissociation (k_d) constants determined by SPR binding assay.

substrate	structure	K_D (nM)	k_a ($\times 10^5$ M ⁻¹ s ⁻¹)	k_d ($\times 10^{-2}$ s ⁻¹)
CDP		450 ± 50	3.4 ± 0.3	15.0 ± 0.8
dCDP		120 ± 30	12 ± 4	12 ± 3
CTP		160 ± 10	3.2 ± 0.3	5.3 ± 0.4
dCTP		47	7.13 ± 0.05	3.41 ± 0.02

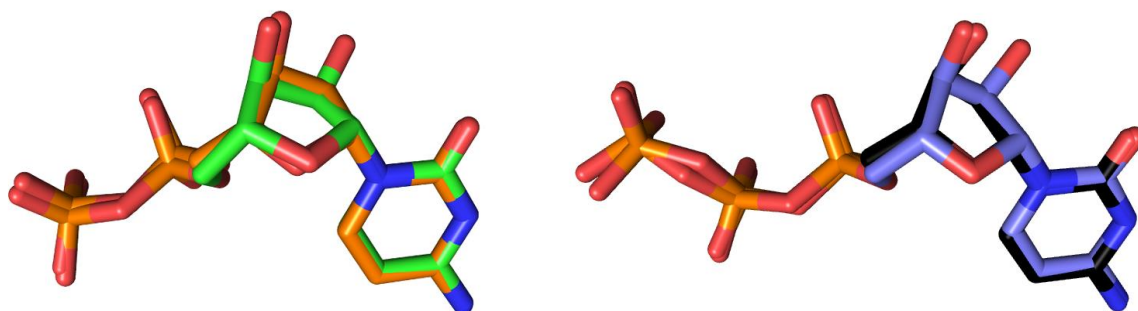


Figure 5.2. Overlays of the binding poses of CDP (green sticks) and dCDP (orange sticks) (left), as well as CTP (blue sticks) and dCTP (black sticks) (right).

Having identified optimised ligands for the nucleoside and DAPA binding pockets, compound development efforts turned to the synthesis of linker functionalised derivatives (Figure 5.3). Such a strategy involves linking the DAPA pocket binders with 2'-deoxycytidine **5.01** to allow the linked compounds to have enhanced binding affinities compared to parent fragments as discussed further below.

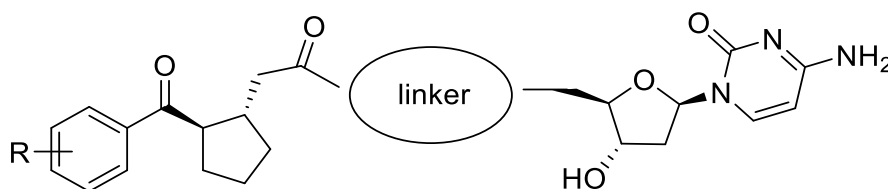


Figure 5.3. Linking DAPA pocket binders to 2'-deoxycytidine **5.01**.

5.2 Design and synthesis of linked compounds

The design of linked compounds, shown in Figure 5.4 and discussed in this chapter, was based on an overlay of crystal structures of *trans*-**4.01** and 2'-deoxycytidine **5.01** bound to *Mtb*DTBS (Figure 5.5). These two compounds appear to bind to distinct parts of the active site. Cyclopentylacetic acid *trans*-**4.01** binds in the DAPA binding pocket, while 2'-deoxycytidine **5.01** binds in nucleoside binding pocket. Sulfate ions from the crystallisation buffer were also observed in the crystal structure to bind in P-loop, where the β -phosphate of CTP binds.

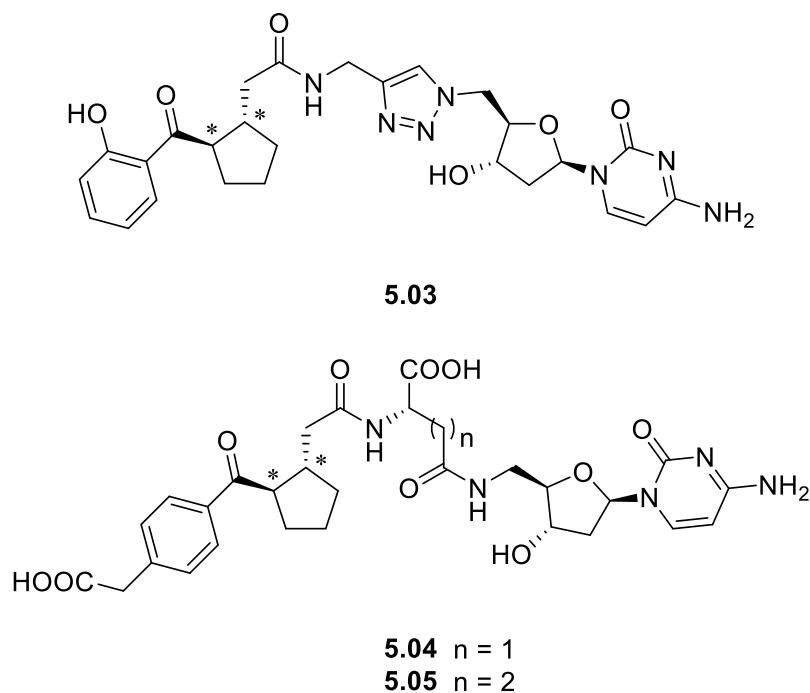


Figure 5.4. Proposed linked compounds **5.03** – **5.05**. * represents relative stereochemical configurations.

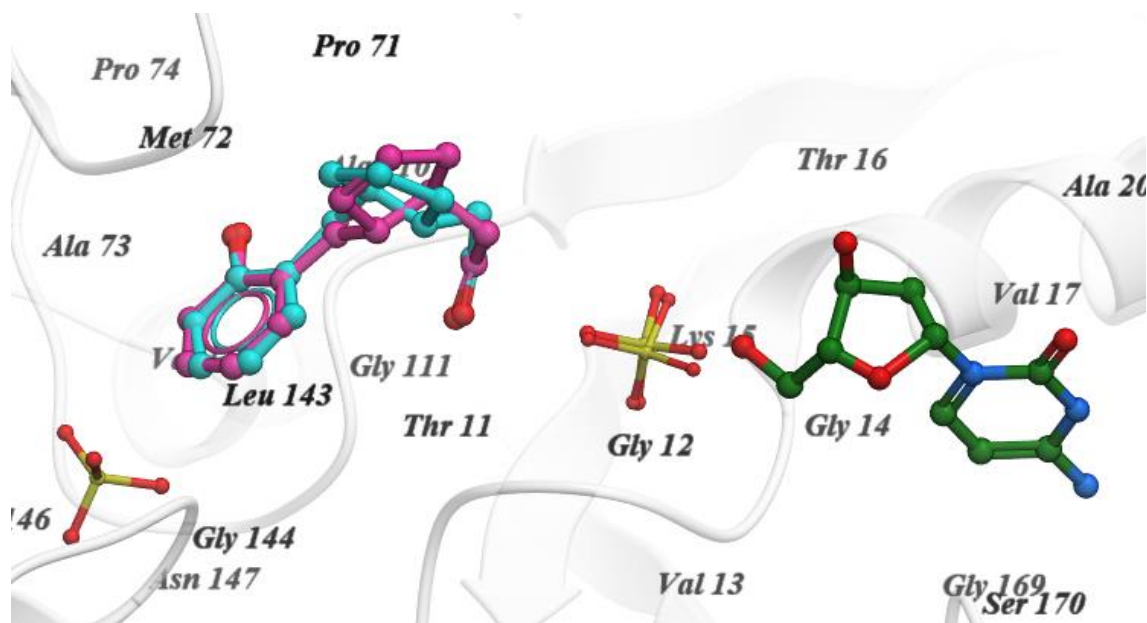


Figure 5.5. Overlay of *trans*-**4.01** (*RS*: magenta, *SR*: cyan), 2'-deoxycytidine **5.01** (green), and sulfate ions (yellow) binding to *MtbDTBS*.

Key features of proposed linked compounds **5.03** – **5.05** are summarised below.

1. Compound **5.03** contains a 1,2,3-triazole linker to link two fragments of *trans*-**4.01** and 2'-deoxycytidine **5.01**, providing a simple robust method of linking the two fragments on binding toward *MtbDTBS*. The triazole linker offers advantages of

reliable and efficient formation through copper(I)-catalysed azide alkyne cycloaddition (CuAAC) as depicted in Figure 5.6.² CuAAC allows linking of a range of azides and alkynes in a facile, selective and high yielding manner that is compatible with a variety of functional groups.² Here we establish the 1,4-triazole as a viable linker between cyclopentylacetic acid analogues and cytidine analogues, with potential to undertake a fragment-based approach in developing DTBS inhibitors.

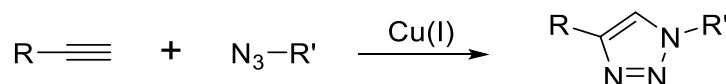


Figure 5.6. Routes to 1,4-triazole (CuAAC) from alkyne and azide.

- Compounds **5.04** and **5.05** contain aspartic acid and glutamic acid respectively, which provide additional carboxyl groups for further potential electrostatic interactions within P-loop of *Mtb*DTBS (Figure 5.7). These compounds also allow an investigation of linker length between the key components (cyclopentylacetic acid analogues and cytidine analogues); the glutamic acid-based linker has one additional methylene group in its side chain compared to the aspartic acid linker.

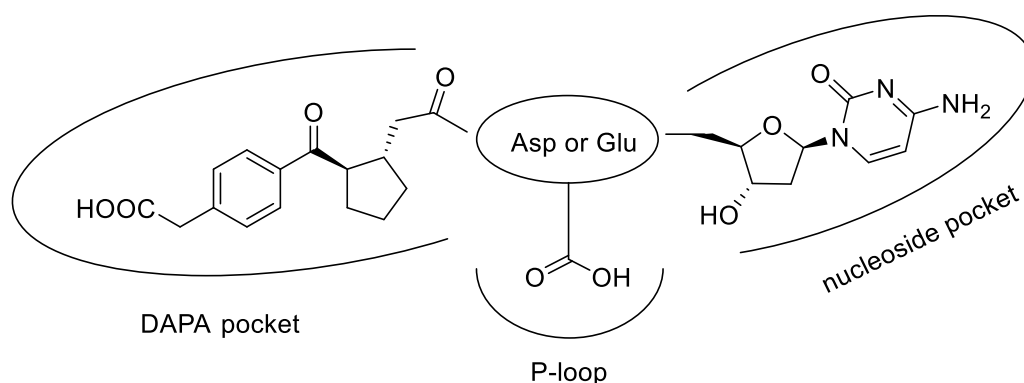
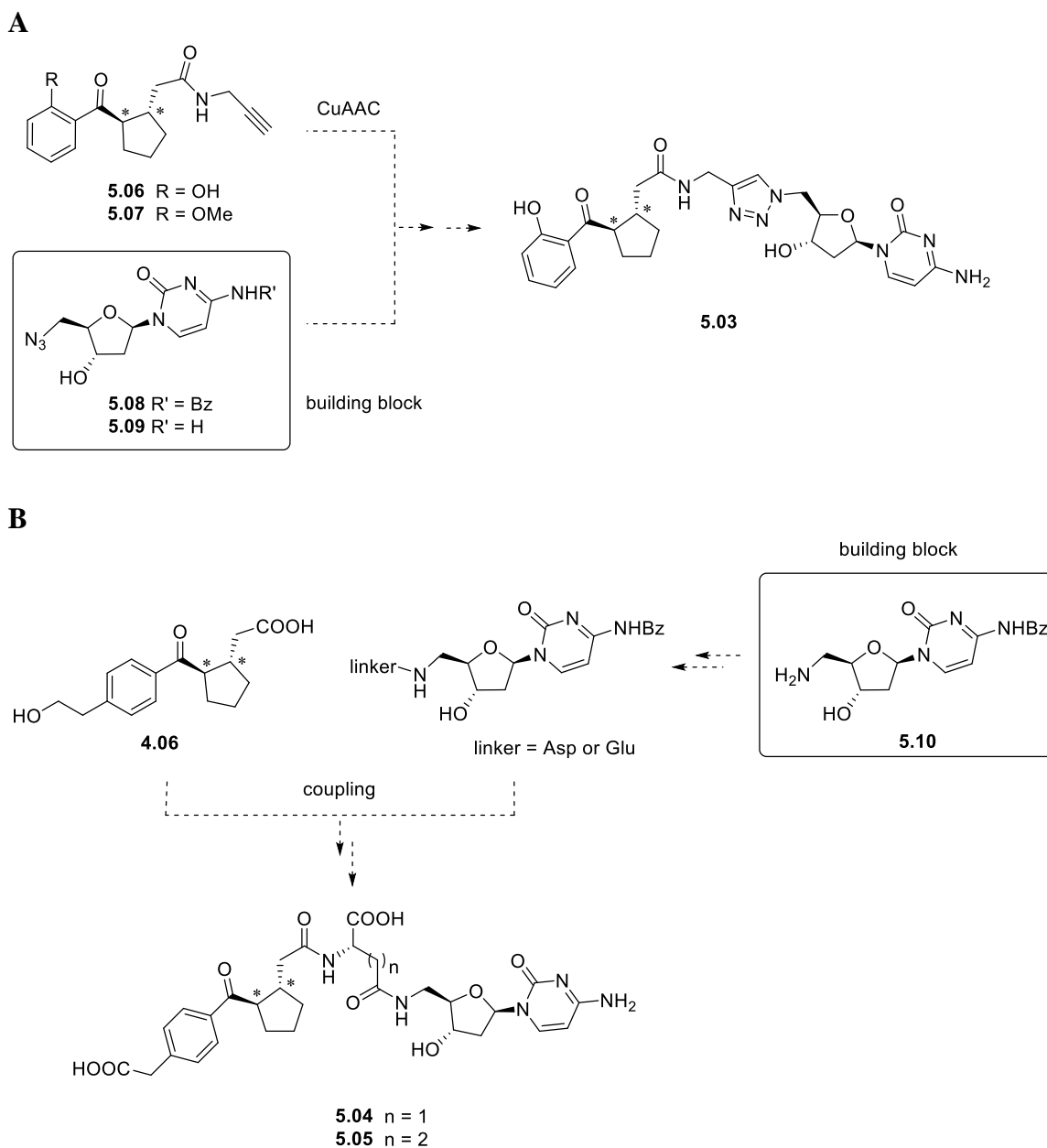


Figure 5.7. Proposed binding poses of **5.04** and **5.05**.

5.2.1 Cytidine building blocks for the synthesis of **5.03** – **5.05**

The synthesis of triazole **5.03** utilises alkyne **5.06/5.07** and azide **5.08/5.09** and involves CuAAC reaction as shown in Scheme 5.1A. The proposed synthesis of amino acid linked compounds **5.04** and **5.05** involves attachment of the linker moiety to cytidine amine **5.10** with subsequent coupling with **4.06** as outlined in Scheme 5.1B.

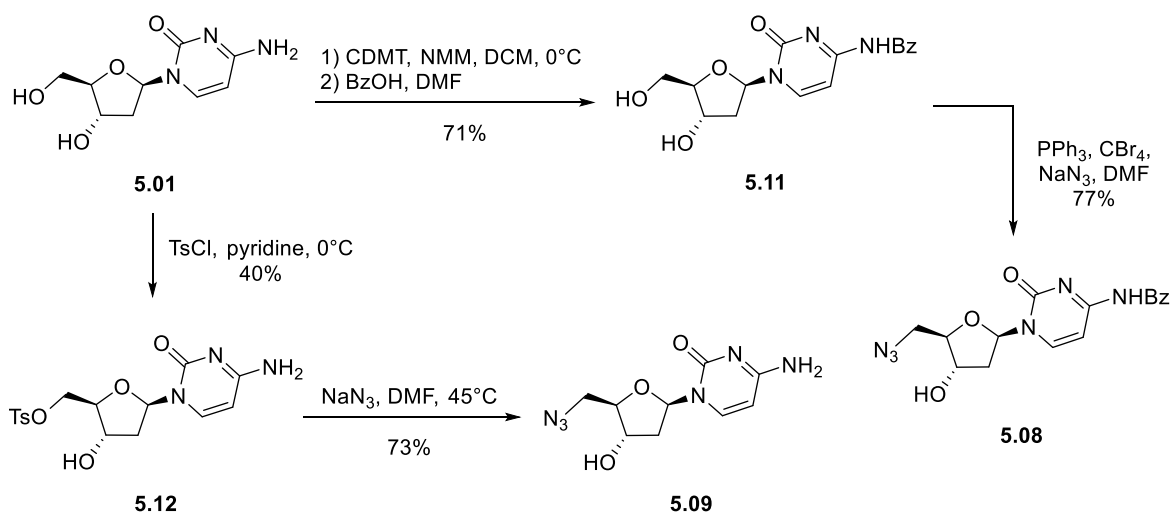


Scheme 5.1. Proposed synthesis of **5.03** – **5.05**. * represents relative stereochemical configurations.

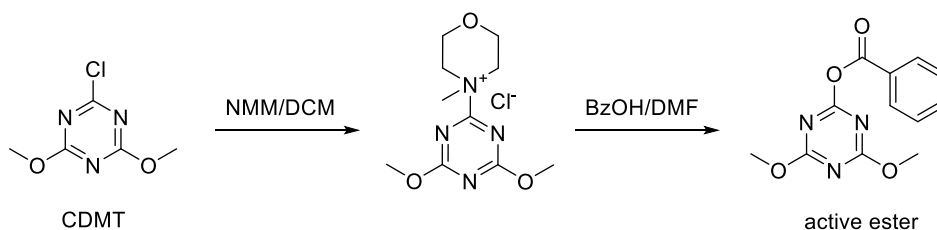
Cytidine azides **5.08** and **5.09**

2'-Deoxycytidine azide analogues **5.08** and **5.09** were prepared as shown in Scheme 5.2. 2-Chloro-4,6-dimethoxy-1,3,5-triazine (CDMT) was first reacted with *N*-methylmorpholine (NMM) to generate 4-(4,6-dimethoxy-1,3,5-triazin-2-yl)-4-methylmorpholinium chloride *in situ* (Scheme 5.3).³ This was followed by the addition of benzoic acid to generate a reactive ester (Scheme 5.3) that was further treated with 2'-deoxycytidine **5.01** to give *N*-benzoylated-2'-deoxycytidine **5.11** in 71% yield. This benzoylation strategy does not require temporary protection of free hydroxyl groups that is required in conventional two

step procedures.⁴ Treatment with triphenylphosphine, carbon tetrabromide, and sodium azide gave 5'-azido-2',5'-dideoxy-*N*⁴-benzoylcytidine azide **5.08** through an Appel reaction⁵ and *in situ* conversion of bromide into azide.⁶ 5'-Azido-2',5'-dideoxycytidine **5.09** required for the synthesis of triazole linked compound **5.03** was also prepared from 2'-deoxycytidine **5.01** as shown in Scheme 5.2. 2'-Deoxycytidine **5.01** was reacted with tosyl chloride in pyridine to give tosylated-2'-deoxycytidine **5.12** in 40% yield. Treatment with sodium azide in DMF gave 5'-azido-2',5'-dideoxycytidine **5.09** in 73% yield.



Scheme 5.2. Synthesis of cytidine azide **5.08** and **5.09**.



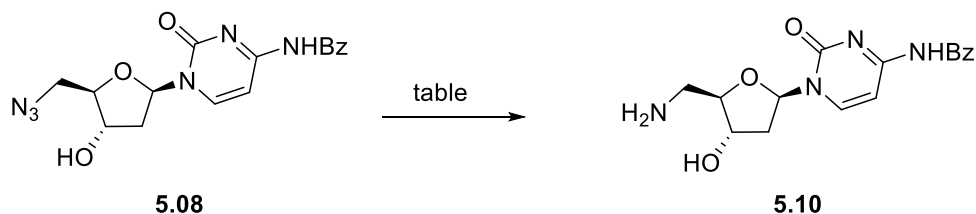
Scheme 5.3. *In situ* generation of active ester of CDMT. The scheme is adapted from Rode *et al.*³

5'-Amino-2',5'-dideoxy-*N*⁴-benzoylcytidine **5.10**

The preparation of 2'-deoxycytidine amine **5.10** was attempted using two different conditions as listed in Table 5.2. Hydrogenation of 2'-deoxycytidine azide **5.08** with palladium on carbon was initially attempted to give **5.10**. However, desired amine **5.10** was not isolated under this condition (Table 5.2, entry 1), rather it gave a complex reaction mixture. Alternatively, the Staudinger reaction⁷, which is a very mild azide reduction, was examined. The 2'-deoxycytidine azide **5.08** was treated with triphenylphosphine and water

in pyridine and the crude product was purified by flash column chromatography to give the desired reduced product **5.10** in 43% yield (Table 5.2, entry 2).

Table 5.2. Synthesis of 2'-deoxycytidine amine **5.10**.

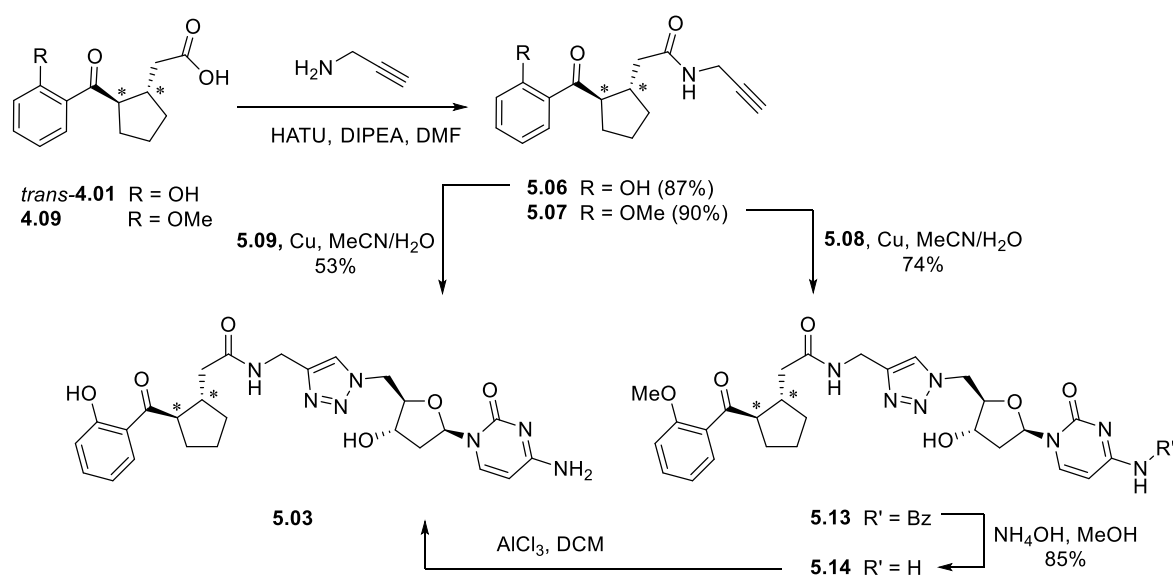


Entry	Reagent	Solvent	Time	Yield (%)
1	10% Pd/C, H ₂	MeOH/DMF (1:1)	2 h	0 ^a
2	Ph ₃ P, H ₂ O	pyridine	6 h	43 ^b

^a unidentified complex mixture; ^b isolated yield after flash chromatography.

5.2.2 Synthesis of triazole linked compound **5.03**

The synthesis of triazole linked compound **5.03** was accomplished as outlined in Scheme 5.4. Carboxylic acid **4.09** was first reacted with propargyl amine, in the presence of HATU and DIPEA, to give alkyne **5.07** in 90% yield. Treatment with azide **5.08**, in the presence

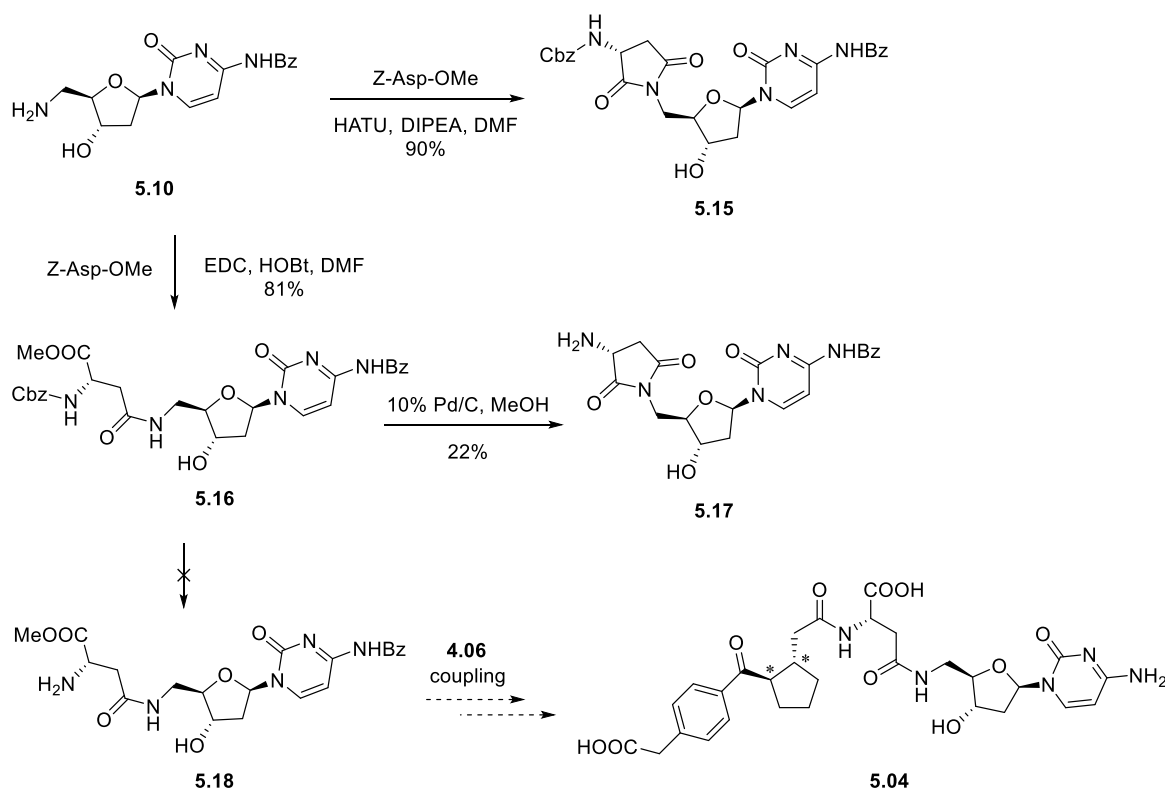


Scheme 5.4. Synthesis of triazole linked compound **5.03**. * represents relative stereochemical configurations.

of 20 mol% copper nano powder, gave triazole **5.13** in 74% yield through a CuAAC reaction. The benzoyl protecting group of **5.13** was removed on treatment with ammonium hydroxide to give triazole linked compound **5.14** in 85% yield. Treatment with anhydrous aluminium chloride in DCM gave a crude mixture of *O*-demethylated compound **5.03** and the starting material **5.14** as confirmed by ^1H NMR which revealed a small singlet methoxy peak of **5.14** at δ 3.87. However, **5.14** could not be separated from **5.03** by normal phase flash chromatography. Thus *trans*-**4.01** was first converted to alkyne **5.06** according to the procedure described for the synthesis of compound **5.07**. Alkyne **5.06** was then reacted with **5.09** through a CuAAC reaction described above using copper nano powder to give triazole linked compound **5.03** in 53% yield after purification by flash chromatography. These results suggest that protection of cytosine amine group is not necessary for the synthesis of triazole linked compounds using a CuAAC reaction.

5.2.3 Synthesis of amino acid linked compound 5.05

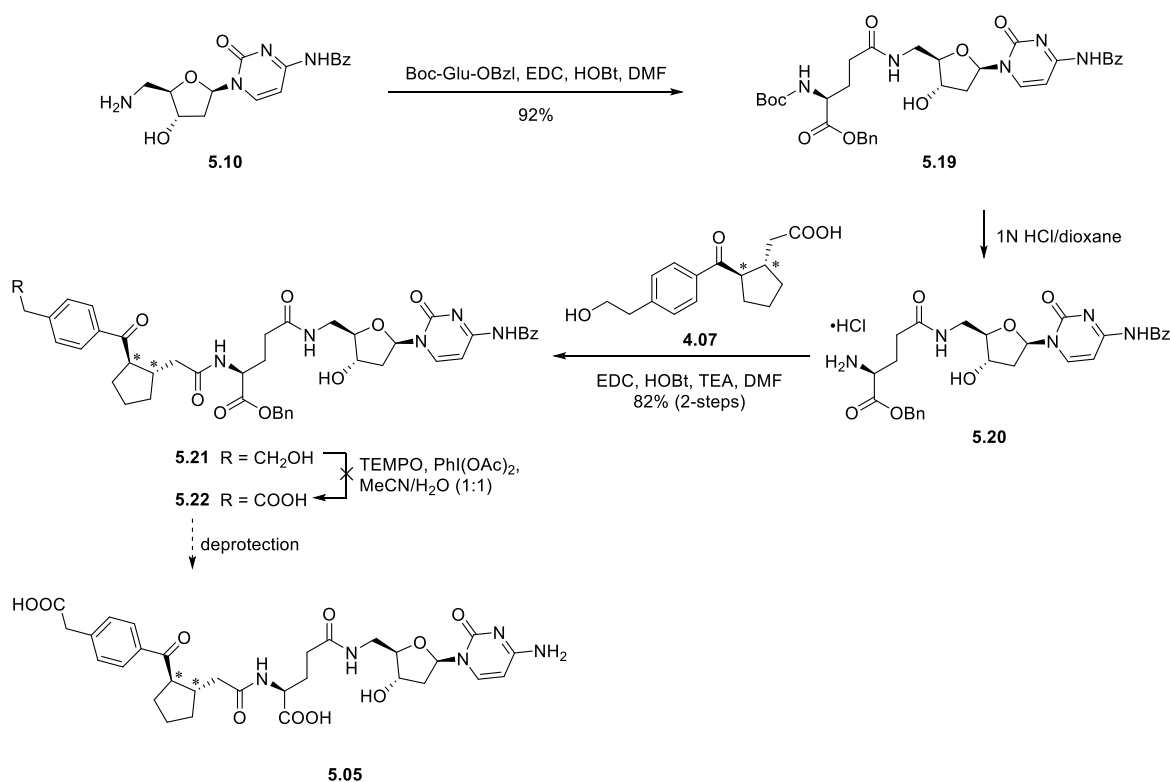
The preparation of cytidine aspartate **5.18** required for the synthesis of linked compound **5.04** was attempted as shown in Scheme 5.5. An initial sequence involving reaction of cytidine amine **5.10** with *Z*-Asp-OMe, HATU, and DIPEA in DMF failed to give cytidine



Scheme 5.5. Attempted synthesis of cytidine aspartate **5.18**. * represents relative stereochemical configurations.

aspartate **5.16**, with only cytidine aspartimide **5.15** being isolated in 90% yield. Formation of aspartimides by intramolecular cyclization is known to be a severe side reaction in the chemical synthesis of aspartic acid containing peptides.⁸⁻⁹ The addition of hydroxybenzotriazole (HOBt) is reported to suppress aspartimide formation, where intramolecular cyclization is much more facile under basic conditions.¹⁰ As expected, reaction of cytidine amine **5.10** with Z-Asp-OMe in the presence of EDC and HOBt gave cytidine aspartate **5.16** in 81% yield. However, subsequent treatment of **5.16** with 10% Pd/C in MeOH in an attempt to prepare **5.18** resulted in a complex mixture, with only Cbz-deprotected aspartimide **5.17** being isolated in 22% yield after flash chromatography. The synthesis of cytidine aspartate **5.18** and the subsequent linked compound **5.04** was therefore not examined further.

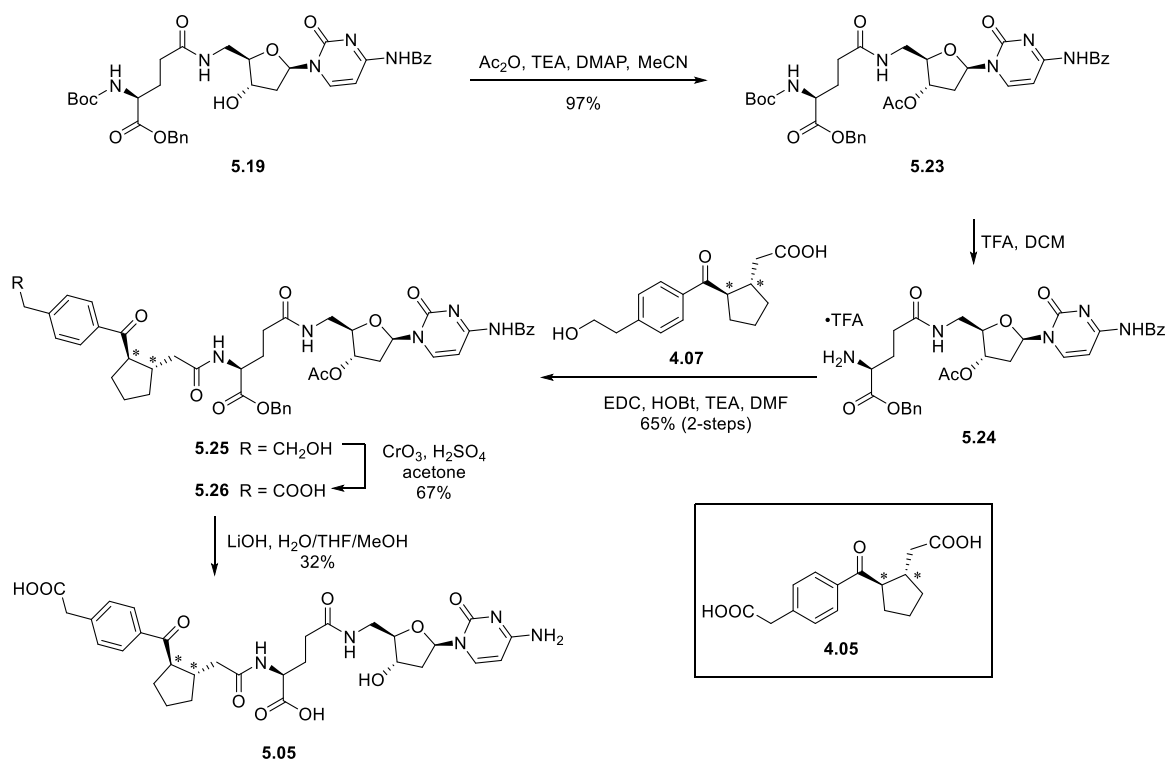
Rozners and Xu¹¹ reported a selective oxidation of a primary alcohol in the presence of a secondary alcohol and a sensitive uracil residue using (2,2,6,6-tetramethylpiperidin-1-yl)oxyl (TEMPO). Based on this observation, we next attempted to synthesise linked compound **5.05**. Access to the glutamate linked compound **5.05** required the conversion of the primary alcohol functionality of **5.21** to the carboxylic acid of **5.22** (Scheme 5.6). The cytidine amine **5.10** was treated with Boc-Glu-OBzl, EDC, and HOBt in DMF to give



Scheme 5.6. Attempted synthesis of **5.22** as a precursor of linked compound **5.05**. * represents relative stereochemical configurations.

cytidine glutamate **5.19** in 92% yield. Deprotection of the Boc group of **5.19** was achieved on treatment with 1N aqueous HCl to give **5.20**, which was directly used in the next step without further purification, see Scheme 5.6. Amine **5.20** was reacted with carboxylic acid **4.07** in the presence of EDC, HOBT and TEA in DMF to give alcohol **5.21** in 82% yield. Carboxylic acid **4.07** was used in this step since use of the dicarboxylic acid **4.05** would present problems with regioselectivity. The alcohol **5.21** was then treated with bis(acetoxy)iodobenzene (BAIB) and catalytic TEMPO in 1:1 MeCN/H₂O using the protocol of Rozners and Xu¹¹ in an attempt to prepare **5.22**. However, only starting material was recovered under these conditions, without evidence for the formation of the desired product **5.22**.

Given the limited success in the selective oxidation of the primary alcohol of **5.21**, an alternative synthetic route to the glutamate linked compound **5.05** was devised. This approach involved protection of the secondary alcohol of **5.19** to give acetate **5.23** with subsequent coupling with **4.07**, as shown in Scheme 5.7. The secondary alcohol **5.19** was thus treated with acetic anhydride, TEA, and DMAP in MeCN to give acetate **5.23** in 97% yield. Deprotection of the Boc group with TFA in DCM gave the aminium salt **5.24**, which was coupled with carboxylic acid **4.07**, in the presence of EDC, HOBT, and TEA, in DMF to give the linked alcohol **5.25** in 65% yield. The alcohol **5.25** was treated with Jones



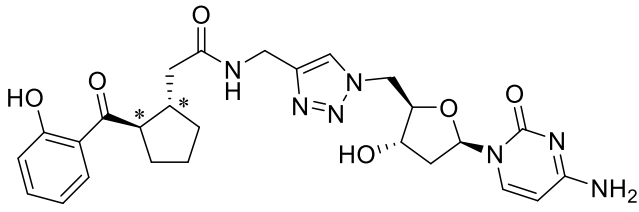
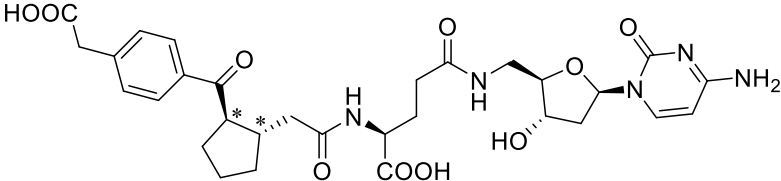
Scheme 5.7. Synthesis of linked compound **5.05**. * represents relative stereochemical configurations.

reagent¹² to give the corresponding carboxylic acid **5.26** in 67% yield. Finally, treatment with lithium hydroxide in 3:1:1 THF/MeOH/H₂O gave the desired linked compound **5.05** in 32% yield after purification by reverse phase flash chromatography. Interestingly, all protecting groups of **5.26** including benzoyl, benzyl, and acetyl groups were removed under these conditions.

5.3 DTBS binding assay results

Compounds **5.03** and **5.05** were assayed against *Mtb*DTBS by collaborators at the Department of Molecular and Biomedical Science, University of Adelaide, using Surface Plasma Resonance (SPR) analysis. The results are summarised in Table 5.3.

Table 5.3. SPR determined binding affinity of linked compounds **5.03** and **5.05** towards *Mtb*DTBS. * represents relative stereochemical configurations.

Compound	K_D (mM)
 <p style="text-align: center;">5.03</p>	0.6 ± 0.2
 <p style="text-align: center;">5.05</p>	0.7 ± 0.2

Linked compound **5.03**, the direct triazole linked analogue of *trans*-**4.01** and 2'-deoxycytidine **5.01**, showed enhanced binding affinity toward *Mtb*DTBS ($K_D = 0.6 \pm 0.2$ mM) compared to the original substituents *trans*-**4.01** ($K_D = 3.4$ mM) and **5.01** ($K_D = >1$ mM). However, the calculated K_D value (0.6 ± 0.2 mM) was beyond the range of concentrations used in the assay due to the limited solubility of linked compound **5.03** (Figure 5.8). Therefore, the K_D value of **5.03** could be subject to larger error than indicated.

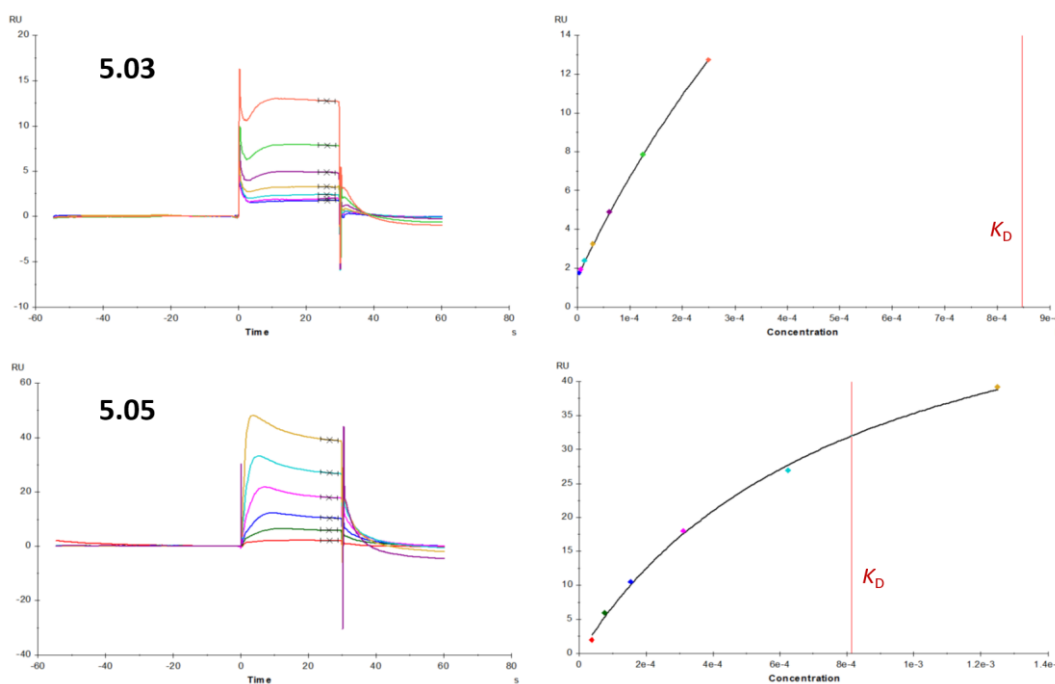


Figure 5.8. SPR sensorgram (left) and concentration vs response plot (right) of **5.03** and **5.05**.

Linked compound **5.05** ($K_D = 0.7 \pm 0.2$ mM) demonstrated a similar level of binding affinity toward *Mtb*DTBS as **5.03** ($K_D = 0.6 \pm 0.2$ mM). Interestingly, the binding affinity of **5.05** was approximately 40-fold weaker than 4-carboxymethylbenzoyl compound **4.05** ($K_D = 17 \pm 1$ μ M). Linked compound **5.05** was expected to have a higher binding affinity toward *Mtb*DTBS than triazole linked compound **5.03** due to the inclusion of both the glutamate linker and **4.05** moiety, which exhibit the highest affinity for *Mtb*DTBS amongst cyclopentylacetic acid analogues discussed in Chapter 4 (Figure 5.9). A carboxyl group of glutamate linker was expected to bind to the P-loop in the binding site. The low binding affinity of **5.05** suggests that the glutamate linker may not interact with the P-loop, possibly due to its flexibility. Excessive conformational flexibility would increase the entropic penalty of binding.¹³ Indeed, the glutamate linker moiety of **5.05** possesses multiple rotatable bonds, affording it more conformational flexibility than the triazole linker of **5.03**.

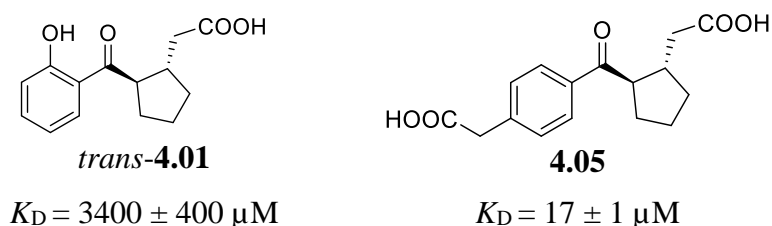


Figure 5.9. Comparison of *trans*-**4.01** and **4.05**. Stereochemical configurations are relative.

5.4 X-ray crystal structure of 5.03 and 5.05 bound to DTBS

The structures of linked compounds **5.03** and **5.05** bound to *Mtb*DTBS were solved by collaborators at the Department of Molecular and Biomedical Science, University of Adelaide as depicted in Figure 5.10 and 5.11. One stereoisomer was modelled only as the inclusion of both stereoisomers did not correlate with the crystallographic data.

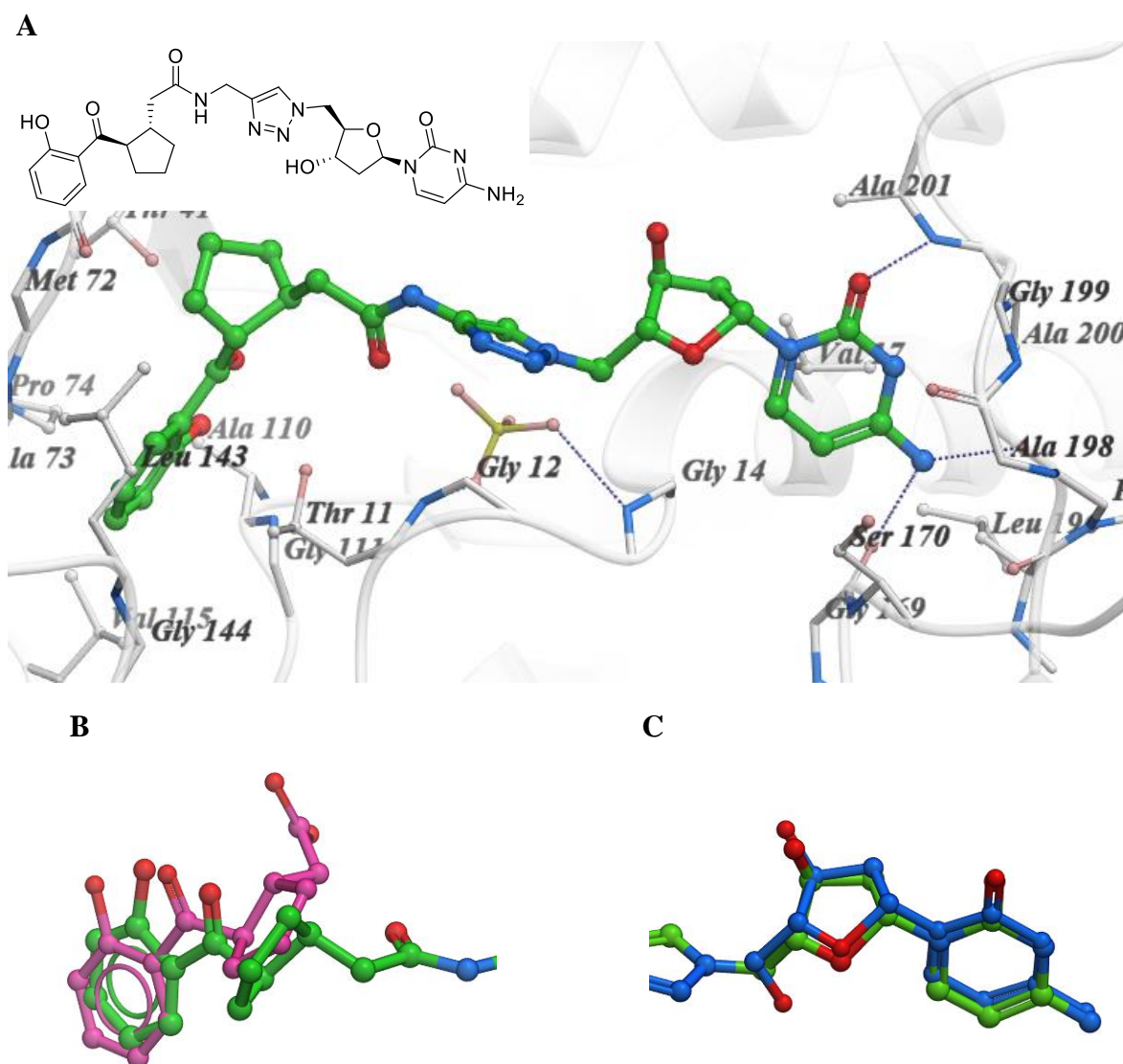


Figure 5.10. The binding mode of linked compound **5.03** to *Mtb*DTBS. (A) **5.03** (green) binds to the *Mtb*DTBS active site above a sulfate ion (yellow) that is bound to the P-loop. (B) The cyclopentylacetic acid moiety of **5.03** (green) exhibits conformational differences from **RS-4.01** binding pose (magenta). (C) The 2'-deoxycytidine moiety of **5.03** (green) overlays well with 2'-deoxycytidine **5.01** (blue).

The X-ray crystal structure of **5.03** bound to *Mtb*DTBS is shown in Figure 5.10. The triazole linker moiety is not bound to the P-loop, but is rather located away from the protein surface, around a sulfate ion bound at this position (Figure 5.10A). The conformation of cyclopentylacetic acid moiety of **5.03** slightly differs from *RS-4.01* binding conformation (Figure 5.10B), whilst the 2'-deoxycytidine moiety of **5.03** binds in the same pose as **5.01** (Figure 5.10C). The conformational difference of cyclopentylacetic acid moiety is presumably due to the conversion of the carboxyl group of **4.01** to the amide group of **5.03**, abrogating several interactions with the enzyme to accommodate the linker

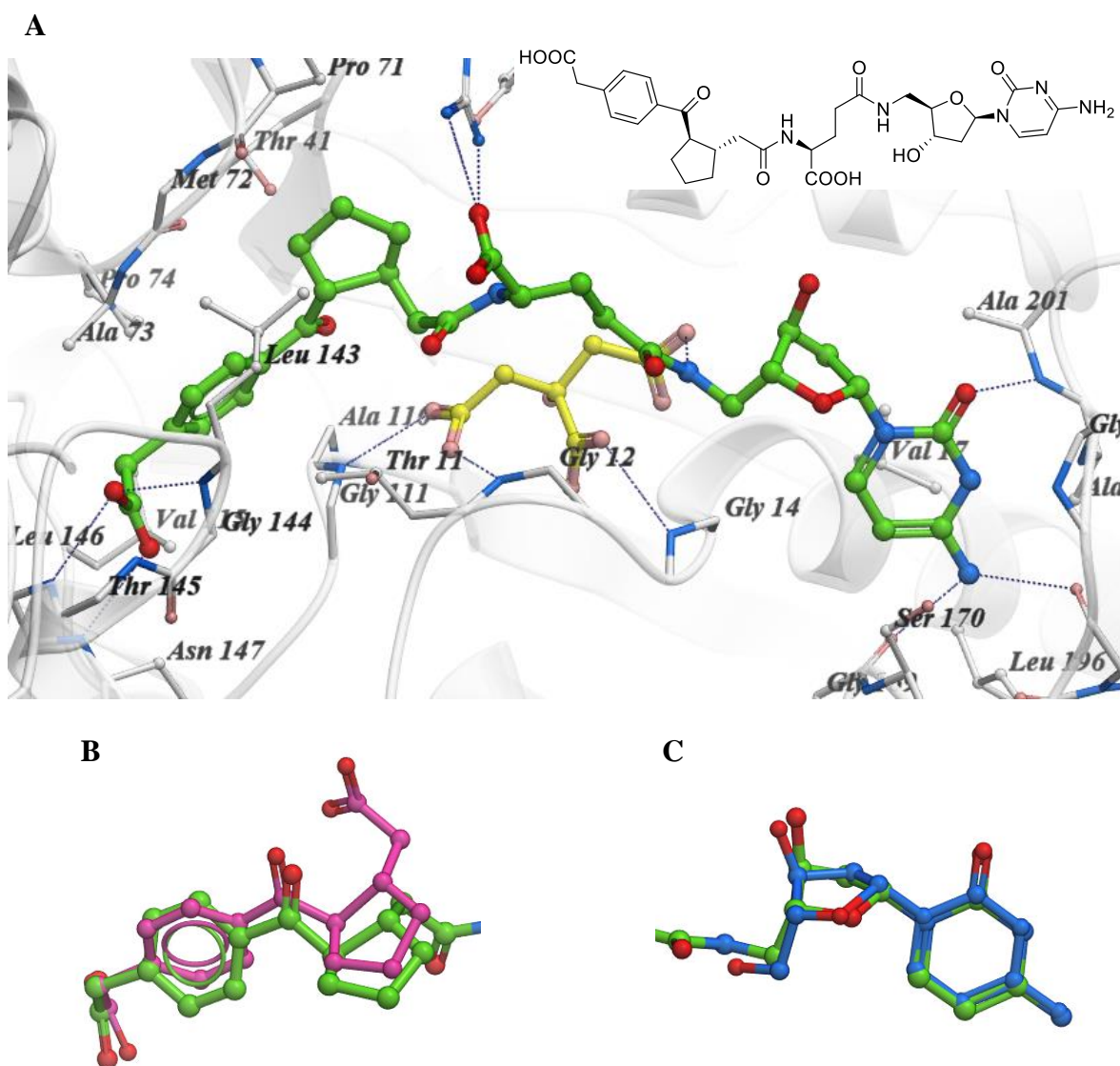


Figure 5.11. The binding mode of linked compound **5.05** to *Mtb*DTBS. (A) **5.05** exhibits a binding conformation adjacent to the crystallographic precipitant, citrate (yellow). (B) The cyclopentylacetic acid moiety of **5.05** (green) exhibits conformational differences from the original *RS-4.05* binding pose (magenta). (C) The 2'-deoxycytidine moiety of **5.05** (green) overlays well with 2'-deoxycytidine **5.01** (blue).

moiety. The carboxyl group of *trans*-**4.01** forms hydrogen bonds with residues Thr11, Lys15 and Gly111 in the active site, whereas the amide carbonyl group of **5.03** does not interact with these amino acid residues. Crystallography results propose that the triazole linker moiety does not favourably interact with the P-loop.

The X-ray crystallographic structure of linked compound **5.05** reveals a similar binding pose to **5.03** as discussed above. The cyclopentylacetic acid and 2'-deoxycytidine moieties bind to the DAPA and nucleoside pockets respectively, but with the linker moiety bound adjacent to the crystallographic precipitant, citrate (Figure 5.11). The linker likely has multiple disordered conformations as the observed electron density for the glutamate linker is weaker than that for the cyclopentylacetic acid and 2'-deoxycytidine moieties (Figure 5.12). The combined binding affinity and X-ray crystallographic data demonstrates that the use of a glutamic acid to link fragments **4.05** and **5.01** does not enhance binding over triazole linked compound **5.03**. Considering that linkers of **5.03** and **5.05** are located around the crystallographic precipitant (sulfate or citrate) instead of binding to the P-loop, the linker moiety requires further optimisation in order to encourage interactions with the P-loop in the binding site.

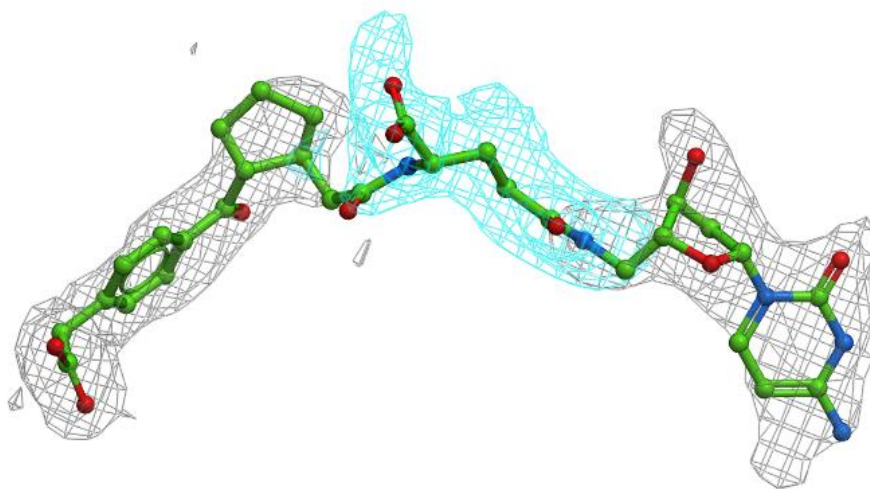


Figure 5.12. Electron density for **5.05** is strong (grey mesh) for cyclopentylacetic acid and 2'-deoxycytidine moieties but weak (cyan mesh) for the glutamate linker moiety.

5.5 Conclusion

The linked compound **5.03** was successfully synthesised by a CuAAC reaction of **5.06** with **5.09** (see Scheme 5.4) and assayed for binding affinity toward *Mtb*DTBS. Triazole linked compound **5.03** ($K_D = 0.6 \pm 0.2$ mM), the direct triazole linked analogue of *trans*-

4.01 and **5.01**, was more potent than the original substituents *trans*-**4.01** ($K_D = 3.4$ mM) and **5.01** ($K_D > 1$ mM). X-ray crystallography of **5.03** bound to *Mtb*DTBS reveals that the cyclopentylacetic acid and cytidine moieties of **5.03** bind to DAPA and nucleoside pockets respectively as per *trans*-**4.01** and **5.01**. The triazole linker moiety does not bind to the P-loop of the enzyme, with a sulfate ion occupying this site.

The linked compound **5.05** was synthesised by attachment of glutamate to cytidine amine **5.10** with subsequent coupling with **4.07** (see Scheme 5.6 and 5.7) and assayed against *Mtb*DTBS. The binding affinity of **5.05** ($K_D = 0.7 \pm 0.2$ mM) was similar to that of **5.03** ($K_D = 0.6 \pm 0.2$ mM). Compound **5.05**, the direct glutamate linked analogue of **4.05** and **5.01**, was approximately 40-fold less potent than the original substituent **4.05**, suggesting the use of a glutamic acid as a linker moiety does not enhance binding over **4.05**. The crystal structure of **5.05** bound to *Mtb*DTBS was determined to reveal that the cyclopentylacetic acid and cytidine moieties adopted poses similar to those previously observed for **4.03** and **5.01**. The glutamate linker moiety is not bound the P-loop, but rather located adjacent to a citrate ion at this position as per the triazole moiety of **5.03**.

Future work toward more potent linked *Mtb*DTBS inhibitors would require optimising the linker moiety between cyclopentylacetic acid **4.05** and 2'-deoxycytidine **5.01**. A carboxyl group of **4.05** forms hydrogen bonds with residues Thr11, Lys15 and Gly111 of *Mtb*DTBS, while the amide carbonyl group of **5.05** does not form a hydrogen bond with the enzyme. Thus, acidic moieties (e.g. acylsulfamide), with a low pK_a value as per the carboxyl group of **4.05**, could be considered to link the fragments **4.05** and **5.01** (Figure 5.13). Given that sulfate and citrate ions are known to bind the P-loop of the enzyme, analogues of sulfate or citrate also should be investigated as a linker moiety.

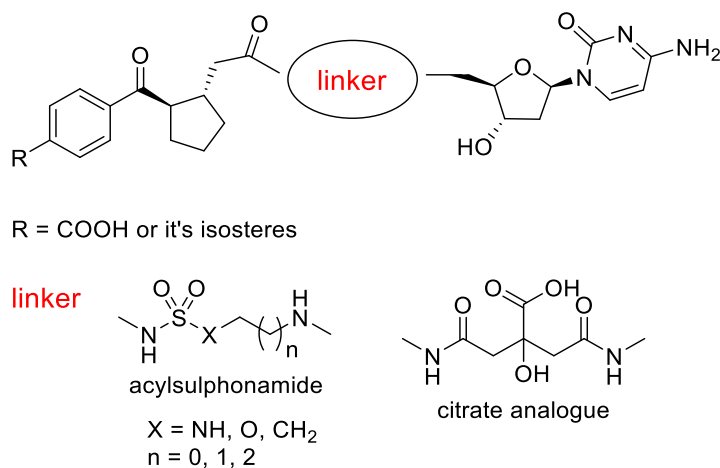


Figure 5.13. Future compound development of linked *Mtb*DTBS inhibitors.

5.6 References for Chapter Five

1. Thompson, A. P.; Salaemae, W.; Pederick, J. L.; Abell, A. D.; Booker, G. W.; Bruning, J. B.; Wegener, K. L.; Polyak, S. W., Mycobacterium tuberculosis Dethiobiotin Synthetase Facilitates Nucleoside Triphosphate Promiscuity through Alternate Binding Modes. *Acs Catalysis* **2018**, *8* (11), 10774-10783.
2. Rostovtsev, V. V.; Green, L. G.; Fokin, V. V.; Sharpless, K. B., A stepwise Huisgen cycloaddition process: Copper(I)-catalyzed regioselective "ligation" of azides and terminal alkynes. *Angewandte Chemie-International Edition* **2002**, *41* (14), 2596-+.
3. Rode, A. B.; Son, S. J.; Hong, I. S., An Efficient One-pot N-Acylation of Deoxy- and Ribo-cytidine Using Carboxylic Acids Activated in situ with 2-Chloro-4,6-dimethoxy-1,3,5-triazine. *Bull. Korean Chem. Soc.* **2010**, *31* (7), 2061-2064.
4. Ti, G. S.; Gaffney, B. L.; Jones, R. A., Transient Protection - Efficient One-Flask Syntheses of Protected Deoxynucleosides. *J. Am. Chem. Soc.* **1982**, *104* (5), 1316-1319.
5. Appel, R., Tertiary Phosphane-Tetrachloromethane, a Versatile Reagent for Chlorination, Dehydration, and P-N Linkage. *Angewandte Chemie-International Edition in English* **1975**, *14* (12), 801-811.
6. Patureau, B. M.; Hudson, R. H. E.; Damha, M. J., Induction of RNase H activity by arabinose-peptide nucleic acid chimeras. *Bioconjugate Chem.* **2007**, *18* (2), 421-430.
7. Gololobov, Y. G.; Zhmurova, I. N.; Kasukhin, L. F., 60 Years of Staudinger Reaction. *Tetrahedron* **1981**, *37* (3), 437-472.
8. Nicolas, E.; Pedroso, E.; Giralt, E., Formation of Aspartimide Peptides in Asp-Gly Sequences. *Tetrahedron Lett.* **1989**, *30* (4), 497-500.
9. Yang, Y.; Sweeney, W. V.; Schneider, K.; Thornqvist, S.; Chait, B. T.; Tam, J. P., Aspartimide Formation in Base-Driven 9-Fluorenylmethoxycarbonyl Chemistry. *Tetrahedron Lett.* **1994**, *35* (52), 9689-9692.
10. Michels, T.; Dolling, R.; Haberkorn, U.; Mier, W., Acid-Mediated Prevention of Aspartimide Formation in Solid Phase Peptide Synthesis. *Org. Lett.* **2012**, *14* (20), 5218-5221.

-
11. Rozners, E.; Xu, Q., Total synthesis of 3',5'-C-branched nucleosides. *Org. Lett.* **2003**, 5 (21), 3999-4001.
 12. Bowden, K.; Heilbron, I. M.; Jones, E. R. H.; Weedon, B. C. L., Researches on Acetylenic Compounds .1. The Preparation of Acetylenic Ketones by Oxidation of Acetylenic Carbinols and Glycols. *J. Chem. Soc.* **1946**, (Jan), 39-45.
 13. Chung, S. M.; Parker, J. B.; Bianchet, M.; Amzel, L. M.; Stivers, J. T., Impact of linker strain and flexibility in the design of a fragment-based inhibitor. *Nat. Chem. Biol.* **2009**, 5 (6), 407-413.

Chapter Six

6.1 General methods

All reagents were obtained from commercial sources and are of reagent grade or as specified. Solvents were also obtained from commercial sources, except for anhydrous THF, anhydrous DCM and anhydrous DMF which were dried over solvent purifier (PS-Micro, Innovative Technology, USA). Reactions were monitored by TLC using precoated plates (silica gel 60 F254, 250 μm , Merck, Darmstadt, Germany), spots were visualised under ultraviolet light at 254 nm and with either sulphuric acid-vanillin spray, potassium permanganate dip or Hanessian's stain. Flash column chromatography was performed with silica gel (40-63 μm 60 Å, Davisil, Grace, Germany). Preparative TLC was carried out on 20 x 20 cm plates coated with silica gel 60 F254 and having a 2 mm thickness which were purchased from Analtech, Inc. Microwave reactions were performed on a CEM Discovery SP with external IR temperature monitoring. Reactions were stirred for 5 min in a sealed container at ambient temperature, followed by 5 min stirring with increased microwave power until the prescribed temperature was reached. Both power and pressure were kept variable. ^1H , ^{13}C and ^{19}F NMR spectra were recorded on a Varian Inova 500 MHz or a Varian Inova 600 MHz. Chemical shifts are given in ppm (δ) relative to the residue signals, which in the case of DMSO- d_6 were 2.50 ppm for ^1H and 39.55 ppm for ^{13}C , CDCl_3 were 7.26 ppm for ^1H and 77.23 ppm for ^{13}C and D_2O was 4.79 for ^1H . Structural assignment was confirmed with COSY, NOESY, HSQC and HMBC. High-resolution mass spectra (HRMS) were recorded on an Agilent 6230 time of flight (TOF) liquid chromatography mass spectra (LC/MS) ($\Delta < 5$ ppm). Infrared mass spectra were recorded on PerkinElmer Spectrum 100 FTIR with a Universal Zinc Selenide crystal ATR attachment.

6.2 Experimental work as described in Chapter 2

General Procedure for CuAAC

Copper nano powder (40 mol %) was added to a stirring suspension of biotin acetylene **8**¹ (1.0 equiv) and corresponding azide (1.5 equiv) in $\text{CH}_3\text{CN}:\text{H}_2\text{O}$ (2:1) (1 mL per 60 mg of **8**). The reaction was sonicated for 15 min and stirred at ambient temperature for 17 hours. The reaction mixture was then concentrated under reduced pressure and the residue purified by column chromatography on silica gel. See individual experiments for details.

General Procedure for Synthesis of 5-Iodo-1,2,3-triazoles

To a solution of 1-iodoalkyne **10** (1.0 equiv) and corresponding azide (1.0 - 1.2 equiv) in dry DMF (1 ml per 10 mg of 1-iodoalkyne) was added CuI (0.05 equiv) and TEA (2.0 equiv) and the mixture was stirred at ambient temperature for 1 day. The mixture was quenched with 10% NH₄OH and extracted with DCM twice. The combined organics were dried over anhydrous sodium sulfate and concentrated under reduced pressure. The resulting residue was purified by column chromatography on silica gel. See individual experiments for details.

General Procedure for Halogen Exchange of 5-Iodo-1,2,3-triazole

To a round-bottomed microwave vial was added 5-iodo-1,2,3-triazole (1.0 equiv) and potassium halide (5.0 equiv). The solids were washed off of the side with acetonitrile (1 ml per 50 mg of triazole) and then deionised water (1 ml per 50 mg of triazole). The vial was placed into the microwave reactor set at a pressure of 200 psi and heated at 180 °C for 5-10 min based on ¹H NMR. After the vial was cooled to ambient temperature, the mixture was diluted with EtOAc and the organic layer was extracted with a Pasteur pipette. The resulting aqueous layer was extracted three additional times and the combined organics were dried over anhydrous sodium sulfate and concentrated under reduced pressure. The residue was purified by column chromatography on silica gel. See individual experiments for details.

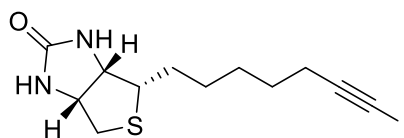
General Procedure for Synthesis of Benzyl Azides

A solution of the benzyl halide (1.0 equiv) and sodium azide (1.3 equiv) in DMF (1 mL per 50mg of benzyl halide) was stirred at ambient temperature for 5 hours. The reaction mixture was diluted with ether and wash with water three times. The organic layer was dried over anhydrous sodium sulfate and concentrated under reduced pressure. See individual experiments for details.

General Procedure for Hydrolysis of Ester

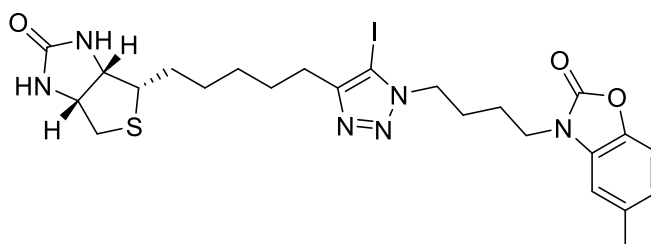
To a mixture of ester (1.0 equiv) in THF:MeOH:H₂O (3:1:1) (1 mL per 10 mg of ester) was added LiOH (2.2 equiv) and the mixture was stirred for 17 hours. The resulting mixture was acidified with 1 M HCl to pH = 4. The mixture was diluted with DCM:MeOH (9:1) and washed with 0.5M HCl, water, and brine. The organic layer was dried over anhydrous sodium sulfate and concentrated under reduced pressure. The residue was purified by column chromatography on silica gel. See individual experiments for details.

(3*aS*,4*S*,6*aR*)-4-(7-iodohept-6-yn-1-yl)tetrahydro-1*H*-thieno[3,4-*d*]imidazol-2(3*H*)-one (**10**)



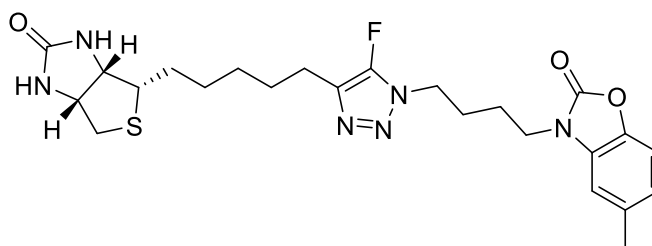
To a solution of biotin acetylene **8**¹ (100 mg, 0.42 mmol) in dry DMF (5 ml) was added CuI (5 mg, 0.08 mmol) and N-iodomorpholine (286 mg, 0.84 mmol). The reaction mixture was stirred at ambient temperature. After full conversion (>99%) was achieved in 1 hour as judged by ¹H NMR, the reaction mixture was filtered through a pad of neutral aluminium oxide, washed with 10% MeOH in DCM (3 x 20 ml) and dried *in vacuo* to give **10** as a pale yellow solid. This material was used without further purification.

3-(4-(5-iodo-4-(5-((3*aS*,4*S*,6*aR*)-2-oxohexahydro-1*H*-thieno[3,4-*d*]imidazol-4-yl)pentyl)-1*H*-1,2,3-triazol-1-yl)butyl)-5-methylbenzo[*d*]oxazol-2(3*H*)-one (**4b**)



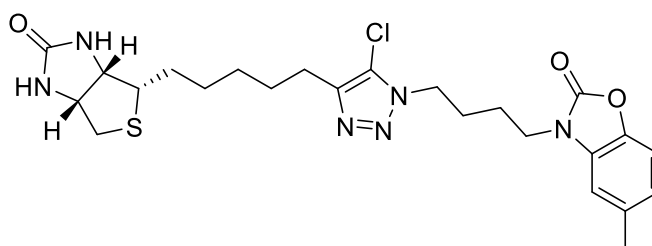
The iodo-acetylene **10** (20 mg, 0.06 mmol) and azide **9**¹ (14 mg, 0.06 mmol) was reacted according to general procedure for synthesis of 5-Iodo-1,2,3-triazoles and was purified by flash chromatography on silica eluting with 5% MeOH in DCM to give a yellowish solid (12 mg, 36%). ¹H NMR (500 MHz; CDCl₃) δ 7.08 (d, *J* = 8.1 Hz, 1H), 6.90 - 6.92 (m, 1H), 6.78 (m, 1H), 5.08 (br s, 1H), 4.86 (br s, 1H), 4.50 - 4.53 (m, 1H), 4.42 (t, *J* = 6.9 Hz, 2H), 4.30 - 4.33 (m, 1H), 3.84 (t, *J* = 6.9 Hz, 2H), 3.14 - 3.19 (m, 1H), 2.93 (dd, *J* = 5.0, 12.8 Hz, 1H), 2.74 (d, *J* = 12.8 Hz, 1H), 2.64 (d, *J* = 7.5 Hz, 2H), 2.40 (s, 3H), 1.97 - 2.02 (m, 2H), 1.79 - 1.84 (m, 2H), 1.64 - 1.72 (m, 4H), 1.38 - 1.49 (m, 4H); ¹³C NMR (125 MHz; CDCl₃) δ 162.8, 154.9, 151.8, 140.7, 134.0, 130.8, 122.9, 109.7, 108.8, 61.9, 60.1, 55.5, 49.7, 41.3, 40.6, 28.9, 28.6, 28.6, 28.4, 26.6, 25.8, 24.5, 21.5; HRMS calcd. for [M + H]⁺ C₂₄H₃₂IN₆O₃S, requires 611.1301, found 611.1298.

3-(4-(5-fluoro-4-(5-((3*aS*,4*S*,6*aR*)-2-oxohexahydro-1*H*-thieno[3,4-*d*]imidazol-4-yl)pentyl)-1*H*-1,2,3-triazol-1-yl)butyl)-5-methylbenzo[*d*]oxazol-2(3*H*)-one (**4c**)



The 5-iodo-triazole **4b** (15 mg, 0.03 mmol) was reacted with potassium fluoride (7 mg, 0.12 mmol) according to general procedure for halogen exchange of 5-Iodo-1,2,3-triazole for 10 min and was purified by flash chromatography on silica eluting with 5% MeOH in DCM to yield 5-fluoro-triazole as an off white solid (11 mg, 89%). ^1H NMR (500 MHz; CDCl_3) δ 7.08 (d, $J = 8.1$ Hz, 1H), 6.90-6.92 (m, 1H), 6.76 - 6.77 (m, 1H), 5.06 (br s, 1H), 4.82 (br s, 1H), 4.49 - 4.52 (m, 1H), 4.30 - 4.33 (m, 1H), 4.27 (t, $J = 6.9$ Hz, 2H), 3.85 (t, $J = 6.9$ Hz, 2H), 3.14 - 3.17 (m, 1H), 2.92 (dd, $J = 5.0, 12.8$ Hz, 1H), 2.73 (d, $J = 12.8$ Hz, 1H), 2.62 (d, $J = 7.5$ Hz, 2H), 2.40 (s, 3H), 1.96 - 2.02 (m, 2H), 1.79 - 1.85 (m, 2H), 1.63 - 1.70 (m, 4H), 1.37 - 1.48 (m, 4H); ^{13}C NMR (125 MHz; CDCl_3) δ 162.8, 154.9, 140.7, 134.0, 130.7, 122.9, 110.0, 109.7, 108.7, 61.9, 60.0, 55.5, 46.1, 41.2, 40.5, 28.9, 28.6, 28.6, 28.0, 26.2, 24.7, 23.4, 21.5, HRMS calcd. for $[\text{M} + \text{H}]^+$ $\text{C}_{24}\text{H}_{32}\text{FN}_6\text{O}_3\text{S}$, requires 503.2241, found 503.2220.

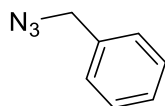
3-(4-(5-chloro-4-(5-((3*aS*,4*S*,6*aR*)-2-oxohexahydro-1*H*-thieno[3,4-*d*]imidazol-4-yl)pentyl)-1*H*-1,2,3-triazol-1-yl)butyl)-5-methylbenzo[*d*]oxazol-2(3*H*)-one (**4d**)



The 5-iodo-triazole **4b** (15 mg, 0.03 mmol) was reacted with potassium chloride (9 mg, 0.12 mmol) according to general procedure for halogen exchange of 5-Iodo-1,2,3-triazole for 10 min and was purified by flash chromatography on silica eluting with 5% MeOH in DCM to yield 5-fluoro-triazole as an off white solid (10 mg, 80%). ^1H NMR (500 MHz; CDCl_3) δ 7.03 (m, 1H), 6.97 - 6.99 (m, 1H), 6.83 (d, $J = 8.1$ Hz, 1H), 5.39 (br s, 1H), 5.08 (br s, 1H), 4.49 - 4.51 (m, 1H), 4.35 (t, $J = 6.9$ Hz, 2H), 4.29 - 4.32 (m, 1H), 3.84 (t, $J = 6.9$ Hz, 2H), 3.13 - 3.17 (m, 1H), 2.91 (dd, $J = 5.0, 12.8$ Hz, 1H), 2.72 (d, $J = 12.8$ Hz, 1H), 2.62 (t, $J = 7.5$ Hz, 2H), 2.38 (s, 3H), 1.95 - 2.01 (m, 2H), 1.77 - 1.83 (m, 2H), 1.63 - 1.73 (m, 4H), 1.36 - 1.47 (m, 4H); ^{13}C NMR (125 MHz; CDCl_3) δ 163.1, 154.8, 143.6, 142.8, 132.7, 128.4,

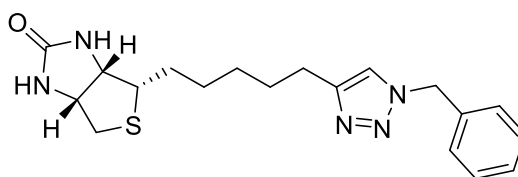
124.3, 122.2, 110.8, 107.8, 62.0, 60.1, 55.6, 47.3, 41.3, 40.5, 28.9, 28.6, 28.5, 28.0, 26.2, 24.6, 24.3, 21.4; HRMS calcd. for $[M + H]^+$ $C_{24}H_{32}ClN_6O_3S$, requires 519.1945, found 519.1909.

(azidomethyl)benzene (**11a**)²



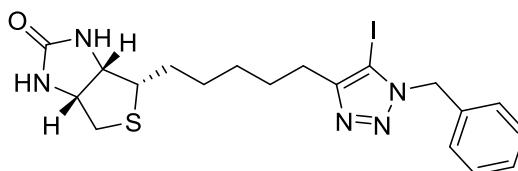
Benzyl bromide (343 mg, 2.00 mmol) and sodium azide (169 mg, 2.60 mmol) was reacted according to general procedure for synthesis of benzyl azides to give a yellow liquid (245 mg, 92%). ¹H NMR (500 MHz, CDCl₃) δ 7.31 - 7.44 (m, 5H), 4.36 (s, 2H).

(3a*S*,4*S*,6a*R*)-4-(5-(1-benzyl-1*H*-1,2,3-triazol-4-yl)pentyl)tetrahydro-1*H*-thieno[3,4-*d*]imidazol-2(3*H*)-one (**5a**)



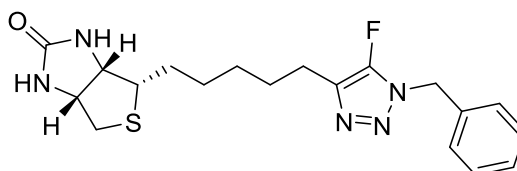
Biotin acetylene **8**¹ (60 mg, 0.25 mmol) was reacted with azide **11a** (51 mg, 0.38 mmol) and Cu nanopowder (6 mg, 0.1 mmol) according to general procedure for CuAAC and purified by flash chromatography on silica gel eluting with 5% MeOH in DCM to give an off white solid (53 mg, 57%). ¹H NMR (500 MHz, CDCl₃) δ 7.33 - 7.41 (m, 3H), 7.25 - 7.29 (m, 2H), 7.20 (s, 1H), 5.50 (s, 2H), 5.14 (br s, 1H), 4.87 (br s, 1H), 4.49 - 4.53 (m, 1H), 4.28 - 4.33 (m, 1H), 3.13 - 3.18 (m, 1H), 2.92 (dd, $J = 5.01, 12.84$ Hz, 1H), 2.67 - 2.75 (m, 3H), 1.60 - 1.73 (m, 4H), 1.36 - 1.50 (m, 4H); ¹³C NMR (125 MHz, CDCl₃) δ 162.9, 148.6, 134.9, 129.1, 128.6, 128.0, 120.6, 61.9, 60.0, 55.5, 54.0, 40.5, 29.0, 28.7, 28.5, 25.5; HRMS calcd for $C_{19}H_{25}N_5OS$ $[M + H]^+$ 372.1858, found 372.1849.

(3a*S*,4*S*,6a*R*)-4-(5-(1-benzyl-5-iodo-1*H*-1,2,3-triazol-4-yl)pentyl)tetrahydro-1*H*-thieno[3,4-*d*]imidazol-2(3*H*)-one (**6a**)



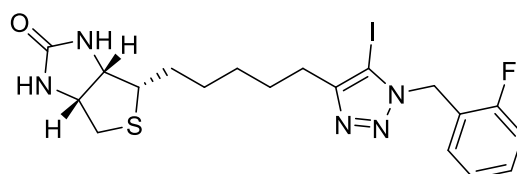
The iodo-acetylene **10** (0.25 mmol) and azide **11a** (37 mg, 0.28 mmol) was reacted according to general procedure for synthesis of 5-Iodo-1,2,3-triazoles and was purified by flash chromatography on silica eluting with 6% MeOH in DCM to give an off white solid (31 mg, 25%). ^1H NMR (500 MHz, CDCl_3) δ 7.30 - 7.40 (m, 3H), 7.25 (s, 2H), 5.58 (s, 2H), 4.90 (br s, 1H), 4.72 (br s, 1H), 4.49 - 4.54 (m, 1H), 4.29 - 4.34 (m, 1H), 3.14 - 3.20 (m, 1H), 2.93 (dd, $J = 5.01, 12.84$ Hz, 1H), 2.73 (d, $J = 12.96$ Hz, 1H), 2.66 (t, $J = 7.58$ Hz, 2H), 1.61 - 1.77 (m, 4H), 1.37 - 1.54 (m, 4H); ^{13}C NMR (125 MHz, CDCl_3) δ 162.7, 152.2, 134.5, 128.8, 128.4, 127.7, 61.9, 60.0, 55.4, 54.2, 40.5, 28.9, 28.6, 28.5, 28.4, 25.9; HRMS calcd for $\text{C}_{19}\text{H}_{24}\text{IN}_5\text{OS}$ [$\text{M} + \text{NH}_3$] $^+$ 515.1090, found 515.1075.

(3*aS*,4*S*,6*aR*)-4-(5-(1-benzyl-5-fluoro-1*H*-1,2,3-triazol-4-yl)pentyl)tetrahydro-1*H*-thieno[3,4-*d*]imidazol-2(3*H*)-one (**7a**)



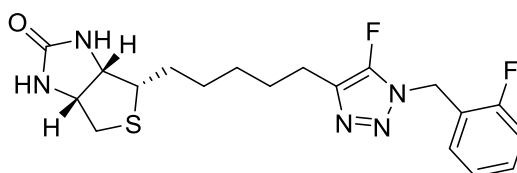
The 5-iodo-triazole **6a** (12 mg, 0.024 mmol) was reacted with potassium fluoride (7 mg, 0.12 mmol) according to general procedure for halogen exchange of 5-Iodo-1,2,3-triazole for 5 min and was purified by flash chromatography on silica eluting with 6% MeOH in DCM to yield 5-fluoro-triazole as an off white solid (6 mg, 64%). ^1H NMR (500 MHz, CDCl_3) δ 7.29 - 7.41 (m, 5H), 5.48 (br s, 1H), 5.39 (s, 2H), 5.15 (s, 1H), 4.48 - 4.52 (m, 1H), 4.28 - 4.32 (m, 1H), 3.12 - 3.17 (m, 1H), 2.91 (dd, $J = 5.01, 12.84$ Hz, 1H), 2.72 (d, $J = 12.96$ Hz, 1H), 2.61 (t, $J = 7.58$ Hz, 2H), 1.60 - 1.75 (m, 4H), 1.35 - 1.51 (m, 4H); ^{13}C NMR (125 MHz, CDCl_3) δ 163.2, 133.8, 129.0, 128.7, 127.9, 62.0, 60.1, 55.6, 50.9, 40.5, 29.0, 28.6, 28.5, 27.9, 23.5, 23.5; ^{19}F NMR (470 MHz, CDCl_3) δ -158.02 (s); HRMS calcd for $\text{C}_{19}\text{H}_{24}\text{FN}_5\text{OS}$ [$\text{M} + \text{Na}$] $^+$ 412.1584, found 412.1603.

(3*aS*,4*S*,6*aR*)-4-(5-(1-(2-fluorobenzyl)-5-iodo-1*H*-1,2,3-triazol-4-yl)pentyl)tetrahydro-1*H*-thieno[3,4-*d*]imidazol-2(3*H*)-one (**6b**)



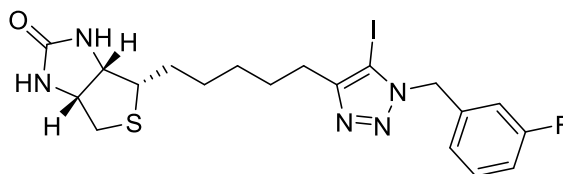
The iodo-acetylene **10** (0.25 mmol) and azide **11b** (42 mg, 0.28 mmol) was reacted according to general procedure for synthesis of 5-Iodo-1,2,3-triazoles and was purified by flash chromatography on silica eluting with 6% MeOH in DCM to give an off white solid (46 mg, 36%). ^1H NMR (500 MHz, CDCl_3) δ 7.28 - 7.37 (m, 1H), 7.08 - 7.15 (m, 2H), 6.98 (t, $J = 7.46$ Hz, 1H), 5.64 (s, 2H), 4.87 (br s, 1H), 4.70 (br s, 1H), 4.50 - 4.55 (m, 1H), 4.30 - 4.35 (m, 1H), 3.15 - 3.20 (m, 1H), 2.94 (dd, $J = 4.89, 12.72$ Hz, 1H), 2.74 (d, $J = 12.96$ Hz, 1H), 2.68 (t, $J = 7.58$ Hz, 2H), 1.65 - 1.77 (m, 4H), 1.38 - 1.52 (m, 4H); ^{13}C NMR (125 MHz, CDCl_3) δ 162.7, 130.3, 130.2, 129.3, 129.2, 124.6, 124.6, 115.7, 115.5, 78.5, 61.9, 60.0, 55.4, 47.6, 47.6, 40.5, 28.9, 28.6, 28.5, 28.4, 25.9; ^{19}F NMR (470 MHz, CDCl_3) δ -117.37 to -117.45 (m); HRMS calcd for $\text{C}_{19}\text{H}_{23}\text{FIN}_5\text{OS}$ [$2\text{M} + \text{Na}$] $^+$ 1053.1202, found 1053.1204.

(3*aS*,4*S*,6*aR*)-4-(5-(5-fluoro-1-(2-fluorobenzyl)-1*H*-1,2,3-triazol-4-yl)pentyl)tetrahydro-1*H*-thieno[3,4-*d*]imidazol-2(3*H*)-one (**7b**)



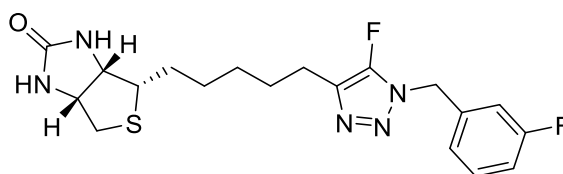
The 5-iodo-triazole **6b** (20 mg, 0.039 mmol) was reacted with potassium fluoride (11 mg, 0.20 mmol) according to general procedure for halogen exchange of 5-Iodo-1,2,3-triazole for 5 min and was purified by flash chromatography on silica eluting with 6% MeOH in DCM to yield 5-fluoro-triazole as an off white solid (12 mg, 76%). ^1H NMR (500 MHz, CDCl_3) δ 7.32 - 7.38 (m, 1H), 7.25 (t, $J = 7.21$ Hz, 1H), 7.08 - 7.18 (m, 2H), 5.67 (br s, 1H), 5.45 (s, 2H), 5.30 (br s, 1H), 4.47 - 4.52 (m, 1H), 4.28 - 4.32 (m, 1H), 3.12 - 3.18 (m, 1H), 2.90 (dd, $J = 5.14, 12.72$ Hz, 1H), 2.72 (d, $J = 12.72$ Hz, 1H), 2.62 (t, $J = 7.58$ Hz, 2H), 1.61 - 1.74 (m, 4H), 1.36 - 1.50 (m, 4H); ^{13}C NMR (125 MHz, CDCl_3) δ 163.4, 130.8, 130.7, 130.1, 130.0, 124.7, 124.7, 115.8, 115.7, 62.0, 60.1, 55.6, 44.2, 44.2, 40.5, 29.0, 28.6, 28.5, 27.9, 23.5, 23.5; ^{19}F NMR (470 MHz, CDCl_3) δ -118.20 to -118.27 (m), -156.78 (d); HRMS calcd for $\text{C}_{19}\text{H}_{23}\text{F}_2\text{N}_5\text{OS}$ [$\text{M} + \text{H}$] $^+$ 408.1669, found 408.1648.

(3*aS*,4*S*,6*aR*)-4-(5-(1-(3-fluorobenzyl)-5-iodo-1*H*-1,2,3-triazol-4-yl)pentyl)tetrahydro-1*H*-thieno[3,4-*d*]imidazol-2(3*H*)-one (**6c**)



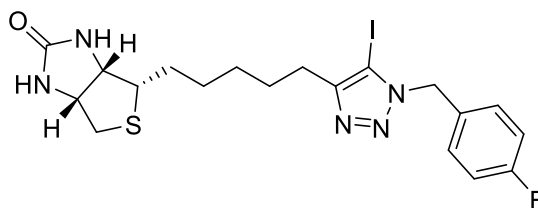
The iodo-acetylene **10** (0.21 mmol) and azide **11c** (35 mg, 0.23 mmol) was reacted according to general procedure for synthesis of 5-Iodo-1,2,3-triazoles and was purified by flash chromatography on silica eluting with 6% MeOH in DCM to give an off white solid (71 mg, 66%). ^1H NMR (500 MHz, $\text{DMSO-}d_6$) δ 7.38 - 7.44 (m, 1H), 7.15 (t, $J = 8.44$ Hz, 1H), 6.99 (d, $J = 9.78$ Hz, 1H), 6.93 (d, $J = 7.83$ Hz, 1H), 6.41 (br s, 1H), 6.33 (br s, 1H), 5.63 (s, 2H), 4.27 - 4.31 (m, 1H), 4.09 - 4.14 (m, 1H), 3.05 - 3.11 (m, 1H), 2.80 (dd, $J = 5.01, 12.35$ Hz, 1H), 2.53 - 2.60 (m, 3H), 1.55 - 1.65 (m, 3H), 1.26 - 1.49 (m, 5H); ^{13}C NMR (125 MHz, $\text{DMSO-}d_6$) δ 163.1, 162.7, 151.3, 138.3, 138.3, 130.9, 130.8, 123.2, 123.2, 114.9, 114.7, 114.2, 114.0, 106.8, 82.7, 61.0, 59.1, 55.5, 52.5, 28.4, 28.3, 28.2, 28.2, 25.4; HRMS calcd for $\text{C}_{19}\text{H}_{23}\text{FIN}_5\text{OS}$ [$\text{M} + \text{H}$] $^+$ 516.0730, found 516.0721.

(3*aS*,4*S*,6*aR*)-4-(5-(5-fluoro-1-(3-fluorobenzyl)-1*H*-1,2,3-triazol-4-yl)pentyl)tetrahydro-1*H*-thieno[3,4-*d*]imidazol-2(3*H*)-one (**7c**)



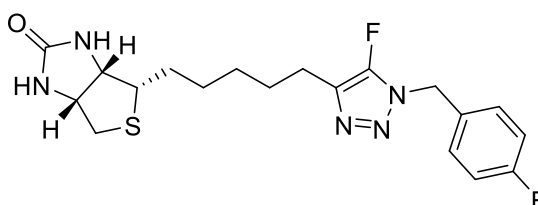
The 5-iodo-triazole **6c** (30 mg, 0.058 mmol) was reacted with potassium fluoride (17 mg, 0.29 mmol) according to general procedure for halogen exchange of 5-Iodo-1,2,3-triazole for 5 min and was purified by flash chromatography on silica eluting with 6% MeOH in DCM to yield 5-fluoro-triazole as an off white solid (18 mg, 76%). ^1H NMR (500 MHz, CDCl_3) δ 7.32 - 7.38 (m, 1H), 6.98 - 7.11 (m, 3H), 5.51 (br s, 1H), 5.38 (s, 2H), 5.18 (br s, 1H), 4.48 - 4.53 (m, 1H), 4.28 - 4.33 (m, 1H), 3.15 (td, $J = 5.47, 8.38$ Hz, 1H), 2.91 (dd, $J = 5.01, 12.84$ Hz, 1H), 2.73 (d, $J = 12.72$ Hz, 1H), 2.63 (t, $J = 7.58$ Hz, 2H), 1.60 - 1.75 (m, 4H), 1.35 - 1.52 (m, 4H); ^{13}C NMR (125 MHz, CDCl_3) δ 163.9, 163.2, 148.9, 136.1, 136.0, 130.8, 130.7, 127.6, 127.5, 123.4, 123.4, 115.9, 115.7, 115.0, 114.8, 62.0, 60.1, 55.6, 50.2, 40.5, 29.0, 28.6, 28.5, 27.9, 23.5, 23.5; ^{19}F NMR (470 MHz, CDCl_3) δ -111.63 to -111.69 (m), -157.01 (s); HRMS calcd for $\text{C}_{19}\text{H}_{23}\text{F}_2\text{N}_5\text{OS}$ [$\text{M} + \text{H}$] $^+$ 408.1669, found 408.1641.

(3*aS*,4*S*,6*aR*)-4-(5-(1-(4-fluorobenzyl)-5-iodo-1*H*-1,2,3-triazol-4-yl)pentyl)tetrahydro-1*H*-thieno[3,4-*d*]imidazol-2(3*H*)-one (**6d**)



The iodo-acetylene **10** (0.21 mmol) and azide **11d** (35 mg, 0.23 mmol) was reacted according to general procedure for synthesis of 5-Iodo-1,2,3-triazoles and was purified by flash chromatography on silica eluting with 6% MeOH in DCM to give an off white solid (69 mg, 64%). ¹H NMR (500 MHz, DMSO-*d*₆) δ 7.16 - 7.25 (m, 4H), 6.41 (br s, 1H), 6.33 (br s, 1H), 5.59 (s, 2H), 4.27 - 4.32 (m, 1H), 4.09 - 4.14 (m, 1H), 3.05 - 3.12 (m, 1H), 2.80 (dd, *J* = 5.14, 12.47 Hz, 1H), 2.52 - 2.60 (m, 3H), 1.52 - 1.65 (m, 3H), 1.25 - 1.49 (m, 5H); ¹³C NMR (125 MHz, DMSO-*d*₆) δ 162.7, 162.6, 151.2, 131.7, 131.7, 129.5, 129.5, 115.6, 115.5, 82.4, 61.0, 59.1, 55.5, 52.4, 28.4, 28.3, 28.2, 28.2, 25.4; HRMS calcd for C₁₉H₂₃FIN₅OS [M + Na]⁺ 538.0550, found 538.0585.

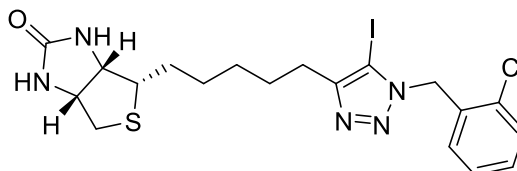
(3*aS*,4*S*,6*aR*)-4-(5-(5-fluoro-1-(4-fluorobenzyl)-1*H*-1,2,3-triazol-4-yl)pentyl)tetrahydro-1*H*-thieno[3,4-*d*]imidazol-2(3*H*)-one (**7d**)



The 5-iodo-triazole **6d** (20 mg, 0.039 mmol) was reacted with potassium fluoride (11 mg, 0.20 mmol) according to general procedure for halogen exchange of 5-Iodo-1,2,3-triazole for 5 min and was purified by flash chromatography on silica eluting with 6% MeOH in DCM to yield 5-fluoro-triazole as an off white solid (11 mg, 69%). ¹H NMR (500 MHz, CDCl₃) δ 7.32 (dd, *J* = 5.14, 8.56 Hz, 2H), 7.04 - 7.10 (m, 2H), 5.41 (br s, 1H), 5.35 (s, 2H), 5.09 (br s, 1H), 4.48 - 4.53 (m, 1H), 4.28 - 4.33 (m, 1H), 3.12 - 3.18 (m, 1H), 2.91 (dd, *J* = 5.14, 12.72 Hz, 1H), 2.73 (d, *J* = 12.72 Hz, 1H), 2.61 (t, *J* = 7.58 Hz, 2H), 1.62 - 1.74 (m, 4H), 1.36 - 1.50 (m, 4H); ¹³C NMR (125 MHz, CDCl₃) δ 163.8, 163.1, 161.9, 129.9, 129.9, 129.6, 116.1, 116.0, 62.0, 60.1, 55.6, 50.2, 40.5, 29.0, 28.6, 28.5, 27.9, 23.5, 23.5; ¹⁹F NMR

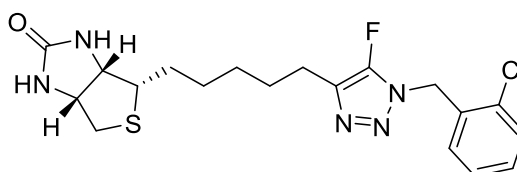
(470 MHz, CDCl₃) δ -112.70 to -112.77 (m), -157.15 (s); HRMS calcd for C₁₉H₂₃F₂N₅OS [2M + Na]⁺ 837.3081, found 837.3065.

(3*aS*,4*S*,6*aR*)-4-(5-(1-(2-chlorobenzyl)-5-iodo-1*H*-1,2,3-triazol-4-yl)pentyl)tetrahydro-1*H*-thieno[3,4-*d*]imidazol-2(3*H*)-one (**6e**)



The iodo-acetylene **10** (0.25 mmol) and azide **11e** (47 mg, 0.28 mmol) was reacted according to general procedure for synthesis of 5-Iodo-1,2,3-triazoles and was purified by flash chromatography on silica eluting with 6% MeOH in DCM to give an off white solid (43 mg, 32%). ¹H NMR (500 MHz, CDCl₃) δ 7.43 (d, *J* = 8.07 Hz, 1H), 7.28 - 7.31 (m, 1H), 7.18 - 7.23 (m, 1H), 6.67 (d, *J* = 7.34 Hz, 1H), 5.70 (s, 2H), 4.91 (br s, 1H), 4.72 (br s, 1H), 4.50 - 4.55 (m, 1H), 4.30 - 4.36 (m, 1H), 3.15 - 3.21 (m, 1H), 2.94 (dd, *J* = 4.65, 12.72 Hz, 1H), 2.67 - 2.77 (m, 3H), 1.63 - 1.80 (m, 4H), 1.39 - 1.55 (m, 4H); ¹³C NMR (125 MHz, CDCl₃) δ 178.5, 162.7, 152.3, 132.5, 132.4, 129.6, 129.5, 128.2, 127.4, 61.9, 60.1, 55.4, 51.4, 40.5, 28.9, 28.6, 28.6, 28.4, 25.9; HRMS calcd for C₁₉H₂₃ClIN₅OS [2M + Na]⁺ 1085.0611, found 1085.0575.

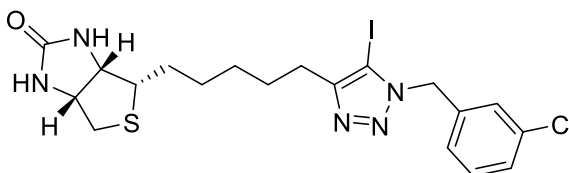
(3*aS*,4*S*,6*aR*)-4-(5-(1-(2-chlorobenzyl)-5-fluoro-1*H*-1,2,3-triazol-4-yl)pentyl)tetrahydro-1*H*-thieno[3,4-*d*]imidazol-2(3*H*)-one (**7e**)



The 5-iodo-triazole **6e** (20 mg, 0.038 mmol) was reacted with potassium fluoride (11 mg, 0.19 mmol) according to general procedure for halogen exchange of 5-Iodo-1,2,3-triazole for 5 min and was purified by flash chromatography on silica eluting with 6% MeOH in DCM to yield 5-fluoro-triazole as an off white solid (10 mg, 62%). ¹H NMR (500 MHz, CDCl₃) δ 7.42 (d, *J* = 7.58 Hz, 1H), 7.24 - 7.34 (m, 2H), 7.10 (d, *J* = 7.34 Hz, 1H), 5.75 (br s, 1H), 5.52 (s, 2H), 5.36 (br s, 1H), 4.47 - 4.52 (m, 1H), 4.28 - 4.33 (m, 1H), 3.12 - 3.18 (m, 1H), 2.90 (dd, *J* = 5.14, 12.72 Hz, 1H), 2.73 (d, *J* = 12.72 Hz, 1H), 2.64 (t, *J* = 7.58 Hz, 2H), 1.61 - 1.76 (m, 4H), 1.36 - 1.51 (m, 4H); ¹³C NMR (125 MHz, CDCl₃) δ 163.4, 133.1,

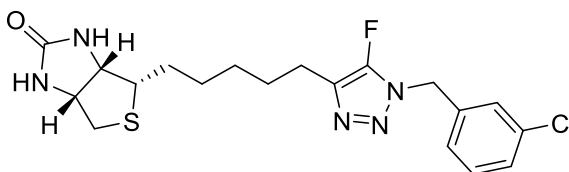
131.6, 130.0, 129.8, 129.4, 127.4, 62.0, 60.1, 55.6, 48.0, 40.5, 29.0, 28.6, 28.5, 27.9, 23.5, 23.5; ^{19}F NMR (470 MHz, CDCl_3) δ -156.18 (s); HRMS calcd for $\text{C}_{19}\text{H}_{23}\text{ClFN}_5\text{OS}$ [$\text{M} + \text{Na}$] $^+$ 554.0255, found 554.0270.

(3*aS*,4*S*,6*aR*)-4-(5-(1-(3-chlorobenzyl)-5-iodo-1*H*-1,2,3-triazol-4-yl)pentyl)tetrahydro-1*H*-thieno[3,4-*d*]imidazol-2(3*H*)-one (**6f**)



The iodo-acetylene **10** (0.25 mmol) and azide **11f** (47 mg, 0.28 mmol) was reacted according to general procedure for synthesis of 5-Iodo-1,2,3-triazoles and was purified by flash chromatography on silica eluting with 6% MeOH in DCM to give an off white solid (55 mg, 41%). ^1H NMR (500 MHz, CDCl_3) δ 7.24 - 7.32 (m, 3H), 7.13 (d, $J = 7.09$ Hz, 1H), 5.54 (s, 2H), 5.15 (br s, 1H), 4.91 (br s, 1H), 4.49 - 4.54 (m, 1H), 4.29 - 4.34 (m, 1H), 3.14 - 3.20 (m, 1H), 2.93 (dd, $J = 5.01, 12.84$ Hz, 1H), 2.73 (d, $J = 12.72$ Hz, 1H), 2.66 (t, $J = 7.46$ Hz, 2H), 1.64 - 1.77 (m, 4H), 1.37 - 1.54 (m, 4H); ^{13}C NMR (125 MHz, CDCl_3) δ 162.9, 152.4, 136.4, 134.8, 130.2, 128.7, 127.9, 125.9, 62.0, 60.1, 55.5, 53.5, 40.5, 28.9, 28.6, 28.5, 28.4, 25.9; HRMS calcd for $\text{C}_{19}\text{H}_{23}\text{ClIN}_5\text{OS}$ [$\text{M} + \text{Na}$] $^+$ 554.0255, found 554.0270.

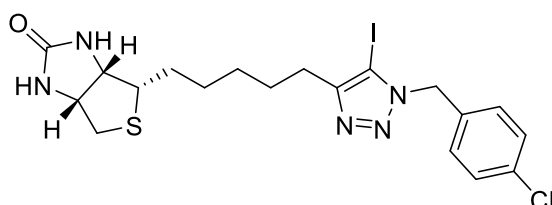
(3*aS*,4*S*,6*aR*)-4-(5-(1-(3-chlorobenzyl)-5-fluoro-1*H*-1,2,3-triazol-4-yl)pentyl)tetrahydro-1*H*-thieno[3,4-*d*]imidazol-2(3*H*)-one (**7f**)



The 5-iodo-triazole **6f** (20 mg, 0.038 mmol) was reacted with potassium fluoride (11 mg, 0.19 mmol) according to general procedure for halogen exchange of 5-Iodo-1,2,3-triazole for 5 min and was purified by flash chromatography on silica eluting with 6% MeOH in DCM to yield 5-fluoro-triazole as an off white solid (12 mg, 74%). ^1H NMR (500 MHz, CDCl_3) δ 7.28 - 7.35 (m, 3H), 7.19 (d, $J = 6.85$ Hz, 1H), 5.72 (br s, 1H), 5.35 (br s, 3H), 4.47 - 5.52 (m, 1H), 4.28 - 4.32 (m, 1H), 3.11 - 3.18 (m, 1H), 2.90 (dd, $J = 5.01, 12.84$ Hz, 1H), 2.72 (d, $J = 12.72$ Hz, 1H), 2.62 (t, $J = 7.58$ Hz, 2H), 1.60 - 1.75 (m, 4H), 1.36 - 1.49 (m, 4H); ^{13}C NMR (125 MHz, CDCl_3) δ 163.4, 151.1, 135.6, 134.9, 130.4, 129.0, 128.0,

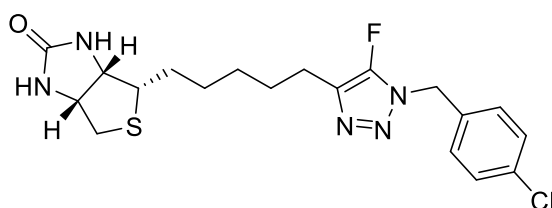
127.6, 127.5, 126.0, 62.0, 60.1, 55.6, 50.1, 40.5, 29.0, 28.6, 28.5, 27.9, 23.5, 23.5; ^{19}F NMR (470 MHz, CDCl_3) δ -156.96 (s); HRMS calcd for $\text{C}_{19}\text{H}_{23}\text{ClFN}_5\text{OS}$ $[\text{M} + \text{H}]^+$ 424.1374, found 424.1363.

(3*aS*,4*S*,6*aR*)-4-(5-(1-(4-chlorobenzyl)-5-iodo-1*H*-1,2,3-triazol-4-yl)pentyl)tetrahydro-1*H*-thieno[3,4-*d*]imidazol-2(3*H*)-one (**6g**)



The iodo-acetylene **10** (0.25 mmol) and azide **11g** (47 mg, 0.28 mmol) was reacted according to general procedure for synthesis of 5-Iodo-1,2,3-triazoles and was purified by flash chromatography on silica eluting with 6% MeOH in DCM to give an off white solid (56 mg, 42%). ^1H NMR (500 MHz, CDCl_3) δ 7.31 - 7.35 (m, 2H), 7.19 - 7.23 (m, 2H), 5.54 (s, 2H), 4.93 (br s, 1H), 4.74 (br s, 1H), 4.50 - 4.54 (m, 1H), 4.30 - 4.34 (m, 1H), 3.14 - 3.19 (m, 1H), 2.93 (dd, $J = 5.14, 12.72$ Hz, 1H), 2.74 (d, $J = 12.72$ Hz, 1H), 2.66 (t, $J = 7.58$ Hz, 2H), 1.64 - 1.76 (m, 4H), 1.38 - 1.53 (m, 4H); ^{13}C NMR (125 MHz, CDCl_3) δ 162.7, 152.4, 134.5, 132.9, 129.2, 129.1, 78.1, 61.9, 60.1, 55.4, 53.5, 40.5, 28.9, 28.6, 28.5, 28.4, 25.9; HRMS calcd for $\text{C}_{19}\text{H}_{23}\text{ClIN}_5\text{OS}$ $[\text{M} + \text{H}]^+$ 532.0435, found 532.0430.

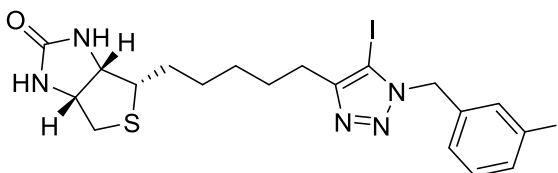
(3*aS*,4*S*,6*aR*)-4-(5-(1-(4-chlorobenzyl)-5-fluoro-1*H*-1,2,3-triazol-4-yl)pentyl)tetrahydro-1*H*-thieno[3,4-*d*]imidazol-2(3*H*)-one (**7g**)



The 5-iodo-triazole **6g** (20 mg, 0.038 mmol) was reacted with potassium fluoride (11 mg, 0.19 mmol) according to general procedure for halogen exchange of 5-Iodo-1,2,3-triazole for 5 min and was purified by flash chromatography on silica eluting with 6% MeOH in DCM to yield 5-fluoro-triazole as an off white solid (13 mg, 81%). ^1H NMR (500 MHz, CDCl_3) δ 7.35 (d, $J = 8.56$ Hz, 2H), 7.25 (d, $J = 8.31$ Hz, 2H), 5.74 (br s, 1H), 5.37 (br s, 1H), 5.35 (s, 2H), 4.47 - 4.52 (m, 1H), 4.27 - 4.32 (m, 1H), 3.11 - 3.17 (m, 1H), 2.90 (dd, $J = 4.89, 12.72$ Hz, 1H), 2.73 (d, $J = 12.96$ Hz, 1H), 2.61 (t, $J = 7.58$ Hz, 2H), 1.60 - 1.75 (m,

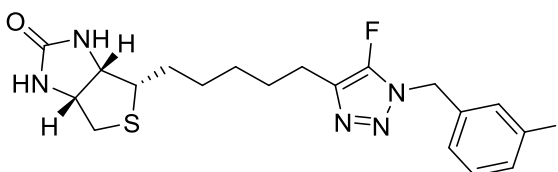
4H), 1.35 - 1.50 (m, 4H); ^{13}C NMR (125 MHz, CDCl_3) δ 163.4, 151.1, 134.8, 132.2, 129.3, 129.2, 62.0, 60.1, 55.6, 50.2, 40.5, 29.0, 28.6, 28.5, 27.9, 23.5, 23.5; ^{19}F NMR (470 MHz, CDCl_3) δ -157.05 (s); HRMS calcd for $\text{C}_{19}\text{H}_{23}\text{ClFN}_5\text{OS}$ $[\text{M} + \text{H}]^+$ 424.1374, found 424.1385.

(3*aS*,4*S*,6*aR*)-4-(5-(5-iodo-1-(3-iodobenzyl)-1*H*-1,2,3-triazol-4-yl)pentyl)tetrahydro-1*H*-thieno[3,4-*d*]imidazol-2(3*H*)-one (**6h**)



The iodo-acetylene **10** (0.25 mmol) and azide **11h** (73 mg, 0.28 mmol) was reacted according to general procedure for synthesis of 5-Iodo-1,2,3-triazoles and was purified by flash chromatography on silica eluting with 6% MeOH in DCM to give an off white solid (85 mg, 55%). ^1H NMR (500 MHz, CDCl_3) δ 7.67 (d, $J = 7.83$ Hz, 1H), 7.63 (s, 1H), 7.21 (d, $J = 7.58$ Hz, 1H), 7.09 (t, $J = 7.70$ Hz, 1H), 5.51 (s, 2H), 4.99 (br s, 1H), 4.78 (br s, 1H), 4.50 - 4.54 (m, 1H), 4.30 - 4.34 (m, 1H), 3.14 - 3.20 (m, 1H), 2.93 (dd, $J = 5.01, 12.84$ Hz, 1H), 2.73 (d, $J = 12.96$ Hz, 1H), 2.67 (t, $J = 7.58$ Hz, 2H), 1.64 - 1.77 (m, 4H), 1.37 - 1.54 (m, 4H); ^{13}C NMR (125 MHz, CDCl_3) δ 162.7, 152.4, 137.6, 136.7, 136.6, 130.6, 127.0, 94.5, 61.9, 60.0, 55.4, 53.2, 40.6, 28.9, 28.6, 28.6, 28.4, 25.9; HRMS calcd for $\text{C}_{19}\text{H}_{23}\text{I}_2\text{N}_5\text{OS}$ $[\text{M} + \text{H}]^+$ 623.9791, found 623.9816.

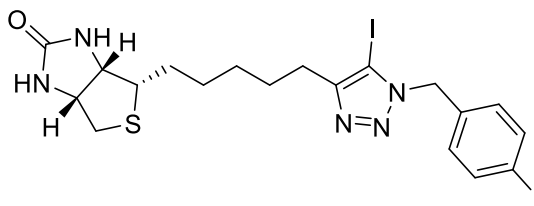
(3*aS*,4*S*,6*aR*)-4-(5-(5-fluoro-1-(3-iodobenzyl)-1*H*-1,2,3-triazol-4-yl)pentyl)tetrahydro-1*H*-thieno[3,4-*d*]imidazol-2(3*H*)-one (**7h**)



The 5-iodo-triazole **6h** (20 mg, 0.032 mmol) was reacted with potassium fluoride (9.3 mg, 0.16 mmol) according to general procedure for halogen exchange of 5-Iodo-1,2,3-triazole for 5 min and was purified by flash chromatography on silica eluting with 6% MeOH in DCM to yield 5-fluoro-triazole as an off white solid (11 mg, 67%). ^1H NMR (500 MHz, CDCl_3) δ 7.69 (d, $J = 8.07$ Hz, 1H), 7.66 (s, 1H), 7.25 - 7.30 (m, 2H), 7.11 (t, $J = 7.83$ Hz, 1H), 5.51 (br s, 1H), 5.32 (s, 2H), 5.17 (br s, 1H), 4.48 - 4.53 (m, 1H), 4.28 - 4.33 (m, 1H), 3.12 - 3.18 (m, 1H), 2.91 (dd, $J = 4.89, 12.72$ Hz, 1H), 2.73 (d, $J = 12.72$ Hz, 1H), 2.63 (t,

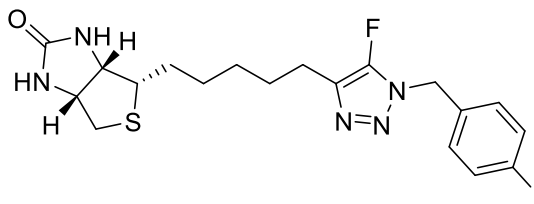
$J = 7.58$ Hz, 2H), 1.60 - 1.76 (m, 4H), 1.36 - 1.51 (m, 4H); ^{13}C NMR (125 MHz, CDCl_3) δ 163.2, 137.9, 136.7, 135.9, 130.7, 127.1, 94.7, 62.0, 60.1, 55.6, 50.0, 40.5, 29.0, 28.6, 28.5, 27.9, 23.5, 23.5; ^{19}F NMR (470 MHz, CDCl_3) δ -156.93 (s); HRMS calcd for $\text{C}_{19}\text{H}_{23}\text{FIN}_5\text{OS}$ $[\text{M}]^+$ 515.0652, found 515.0647.

(3*aS*,4*S*,6*aR*)-4-(5-(5-iodo-1-(4-iodobenzyl)-1*H*-1,2,3-triazol-4-yl)pentyl)tetrahydro-1*H*-thieno[3,4-*d*]imidazol-2(3*H*)-one (**6i**)



The iodo-acetylene **10** (0.21 mmol) and azide **11i** (60 mg, 0.23 mmol) was reacted according to general procedure for synthesis of 5-Iodo-1,2,3-triazoles and was purified by flash chromatography on silica eluting with 6% MeOH in DCM to give an off white solid (121 mg, 92%). ^1H NMR (500 MHz, CDCl_3) δ 7.67 - 7.71 (m, 2H), 6.99 - 7.03 (m, 2H), 5.51 (s, 2H), 4.84 (br s, 1H), 4.68 (br s, 1H), 4.51 - 4.54 (m, 1H), 4.30 - 4.34 (m, 1H), 3.15 - 3.20 (m, 1H), 2.94 (dd, $J = 5.01, 12.84$ Hz, 1H), 2.74 (d, $J = 12.96$ Hz, 1H), 2.66 (t, $J = 7.58$ Hz, 2H), 1.64 - 1.76 (m, 4H), 1.37 - 1.52 (m, 4H); ^{13}C NMR (125 MHz, CDCl_3) δ 162.6, 152.4, 138.0, 134.1, 129.6, 107.3, 94.2, 61.9, 60.0, 55.4, 53.6, 40.6, 28.8, 28.6, 28.5, 28.4, 25.9; HRMS calcd for $\text{C}_{19}\text{H}_{23}\text{I}_2\text{N}_5\text{OS}$ $[\text{M} + \text{H}]^+$ 623.9791, found 623.9820.

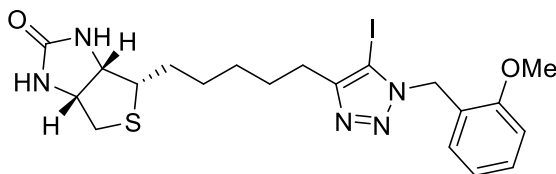
(3*aS*,4*S*,6*aR*)-4-(5-(5-fluoro-1-(4-iodobenzyl)-1*H*-1,2,3-triazol-4-yl)pentyl)tetrahydro-1*H*-thieno[3,4-*d*]imidazol-2(3*H*)-one (**7i**)



The 5-iodo-triazole **6i** (20 mg, 0.032 mmol) was reacted with potassium fluoride (9.3 mg, 0.16 mmol) according to general procedure for halogen exchange of 5-Iodo-1,2,3-triazole for 5 min and was purified by flash chromatography on silica eluting with 6% MeOH in DCM to yield 5-fluoro-triazole as an off white solid (11 mg, 67%). ^1H NMR (500 MHz, CDCl_3) δ 7.70 - 7.74 (m, 2H), 7.04 - 7.09 (m, 2H), 5.33 (s, 2H), 4.97 (br s, 1H), 4.77 (br s, 1H), 4.50 - 4.54 (m, 1H), 4.29 - 4.34 (m, 1H), 3.13 - 3.19 (m, 1H), 2.93 (dd, $J = 5.14, 12.96$

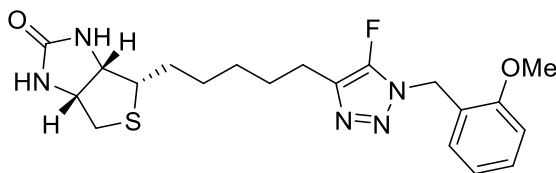
Hz, 1H), 2.73 (d, $J = 12.96$ Hz, 1H), 2.62 (t, $J = 7.58$ Hz, 2H), 1.62 - 1.74 (m, 4H), 1.36 - 1.52 (m, 4H); ^{13}C NMR (125 MHz, CDCl_3) δ 162.8, 138.2, 133.4, 129.8, 94.6, 61.9, 60.0, 55.4, 50.3, 40.5, 28.9, 28.6, 28.5, 27.9, 23.5, 23.4; ^{19}F NMR (470 MHz, CDCl_3) δ -157.09 (s); HRMS calcd for $\text{C}_{19}\text{H}_{23}\text{FIN}_5\text{OS}$ [$\text{M} + \text{H}$] $^+$ 516.0730, found 516.0766.

(3*aS*,4*S*,6*aR*)-4-(5-(5-iodo-1-(2-methoxybenzyl)-1*H*-1,2,3-triazol-4-yl)pentyl)tetrahydro-1*H*-thieno[3,4-*d*]imidazol-2(3*H*)-one (**6j**)



The iodo-acetylene **10** (0.25 mmol) and azide **11j** (49 mg, 0.30 mmol) was reacted according to general procedure for synthesis of 5-Iodo-1,2,3-triazoles and was purified by flash chromatography on silica eluting with 5% MeOH in DCM to give an off white solid (34 mg, 26%). ^1H NMR (500 MHz, $\text{DMSO}-d_6$) δ 7.28 - 7.33 (m, 1H), 7.05 (d, $J = 8.31$ Hz, 1H), 6.89 (t, $J = 7.46$ Hz, 1H), 6.60 (d, $J = 7.34$ Hz, 1H), 6.43 (br s, 1H), 6.34 (br s, 1H), 5.50 (s, 2H), 4.27 - 4.32 (m, 1H), 4.10 - 4.14 (m, 1H), 3.83 (s, 3H), 3.06 - 3.12 (m, 1H), 2.81 (dd, $J = 5.14, 12.47$ Hz, 1H), 2.54 - 2.60 (m, 3H), 1.56 - 1.65 (m, 3H), 1.26 - 1.49 (m, 5H); ^{13}C NMR (125 MHz, $\text{DMSO}-d_6$) δ 162.7, 156.2, 150.8, 129.3, 127.7, 123.4, 120.4, 111.0, 83.0, 61.0, 59.2, 55.5, 48.5, 28.5, 28.4, 28.3, 28.2, 28.2, 25.4; HRMS calcd for $\text{C}_{20}\text{H}_{26}\text{IN}_5\text{O}_2\text{S}$ [$\text{M} + \text{K}$] $^+$ 566.0489, found 566.0520.

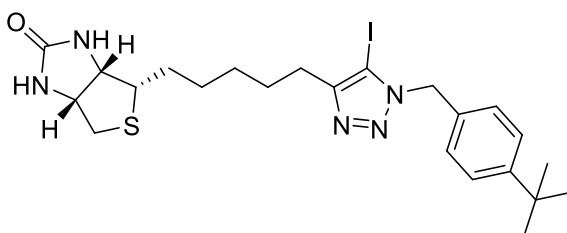
(3*aS*,4*S*,6*aR*)-4-(5-(5-fluoro-1-(2-methoxybenzyl)-1*H*-1,2,3-triazol-4-yl)pentyl)tetrahydro-1*H*-thieno[3,4-*d*]imidazol-2(3*H*)-one (**7j**)



The 5-iodo-triazole **6j** (17 mg, 0.032 mmol) was reacted with potassium fluoride (9.3 mg, 0.16 mmol) according to general procedure for halogen exchange of 5-Iodo-1,2,3-triazole for 5 min and was purified by flash chromatography on silica eluting with 6% MeOH in DCM to yield 5-fluoro-triazole as an off white solid (10 mg, 74%). ^1H NMR (500 MHz, CDCl_3) δ 7.29 - 7.35 (m, 1H), 7.10 (d, $J = 7.34$ Hz, 1H), 6.88-6.96 (m, 2H), 5.75 (br s, 1H), 5.40 (s, 2H), 5.35 (br s, 1H), 4.46 - 4.51 (m, 1H), 4.27 - 4.32 (m, 1H), 3.85 (s, 3H), 3.11 -

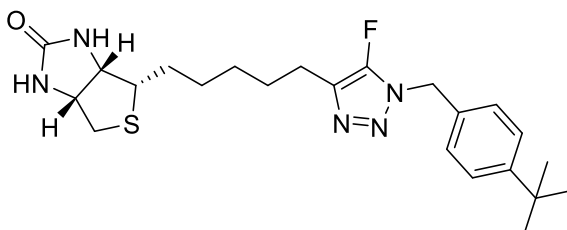
3.17 (m, 1H), 2.89 (dd, $J = 4.89, 12.72$ Hz, 1H), 2.72 (d, $J = 12.72$ Hz, 1H), 2.62 (t, $J = 7.58$ Hz, 2H), 1.61 - 1.76 (m, 4H), 1.36 - 1.51 (m, 4H); ^{13}C NMR (125 MHz, CDCl_3) δ 163.4, 156.9, 130.0, 129.2, 122.3, 120.7, 110.5, 62.0, 60.1, 55.7, 55.4, 45.7, 40.5, 29.0, 28.7, 28.5, 28.0, 23.6, 23.5; ^{19}F NMR (470 MHz, CDCl_3) δ -156.43 (s); HRMS calcd for $\text{C}_{20}\text{H}_{26}\text{FN}_5\text{O}_2\text{S}$ $[\text{M} + \text{H}]^+$ 420.1869, found 420.1887.

(3*aS*,4*S*,6*aR*)-4-(5-(1-(4-(*tert*-butyl)benzyl)-5-iodo-1*H*-1,2,3-triazol-4-yl)pentyl)tetrahydro-1*H*-thieno[3,4-*d*]imidazol-2(3*H*)-one (**6k**)



The iodo-acetylene **10** (0.25 mmol) and azide **11k** (53 mg, 0.28 mmol) was reacted according to general procedure for synthesis of 5-Iodo-1,2,3-triazoles and was purified by flash chromatography on silica eluting with 5% MeOH in DCM to give an off white solid (41 mg, 30%). ^1H NMR (500 MHz, CDCl_3) δ 7.34 - 7.39 (m, 2H), 7.19 - 7.24 (m, 2H), 5.53 (s, 2H), 5.27 (br s, 1H), 4.99 (br s, 1H), 4.49 - 4.54 (m, 1H), 4.29 - 4.34 (m, 1H), 3.14 - 3.20 (m, 1H), 2.92 (dd, $J = 5.01, 12.84$ Hz, 1H), 2.73 (d, $J = 12.72$ Hz, 1H), 2.65 (t, $J = 7.58$ Hz, 2H), 1.61 - 1.77 (m, 4H), 1.37 - 1.53 (m, 4H), 1.31 (s, 9H); ^{13}C NMR (125 MHz, CDCl_3) δ 163.0, 152.1, 151.5, 131.4, 127.6, 125.7, 61.9, 60.1, 55.5, 53.8, 40.5, 34.6, 31.3, 29.0, 28.6, 28.5, 28.4, 26.0; HRMS calcd for $\text{C}_{23}\text{H}_{32}\text{IN}_5\text{OS}$ $[\text{M} + \text{K}]^+$ 592.1009, found 592.0987.

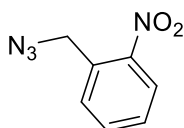
(3*aS*,4*S*,6*aR*)-4-(5-(1-(4-(*tert*-butyl)benzyl)-5-fluoro-1*H*-1,2,3-triazol-4-yl)pentyl)tetrahydro-1*H*-thieno[3,4-*d*]imidazol-2(3*H*)-one (**7k**)



The 5-iodo-triazole **6k** (25 mg, 0.045 mmol) was reacted with potassium fluoride (14 mg, 0.23 mmol) according to general procedure for halogen exchange of 5-Iodo-1,2,3-triazole for 5 min and was purified by flash chromatography on silica eluting with 6% MeOH in DCM to yield 5-fluoro-triazole as an off white solid (14 mg, 70%). ^1H NMR (500 MHz,

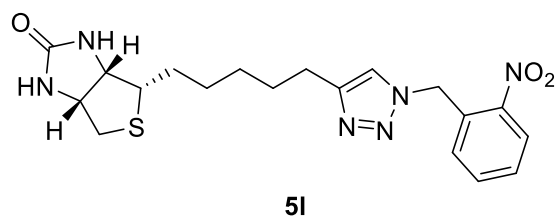
CDCl_3) δ 7.37 - 7.41 (m, 2H), 7.23 - 7.27 (m, 2H), 5.54 (br s, 1H), 5.34 (s, 2H), 5.18 (br s, 1H), 4.48 - 4.52 (m, 1H), 4.28 - 4.33 (m, 1H), 3.12 - 3.18 (m, 1H), 2.90 (dd, $J = 5.14, 12.72$ Hz, 1H), 2.72 (d, $J = 12.72$ Hz, 1H), 2.61 (t, $J = 7.58$ Hz, 2H), 1.60 - 1.76 (m, 4H), 1.37 - 1.50 (m, 4H), 1.31 (s, 9H); ^{13}C NMR (125 MHz, CDCl_3) δ 163.2, 151.8, 130.8, 127.7, 127.4, 125.9, 62.0, 60.1, 55.6, 50.6, 40.5, 34.6, 31.2, 29.0, 28.6, 28.5, 28.0, 23.6, 23.5; ^{19}F NMR (470 MHz, CDCl_3) δ -157.02 (s); HRMS calcd for $\text{C}_{23}\text{H}_{32}\text{FN}_5\text{OS}$ $[\text{M}]^+$ 445.2312, found 445.2320.

1-(azidomethyl)-2-nitrobenzene (**111**)³

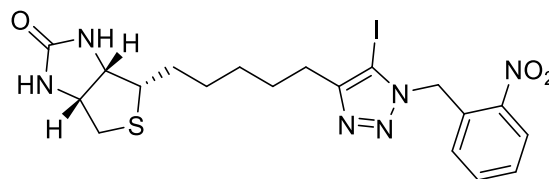


2-nitrobenzyl chloride (500 mg, 2.91 mmol) and sodium azide (246 mg, 3.78 mmol) was reacted according to general procedure for synthesis of benzyl azides to give a yellow liquid (489 mg, 94%). ^1H NMR (500 MHz, CDCl_3) δ 8.13 (d, $J = 8.31$ Hz, 1H), 7.66 - 7.73 (m, 2H), 7.51 - 7.55 (m, 1H), 4.87 (s, 2H)

(3*aS*,4*S*,6*aR*)-4-(5-(5-iodo-1-(2-nitrobenzyl)-1*H*-1,2,3-triazol-4-yl)pentyl)tetrahydro-1*H*-thieno[3,4-*d*]imidazol-2(3*H*)-one (**61**) and (3*aS*,4*S*,6*aR*)-4-(5-(1-(2-nitrobenzyl)-1*H*-1,2,3-triazol-4-yl)pentyl)tetrahydro-1*H*-thieno[3,4-*d*]imidazol-2(3*H*)-one (**51**)



51



61

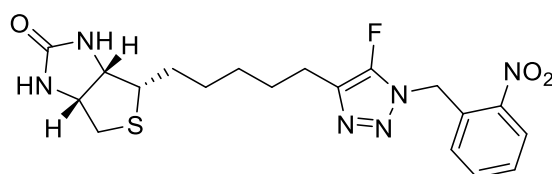
The iodo-acetylene **10** (0.50 mmol) and azide **111** (98 mg, 0.55 mmol) was reacted according to general procedure for synthesis of 5-Iodo-1,2,3-triazoles and was purified by flash chromatography on silica eluting with 5% MeOH in DCM to give **61** (81 mg, 30%) as a yellow solid and **51** (40 mg, 19%) as a yellow solid.

61. ^1H NMR (500 MHz, $\text{DMSO}-d_6$) δ 8.17 (d, $J = 7.34$ Hz, 1H), 7.73 (t, $J = 7.58$ Hz, 1H), 7.64 (t, $J = 7.58$ Hz, 1H), 6.76 (d, $J = 7.34$ Hz, 1H), 6.42 (br s, 1H), 6.34 (br s, 1H), 5.93 (s, 2H), 4.27 - 4.32 (m, 1H), 4.10 - 4.15 (m, 1H), 3.06 - 3.12 (m, 1H), 2.81 (dd, $J = 5.01, 12.35$ Hz, 1H), 2.54 - 2.62 (m, 3H), 1.56 - 1.67 (m, 3H), 1.27 - 1.50 (m, 5H); ^{13}C NMR (125 MHz,

DMSO- d_6) δ 162.7, 151.3, 147.4, 134.4, 130.4, 129.5, 129.2, 125.2, 83.6, 61.0, 59.2, 55.5, 50.6, 28.4, 28.4, 28.3, 28.2, 25.4; HRMS calcd for $C_{19}H_{23}IN_6O_3S$ $[M + H]^+$ 543.0675, found 543.0688.

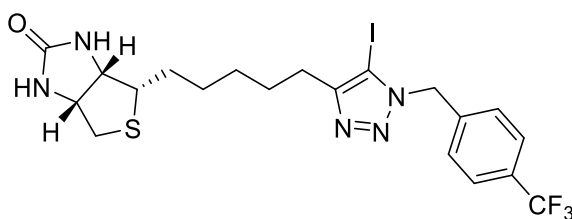
5l. 1H NMR (500 MHz, $CDCl_3$) δ 8.15 (d, $J = 8.07$ Hz, 1H), 7.63 (t, $J = 7.46$ Hz, 1H), 7.54 (t, $J = 7.83$ Hz, 1H), 7.44 (s, 1H), 7.08 (d, $J = 7.58$ Hz, 1H), 5.92 (s, 2H), 4.96 (br s, 1H), 4.73 (br s, 1H), 4.50 - 4.54 (m, 1H), 4.30 - 4.34 (m, 1H), 3.15 - 3.20 (m, 1H), 2.94 (dd, $J = 5.01, 12.84$ Hz, 1H), 2.71 - 2.78 (m, 3H), 1.62 - 1.76 (m, 4H), 1.39 - 1.52 (m, 4H); ^{13}C NMR (125 MHz, $CDCl_3$) δ 162.7, 134.3, 131.0, 130.3, 129.5, 125.3, 121.8, 61.9, 60.0, 55.4, 50.6, 40.5, 29.0, 28.7, 28.6, 25.5; HRMS calcd for $C_{19}H_{24}N_6O_3S$ $[M + K]^+$ 455.1268, found 455.1297.

(3*aS*,4*S*,6*aR*)-4-(5-(5-fluoro-1-(2-nitrobenzyl)-1*H*-1,2,3-triazol-4-yl)pentyl)tetrahydro-1*H*-thieno[3,4-*d*]imidazol-2(3*H*)-one (**7l**)



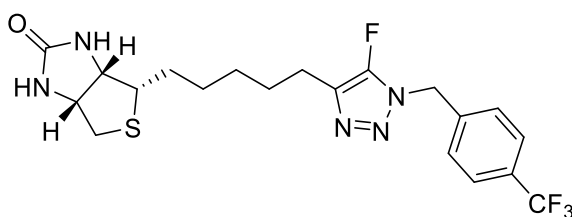
The 5-iodo-triazole **6l** (46 mg, 0.085 mmol) was reacted with potassium fluoride (25 mg, 0.43 mmol) according to general procedure for halogen exchange of 5-Iodo-1,2,3-triazole for 5 min and was purified by flash chromatography on silica eluting with 6% MeOH in DCM to yield 5-fluoro-triazole as a yellow solid (27 mg, 73%). 1H NMR (500 MHz, $CDCl_3$) δ 8.21 (dd, $J = 1.22, 8.31$ Hz, 1H), 7.65 (dt, $J = 1.22, 7.70$ Hz, 1H), 7.53 - 7.58 (m, 1H), 6.99 (d, $J = 7.83$ Hz, 1H), 5.85 (s, 2H), 5.48 (br s, 1H), 5.11 (br s, 1H), 4.49 - 4.54 (m, 1H), 4.30 - 4.34 (m, 1H), 3.14 - 3.20 (m, 1H), 2.92 (dd, $J = 5.01, 12.84$ Hz, 1H), 2.74 (d, $J = 12.72$ Hz, 1H), 2.68 (t, $J = 7.58$ Hz, 2H), 1.62 - 1.79 (m, 4H), 1.38 - 1.54 (m, 4H); ^{13}C NMR (125 MHz, $CDCl_3$) δ 163.2, 151.6, 134.5, 129.9, 129.6, 129.2, 125.6, 62.0, 60.1, 55.6, 47.7, 40.5, 28.9, 28.6, 28.6, 28.1, 27.9, 23.5, 23.5; ^{19}F NMR (470 MHz, $CDCl_3$) δ -156.42 (s); HRMS calcd for $C_{19}H_{23}FN_6O_3S$ $[M + H]^+$ 435.1614, found 435.1618.

(3*aS*,4*S*,6*aR*)-4-(5-(5-iodo-1-(4-(trifluoromethyl)benzyl)-1*H*-1,2,3-triazol-4-yl)pentyl)tetrahydro-1*H*-thieno[3,4-*d*]imidazol-2(3*H*)-one (**6m**)



To a mixture of biotin acetylene **8**¹ (50 mg, 0.21 mmol), LiI (112 mg, 0.84 mmol), and Cu(ClO₄)₂·6H₂O (195 mg, 0.53 mmol) in THF (3 mL) was added TEA (68 μL) and the mixture was stirred for 30 min. To the reaction mixture was added azide **11m** (42 mg, 0.21 mmol) and the mixture was stirred for 5 hours. The mixture was quenched with 10% NH₄OH and extracted with DCM twice. The combined organics were dried over anhydrous sodium sulfate and concentrated under reduced pressure. The resulting residue was purified by flash chromatography on silica eluting with 5% MeOH in DCM to give an off white solid (88 mg, 74%). ¹H NMR (500 MHz, DMSO-*d*₆) δ 7.72 - 7.78 (m, 2H), 7.31 - 7.36 (m, 2H), 6.42 (br s, 1H), 6.34 (br s, 1H), 5.73 (s, 2H), 4.26 - 4.32 (m, 1H), 4.09 - 4.14 (m, 1H), 3.05 - 3.12 (m, 1H), 2.81 (dd, *J* = 5.01, 12.35 Hz, 1H), 2.53 - 2.60 (m, 3H), 1.55 - 1.67 (m, 3H), 1.26 - 1.50 (m, 5H); ¹³C NMR (125 MHz, DMSO-*d*₆) δ 162.7, 151.4, 140.3, 128.0, 125.7, 125.7, 125.6, 82.8, 61.0, 59.2, 55.5, 52.6, 28.5, 28.4, 28.3, 28.2, 25.4; ¹⁹F NMR (470 MHz, DMSO-*d*₆) δ -61.05 (s); HRMS calcd for C₂₀H₂₃F₃IN₅OS [M + H]⁺ 566.0698, found 566.0668.

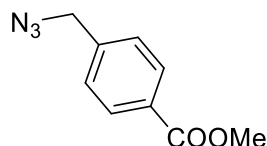
(3*aS*,4*S*,6*aR*)-4-(5-(5-fluoro-1-(4-(trifluoromethyl)benzyl)-1*H*-1,2,3-triazol-4-yl)pentyl)tetrahydro-1*H*-thieno[3,4-*d*]imidazol-2(3*H*)-one (**7m**)



The 5-iodo-triazole **6m** (35 mg, 0.062 mmol) was reacted with potassium fluoride (18 mg, 0.31 mmol) according to general procedure for halogen exchange of 5-Iodo-1,2,3-triazole for 5 min and was purified by flash chromatography on silica eluting with 6% MeOH in DCM to yield 5-fluoro-triazole as an off white solid (21 mg, 74%). ¹H NMR (500 MHz, CDCl₃) δ 7.63 - 7.67 (m, 2H), 7.41 - 7.45 (m, 2H), 5.41 - 5.47 (m, 3H), 5.11 (br s, 1H), 4.49 - 4.53 (m, 1H), 4.29 - 4.33 (m, 1H), 3.13 - 3.18 (m, 1H), 2.92 (dd, *J* = 5.01, 12.84 Hz, 1H), 2.73 (d, *J* = 12.72 Hz, 1H), 2.63 (t, *J* = 7.58 Hz, 2H), 1.61 - 1.75 (m, 4H), 1.36 - 1.52 (m, 4H); ¹³C NMR (125 MHz, CDCl₃) δ 163.2, 151.2, 137.6, 128.2, 127.7, 127.6, 126.1, 126.1,

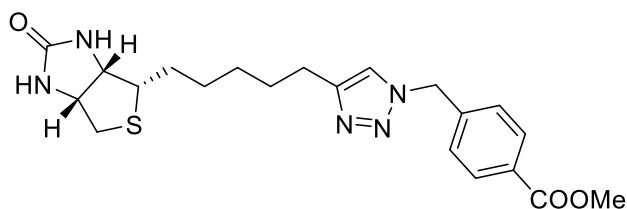
126.1, 126.0, 62.0, 60.1, 55.6, 50.2, 40.5, 29.0, 28.6, 28.5, 27.9, 23.5, 23.5; ^{19}F NMR (470 MHz, CDCl_3) δ -62.80 (s), -157.08 (s); HRMS calcd for $\text{C}_{20}\text{H}_{23}\text{F}_4\text{N}_5\text{OS}$ $[\text{M} + \text{H}]^+$ 458.1637, found 458.1632.

methyl 4-(azidomethyl)benzoate (**11n**)⁴



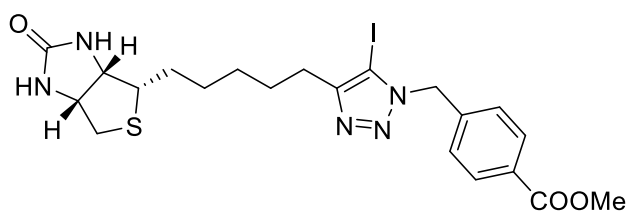
To the suspension of 4-(bromomethyl)benzoic acid (431 mg, 2.00 mmol) in MeOH (12.5 mL) was added dropwise SOCl_2 (435 μL , 6.00 mmol) and the mixture was stirred for 20 hours at ambient temperature. The resulting clear solution was concentrated under reduced pressure to give a dark yellow liquid. The yellow liquid was treated with sodium azide (169 mg, 2.60 mmol) according to general procedure for synthesis of benzyl azides to give a yellow liquid (366 mg, 96%). ^1H NMR (500 MHz, CDCl_3) δ 8.05 - 8.09 (m, 2H), 7.39 - 7.42 (m, 2H), 4.43 (s, 2H), 3.94 (s, 3H).

Methyl 4-((4-(5-((3aS,4S,6aR)-2-oxohexahydro-1H-thieno[3,4-d]imidazol-4-yl)pentyl)-1H-1,2,3-triazol-1-yl)methyl)benzoate (**5n**)



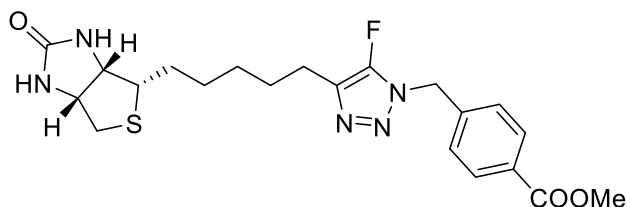
Biotin acetylene **8**¹ (60 mg, 0.25 mmol) was reacted with azide **11n** (73 mg, 0.38 mmol) and Cu nanopowder (6 mg, 0.1 mmol) according to general procedure for CuAAC and purified by flash chromatography on silica gel eluting with 5% MeOH in DCM to give an off white solid (41 mg, 38%). ^1H NMR (500 MHz, CDCl_3) δ 8.04 (d, J = 8.31 Hz, 2H), 7.31 (d, J = 8.31 Hz, 2H), 7.23 (s, 1H), 5.57 (s, 2H), 5.06 (br s, 1H), 4.81 (br s, 1H), 4.49 - 4.54 (m, 1H), 4.29 - 4.34 (m, 1H), 3.93 (s, 3H), 3.13 - 3.18 (m, 1H), 2.92 (dd, J = 5.01, 12.84 Hz, 1H), 2.68 - 2.76 (m, 3H), 1.59 - 1.74 (m, 4H), 1.35 - 1.51 (m, 4H); ^{13}C NMR (125 MHz, CDCl_3) δ 166.4, 162.8, 148.8, 139.8, 130.5, 130.3, 127.7, 120.7, 61.9, 60.0, 55.5, 53.5, 52.3, 40.5, 29.0, 29.0, 28.7, 28.5, 25.5; HRMS calcd for $\text{C}_{21}\text{H}_{27}\text{N}_5\text{O}_3\text{S}$ $[\text{M} + \text{H}]^+$ 430.1913, found 430.1907.

Methyl 4-((5-iodo-4-(5-((3a*S*,4*S*,6a*R*)-2-oxohexahydro-1*H*-thieno[3,4-*d*]imidazol-4-yl)pentyl)-1*H*-1,2,3-triazol-1-yl)methyl)benzoate (**6n**)



The iodo-acetylene **10** (0.50 mmol) and azide **11n** (115 mg, 0.60 mmol) was reacted according to general procedure for synthesis of 5-Iodo-1,2,3-triazoles and was purified by flash chromatography on silica eluting with 5% MeOH in DCM to give an off white solid (124 mg, 45%). ¹H NMR (500 MHz, DMSO-*d*₆) δ 7.95 (d, *J* = 8.31 Hz, 2H), 7.25 (d, *J* = 8.07 Hz, 2H), 6.42 (br s, 1H), 6.34 (br s, 1H), 5.71 (s, 2H), 4.27 - 4.32 (m, 1H), 4.09 - 4.15 (m, 1H), 3.84 (s, 3H), 3.06 - 3.11 (m, 1H), 2.80 (dd, *J* = 5.01, 12.35 Hz, 1H), 2.53 - 2.60 (m, 3H), 1.55 - 1.65 (m, 3H), 1.25 - 1.49 (m, 5H); ¹³C NMR (125 MHz, DMSO-*d*₆) δ 165.8, 162.7, 151.3, 140.8, 129.6, 129.2, 127.4, 82.8, 61.0, 59.2, 55.5, 52.8, 52.2, 28.4, 28.4, 28.3, 28.2, 25.4; HRMS calcd for C₂₁H₂₆IN₅O₃S [M + Na]⁺ 578.0699, found 578.0688.

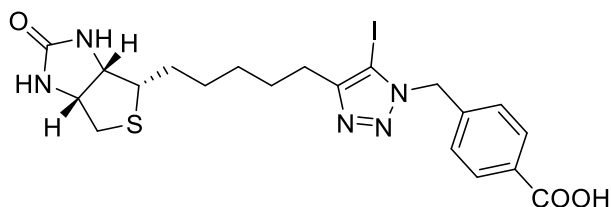
Methyl 4-((5-fluoro-4-(5-((3a*S*,4*S*,6a*R*)-2-oxohexahydro-1*H*-thieno[3,4-*d*]imidazol-4-yl)pentyl)-1*H*-1,2,3-triazol-1-yl)methyl)benzoate (**7n**)



The 5-iodo-triazole **6n** (41 mg, 0.074 mmol) was reacted with potassium fluoride (21 mg, 0.37 mmol) according to general procedure for halogen exchange of 5-Iodo-1,2,3-triazole for 5 min and was purified by flash chromatography on silica eluting with 6% MeOH in DCM to yield 5-fluoro-triazole as an off white solid (18 mg, 54%). ¹H NMR (500 MHz, CDCl₃) δ 8.02 - 8.06 (m, 2H), 7.34 - 7.38 (m, 2H), 5.46 (br s, 1H), 5.44 (s, 2H), 5.13 (br s, 1H), 4.48 - 4.53 (m, 1H), 4.28 - 4.33 (m, 1H), 3.92 (s, 3H), 3.12 - 3.18 (m, 1H), 2.91 (dd, *J* = 5.14, 12.72 Hz, 1H), 2.73 (d, *J* = 12.72 Hz, 1H), 2.63 (t, *J* = 7.58 Hz, 2H), 1.60 - 1.75 (m, 4H), 1.36 - 1.51 (m, 4H); ¹³C NMR (125 MHz, CDCl₃) δ 166.4, 163.2, 138.5, 130.6, 130.3, 127.7, 107.3, 62.0, 60.1, 55.6, 52.3, 50.4, 40.5, 29.0, 28.6, 28.5, 27.9, 23.5, 23.5; ¹⁹F NMR

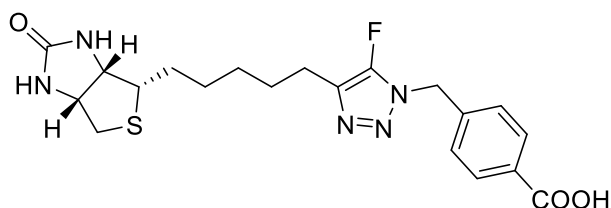
(470 MHz, CDCl₃) δ -157.01 (s); HRMS calcd for C₂₁H₂₆FN₅O₃S [M + H]⁺ 448.1818, found 448.1811.

4-((5-iodo-4-(5-((3*aS*,4*S*,6*aR*)-2-oxohexahydro-1*H*-thieno[3,4-*d*]imidazol-4-yl)pentyl)-1*H*-1,2,3-triazol-1-yl)methyl)benzoic acid (**6o**)



The ester **6n** (20 mg, 0.036 mmol) was reacted with LiOH (2 mg, 0.08 mmol) according to general procedure for hydrolysis of ester and was purified by flash chromatography on silica eluting with 30% MeOH in DCM to yield carboxylic acid as an off white solid (8 mg, 41%). ¹H NMR (500 MHz, DMSO-*d*₆) δ 7.90 - 7.96 (m, 2H), 7.19 - 7.26 (m, 2H), 6.42 (br s, 1H), 6.34 (br s, 1H), 5.69 (s, 2H), 4.26 - 4.32 (m, 1H), 4.09 - 4.14 (m, 1H), 3.05 - 3.12 (m, 1H), 2.81 (dd, *J* = 5.14, 12.47 Hz, 1H), 2.54 - 2.60 (m, 3H), 1.55 - 1.65 (m, 3H), 1.26 - 1.50 (m, 5H); ¹³C NMR (125 MHz, DMSO-*d*₆) δ 166.9, 162.7, 151.3, 140.2, 129.7, 127.2, 82.7, 61.0, 59.2, 55.5, 52.8, 28.5, 28.4, 28.3, 28.2, 27.5, 25.4; HRMS calcd for C₂₀H₂₄IN₅O₃S [M + H]⁺ 542.0723, found 542.0767.

4-((5-fluoro-4-(5-((3*aS*,4*S*,6*aR*)-2-oxohexahydro-1*H*-thieno[3,4-*d*]imidazol-4-yl)pentyl)-1*H*-1,2,3-triazol-1-yl)methyl)benzoic acid (**7o**)

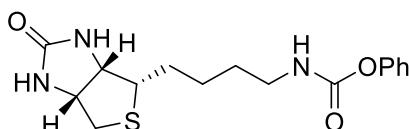


The ester **7n** (8 mg, 0.018 mmol) was reacted with LiOH (1 mg, 0.04 mmol) according to general procedure for hydrolysis of ester and was purified by flash chromatography on silica eluting with 30% MeOH in DCM to yield carboxylic acid as an off white solid (6 mg, 77%). ¹H NMR (500 MHz, DMSO-*d*₆) δ 7.81 - 7.87 (m, 2H), 7.14 - 7.18 (m, 2H), 6.43 (br s, 1H), 6.35 (br s, 1H), 5.49 (s, 2H), 4.27 - 4.31 (m, 1H), 4.09 - 4.13 (m, 1H), 3.04 - 3.10 (m, 1H), 2.80 (dd, *J* = 5.14, 12.47 Hz, 1H), 2.52 - 2.59 (m, 3H), 1.53 - 1.63 (m, 3H), 1.22 - 1.46 (m, 5H); ¹³C NMR (125 MHz, DMSO-*d*₆) δ 168.9, 162.7, 150.8, 129.4, 126.5, 61.1, 59.2, 55.5,

50.0, 37.3, 28.4, 28.2, 28.2, 27.7, 22.9; ^{19}F NMR (470 MHz, $\text{DMSO-}d_6$) δ -156.77 (s); HRMS calcd for $\text{C}_{20}\text{H}_{24}\text{FN}_5\text{O}_3\text{S}$ $[\text{M} + \text{H}]^+$ 434.1662, found 434.1656.

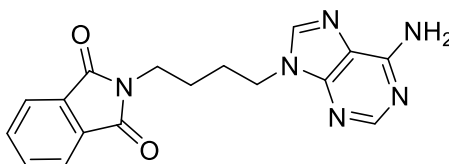
6.3 Experimental work as described in Chapter 3

Phenyl (4-((3*aS*,4*S*,6*aR*)-2-oxohexahydro-1*H*-thieno[3,4-*d*]imidazol-4-yl)butyl)carbamate (12)



To a mixture of compound **11**⁵ (300 mg, 1.19 mmol) in water/THF (9:1, 3.33 mL) were added diphenyl carbonate (255 mg, 1.19 mmol) and TEA (0.33 mL, 2.38 mmol) and the mixture was stirred for 6 h. The mixture was poured into water and extracted with DCM. The organic layer was washed with cold aqueous 10 % NaOH solution and brine. The organic layer was dried over Na_2SO_4 and concentrated. The residue was purified by flash chromatography on silica (DCM:MeOH = 10:1) to yield a white solid (223 mg, 56 %). ^1H NMR (500 MHz, $\text{DMSO-}d_6$) δ 7.71 (t, $J = 5.7$ Hz, 1H), 7.40 – 7.33 (m, 2H), 7.22 – 7.15 (m, 1H), 7.11 – 7.06 (m, 2H), 6.43 (s, 1H), 6.35 (s, 1H), 4.31 (ddt, $J = 7.6, 5.0, 1.1$ Hz, 1H), 4.14 (ddd, $J = 7.8, 4.5, 1.9$ Hz, 1H), 3.12 (ddd, $J = 8.2, 6.4, 4.4$ Hz, 1H), 3.05 (q, $J = 6.6$ Hz, 2H), 2.83 (dd, $J = 12.4, 5.1$ Hz, 1H), 2.58 (d, $J = 12.4$ Hz, 1H), 1.69 – 1.58 (m, 1H), 1.57 – 1.27 (m, 5H); ^{13}C NMR (126 MHz, $\text{DMSO-}d_6$) δ 162.7, 154.3, 151.1, 129.2, 124.8, 121.7, 60.9, 59.2, 55.4, 40.2, 39.8, 29.2, 28.0, 25.8.

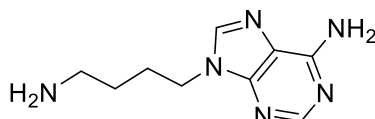
2-(4-(6-Amino-9*H*-purin-9-yl)butyl)isoindoline-1,3-dione (20)



To a suspension of adenine (1.1 g, 8.14 mmol) in DMF (11 mL) was added K_2CO_3 (1.8 g, 13.23 mmol) and *N*-(4-bromobutyl)phthalamide **19** (2.75 g, 9.75 mmol) and the mixture was stirred at 70 °C overnight. The mixture was allowed to cool down to room temperature and partitioned between EtOAc and water. The aqueous phase was extracted with EtOAc. The combined organics were washed with brine and water, dried over Na_2SO_4 , filtrated and concentrated under reduced pressure. The solid obtained was triturated from diethyl ether

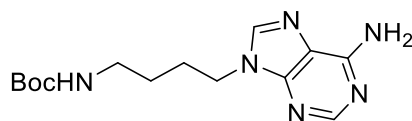
affording the title compound as a pale yellow solid (2.5 g, 84%). ^1H NMR (500 MHz, $\text{DMSO-}d_6$) δ 8.12 (s, 1H), 8.07 (s, 1H), 7.84 (m, 4H), 7.16 (s, 2H), 4.17 (t, $J = 6.7$ Hz, 2H), 3.61 (t, $J = 6.7$ Hz, 2H), 1.83 (dd, $J = 14.7, 6.9$ Hz, 2H), 1.56 (dt, $J = 13.8, 6.9$ Hz, 2H); ^{13}C NMR (125 MHz, $\text{DMSO-}d_6$) δ 167.9, 155.9, 152.3, 149.5, 140.8, 134.3, 131.6, 123.0, 118.7, 42.4, 36.8, 26.7, 25.1; IR (ATR) ν : 3113 (NH_2), 1698 (C=O), 1600 (N=C and C=C) cm^{-1} .

9-(4-Aminobutyl)-9H-purin-6-amine (**21**)



To a suspension of 2-(4-(6-amino-9H-purin-9-yl)butyl)isoindoline-1,3-dione **20** (2.5 g, 7.43 mmol) in ethanol (125 mL) was added hydrazine hydrate (3.5 mL, 114.45 mmol) and the mixture was stirred at reflux overnight. The mixture was allowed to cool down to room temperature and concentrated under reduced pressure. A solid was formed which was filtrated and washed with DCM. Trituration from MeOH afforded the title compound (1.0 g, 67%) as a colourless solid. ^1H NMR (500 MHz, $\text{DMSO-}d_6$) δ 8.12 (s, 1H), 8.11 (s, 1H), 7.14 (2, 2H), 4.11 (t, $J = 7.1$ Hz, 2H), 3.08 (br s, 2H), 2.51 (t, $J = 6.9$ Hz, 2H), 1.79 (dd, $J = 14.9, 7.3$ Hz, 2H), 1.28 (dd, $J = 14.9, 7.3$ Hz, 2H); ^{13}C NMR (125 MHz, $\text{DMSO-}d_6$) δ 155.9, 152.3, 149.5, 140.8, 118.7, 42.8, 41.0, 30.0, 26.9; HRMS calcd. for $[\text{M} + \text{H}^+]$ $\text{C}_9\text{H}_{15}\text{N}_6$: requires 207.1358, found 207.1365; IR (ATR) ν : 3149 (NH_2), 2932 ($=\text{C-H}$), 1677 (N=C and C=C) cm^{-1} .

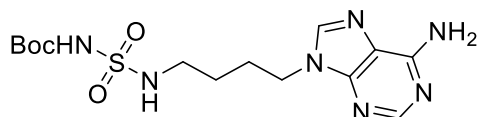
tert-Butyl (4-(6-amino-9H-purin-9-yl)butyl)carbamate (**14**)



To a suspension of adenine (1.10 g, 8.14 mmol) in DMF (12 mL) was added Cs_2CO_3 (3.98 g, 12.2 mmol) and bromide **13**⁶ (2.45 g, 9.77 mmol). The mixture was stirred overnight, poured onto water and extracted with EtOAc twice. The combined organic layers were washed with brine and water. The organic layer was dried over Na_2SO_4 and concentrated under reduced pressure. The residue was purified by flash chromatography on silica (DCM:MeOH = 15:1 \rightarrow 10:1) to yield a white solid (1.70 g, 68 %). ^1H NMR (500 MHz, $\text{DMSO-}d_6$) δ 8.12 (s, 1H), 8.11 (s, 1H), 7.16 (s, 2H), 6.80 (t, $J = 5.8$ Hz, 1H), 4.12 (t, $J = 7.0$

Hz, 2H), 2.92 (q, $J = 6.6$ Hz, 2H), 1.76 (m, 2H), 1.38 – 1.28 (m, 11H); ^{13}C NMR (126 MHz, DMSO- d_6) δ 155.9, 155.6, 152.3, 149.5, 140.8, 118.7, 77.4, 42.6, 28.2, 26.8, 26.7.

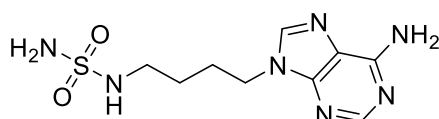
tert-Butyl (*N*-(4-(6-amino-9*H*-purin-9-yl)butyl)sulfamoyl)carbamate (**17**)



Method 1. To a solution of amine **21** (1.6 g, 7.75 mmol) in DCM (16 ml) was added TEA (2.1 mL, 15.5 mmol), followed by addition of sulfamoylating agent **16**⁷ (2.6 g, 7.75 mmol). The reaction mixture was stirred at room temperature for 12 h. The mixture was concentrated under reduced pressure and the residue was purified by flash chromatography on silica (5% MeOH in DCM) to give a crystalline white solid (664 mg, 23%). ^1H NMR (500 MHz, DMSO- d_6) δ 10.77 (s, 1H), 8.12 (s, 1H), 8.11 (s, 1H), 7.58 (t, $J = 5.8$ Hz, 1H), 7.16 (s, 2H), 4.12 (t, $J = 7.0$ Hz, 2H), 2.90 (q, $J = 6.6$ Hz, 2H), 1.80 (q, $J = 7.4$ Hz, 2H), 1.41 (m, 2H), 1.38 (s, 9H); ^{13}C NMR (125 MHz, DMSO- d_6) δ 155.9, 152.3, 150.6, 149.5, 140.7, 118.7, 81.1, 42.4, 42.2, 27.7, 26.7, 25.8.; IR (ATR) ν : 3455 (NH₂), 3358 (N–H), 2980 (=C–H), 1714 (C=O), 1643 (N=C and C=C), 1329 (SO₂) cm^{-1} .

Method 2. To a mixture of compound **14** (613 mg, 2.00 mmol) in DCM (9 mL) was added TFA (0.83 mL, 10.8 mmol) and the mixture was stirred for 3 hours. TEA (1.5 mL) was added dropwise to the reaction mixture to form a white solid. The solid was collected by filtration and washed with DCM. To a mixture of the collected solid in THF (20mL) were added TEA (0.45 mL, 4.00 mmol) and sulfamoylating agent **16**⁷ (602 mg 2.00 mmol) and the mixture was stirred at 60°C overnight. The mixture was concentrated under reduced pressure and the residue was purified by flash chromatography on silica (DCM:MeOH = 20:1 → 15:1) to yield a white solid (116 mg, 15 %).

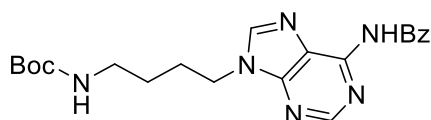
N-(4-(6-Amino-9*H*-purin-9-yl)butyl)-sulfamide (**18**)



A solution of compound **17** (664 mg, 1.72 mmol) in DCM (12 mL) cooled down to 0 °C was treated with TFA (1.2 mL) and stirred at room temperature. After 2 h TFA (1.2 mL) was added. After being stirred at room temperature overnight the solvent was removed under

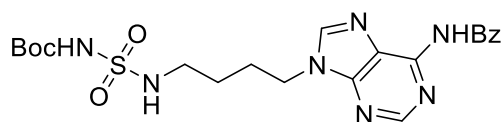
reduced pressure. The title compound was obtained as a colourless solid (641 mg) and was used without further purification. HRMS (ESI) calcd. for $C_9H_{15}N_7NaO_2S$ [$M + Na^+$]: 308.0906, found 308.0883; IR (ATR) ν : 3324 (NH₂), 3212 (N–H), 3011 (=C–H), 1626 (N=C and C=C), 1332 (SO₂) cm^{-1} .

tert-Butyl (4-(6-benzamido-9*H*-purin-9-yl)butyl)carbamate (**22**)



To a mixture of compound **14** (1.03 g, 3.36 mmol) in pyridine (5 mL) was slowly added BzCl (0.39 mL, 3.36 mmol) and the mixture was stirred at 100 °C for 1 h. The mixture was concentrated under reduced pressure and the residue was purified by flash chromatography on silica (DCM:MeOH = 20:1) to yield a white solid (0.83 g, 60 %). ¹H NMR (600 MHz, CDCl₃) δ 9.30 (s, 1H), 8.74 (s, 1H), 8.06 – 7.93 (m, 3H), 7.59 – 7.52 (m, 1H), 7.47 (t, J = 7.8 Hz, 2H), 4.71 (t, J = 6.2 Hz, 1H), 4.28 (t, J = 7.3 Hz, 2H), 3.16 (q, J = 6.7 Hz, 2H), 2.40 (s, 1H), 1.92 (m, 2H), 1.50 (m, 2H), 1.39 (s, 9H); ¹³C NMR (151 MHz, CDCl₃) δ 164.9, 156.2, 152.6, 152.2, 149.6, 143.1, 133.7, 132.8, 128.9, 128.0, 123.1, 79.5, 43.7, 39.6, 28.5, 27.4, 27.2.

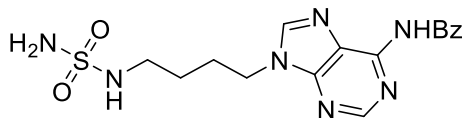
tert-Butyl (*N*-(4-(6-benzamido-9*H*-purin-9-yl)butyl)sulfamoyl)carbamate (**24**)



To a mixture of compound **22** (820 mg, 2.00 mmol) in DCM (9 mL) was added TFA (0.83 mL, 10.8 mmol) and the mixture was stirred for 3 hours. TEA (1.5 mL) was added dropwise to the reaction mixture to form a white solid. The solid was collected by filtration and washed with DCM. To a mixture of the collected solid in THF (20mL) were added TEA (0.45 mL, 4.00 mmol) and sulfamoylating agent **16**⁷ (602 mg 2.00 mmol) and the mixture was stirred at 60°C overnight. The mixture was concentrated under reduced pressure and the residue was purified by flash chromatography on silica (DCM:acetone:MeOH = 50:25:1) to yield a white solid (320 mg, 34 %). ¹H NMR (500 MHz, CDCl₃) δ 9.26 (br s, 1H), 8.79 (s, 1H), 8.10 – 7.99 (m, 3H), 7.66 – 7.57 (m, 1H), 7.52 (t, J = 7.6 Hz, 2H), 5.81 (br s, 1H), 4.33 (t, J = 7.1 Hz, 2H), 3.14 (q, J = 5.9 Hz, 2H), 2.03 (m, 2H), 1.69 – 1.55 (m, 2H), 1.46 (s, 9H); ¹³C NMR

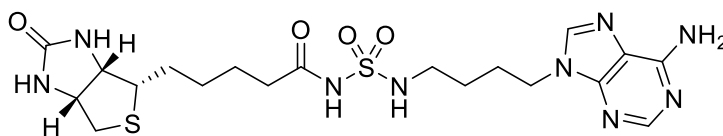
(126 MHz, CDCl₃) δ 152.6, 152.4, 150.6, 149.7, 143.2, 133.7, 132.9, 128.9, 128.2, 123.3, 83.9, 68.1, 43.6, 43.1, 28.1, 27.3, 26.2.

N-(9-(4-(Sulfamoylamino)butyl)-9*H*-purin-6-yl)benzamide (**25**)



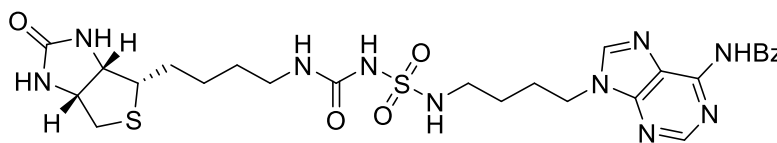
To a mixture of compound **24** (140 mg, 0.286 mmol) in DCM (5 mL) was added TFA (0.5 mL) and the mixture was stirred for 2 h. The mixture was concentrated under reduced pressure and the residue was purified by flash chromatography on silica (DCM:MeOH = 6:1) to yield a white solid (105 mg, 94 %). ¹H NMR (500 MHz, DMSO-*d*₆) δ 11.11 (br s, 1H), 8.73 (s, 1H), 8.50 (s, 1H), 8.09 – 8.00 (m, 2H), 7.69 – 7.60 (m, 1H), 7.55 (t, *J* = 7.7 Hz, 2H), 6.47 (m, 3H), 4.28 (t, *J* = 7.1 Hz, 2H), 2.91 (q, *J* = 6.5 Hz, 2H), 1.91 (m, 2H), 1.52 – 1.40 (m, 2H); ¹³C NMR (126 MHz, DMSO-*d*₆) δ 152.4, 151.3, 150.0, 144.7, 133.5, 132.3, 128.42, 128.40, 125.3, 43.0, 41.9, 26.7, 26.1.

N-(*N*-(4-(6-Amino-9*H*-purin-9-yl)butyl)sulfamoyl)-5-((3*aS*,4*S*,6*aR*)-2-oxohexahydro-1*H*-thieno[3,4-*d*]imidazol-4-yl)pentanamide (**6**)



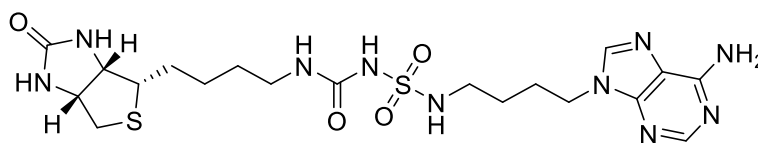
To a mixture of sulfamide **18** (258 mg, 1.00 mmol) in DMF (3 ml) was added Cs₂CO₃ (232 mg, 1.20 mmol) and biotin-NHS **26**⁸ (375 mg, 1.10 mmol). The mixture was concentrated under reduced pressure and the residue was purified by flash chromatography on silica (10% MeOH in DCM) to give the title compound as a crystalline solid (178 mg, 35%). ¹H NMR (500 MHz, DMSO-*d*₆) δ 11.25 (br s, 1H), 8.13 (s, 1H), 8.11 (s, 1H), 7.59 (t, *J* = 5.7 Hz, 1H), 7.20 (s, 2H), 6.50 (s, 1H), 6.38 (s, 1H), 4.30 (dd, *J* = 7.6, 5.2 Hz, 1H), 4.20 – 4.07 (m, 3H), 3.12 – 3.04 (m, 1H), 2.88 (dd, *J* = 12.9, 6.7 Hz, 2H), 2.80 (dd, *J* = 12.4, 5.1 Hz, 1H), 2.57 (d, *J* = 12.4 Hz, 1H), 2.18 (t, *J* = 7.4 Hz, 2H), 1.91 – 1.73 (m, 2H), 1.67 – 1.55 (m, 1H), 1.55 – 1.36 (m, 5H), 1.35 – 1.21 (m, 2H); ¹³C NMR (125 MHz, DMSO-*d*₆): 171.6, 162.8, 156.0, 152.4, 149.6, 140.8, 118.7, 61.1, 59.2, 55.4, 48.6, 42.5, 42.2, 35.0, 28.0, 26.8, 25.8, 24.4; HRMS (ESI) calcd. for C₁₉H₃₀N₉O₄S₂ [M + H⁺]: 512.1857, found 512.1834; IR (ATR) ν : 3315 (NH₂), 3283 (N–H), 1638 (C=O), 1342 (SO₂) cm⁻¹.

N-(9-(4-((*N*-((4-((3*aS*,4*S*,6*aR*)-2-Oxohexahydro-1*H*-thieno[3,4-*d*]imidazol-4-yl)butyl)carbamoyl)sulfamoyl)amino)butyl)-9*H*-purin-6-yl)benzamide (**27**)



To a mixture of compound **12** (77 mg, 0.23 mmol) and compound **25** (74 mg, 0.19 mmol) in MeCN (10 mL) was added DBU (43 μ L, 0.29 mmol) and the resulting mixture was refluxed for 17 h. The solvent was evaporated under reduced pressure. The residue was dissolved in EtOAc and the organic layer was washed with 0.1N HCl, brine, and water. The organic layer was dried over Na₂SO₄ and concentrated under reduced pressure. The residue was purified by flash chromatography on silica (DCM:MeOH = 9:1) to yield a white solid (58 mg, 48%). ¹H NMR (500 MHz, DMSO-*d*₆) δ 11.11 (br s, 1H), 9.74 (br s, 1H), 8.72 (s, 1H), 8.47 (s, 1H), 8.09 – 8.00 (m, 2H), 7.70 – 7.60 (m, 1H), 7.55 (t, *J* = 7.7 Hz, 2H), 7.35 (br s, 1H), 6.41 (s, 1H), 6.34 (s, 1H), 6.26 (m, 1H), 4.27 (m, 3H), 4.11 (ddd, *J* = 7.5, 4.5, 1.7 Hz, 1H), 3.07 (ddd, *J* = 8.4, 6.3, 4.4 Hz, 1H), 3.01 (q, *J* = 6.6 Hz, 2H), 2.93 (m, 2H), 2.79 (dd, *J* = 12.5, 5.1 Hz, 1H), 2.56 (d, *J* = 12.5 Hz, 1H), 1.89 (m, 2H), 1.62 (m, 1H), 1.54 – 1.24 (m, 7H); ¹³C NMR (126 MHz, DMSO-*d*₆) δ 162.7, 152.4, 152.30, 152.29, 151.3, 150.0, 144.6, 132.3, 128.42, 128.40, 125.3, 61.0, 59.2, 55.4, 42.8, 42.1, 39.8, 29.4, 27.9, 26.6, 25.9, 25.8.

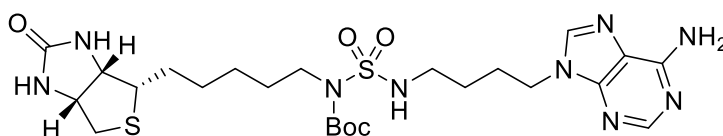
(3*aS*,4*S*,6*aR*)-4-(4-(((4-(6-Amino-9*H*-purin-9-yl)butyl)sulfamoyl)carbamoyl)amino)butyl)tetrahydro-1*H*-thieno[3,4-*d*]imidazol-2(3*H*)-one (**7**)



To a solution of compound **27** (50 mg, 0.079 mmol) in MeOH (1.6 mL) was added 30 % NH₄OH (2.4 mL) and the mixture was stirred overnight. The mixture was concentrated under reduced pressure and the residue was purified by flash chromatography on silica (DCM:MeOH = 4:1) to yield a white solid (22 mg, 53 %). ¹H NMR (500 MHz, DMSO-*d*₆) δ 9.74 (br s, 1H), 8.13 (s, 1H), 8.11 (s, 1H), 7.33 (br s, 1H), 7.17 (s, 2H), 6.47 (s, 1H), 6.35 (s, 1H), 6.21 (br s, 1H), 4.29 (dd, *J* = 7.7, 5.0 Hz, 1H), 4.17 – 4.09 (m, 3H), 3.08 (ddd, *J* = 8.6, 6.2, 4.4 Hz, 1H), 3.01 (q, *J* = 6.6 Hz, 2H), 2.90 (q, *J* = 6.6 Hz, 2H), 2.80 (dd, *J* = 12.4, 5.1 Hz, 1H), 2.57 (d, *J* = 12.4 Hz, 1H), 1.87 – 1.77 (m, 2H), 1.67 – 1.56 (m, 1H), 1.51 – 1.19

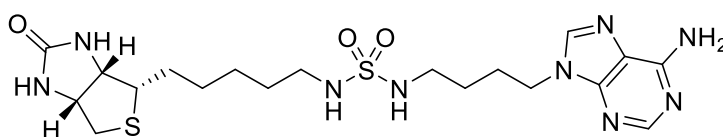
(m, 7H); ^{13}C NMR (126 MHz, $\text{DMSO-}d_6$) δ 162.7, 155.9, 152.3, 149.5, 140.7, 118.7, 61.0, 59.2, 55.5, 42.4, 42.1, 38.8, 29.4, 28.0, 26.8, 25.82, 25.78; HRMS (ESI) calcd. for $\text{C}_{19}\text{H}_{30}\text{N}_{10}\text{O}_4\text{S}_2$ [$\text{M} + \text{H}^+$]: 527.1966, found 527.1966.

tert-Butyl $(N$ -(4-(6-amino-9*H*-purin-9-yl)butyl)sulfamoyl)(5-((3*aS*,4*S*,6*aR*)-2-oxohexahydro-1*H*-thieno[3,4-*d*]imidazol-4-yl)pentyl)carbamate (**29**)



To a mixture of sulfamide **17** (50 mg, 0.13 mmol) in DMF (2 mL) was added K_2CO_3 (27 mg, 0.20 mmol) and biotin bromide **28**⁵ (42 mg, 0.14 mmol). The mixture was concentrated under reduced pressure and the residue was purified by flash chromatography on silica (DCM:MeOH = 15:1) to give a white solid (38 mg, 49%). ^1H NMR (500 MHz, $\text{DMSO-}d_6$) δ 8.12 (s, 1H), 8.11 (s, 1H), 7.61 (br s, 1H), 7.16 (s, 2H), 6.47 (s, 1H), 6.34 (s, 1H), 4.35 – 4.25 (m, 1H), 4.12 (m, 3H), 3.48 (t, $J = 7.5$ Hz, 2H), 3.14 – 3.04 (m, 1H), 2.88 (m, 2H), 2.81 (dd, $J = 12.4, 5.1$ Hz, 1H), 2.57 (d, $J = 12.4$ Hz, 1H), 1.82 (m, 2H), 1.59 (m, 1H), 1.55 – 1.19 (m, 18H); ^{13}C NMR (126 MHz, $\text{DMSO-}d_6$) δ 162.7, 155.9, 152.3, 151.1, 149.6, 140.7, 118.7, 82.4, 61.0, 59.2, 55.5, 47.4, 42.4, 42.3, 29.1, 28.3, 28.2, 27.6, 26.7, 26.1, 25.7.

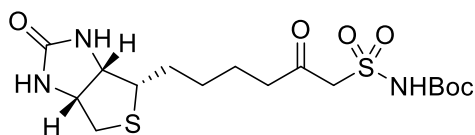
N-(4-(6-Amino-9*H*-purin-9-yl)butyl)-*N*-(5-((3*aS*,4*S*,6*aR*)-2-oxohexahydro-1*H*-thieno[3,4-*d*]imidazol-4-yl)pentyl)sulfuric diamide (**8**)



To a mixture of compound **29** (21 mg, 0.035 mmol) in DCM (0.5 mL) was added TFA (24 μL , 0.32 mmol) and the mixture was stirred overnight. The mixture was quenched with TEA and concentrated under reduced pressure. The residue was purified by flash chromatography on silica (DCM:MeOH = 5:1) to yield a white solid (14 mg, 80 %). ^1H NMR (500 MHz, $\text{DMSO-}d_6$) δ 8.12 (d, 2H), 7.18 (s, 2H), 6.75 (t, $J = 5.9$ Hz, 1H), 6.71 (t, $J = 5.9$ Hz, 1H), 6.48 (s, 1H), 6.36 (s, 1H), 4.30 (dd, $J = 7.7, 5.1$ Hz, 1H), 4.13 (m, 3H), 3.08 (ddd, $J = 8.5, 6.1, 4.3$ Hz, 1H), 2.87 – 2.77 (m, 3H), 2.73 (m, 2H), 2.57 (d, $J = 12.4$ Hz, 1H), 1.82 (m, 2H), 1.58 (m, 1H), 1.51 – 1.18 (m, 9H); ^{13}C NMR (126 MHz, $\text{DMSO-}d_6$) δ 162.8, 155.9, 152.3,

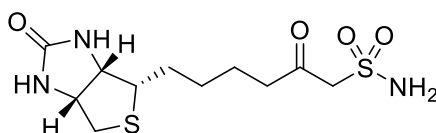
149.5, 140.8, 118.7, 61.0, 59.2, 55.5, 42.5, 42.1, 41.6, 39.8, 28.7, 28.3, 28.2, 27.0, 26.3, 26.1; HRMS (ESI) calcd. for C₁₉H₃₁N₉O₃S₂ [M + H⁺]: 498.2064, found 498.2069.

tert-Butyl ((2-oxo-6-((3*a*S,4*S*,6*a*R)-2-oxohexahydro-1*H*-thieno[3,4-*d*]imidazol-4-yl)hexyl)sulfonyl)carbamate (**32**)



To a mixture of sulfonamide **31**⁹ (0.90 g, 4.59 mmol) in anhydrous THF (30 mL) was added dropwise LDA (1.0 M in THF/hexane; 14.22 mL, 14.22 mmol) at 0°C and the mixture was stirred for 1 h at 0°C. Biotin ester **30**¹⁰ (1.38 g, 5.07 mmol) was added and the reaction mixture was stirred for 3 h at 0°C. The mixture was warmed to room temperature and stirred overnight. The reaction mixture was quenched with saturated aq NaCl (15 mL) and 0.5 M aq NaH₂PO₄ (15 mL) and extracted with EtOAc (2 X 15 mL). The aqueous layer was extracted with 10 % MeOH/DCM (6 X 15 mL) and the combined DCM extracts were dried over Na₂SO₄. The mixture was concentrated under reduced pressure and the residue was purified by flash chromatography on silica (DCM:MeOH = 15:1) to yield a white solid (223 mg, 17 %). ¹H NMR (500 MHz, DMSO-*d*₆) δ 11.45 (br s, 1H), 6.41 (s, 1H), 6.34 (s, 1H), 4.52 (s, 2H), 4.30 (dd, *J* = 7.7, 5.1 Hz, 1H), 4.12 (ddd, *J* = 7.5, 4.5, 1.8 Hz, 1H), 3.09 (ddd, *J* = 8.5, 6.3, 4.4 Hz, 1H), 2.81 (dd, *J* = 12.4, 5.1 Hz, 1H), 2.64 (td, *J* = 7.0, 4.1 Hz, 2H), 2.57 (d, *J* = 12.4 Hz, 1H), 1.60 (m, 1H), 1.54 – 1.21 (m, 14H); ¹³C NMR (126 MHz, DMSO-*d*₆) δ 198.9, 162.7, 61.8, 61.0, 59.2, 55.3, 42.9, 31.3, 28.1, 27.8, 27.7, 22.6.

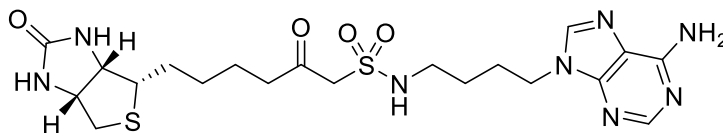
2-Oxo-6-((3*a*S,4*S*,6*a*R)-2-oxohexahydro-1*H*-thieno[3,4-*d*]imidazol-4-yl)hexane-1-sulfonamide (**33**)



To a solution of compound **32** (50 mg, 0.12 mmol) in DCM (1 mL) was added TFA (81 μL) and the mixture was stirred overnight. The mixture was concentrated under reduced pressure and was used without further purification. ¹H NMR (500 MHz, DMSO-*d*₆) δ 7.10 (br s, 2H), 4.30 (ddd, *J* = 7.7, 5.1, 1.0 Hz, 1H), 4.17 (s, 2H), 4.12 (dd, *J* = 7.7, 4.4 Hz, 1H), 3.09 (ddd, *J* = 8.5, 6.3, 4.4 Hz, 1H), 2.82 (dd, *J* = 12.4, 5.1 Hz, 1H), 2.72 – 2.59 (m, 2H), 2.57 (d, *J* =

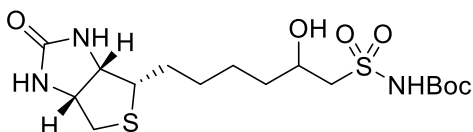
12.4 Hz, 1H), 1.66 – 1.56 (m, 1H), 1.55 – 1.41 (m, 3H), 1.38 – 1.23 (m, 2H); ^{13}C NMR (126 MHz, DMSO- d_6) δ 200.1, 162.7, 65.6, 61.0, 59.2, 55.3, 42.5, 28.1, 27.9, 22.7.

N-(4-(6-Amino-9*H*-purin-9-yl)butyl)-2-oxo-6-((3*aS*,4*S*,6*aR*)-2-oxohexahydro-1*H*-thieno[3,4-*d*]imidazol-4-yl)hexane-1-sulfonamide (**9**)



To a mixture of compound **33** (27 mg, 0.084 mmol) and adenine bromide **34**¹¹ (25 mg, 0.093 mmol) in DMF (1 mL) was added Cs₂CO₃ (33 mg, 0.10 mmol) and the mixture was stirred overnight. The mixture was concentrated under reduced pressure and the residue was purified by flash chromatography on silica (DCM:MeOH = 5:1) to yield a white solid (22 mg, 51 %). ^1H NMR (500 MHz, DMSO- d_6) δ 8.13 (s, 1H), 8.12 (s, 1H), 7.34 (t, J = 5.8 Hz, 1H), 7.18 (s, 2H), 6.44 (s, 1H), 6.36 (s, 1H), 4.32 – 4.27 (m, 1H), 4.21 (s, 2H), 4.17 – 4.10 (m, 3H), 3.08 (ddd, J = 8.5, 6.2, 4.4 Hz, 1H), 2.96 (m, 2H), 2.81 (dd, J = 12.5, 5.1 Hz, 1H), 2.62 (td, J = 7.1, 2.8 Hz, 2H), 2.57 (d, J = 12.4 Hz, 1H), 1.87 – 1.77 (m, 2H), 1.59 (m, 1H), 1.52 – 1.20 (m, 7H); ^{13}C NMR (126 MHz, DMSO- d_6) δ 200.1, 162.7, 155.9, 152.4, 149.5, 140.8, 118.7, 62.1, 61.0, 59.2, 55.3, 42.7, 42.4, 42.0, 28.1, 27.9, 26.7, 26.6, 22.7; HRMS (ESI) calcd. for C₂₀H₃₀N₈O₄S₂ [M + H⁺]: 511.1904, found 511.1910.

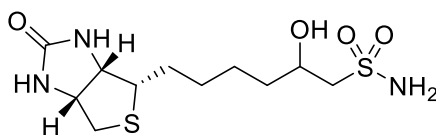
tert-Butyl ((2-hydroxy-6-((3*aS*,4*S*,6*aR*)-2-oxohexahydro-1*H*-thieno[3,4-*d*]imidazol-4-yl)hexyl)sulfonyl)carbamate (**35**)



To a mixture of compound **32** (84 mg, 0.20 mmol) in MeOH (2 mL) was added NaBH₄ (8 mg, 0.21 mmol) and the mixture was stirred for 4 h. The reaction mixture was quenched with adding HCl to adjust pH of around 5. The mixture was concentrated under reduced pressure and the residue was purified by flash chromatography on silica (DCM:MeOH = 5:1) to yield a white solid (78 mg, 92 %). ^1H NMR (500 MHz, DMSO- d_6) δ 11.05 (br s, 1H), 6.41 (s, 1H), 6.34 (s, 1H), 4.93 (br s, 1H), 4.30 (dd, J = 7.7, 5.1 Hz, 1H), 4.16 – 4.10 (m, 1H), 3.87 (br s, 1H), 3.45 – 3.33 (m, 2H), 3.10 (ddd, J = 8.5, 6.1, 4.4 Hz, 1H), 2.82 (dd, J = 12.4, 5.1 Hz, 1H), 2.57 (d, J = 12.4 Hz, 1H), 1.60 (m, 1H), 1.55 – 1.20 (m, 16H); ^{13}C NMR (126

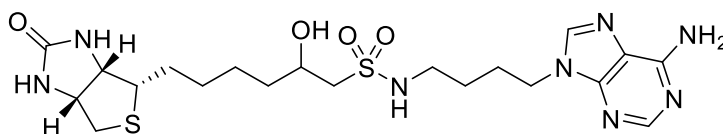
MHz, DMSO-*d*₆) δ 162.7, 150.6, 81.9, 65.49, 65.47, 61.03, 61.00, 60.7, 59.2, 58.4, 55.5, 55.4, 39.8, 36.41, 36.38, 29.2, 28.5, 28.4, 28.3, 28.2, 27.7, 24.70, 24.67.

2-Hydroxy-6-((3*aS*,4*S*,6*aR*)-2-oxohexahydro-1*H*-thieno[3,4-*d*]imidazol-4-yl)hexane-1-sulfonamide (**36**)



To a solution of compound **37** (56 mg, 0.13 mmol) in DCM (1 mL) was added TFA (81 μ L) and the mixture was stirred overnight. The mixture was concentrated under reduced pressure and was used without further purification.

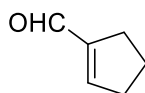
N-(4-(6-Amino-9*H*-purin-9-yl)butyl)-2-hydroxy-6-((3*aS*,4*S*,6*aR*)-2-oxohexahydro-1*H*-thieno[3,4-*d*]imidazol-4-yl)hexane-1-sulfonamide (**10**)



To a mixture of compound **36** (21 mg, 0.064 mmol) and adenine bromide **34**¹¹ (19 mg, 0.070 mmol) in DMF (1 mL) was added Cs₂CO₃ (25 mg, 0.077 mmol) and the mixture was stirred overnight. The mixture was concentrated under reduced pressure and the residue was purified by flash chromatography on silica (DCM:MeOH = 10:1 \rightarrow 5:1) to yield a white solid (22 mg, 67 %). ¹H NMR (500 MHz, Methanol-*d*₄) δ 8.22 (s, 1H), 8.15 (d, *J* = 2.0 Hz, 1H), 4.55 (br s, 1H), 4.50 (dd, *J* = 7.9, 5.0 Hz, 1H), 4.35 – 4.25 (m, 2H), 4.06 (m, 1H), 3.22 (dt, *J* = 9.8, 5.3 Hz, 1H), 3.17 – 3.08 (m, 3H), 2.97 – 2.90 (m, 1H), 2.71 (d, *J* = 12.7 Hz, 1H), 2.02 – 1.94 (m, 2H), 1.79 – 1.70 (m, 1H), 1.65 – 1.37 (m, 7H); ¹³C NMR (126 MHz, Methanol-*d*₄) δ 166.1, 157.3, 153.7, 150.7, 142.8, 120.1, 68.1, 68.0, 67.9, 63.43, 63.41, 63.39, 61.6, 59.6, 59.02, 58.97, 57.10, 57.08, 44.4, 43.3, 41.0, 37.8, 37.7, 37.5, 30.1, 30.01, 30.00, 29.8, 29.7, 29.6, 28.3, 28.2, 26.2.; HRMS (ESI) calcd. for C₂₀H₃₂N₈O₄S₂ [M + H⁺]: 513.2061, found 513.2066.

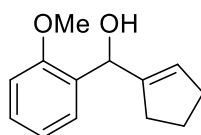
6.4 Experimental work as described in Chapter 4

cyclopent-1-ene-1-carbaldehyde (**4.14**)



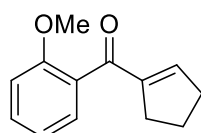
To a solution of sodium periodate (7.1 g, 33.2 mmol) in water (62 mL) was added an ethyl ether solution (37 mL) of trans-1,2-cyclohexanediol **4.15** (3.0 g, 25.8 mmol). The solution was stirred for 30 min at ambient temperature. To the solution was added 20% aqueous KOH (10 mL) and the solution was stirred for 1 hour. The resulting organic layer was washed with water and brine. The organic layer was dried over anhydrous sodium sulfate and concentrated under reduced pressure to give a pale-yellow oil (1.20 g, 48%). ^1H NMR (500 MHz, CDCl_3) δ 9.80 (s, 1H), 6.89 – 6.86 (m, 1H), 2.61 (tq, $J = 7.5, 2.4$ Hz, 2H), 2.54 (tq, $J = 8.1, 2.2$ Hz, 2H), 2.06 – 1.96 (m, 2H); ^{13}C NMR (126 MHz, CDCl_3) δ 190.0, 153.2, 148.1, 33.8, 28.5, 23.0.

cyclopent-1-en-1-yl(2-methoxyphenyl)methanol (**4.12**)



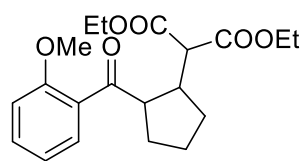
To a solution of 2-bromoanisole **4.13** (1.12 g, 6.0 mmol) in anhydrous THF (30 mL) was added *n*-BuLi (2 M solution, 3.1 mL, 6.2 mmol) at -78°C over 10 min. After 1 hour, a solution of **4.14** (0.38 g, 4.0 mmol) in anhydrous THF (10 mL) was added to the mixture at -78°C over 10 min and the mixture was stirred at -78°C for 4 h. The reaction mixture was quenched with water. The mixture was extracted with EtOAc (30 mL) three times and the organics were washed with water (40 mL) and brine. The organic layer was dried over anhydrous sodium sulfate and concentrated under reduced pressure. The residue was purified by flash chromatography on silica eluting with 5% \rightarrow 10% EtOAc in hexane to give a colourless oil (0.52 g, 64%). ^1H NMR (500 MHz, CDCl_3) δ 7.31 – 7.23 (m, 2H), 6.96 (td, $J = 7.4, 1.1$ Hz, 1H), 6.90 (d, $J = 8.1$ Hz, 1H), 5.64 (q, $J = 2.0$ Hz, 1H), 5.55 (d, $J = 5.8$ Hz, 1H), 3.86 (s, 3H), 2.74 (d, $J = 6.0$ Hz, 1H), 2.41 – 2.19 (m, 4H), 1.95 – 1.82 (m, 2H); ^{13}C NMR (126 MHz, CDCl_3) δ 157.1, 146.0, 130.8, 128.7, 127.9, 125.7, 120.9, 110.9, 70.1, 55.6, 32.6, 32.5, 23.5.

cyclopent-1-en-1-yl(2-methoxyphenyl)methanone (**4.11**)



To a solution of the alcohol **4.12** (440 mg, 2.15 mmol) in DCM (14 mL) was added Dess-Martin Periodinane (1.37 g, 3.23 mmol) and the mixture was stirred overnight. DCM was evaporated and EtOAc (13 mL) an aqueous solution of 1:1 10 % sodium thiosulphate to saturated sodium bicarbonate (13 mL) was then added. After stirring for 10 min, the biphasic mixture was extracted with EtOAc (20 mL) three times. The combined organic phase was washed with saturated sodium bicarbonate (20 mL) and dried over anhydrous sodium sulphate. The organic phase was concentrated under reduced pressure and purified by flash chromatography on silica eluting with 5% EtOAc in hexane to give a colourless oil (321 mg, 74%). ^1H NMR (500 MHz, CDCl_3) δ 7.41 – 7.36 (m, 1H), 7.25 (dd, $J = 7.5, 1.8$ Hz, 1H), 7.00 – 6.94 (m, 2H), 6.42 (ddt, $J = 4.0, 2.9, 1.8$ Hz, 1H), 3.81 (s, 3H), 2.76 – 2.68 (m, 2H), 2.56 (tq, $J = 7.5, 2.5$ Hz, 2H), 2.06 – 1.97 (m, 2H); ^{13}C NMR (126 MHz, CDCl_3) δ 194.4, 156.9, 148.7, 146.5, 131.1, 130.3, 128.9, 120.2, 111.6, 55.9, 34.3, 30.7, 23.2.

diethyl 2-(2-(2-methoxybenzoyl)cyclopentyl)malonate (**4.16**)



(*cis* : *trans* = 1 : 2.5)

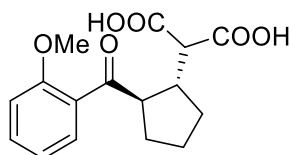
NaH (60% dispersion in mineral oil; 11 mg, 0.27 mmol) was added slowly with ice-cooling under an N_2 atmosphere to a solution of **4.11** (319 mg, 1.58 mmol) and diethylmalonate (320 μL , 2.11 mmol) in EtOH (5 mL). The reaction mixture was stirred at ambient temperature for 15 min and then refluxed at 80°C for 24 h. The reaction was quenched by addition of water. Ethanol was evaporated and the residue was extracted with EtOAc twice. The combined organic phase was dried over anhydrous sodium sulphate. The organic phase was concentrated under reduced pressure and purified by flash chromatography on silica eluting with 5% \rightarrow 10% EtOAc in hexane to give **4.16** (1 : 2.5, *cis* : *trans*) as a colourless oil (498 mg, 87%). A sample of the mixture was further purified to give pure *cis* and pure *trans* for characterisation.

cis-**4.16**. ^1H NMR (500 MHz, CDCl_3) δ 7.57 (dd, $J = 7.7, 1.8$ Hz, 1H), 7.42 (ddd, $J = 8.2, 7.3, 1.8$ Hz, 1H), 6.98 (td, $J = 7.5, 1.0$ Hz, 1H), 6.93 (dd, $J = 8.4, 0.9$ Hz, 1H), 4.26 – 4.15 (m, 2H), 4.12 (ddd, $J = 8.4, 7.0, 3.5$ Hz, 1H), 3.95 (dq, $J = 10.8, 7.2$ Hz, 1H), 3.88 (s, 3H), 3.86 – 3.79 (m, 2H), 2.76 – 2.66 (m, 1H), 2.03 (dtd, $J = 13.0, 8.7, 6.0$ Hz, 1H), 1.96 – 1.75 (m, 4H), 1.73 – 1.63 (m, 1H), 1.27 (t, $J = 7.1$ Hz, 3H), 1.03 (t, $J = 7.1$ Hz, 3H); ^{13}C NMR

(126 MHz, CDCl₃) δ 206.0, 169.7, 169.3, 158.3, 133.2, 130.4, 129.6, 120.6, 111.7, 61.4, 61.1, 55.7, 53.4, 51.4, 43.6, 30.8, 30.0, 23.6, 14.3, 13.9.

trans-**4.16**. ¹H NMR (500 MHz, CDCl₃) δ 7.62 (dd, $J = 7.6, 1.8$ Hz, 1H), 7.43 (ddd, $J = 8.4, 7.4, 1.8$ Hz, 1H), 7.00 (td, $J = 7.5, 1.0$ Hz, 1H), 6.95 (dd, $J = 8.3, 1.0$ Hz, 1H), 4.24 – 4.10 (m, 2H), 4.04 (q, $J = 7.1$ Hz, 2H), 3.88 (s, 3H), 3.79 (ddd, $J = 9.8, 7.3, 5.9$ Hz, 1H), 3.42 (d, $J = 8.2$ Hz, 1H), 3.21 (p, $J = 8.1$ Hz, 1H), 2.11 – 1.96 (m, 2H), 1.77 – 1.61 (m, 3H), 1.56 – 1.48 (m, 1H), 1.24 (t, $J = 7.1$ Hz, 3H), 1.16 (t, $J = 7.1$ Hz, 3H); ¹³C NMR (126 MHz, CDCl₃) δ 204.9, 169.1, 169.0, 158.2, 133.1, 130.6, 129.0, 120.8, 111.6, 61.31, 61.26, 56.1, 55.7, 54.2, 41.0, 31.8, 31.3, 25.2, 14.2, 14.1.

(\pm)-2-(*trans*-2-(2-methoxybenzoyl)cyclopentyl)malonic acid (**4.10**)



4.10 (*trans*)

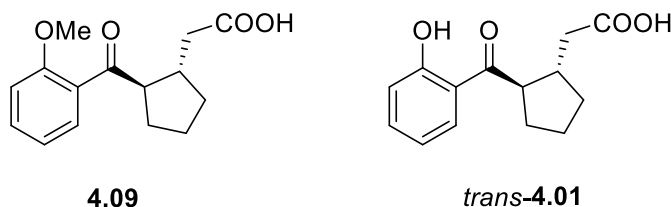
Stereochemical configurations are relative.

Method 1. A mixture of **4.16** (1 : 2.5, *cis* : *trans*; 650 mg, 1.79 mmol) in 6N aqueous HCl (10 mL) was stirred at 90°C for 2 days. The mixture was concentrated under reduced pressure and purified by flash chromatography on silica eluting with 25% → 80% EtOAc in hexane to give **4.10** (*trans*) as a white solid (346 mg, 63%).

Method 2. A mixture of **4.16** (1 : 2.5, *cis* : *trans*; 186 mg, 0.51 mmol), THF (7.7 mL), and 20% aqueous NaOH (2.6 mL) was refluxed at 80°C for 6 h. THF was evaporated and the residue was extracted with ether, then with 10% aqueous NaOH three times. The aqueous layer was acidified with conc. HCl and extracted with DCM three times. The combined organic layer was dried over anhydrous sodium sulphate and concentrated under reduced pressure. The residue was triturated with hexane to give **4.10** (*trans*) as a pale yellow solid (145 mg, 93%). ¹H NMR (500 MHz, DMSO-*d*₆) δ 12.60 (br s, 2H), 7.52 – 7.42 (m, 2H), 7.11 (d, $J = 8.4$ Hz, 1H), 6.99 (t, $J = 7.4$ Hz, 1H), 3.82 (s, 3H), 3.63 (dt, $J = 9.4, 5.7$ Hz, 1H), 3.20 (d, $J = 9.0$ Hz, 1H), 2.98 – 2.87 (m, 1H), 1.97 – 1.79 (m, 2H), 1.67 – 1.39 (m, 4H); ¹³C NMR (126 MHz, DMSO-*d*₆) δ 204.3, 170.30, 170.25, 157.5, 132.9, 129.6, 128.7, 120.3, 112.2, 55.8, 55.7, 53.6, 40.4, 30.9, 30.8, 24.7; HRMS calcd for C₁₆H₁₈O₆ [M + H]⁺ 307.1176, found 307.1176.

The reaction was repeated on separate samples of *cis* and *trans* to give **4.10** (*trans*) in both cases.

(±)-2-(*trans*-2-(2-methoxybenzoyl)cyclopentyl)acetic acid (**4.09**) and (±)-2-(*trans*-2-(2-hydroxybenzoyl)cyclopentyl)acetic acid (*trans*-**4.01**)



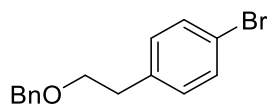
Stereochemical configurations are relative.

Method 1. A mixture of **4.16** (650 mg, 1.79 mmol) in 6N aqueous HCl (10 mL) was stirred at 90°C for 2 days. The mixture was concentrated under reduced pressure and purified by flash chromatography on silica eluting with 25% → 33% EtOAc in hexane to give **4.09** as a yellow oil (134 mg, 29%) and *trans*-**4.01** as a yellow oil (29 mg, 7%).

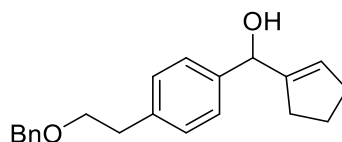
Method 2. A solution of **4.10** (340 mg, 1.11 mmol) in AcOH (5 mL) was refluxed at 120°C for 6 h. The solvent was evaporated and the residue was treated with water. The aqueous phase was extracted with DCM three times. The combined organic phase was dried over anhydrous sodium sulphate and concentrated under reduced pressure. The residue was purified by flash chromatography on silica eluting with 66% EtOAc in hexane to give **4.09** as a colourless oil (229 mg, 79%) and *trans*-**4.01** as a colourless oil (13 mg, 5%).

4.09. ¹H NMR (500 MHz, CDCl₃) δ 7.54 (dd, *J* = 7.6, 1.8 Hz, 1H), 7.43 (ddd, *J* = 8.3, 7.3, 1.8 Hz, 1H), 6.99 (td, *J* = 7.5, 1.0 Hz, 1H), 6.95 (dd, *J* = 8.3, 1.0 Hz, 1H), 3.88 (s, 3H), 3.49 (dt, *J* = 9.2, 7.4 Hz, 1H), 2.84 – 2.71 (m, 1H), 2.53 (dd, *J* = 15.5, 5.8 Hz, 1H), 2.33 (dd, *J* = 15.5, 8.6 Hz, 1H), 2.10 – 1.94 (m, 2H), 1.83 – 1.64 (m, 3H), 1.37 (dq, *J* = 12.5, 8.3 Hz, 1H); ¹³C NMR (126 MHz, CDCl₃) δ 206.1, 179.0, 157.9, 133.0, 130.0, 129.5, 120.8, 111.5, 56.5, 55.6, 39.3, 39.1, 32.7, 30.6, 24.7.

trans-**4.01**. ¹H NMR (500 MHz, CDCl₃) δ 12.46 (s, 1H), 7.77 (dd, *J* = 8.1, 1.6 Hz, 1H), 7.47 (ddd, *J* = 8.6, 7.2, 1.6 Hz, 1H), 6.99 (dd, *J* = 8.4, 1.2 Hz, 1H), 6.91 (ddd, *J* = 8.2, 7.1, 1.2 Hz, 1H), 3.53 (dt, *J* = 9.6, 7.5 Hz, 1H), 2.97 – 2.84 (m, 1H), 2.49 (dd, *J* = 15.4, 6.4 Hz, 1H), 2.38 (dd, *J* = 15.3, 7.9 Hz, 1H), 2.24 – 2.07 (m, 2H), 1.87 – 1.72 (m, 3H), 1.51 – 1.37 (m, 1H); ¹³C NMR (126 MHz, CDCl₃) δ 208.4, 178.273, 163.1, 136.4, 130.3, 119.4, 119.0, 118.7, 51.5, 38.7, 38.5, 32.6, 32.3, 24.9.

1-(2-(benzyloxy)ethyl)-4-bromobenzene (**4.18**)

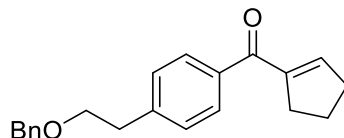
To a slurry of NaH (60%, 0.92 g) in DMF (30 mL) was added dropwise 2-(4-bromophenyl)ethanol **4.17** (2.80 mL, 20.0 mmol) at 0°C, and the mixture was stirred at ambient temperature for 1 h. To the reaction mixture was added dropwise benzyl bromide (2.72 mL, 23.0 mmol) at 0°C and the mixture was stirred at room temperature for 6 h. The resulting mixture was partitioned between saturated aqueous NH₄Cl and EtOAc. The organic layer was dried over anhydrous sodium sulphate and concentrated under reduced pressure. The residue was purified by flash chromatography on silica eluting with 0% → 15% EtOAc in hexane to give a colourless oil (4.52 g, 78%). ¹H NMR (500 MHz, CDCl₃) δ 7.45 – 7.39 (m, 2H), 7.38 – 7.28 (m, 5H), 7.12 (dt, *J* = 8.3, 2.6 Hz, 2H), 4.54 – 4.50 (m, 2H), 3.69 (td, *J* = 6.9, 2.1 Hz, 2H), 2.89 (td, *J* = 6.9, 2.1 Hz, 2H); ¹³C NMR (126 MHz, CDCl₃) δ 138.4, 138.3, 131.53, 131.52, 130.9, 130.8, 128.54, 128.53, 127.8, 120.17, 120.16, 73.2, 70.9, 35.93, 35.92.

(±)-(4-(2-(benzyloxy)ethyl)phenyl)(cyclopent-1-en-1-yl)methanol (**4.19**)

To a solution of **4.18** (4.37 g, 15 mmol) in anhydrous THF (75 mL) was added n-BuLi (2 M solution, 7.75 mL, 15.5 mmol) at -78°C over 15 min. After 1 hour, a solution of **4.14** (0.96 g, 10 mmol) in anhydrous THF (25 mL) was added to the mixture at -78°C over 15 min and the mixture was stirred at -78°C for 4 h. The reaction mixture was quenched with water (50 mL). The mixture was extracted with EtOAc (50 mL) three times and the organics were washed with water (70 mL) and brine. The organic layer was dried over anhydrous sodium sulphate and concentrated under reduced pressure. The residue was purified by flash chromatography on silica eluting with 10% → 20% EtOAc in hexane to give a colourless oil (2.37 g, 77%). ¹H NMR (500 MHz, CDCl₃) δ 7.38 – 7.26 (m, 7H), 7.24 – 7.18 (m, 2H), 5.71 (td, *J* = 2.2, 1.4 Hz, 1H), 5.31 (t, *J* = 2.8 Hz, 1H), 4.54 (s, 2H), 3.70 (t, *J* = 7.1 Hz, 2H), 2.94 (t, *J* = 7.2 Hz, 2H), 2.41 – 2.33 (m, 2H), 2.26 – 2.18 (m, 2H), 1.94 – 1.83 (m, 3H); ¹³C

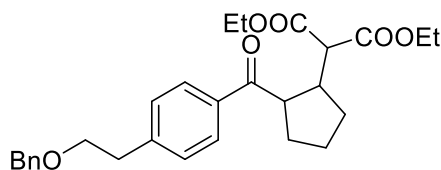
NMR (126 MHz, CDCl₃) δ 146.7, 140.6, 138.6, 138.5, 129.1, 128.5, 127.74, 127.68, 126.6, 126.1, 74.0, 73.1, 71.3, 36.2, 32.4, 31.8, 23.5.

(4-(2-(benzyloxy)ethyl)phenyl)(cyclopent-1-en-1-yl)methanone (**4.20**)



To a solution of the alcohol **4.19** (2.23 g, 7.23 mmol) in DCM (45 mL) was added Dess-Martin Periodinane (4.60 g, 10.85 mmol) and the mixture was stirred overnight. DCM was evaporated and EtOAc (30 mL) an aqueous solution of 1:1 10 % sodium thiosulphate to saturated sodium bicarbonate (30 mL) was then added. After stirring for 10 min, the biphasic mixture was extracted with EtOAc three times. The combined organic phase was washed with saturated sodium bicarbonate (60 mL) and dried over anhydrous sodium sulphate. The organic phase was concentrated under reduced pressure and purified by flash chromatography on silica eluting with 7.5% EtOAc in hexane to give a colourless oil (1.73 g, 78%). ¹H NMR (500 MHz, CDCl₃) δ 7.72 – 7.67 (m, 2H), 7.39 – 7.28 (m, 7H), 6.54 (h, *J* = 2.0 Hz, 1H), 4.54 (s, 2H), 3.73 (t, *J* = 6.9 Hz, 2H), 2.99 (t, *J* = 6.9 Hz, 2H), 2.76 (ddt, *J* = 9.9, 7.2, 2.2 Hz, 2H), 2.63 (tq, *J* = 7.5, 2.5 Hz, 2H), 2.02 (p, *J* = 7.6 Hz, 2H); ¹³C NMR (126 MHz, CDCl₃) δ 194.1, 146.4, 144.7, 143.6, 138.4, 137.2, 129.2, 128.9, 128.5, 127.72, 127.69, 73.2, 70.8, 36.4, 34.5, 32.1, 22.9.

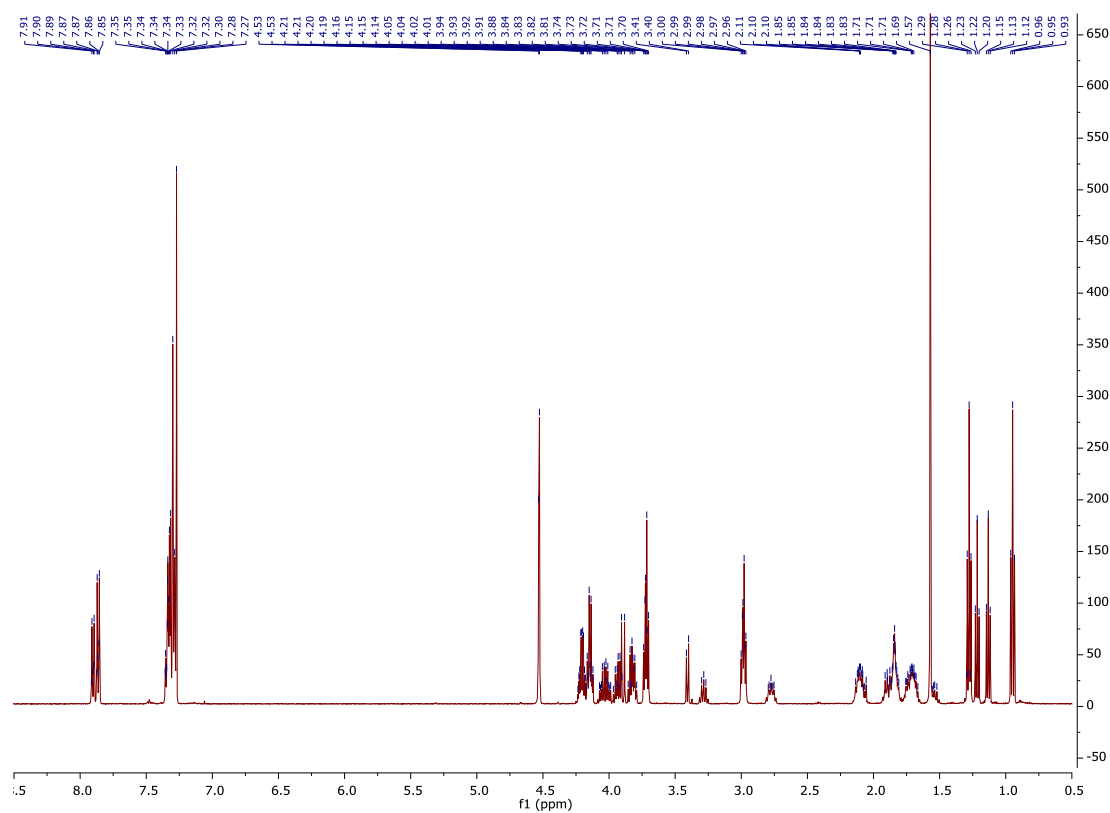
diethyl 2-(2-(4-(2-(benzyloxy)ethyl)benzoyl)cyclopentyl)malonate (**4.21**)



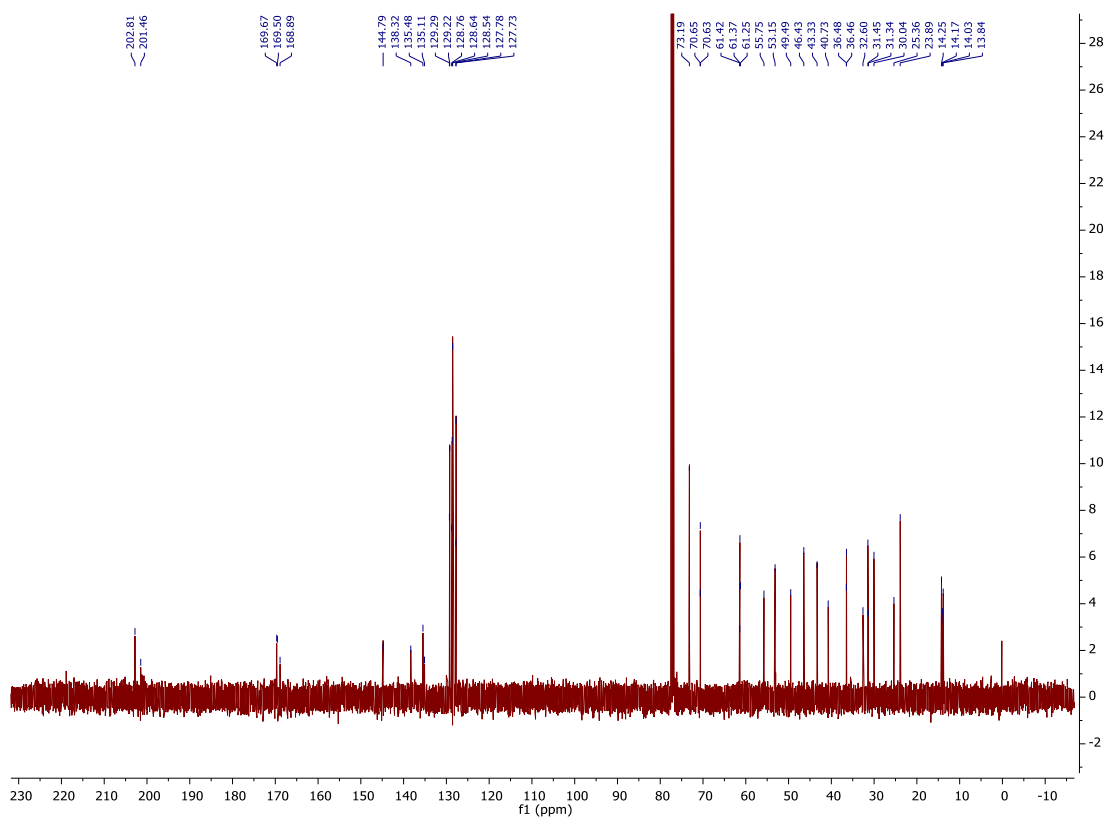
NaH (60% dispersion in mineral oil; 40 mg, 1.0 mmol) was added slowly with ice-cooling under an N₂ atmosphere to a solution of **4.20** (1.73 g, 5.65 mmol) and diethylmalonate (1.14 mL, 7.15 mmol) in EtOH (18 mL). The reaction mixture was stirred at ambient temperature for 15 min and then refluxed at 80°C for 24 h. The reaction was quenched by addition of water. Ethanol was evaporated and the residue was extracted with EtOAc twice. The combined organic phase was dried over anhydrous sodium sulphate. The organic phase was concentrated under reduced pressure and purified by flash chromatography on silica eluting

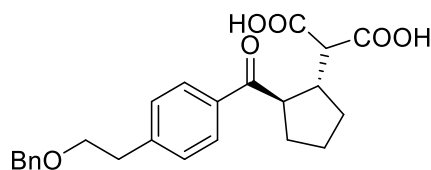
with 10% → 15% EtOAc in hexane to give **4.21** (colourless oil) as a mixture of stereoisomers (2.29 g, 87%).

^1H NMR of **4.21**



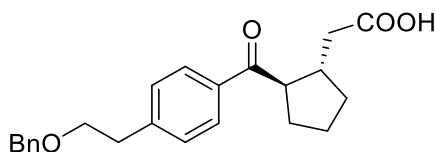
^{13}C NMR of **4.21**



(\pm) -2-(*trans*-2-(4-(2-(benzyloxy)ethyl)benzoyl)cyclopentyl)malonic acid (**4.22**)

Stereochemical configurations are relative.

A mixture of **4.21** (2.27 g, 4.87 mmol), THF (75 mL), and 20% aqueous NaOH (5 mL) was refluxed at 80°C for 6 h. THF was evaporated and the residue was extracted with ether, then with 10% aqueous NaOH three times. The aqueous layer was acidified with conc. HCl and extracted with DCM three times. The combined organic layer was dried over anhydrous sodium sulphate and concentrated under reduced pressure. The residue was triturated with hexane to give a pale yellow solid (1.81 g, 91%). ¹H NMR (500 MHz, DMSO-*d*₆) δ 12.60 (br s, 2H), 7.84 (d, *J* = 8.0 Hz, 2H), 7.38 (d, *J* = 8.0 Hz, 2H), 7.35 – 7.29 (m, 2H), 7.29 – 7.23 (m, 3H), 4.48 (s, 2H), 3.76 (dt, *J* = 9.7, 6.2 Hz, 1H), 3.68 (t, *J* = 6.7 Hz, 2H), 3.24 (d, *J* = 9.6 Hz, 1H), 3.05 – 2.97 (m, 1H), 2.92 (t, *J* = 6.7 Hz, 2H), 2.06 (ddt, *J* = 12.5, 9.9, 7.2 Hz, 1H), 1.96 – 1.86 (m, 1H), 1.66 (tdd, *J* = 11.4, 6.8, 4.8 Hz, 1H), 1.57 – 1.36 (m, 3H); ¹³C NMR (126 MHz, DMSO-*d*₆) δ 201.1, 170.37, 170.35, 144.7, 138.4, 134.6, 129.1, 128.3, 128.2, 127.42, 127.38, 71.8, 70.0, 56.0, 48.9, 40.1, 35.4, 32.1, 31.1, 25.0.

 (\pm) -2-(*trans*-2-(4-(2-(benzyloxy)ethyl)benzoyl)cyclopentyl)acetic acid (**4.23**)

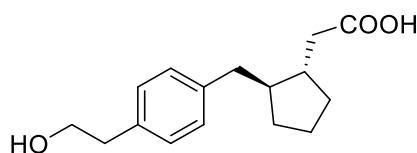
Stereochemical configurations are relative.

Method 1. A solution of **4.22** (1.70 g, 4.14 mmol) in AcOH (16 mL) was refluxed at 120°C for 10 h. The solvent was evaporated and the residue was treated with water. The aqueous phase was extracted with DCM three times. The combined organic phase was dried over anhydrous sodium sulphate and concentrated under reduced pressure. The residue was purified by flash chromatography on silica eluting with 33% EtOAc in hexane to give a colourless oil (1.18 g, 78%).

Method 2. To a mixture of **4.22** (1.00g, 2.44 mmol) in THF (10 mL) was portionwise added CDI (0.44 g, 2.68 mmol) and the mixture was stirred for 1 h. To the reaction mixture was

added 1 mL aqueous solution of NaOH (0.15 g, 3.65 mmol) and the mixture was stirred for 2 h. THF was evaporated and acidified with 1N HCl. The mixture was extracted with DCM twice and the combined organic phase was dried over anhydrous sodium sulphate. The organic phase was concentrated under reduced pressure and purified by flash chromatography on silica eluting with 33% EtOAc in hexane to give a colourless oil (0.63 g, 72%). ^1H NMR (500 MHz, CDCl_3) δ 7.92 – 7.86 (m, 2H), 7.38 – 7.28 (m, 7H), 4.53 (s, 2H), 3.73 (t, $J = 6.8$ Hz, 2H), 3.53 – 3.45 (m, 1H), 2.99 (t, $J = 6.8$ Hz, 2H), 2.93 – 2.82 (m, 1H), 2.49 (dd, $J = 15.3, 6.2$ Hz, 1H), 2.35 (dd, $J = 15.3, 8.0$ Hz, 1H), 2.19 – 2.04 (m, 2H), 1.83 – 1.68 (m, 3H), 1.43 (dq, $J = 12.2, 8.2$ Hz, 1H); ^{13}C NMR (126 MHz, CDCl_3) δ 201.8, 177.3, 144.9, 138.3, 135.3, 129.3, 128.7, 128.5, 127.78, 127.76, 73.2, 70.6, 52.0, 38.7, 38.6, 36.5, 32.6, 31.7, 24.9.

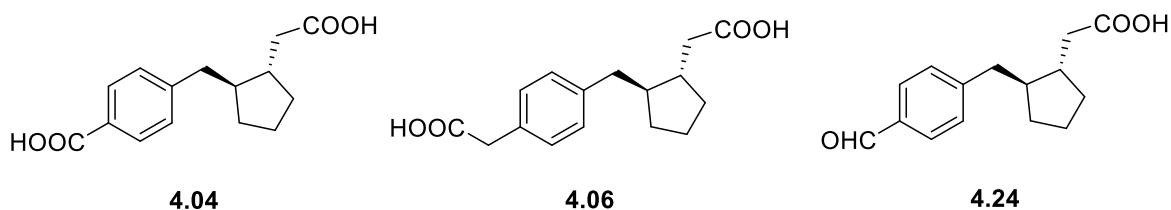
(\pm)-2-(*trans*-2-(4-(2-hydroxyethyl)benzyl)cyclopentyl)acetic acid (**4.08**)



Stereochemical configurations are relative.

4.23 (550 mg, 1.50 mmol) in EtOH (15 mL) was hydrogenated under Pd/C (10%, 55 mg) and H_2 balloon for 2 h. The mixture was filtered over a Celite[®] pad, washed with EtOH, and concentrated under reduced pressure. The residue was purified by flash chromatography on silica eluting with 3.3% → 10% MeOH in DCM to give a colourless oil (350 mg, 89%). ^1H NMR (500 MHz, CDCl_3) δ 7.18 – 7.09 (m, 4H), 3.86 (td, $J = 6.6, 0.9$ Hz, 2H), 2.85 (t, $J = 6.5$ Hz, 2H), 2.75 (dd, $J = 13.5, 5.6$ Hz, 1H), 2.49 (dd, $J = 13.4, 8.4$ Hz, 1H), 2.40 (dd, $J = 15.0, 5.1$ Hz, 1H), 2.18 (dd, $J = 14.9, 8.4$ Hz, 1H), 2.05 – 1.91 (m, 2H), 1.83 – 1.69 (m, 2H), 1.66 – 1.51 (m, 2H), 1.37 – 1.24 (m, 2H); ^{13}C NMR (126 MHz, CDCl_3) δ 178.1, 139.7, 135.9, 129.3, 129.1, 63.9, 47.4, 41.6, 40.8, 39.5, 38.7, 32.6, 32.3, 23.7.

(\pm)-4-((*trans*-2-(carboxymethyl)cyclopentyl)methyl)benzoic acid (**4.04**), (\pm)-2-(*trans*-2-(4-(carboxymethyl)benzyl)cyclopentyl)acetic acid (**4.06**), and (\pm)-2-(*trans*-2-(4-formylbenzyl)cyclopentyl)acetic acid (**4.24**)



Stereochemical configurations are relative.

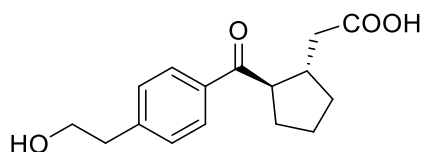
To a solution of **4.08** (220 mg, 0.84 mmol) in DMF (10 mL) was added PDC (1.58 g, 4.19 mmol) and the mixture was stirred for 24 h. The mixture was poured onto water and extracted with EtOAc three times. The combined organic phase was washed with brine and water, dried over anhydrous sodium sulphate, and concentrated under reduced pressure. The residue was purified by flash chromatography on silica eluting with 2.5% → 5% MeOH in DCM to give **4.24** as a white solid (31 mg, 15%) and a mixture of **4.04** and **4.06**. The mixture of **4.04** and **4.06** was purified by flash chromatography on silica eluting with 25% → 50% EtOAc in hexane to give **4.04** as a white solid (35 mg, 16%) and **4.06** as a white solid (71 mg, 31%).

4.04. $^1\text{H NMR}$ (500 MHz, $\text{DMSO-}d_6$) δ 12.37 (br s, 2H), 7.84 (d, $J = 7.9$ Hz, 2H), 7.29 (d, $J = 7.9$ Hz, 2H), 2.87 (dd, $J = 13.3, 4.9$ Hz, 1H), 2.44 (dd, $J = 13.3, 9.5$ Hz, 1H), 2.36 (dd, $J = 15.2, 4.3$ Hz, 1H), 2.06 (dd, $J = 15.1, 8.7$ Hz, 1H), 1.84 (tq, $J = 13.5, 7.8, 6.5$ Hz, 2H), 1.72 (tt, $J = 13.8, 6.9$ Hz, 1H), 1.60 – 1.42 (m, 3H), 1.27 – 1.15 (m, 2H); $^{13}\text{C NMR}$ (126 MHz, $\text{DMSO-}d_6$) δ 174.1, 167.3, 146.8, 129.3, 128.9, 128.3, 46.3, 41.5, 40.0, 39.0, 31.8, 31.2, 22.7; HRMS calcd for $\text{C}_{15}\text{H}_{18}\text{O}_4$ $[\text{M} + \text{H}]^+$ 263.1278, found 263.1284.

4.06. $^1\text{H NMR}$ (500 MHz, $\text{DMSO-}d_6$) δ 12.08 (s, 2H), 7.14 (d, $J = 7.9$ Hz, 2H), 7.10 (d, $J = 8.2$ Hz, 2H), 3.50 (s, 2H), 2.78 (dd, $J = 13.4, 4.8$ Hz, 1H), 2.41 – 2.28 (m, 2H), 2.05 (dd, $J = 15.1, 9.0$ Hz, 1H), 1.89 – 1.76 (m, 2H), 1.72 – 1.62 (m, 1H), 1.60 – 1.41 (m, 3H), 1.25 – 1.15 (m, 2H); $^{13}\text{C NMR}$ (126 MHz, $\text{DMSO-}d_6$) δ 174.1, 172.8, 139.6, 132.2, 129.1, 128.6, 46.5, 41.4, 40.3, 39.6, 39.0, 31.8, 31.2, 22.8; HRMS calcd for $\text{C}_{16}\text{H}_{20}\text{O}_4$ $[\text{M} + \text{Na}]^+$ 299.1254, found 299.1262.

4.24. $^1\text{H NMR}$ (500 MHz, CDCl_3) δ 9.98 (s, 1H), 7.81 (d, $J = 8.1$ Hz, 2H), 7.34 (d, $J = 7.9$ Hz, 2H), 2.92 (dd, $J = 13.4, 5.3$ Hz, 1H), 2.55 (dd, $J = 13.4, 9.3$ Hz, 1H), 2.46 (dd, $J = 15.1, 4.8$ Hz, 1H), 2.24 (dd, $J = 15.2, 8.5$ Hz, 1H), 2.05 – 1.94 (m, 2H), 1.87 – 1.78 (m, 1H), 1.75 – 1.52 (m, 3H), 1.39 – 1.24 (m, 2H); $^{13}\text{C NMR}$ (126 MHz, CDCl_3) δ 192.2, 178.0, 149.1, 134.7, 130.1, 129.7, 47.1, 41.9, 41.3, 39.2, 32.4, 32.1, 23.5; HRMS calcd for $\text{C}_{15}\text{H}_{18}\text{O}_3$ $[\text{M} + \text{H}]^+$ 247.1329, found 247.1338.

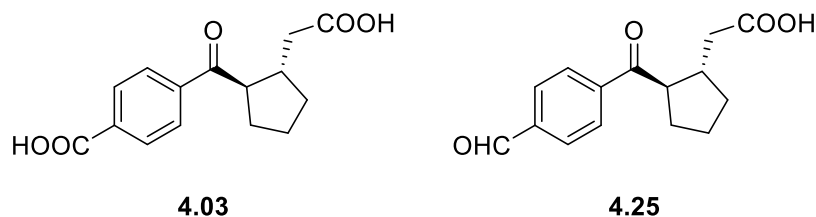
(±)-2-(*trans*-2-(4-(2-hydroxyethyl)benzoyl)cyclopentyl)acetic acid (**4.07**)



Stereochemical configurations are relative.

To a solution of **4.23** (135 mg, 0.37 mmol) in anhydrous DCM (10 mL) was added anhydrous FeCl₃ (179 mg, 1.11 mmol) and the mixture was stirred for 3.5 h. The reaction was quenched with water and diluted with DCM. The mixture was washed with brine and water, dried over anhydrous sodium sulphate, and concentrated under reduced pressure. The residue was purified by flash chromatography on silica eluting with 5% MeOH in DCM to give a white solid (56 mg, 55%). ¹H NMR (500 MHz, CDCl₃) δ 7.89 (d, *J* = 8.3 Hz, 2H), 7.32 (d, *J* = 8.1 Hz, 2H), 3.89 (t, *J* = 6.5 Hz, 2H), 3.49 (dt, *J* = 9.1, 7.1 Hz, 1H), 2.92 (t, *J* = 6.5 Hz, 2H), 2.84 (dt, *J* = 8.9, 7.5 Hz, 1H), 2.45 (dd, *J* = 15.3, 6.7 Hz, 1H), 2.36 (dd, *J* = 15.3, 7.6 Hz, 1H), 2.17 – 2.01 (m, 2H), 1.84 – 1.67 (m, 3H), 1.42 (dq, *J* = 12.3, 8.2 Hz, 1H); ¹³C NMR (126 MHz, CDCl₃) δ 202.1, 177.8, 144.4, 135.5, 129.4, 128.9, 63.3, 51.9, 39.2, 38.9, 38.8, 32.7, 31.7, 24.9; HRMS calcd for C₁₆H₂₀O₄ [M + Na]⁺ 299.1254, found 299.1254.

(±)-4-(*trans*-2-(carboxymethyl)cyclopentane-1-carbonyl)benzoic acid (**4.03**) and (±)-2-(*trans*-2-(4-formylbenzoyl)cyclopentyl)acetic acid (**4.25**)



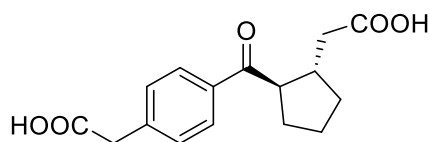
Stereochemical configurations are relative.

To a solution of **4.07** (35 mg, 0.127 mmol) in DMF (2 mL) was added PDC (239 mg, 0.635 mmol) and the mixture was stirred for 24 h. The mixture was poured onto water and extracted with EtOAc three times. The combined organic phase was washed with brine and water, dried over anhydrous sodium sulphate, and concentrated under reduced pressure. The residue was purified by flash chromatography on silica eluting with 5% → 10% MeOH in DCM to give **4.25** as a white solid (4 mg, 12%) and impure **4.03**. This sample of **4.03** was further purified by preparative TLC eluting with 0.5% AcOH in hexane/EtOAc (1:3) to give **4.03** as a white solid (9 mg, 26%).

4.03. ^1H NMR (500 MHz, CDCl_3) δ 8.07 (d, $J = 8.3$ Hz, 2H), 8.00 (d, $J = 8.4$ Hz, 2H), 3.64 – 3.53 (m, 1H), 2.87 (h, $J = 7.8$ Hz, 1H), 2.50 (dd, $J = 15.1, 6.3$ Hz, 1H), 2.41 (dd, $J = 15.1, 8.6$ Hz, 1H), 2.11 (dq, $J = 15.1, 9.8, 7.6$ Hz, 2H), 1.84 – 1.74 (m, 3H), 1.52 – 1.38 (m, 1H); ^{13}C NMR (126 MHz, CDCl_3) δ 202.8, 176.7, 168.9, 140.9, 133.3, 130.4, 128.4, 51.8, 39.8, 39.4, 33.3, 32.1, 25.5; HRMS calcd for $\text{C}_{15}\text{H}_{16}\text{O}_5$ $[\text{M} + \text{Na}]^+$ 299.0890, found 299.0894.

4.25. ^1H NMR (500 MHz, CDCl_3) δ 10.11 (s, 1H), 8.09 (d, $J = 8.3$ Hz, 2H), 7.98 (d, $J = 8.3$ Hz, 2H), 3.57 – 3.49 (m, 1H), 2.94 – 2.84 (m, 1H), 2.51 – 2.38 (m, 2H), 2.20 – 2.07 (m, 2H), 1.85 – 1.71 (m, 3H), 1.44 (dq, $J = 12.5, 8.1$ Hz, 1H); ^{13}C NMR (126 MHz, CDCl_3) δ 201.8, 191.8, 177.6, 141.5, 139.0, 130.0, 129.0, 52.5, 38.7, 38.6, 32.8, 31.6, 25.0; HRMS calcd for $\text{C}_{15}\text{H}_{16}\text{O}_4$ $[\text{M} + \text{Na}]^+$ 283.0941, found 283.0949.

(\pm)-2-(*trans*-2-(4-(carboxymethyl)benzoyl)cyclopentyl)acetic acid (**4.05**)

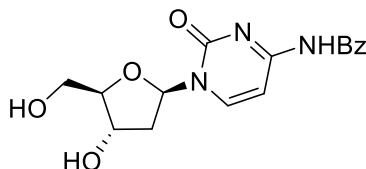


Stereochemical configurations are relative.

A solution of **4.07** (60 mg, 0.22 mmol) in acetone (3 mL) was treated with Jones reagent (0.33 mL of a 2.7 M solution, prepared via standard method) slowly dropwise at 0°C for 10 min. The resulting reaction mixture was stirred at 0°C for 1 h and then was quenched with isopropanol. The mixture was filtered with a pad of Celite[®] and the pad of Celite[®] was washed with EtOAc. The combined organic phase was washed with brine and water, dried over anhydrous sodium sulphate, and concentrated under reduced pressure. The residue was purified by flash chromatography on silica eluting with 5% \rightarrow 10% MeOH in DCM to give a white solid (58 mg, 91%). ^1H NMR (500 MHz, $\text{DMSO-}d_6$) δ 12.22 (br s, 2H), 7.90 (d, $J = 8.2$ Hz, 2H), 7.40 (d, $J = 8.0$ Hz, 2H), 3.67 (s, 2H), 3.56 (dt, $J = 9.1, 7.1$ Hz, 1H), 2.63 (h, $J = 7.7$ Hz, 1H), 2.30 (dd, $J = 15.3, 6.4$ Hz, 1H), 2.22 (dd, $J = 15.3, 8.2$ Hz, 1H), 2.13 – 2.00 (m, 1H), 1.96 – 1.85 (m, 1H), 1.75 – 1.64 (m, 1H), 1.63 – 1.49 (m, 2H), 1.40 – 1.27 (m, 1H); ^{13}C NMR (126 MHz, $\text{DMSO-}d_6$) δ 201.4, 173.7, 172.1, 140.4, 135.1, 129.8, 128.3, 51.0, 40.5, 38.8, 38.3, 32.2, 31.0, 24.5; HRMS calcd for $\text{C}_{16}\text{H}_{18}\text{O}_5$ $[\text{M} + \text{Na}]^+$ 313.1046, found 313.1045.

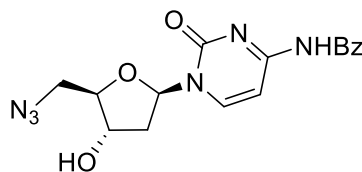
6.5 Experimental work as described in Chapter 5

N-(1-((2*R*,4*S*,5*R*)-4-hydroxy-5-(hydroxymethyl)tetrahydrofuran-2-yl)-2-oxo-1,2-dihydropyrimidin-4-yl)benzamide (**5.11**)



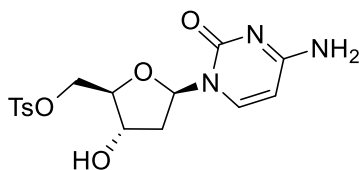
To a solution of 2-chloro-4,6-dimethoxy-1,3,5-triazine (CDMT) (776 mg, 4.4 mmol) in DCM (20 mL) was added NMM (0.66 mL, 6.0 mmol) under ice-bath. A white suspension was formed after 30 min, and benzoic acid (537 mg, 4.4 mmol) was added, resulting in the formation of a pink suspension. After stirring the mixture for 1 h, a solution of 2'-deoxycytidine **5.01** (400 mg, 1.76 mmol) in DMF (12 mL) was added dropwise and stirred at ambient temperature for 24 h. The resulting clear solution was concentrated under reduced pressure, dissolved in a minimum amount of water, and extracted with EtOAc (40 mL) four times. The combined organic phase was dried over anhydrous sodium sulphate and concentrated under reduced pressure. The residue was purified by flash chromatography on silica eluting with 2.5% → 5% → 10% MeOH in DCM to give a white solid (414 mg, 71%). ^1H NMR (500 MHz, DMSO- d_6) δ 11.22 (br s, 1H), 8.39 (d, $J = 7.5$ Hz, 1H), 8.00 (dd, $J = 8.4, 1.4$ Hz, 2H), 7.67–7.57 (m, 1H), 7.51 (t, $J = 7.8$ Hz, 2H), 7.35 (d, $J = 7.4$ Hz, 1H), 6.13 (t, $J = 6.3$ Hz, 1H), 5.27 (d, $J = 4.2$ Hz, 1H), 5.06 (t, $J = 5.2$ Hz, 1H), 4.23 (dq, $J = 7.5, 4.0$ Hz, 1H), 3.87 (q, $J = 3.8$ Hz, 1H), 3.70–3.52 (m, 2H), 2.31 (ddd, $J = 13.3, 6.1, 3.9$ Hz, 1H), 2.05 (dt, $J = 13.0, 6.3$ Hz, 1H); ^{13}C NMR (126 MHz, DMSO- d_6) δ 167.3, 163.0, 154.4, 145.0, 133.1, 132.7, 128.4, 95.9, 87.9, 86.2, 69.9, 60.9, 40.9. ^1H NMR and ^{13}C NMR were consistent with literature.¹²

N-(1-((2*R*,4*S*,5*R*)-5-(azidomethyl)-4-hydroxytetrahydrofuran-2-yl)-2-oxo-1,2-dihydropyrimidin-4-yl)benzamide (**5.08**)



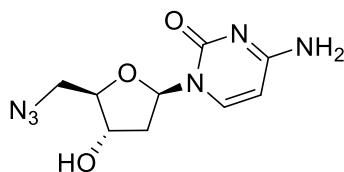
To a mixture of **5.11** (5.49 g, 16.6 mmol), Ph_3P (4.44 g, 16.9 mmol) and NaN_3 (1.83 g, 28.1 mmol) in anhydrous DMF (55 mL) was added CBr_4 (5.61 g, 16.9 mmol) and the reaction mixture was stirred for 24 h. The reaction was quenched by the addition of MeOH and stirring was continued for 1 h. The solvent was evaporated and the residue was purified by flash chromatography on silica eluting with 5% MeOH in DCM to give a white solid (4.53 g, 77%). ^1H NMR (500 MHz, CDCl_3) δ 8.93 (br s, 1H), 8.16 (d, $J = 7.5$ Hz, 1H), 7.95 – 7.89 (m, 2H), 7.66 – 7.60 (m, 1H), 7.53 (dd, $J = 8.3, 7.2$ Hz, 2H), 6.32 (t, $J = 6.3$ Hz, 1H), 4.44 (dt, $J = 6.7, 4.2$ Hz, 1H), 4.20 (q, $J = 3.9$ Hz, 1H), 3.80 (dd, $J = 13.2, 3.5$ Hz, 1H), 3.67 (dd, $J = 13.2, 4.0$ Hz, 1H), 2.74 (ddd, $J = 13.9, 6.2, 4.2$ Hz, 1H), 2.21 (dt, $J = 13.6, 6.6$ Hz, 1H); ^{13}C NMR (126 MHz, CDCl_3) δ 162.6, 144.4, 133.4, 133.1, 129.2, 127.8, 97.2, 87.3, 85.2, 71.6, 52.4, 41.8.

((2*R*,3*S*,5*R*)-5-(4-amino-2-oxypyrimidin-1(2*H*)-yl)-3-hydroxytetrahydrofuran-2-yl)methyl 4-methylbenzenesulfonate (**5.12**)



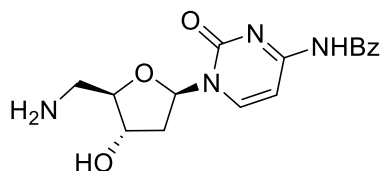
2'-Deoxycytidine **5.01** (250 mg, 1.10 mmol) was dissolved in anhydrous pyridine (3 mL) and concentrated under reduced pressure three times to remove any traces of water. The residue was dissolved in anhydrous pyridine (10 mL) and TsCl (220 mg, 1.16 mmol) was added. The mixture was stirred at 5 °C for 19 h and TsCl (54 mg, 0.28 mmol) added more. After another 4 hr, TLC analysis indicated full conversion and the solvent was removed under reduced pressure. The residue was purified by flash chromatography on silica eluting with 12% MeOH in DCM to give a white solid (166 mg, 40%). Contains an impurity, looks like TsOH. ^1H NMR (500 MHz, $\text{DMSO}-d_6$) δ 8.23 (br s, 1H), 7.80 (d, $J = 8.5$ Hz, 2H), 7.71 (br s, 1H), 7.59 (d, $J = 7.5$ Hz, 1H), 7.48 (d, $J = 8.0$ Hz, 2H), 6.10 (t, $J = 6.5$ Hz, 1H), 5.84 (d, $J = 7.5$ Hz, 1H), 5.45 (br s, 1H), 4.25 (dd, $J = 11.0, 3.5$ Hz, 1H), 4.17 (dd, $J = 11.0, 6.0$ Hz, 1H), 4.12 (d, $J = 5.0$ Hz, 1H), 3.89 (dt, $J = 7.5, 3.5$ Hz, 1H), 2.43 (s, 3H), 2.14 (ddd, $J = 13.5, 6.5, 4.5$ Hz, 1H), 2.07 (dt, $J = 13.5, 6.5$ Hz, 1H); HRMS calcd for $\text{C}_{16}\text{H}_{20}\text{N}_3\text{O}_6\text{S}$ [$\text{M} + \text{H}$] $^+$ 382.1067, found 382.1061.

4-amino-1-((2*R*,4*S*,5*R*)-5-(azidomethyl)-4-hydroxytetrahydrofuran-2-yl)pyrimidin-2(1*H*)-one (**5.09**)



Tosylate **5.12** (0.15 g, 0.40 mmol) was dissolved in anhydrous DMF (4 ml) and NaN_3 (39 mg, 0.60 mmol) was added. The mixture was heated to 45°C . After 18 hr, more NaN_3 (13 mg, 0.20 mmol) was added. When TLC analysis indicated full conversion of the starting material, the solvent was removed under reduced pressure. The residue was purified by flash chromatography on silica eluting with 18% MeOH in DCM to give a colourless film (46 mg, 46%). ^1H NMR (500 MHz, $\text{DMSO}-d_6$) δ 7.63 (d, $J = 7.5$ Hz, 1H), 7.35 (br s, 1H), 7.22 (br s, 1H), 6.21 (t, $J = 7.0$ Hz, 1H), 5.77 (d, $J = 7.5$ Hz, 1H), 5.39 (d, $J = 4.0$ Hz, 1H), 4.17 – 4.12 (m, 1H), 3.84 (dt, $J = 6.0, 4.0$ Hz, 1H), 3.61 – 3.50 (m, 2H), 2.16 – 2.03 (m, 2H); ^{13}C NMR (126 MHz, $\text{DMSO}-d_6$) δ 165.1, 154.5, 141.2, 94.4, 84.8, 84.5, 70.8, 51.8, 39.2.; HRMS calcd for $\text{C}_9\text{H}_{12}\text{N}_6\text{O}_3$ $[\text{M} + \text{Na}]^+$ 275.0863, found 275.0874.

N-(1-((2*R*,4*S*,5*R*)-5-(aminomethyl)-4-hydroxytetrahydrofuran-2-yl)-2-oxo-1,2-dihydropyrimidin-4-yl)benzamide (**5.10**)



Method 1 (Table 5.1 entry 1)

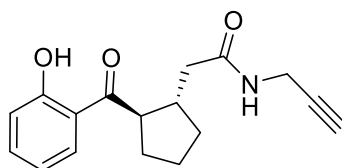
The mixture of **5.08** (200 mg, 0.604 mmol) and 10% Pd/C (20 mg) in MeOH/DMF (1:1; 2 mL) was stirred under H_2 gas balloon for 2 h. The mixture was filtered over a Celite[®] pad, washed with MeOH, and concentrated under reduced pressure. The residue was triturated with DCM. ^1H NMR of crude material confirmed the presence of a complex mixture only.

Method 2 (Table 5.1 entry 2)

To the solution of **5.08** (4.33 g, 12.15 mmol) in anhydrous pyridine (60 mL) was added Ph_3P (3.66 g, 13.97 mmol). After 3 h, water (12 mL) was added and stirring was continued for 3 h. The mixture was diluted with water and extracted with EtOAc twice. The aqueous phase was concentrated under reduced pressure and the residue was purified by flash chromatography on silica eluting with 15% → 30% MeOH in DCM to give a white solid

(1.72 g, 43%). ^1H NMR (500 MHz, $\text{DMSO-}d_6$) δ 8.39 (d, $J = 7.5$ Hz, 1H), 8.03 – 7.97 (m, 2H), 7.62 (t, $J = 7.4$ Hz, 1H), 7.51 (t, $J = 7.7$ Hz, 2H), 7.34 (d, $J = 7.4$ Hz, 1H), 6.12 (t, $J = 6.4$ Hz, 1H), 5.21 (s, 1H), 4.19 (dt, $J = 6.9, 3.7$ Hz, 1H), 3.78 (td, $J = 5.2, 3.4$ Hz, 1H), 2.77 (d, $J = 5.3$ Hz, 2H), 2.30 (ddd, $J = 13.5, 6.3, 3.8$ Hz, 1H), 2.05 (dt, $J = 13.2, 6.4$ Hz, 1H); ^{13}C NMR (126 MHz, $\text{DMSO-}d_6$) δ 167.5, 162.9, 154.3, 145.2, 133.2, 132.7, 128.40, 128.39, 96.2, 88.6, 85.9, 70.6, 43.4, 40.6.

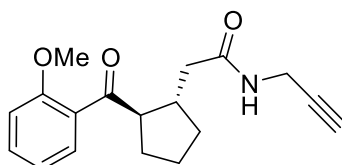
(\pm)-2-(*trans*-2-(2-hydroxybenzoyl)cyclopentyl)-*N*-(prop-2-yn-1-yl)acetamide (**5.06**)



Stereochemical configurations are relative.

To a solution of *trans*-**4.01** (38 mg, 0.15 mmol) and propargyl amine (11 μL , 0.17 mmol) in DMF (1 mL) were added HATU (87 mg, 0.23 mmol) and DIPEA (80 μL , 0.46 mmol), and the mixture was stirred for 2 h. Saturated aqueous NH_4Cl was added and extracted with EtOAc three times. The combined organic phase was dried over anhydrous sodium sulphate and concentrated under reduced pressure. The residue was purified by flash chromatography on silica eluting with 30% \rightarrow 50% EtOAc in hexane to give a white solid (38 mg, 87%). ^1H NMR (500 MHz, CDCl_3) δ 12.44 (s, 1H), 7.79 (dd, $J = 8.0, 1.5$ Hz, 1H), 7.49 – 7.44 (m, 1H), 6.98 (dd, $J = 8.5, 1.0$ Hz, 1H), 6.93 – 6.88 (m, 1H), 5.65 (br s, 1H), 3.97 (dd, $J = 5.0, 2.5$ Hz, 2H), 3.59 (dd, $J = 16.0, 8.5$ Hz, 1H), 2.89 – 2.79 (m, 1H), 2.33 (dd, $J = 14.5, 7.0$ Hz, 1H), 2.25 (dd, $J = 14.5, 7.5$ Hz, 1H), 2.21 – 2.13 (m, 2H), 2.12 – 2.03 (m, 1H), 1.85 – 1.70 (m, 3H), 1.52 – 1.42 (m, 1H); ^{13}C NMR (126 MHz, CDCl_3) δ 208.7, 171.4, 163.1, 136.5, 130.5, 119.1, 118.7, 79.5, 71.7, 51.6, 41.1, 39.4, 32.7, 32.3, 29.3, 24.9; HRMS calcd for $\text{C}_{17}\text{H}_{23}\text{N}_2\text{O}_3$ [$\text{M} + \text{NH}_4$] $^+$ 303.1703, found 303.1706.

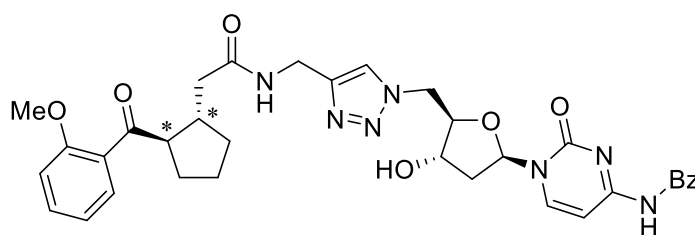
(\pm)-2-(*trans*-2-(2-methoxybenzoyl)cyclopentyl)-*N*-(prop-2-yn-1-yl)acetamide (**5.07**)



Stereochemical configurations are relative.

To a solution of **4.09** (220 mg, 0.839 mmol) and propargyl amine (59 μ L, 0.923 mmol) in DMF (4 mL) were added HATU (479 mg, 1.26 mmol) and DIPEA (439 μ L, 2.52 mmol), and the mixture was stirred for 2 h. Saturated aqueous NH_4Cl was added and extracted with EtOAc three times. The combined organic phase was dried over anhydrous sodium sulphate and concentrated under reduced pressure. The residue was purified by flash chromatography on silica eluting with 30% \rightarrow 50% EtOAc in hexane to give a white solid (225 mg, 90%). ^1H NMR (500 MHz, CDCl_3) δ 7.55 (dd, $J = 7.7, 1.8$ Hz, 1H), 7.45 (ddd, $J = 8.1, 7.3, 1.8$ Hz, 1H), 7.01 (td, $J = 7.5, 1.0$ Hz, 1H), 6.96 (dd, $J = 8.4, 1.0$ Hz, 1H), 5.84 (br s, 1H), 4.06 – 3.93 (m, 2H), 3.89 (s, 3H), 3.47 (dt, $J = 9.4, 7.4$ Hz, 1H), 2.78 – 2.66 (m, 1H), 2.41 (dd, $J = 14.4, 6.2$ Hz, 1H), 2.27 – 2.16 (m, 2H), 2.08 – 1.97 (m, 2H), 1.78 – 1.62 (m, 3H), 1.47 – 1.34 (m, 1H); ^{13}C NMR (126 MHz, CDCl_3) δ 206.3, 171.9, 158.0, 133.1, 130.1, 129.4, 120.9, 111.6, 79.8, 71.6, 57.1, 55.7, 41.9, 39.6, 32.9, 30.8, 29.2, 24.7.

N-(1-((2*R*,4*S*,5*R*)-4-hydroxy-5-((4-((2-(*trans*-2-(2-methoxybenzoyl)cyclopentyl)acetamido)methyl)-1*H*-1,2,3-triazol-1-yl)methyl)tetrahydrofuran-2-yl)-2-oxo-1,2-dihydropyrimidin-4-yl)benzamide (**5.13**)

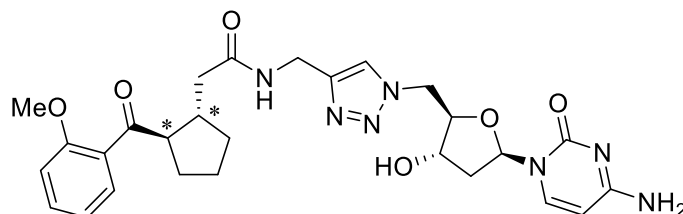


* represents relative stereochemical configurations.

5.07 (53 mg, 0.15 mmol) and **5.08** (45 mg, 0.15 mmol) were dissolved in MeCN/ H_2O (2:1; 1 mL) and copper nano powder (4 mg, 0.06 mmol) was added. The mixture was sonicated for 30 min and stirred overnight. The mixture was concentrated under reduced pressure and the residue was purified by flash chromatography on silica eluting with 10% \rightarrow 20% MeOH in DCM to give **5.13** (white solid) as a mixture of diastereomers (72 mg, 74%). ^1H NMR (500 MHz, CDCl_3) δ 9.07 (br s, 1H), 7.93 (d, $J = 7.7$ Hz, 2H), 7.80 – 7.57 (m, 3H), 7.55 – 7.36 (m, 4H), 7.00 – 6.88 (m, 2H), 6.84 – 6.75 (m, 1H), 6.12 (q, $J = 5.8$ Hz, 1H), 4.81 – 4.70 (m, 1H), 4.70 – 4.49 (m, 2H), 4.46 (d, $J = 5.5$ Hz, 1H), 4.43 – 4.33 (m, 2H), 4.33 – 4.23 (m, 1H), 3.84 (s, 3H), 3.46 (dq, $J = 16.3, 8.1$ Hz, 1H), 2.80 – 2.61 (m, 1H), 2.56 (dq, $J = 12.1, 6.0$ Hz, 1H), 2.34 (ddd, $J = 20.9, 13.9, 6.9$ Hz, 1H), 2.27 – 2.06 (m, 2H), 2.03 – 1.87 (m, 2H), 1.69 – 1.52 (m, 3H), 1.41 – 1.21 (m, 2H); ^{13}C NMR (126 MHz, CDCl_3) δ 206.51, 206.35, 172.90, 172.85, 157.88, 157.86, 133.37, 133.33, 133.13, 133.11, 130.10, 130.00,

129.31, 129.21, 129.14, 129.12, 127.91, 120.84, 111.70, 111.66, 84.42, 84.18, 71.07, 70.58, 57.11, 56.97, 55.72, 41.96, 40.27, 39.58, 39.44, 35.14, 35.05, 33.34, 33.13, 31.17, 31.00, 24.75, 24.72.

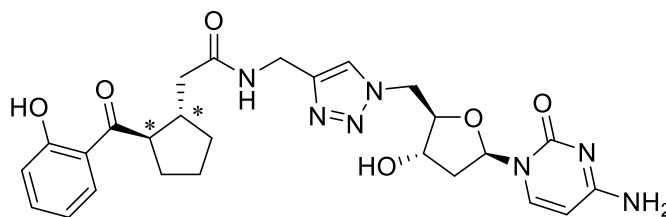
N-((1-(((2*R*,3*S*,5*R*)-5-(4-amino-2-oxopyrimidin-1(2*H*)-yl)-3-hydroxytetrahydrofuran-2-yl)methyl)-1*H*-1,2,3-triazol-4-yl)methyl)-2-(*trans*-2-(2-methoxybenzoyl)cyclopentyl)acetamide (**5.14**)



* represents relative stereochemical configurations.

To a solution of **5.13** (67 mg, 0.10 mmol) in MeOH (2 mL) was added 30% NH₄OH (3 mL) and the mixture was stirred overnight. The mixture was concentrated under reduced pressure and the residue was purified by flash chromatography on silica eluting with 20% MeOH in DCM to give **5.14** (white solid) as a mixture of diastereomers (48 mg, 85%). ¹H NMR (500 MHz, MeOH-*d*₄) δ 7.81 (s, 1H), 7.51 – 7.45 (m, 3H), 7.11 – 7.06 (m, 1H), 7.00 (t, *J* = 7.5 Hz, 1H), 6.17 (t, *J* = 6.6 Hz, 1H), 5.90 (dd, *J* = 7.5, 3.5 Hz, 1H), 4.71 (ddd, *J* = 14.4, 3.8, 1.9 Hz, 1H), 4.66 – 4.56 (m, 1H), 4.41 – 4.26 (m, 3H), 4.18 – 4.12 (m, 1H), 3.87 (s, 3H), 3.52 (dt, *J* = 9.5, 7.1 Hz, 1H), 2.78 – 2.68 (m, 1H), 2.37 – 2.26 (m, 2H), 2.20 (ddd, *J* = 13.7, 8.3, 2.0 Hz, 1H), 2.14 – 1.98 (m, 2H), 1.95 – 1.86 (m, 1H), 1.76 – 1.57 (m, 3H), 1.39 – 1.28 (m, 1H); ¹³C NMR (126 MHz, MeOH-*d*₄) δ 208.32, 208.26, 175.03, 175.02, 167.63, 159.43, 158.03, 146.46, 146.41, 142.65, 142.58, 134.34, 130.79, 125.32, 125.27, 121.65, 112.94, 112.93, 96.39, 96.37, 87.94, 87.87, 85.66, 72.45, 57.87, 56.12, 52.75, 52.73, 42.31, 42.29, 41.38, 41.29, 40.68, 40.62, 35.54, 33.79, 33.77, 31.78, 31.75, 25.60.

N-((1-(((2*R*,3*S*,5*R*)-5-(4-amino-2-oxopyrimidin-1(2*H*)-yl)-3-hydroxytetrahydrofuran-2-yl)methyl)-1*H*-1,2,3-triazol-4-yl)methyl)-2-(*trans*-2-(2-hydroxybenzoyl)cyclopentyl)acetamide (**5.03**)

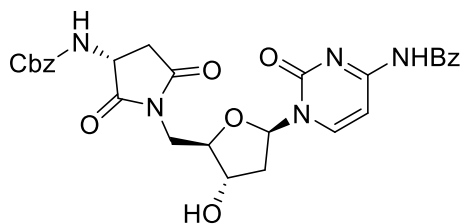


* represents relative stereochemical configurations.

Method 1. To a mixture of **5.14** (39 mg, 0.071 mmol) in DCM (2 mL) was added AlCl_3 (47 mg, 0.35 mmol) and the mixture was stirred overnight. The reaction was quenched with water and the solvents were evaporated. The residue was purified by flash chromatography on silica eluting with 1% TEA in MeOH/DCM (7:1) to give a mixture of the starting material **5.14** and desired product **5.03** based on ^1H NMR.

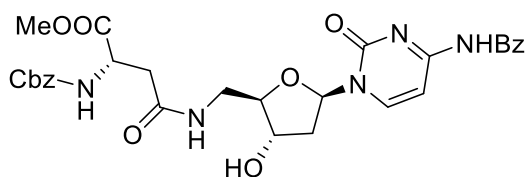
Method 2. **5.06** (15 mg, 0.053 mmol) and **5.09** (13 mg, 0.053 mmol) were dissolved in MeCN/ H_2O (2:1; 1 mL) and copper nano powder (2 mg) was added. The mixture was sonicated for 30 min and stirred overnight. The mixture was concentrated under reduced pressure and the residue was purified by flash chromatography on silica eluting with 1% TEA in MeOH/DCM (7:1) to give **5.03** (white solid) as a mixture of diastereomers (15 mg, 53%). ^1H NMR (500 MHz, MeOH- d_4) δ 7.89 (ddd, $J = 8.3, 2.7, 1.6$ Hz, 1H), 7.79 (d, $J = 2.9$ Hz, 1H), 7.52 – 7.46 (m, 2H), 6.97 – 6.90 (m, 2H), 6.18 (t, $J = 6.6$ Hz, 1H), 5.89 (dd, $J = 7.5, 3.2$ Hz, 1H), 4.73 (dd, $J = 14.4, 3.7$ Hz, 1H), 4.64 (ddd, $J = 14.4, 7.2, 3.7$ Hz, 1H), 4.38 – 4.30 (m, 2H), 4.25 (dd, $J = 15.3, 3.0$ Hz, 1H), 4.15 (dtd, $J = 6.5, 4.0, 2.2$ Hz, 1H), 3.66 (dtd, $J = 9.6, 7.0, 2.7$ Hz, 1H), 2.84 (dtd, $J = 9.9, 7.6, 2.4$ Hz, 1H), 2.37 – 2.24 (m, 3H), 2.22 – 2.07 (m, 2H), 2.03 – 1.93 (m, 1H), 1.84 – 1.64 (m, 3H), 1.49 – 1.39 (m, 1H); ^{13}C NMR (126 MHz, MeOH- d_4) δ 210.32, 210.31, 174.90, 167.48, 163.78, 142.78, 142.70, 141.64, 137.33, 137.32, 131.85, 129.79, 126.96, 125.28, 120.68, 120.17, 120.16, 119.07, 88.03, 87.94, 85.68, 72.46, 52.79, 52.75, 52.70, 41.79, 40.99, 40.95, 40.61, 40.57, 35.50, 33.78, 33.76, 33.28, 25.73; HRMS calcd for $\text{C}_{26}\text{H}_{31}\text{N}_7\text{O}_6$ $[\text{M} + \text{H}]^+$ 538.2409, found 538.2406.

benzyl ((*R*)-1-(((2*R*,3*S*,5*R*)-5-(4-benzamido-2-oxopyrimidin-1(2*H*)-yl)-3-hydroxytetrahydrofuran-2-yl)methyl)-2,5-dioxopyrrolidin-3-yl)carbamate (**5.15**)



To a mixture of **5.10** (200 mg, 0.605 mmol) and Z-Asp-OMe (204 mg, 0.727 mmol) in DMF (2 mL) were added HATU (276 mg, 0.727 mmol) and DIPEA (0.38 mL, 2.180 mmol), and the mixture was stirred for 2 hours. The resulting mixture was poured onto brine and extracted with DCM three times. The combined organic phase was dried over anhydrous sodium sulphate and concentrated under reduced pressure. The residue was purified by flash chromatography on silica eluting with 5% → 10% MeOH in DCM to give a white (305 mg, 90%). ¹H NMR (500 MHz, DMSO-*d*₆) δ 11.22 (s, 1H), 8.26 (d, *J* = 7.5 Hz, 1H), 8.04 – 7.99 (m, 2H), 7.97 (d, *J* = 8.0 Hz, 1H), 7.66 – 7.60 (m, 1H), 7.52 (t, *J* = 7.7 Hz, 2H), 7.43 – 7.25 (m, 5H), 6.11 (t, *J* = 6.6 Hz, 1H), 5.40 (d, *J* = 4.1 Hz, 1H), 5.03 (s, 2H), 4.49 (td, *J* = 8.7, 5.6 Hz, 1H), 4.25 – 4.18 (m, 1H), 4.10 – 4.02 (m, 1H), 3.80 – 3.59 (m, 2H), 3.04 (dd, *J* = 17.6, 9.3 Hz, 1H), 2.60 (dd, *J* = 17.6, 5.6 Hz, 1H), 2.37 – 2.27 (m, 1H), 2.14 (dt, *J* = 13.4, 6.6 Hz, 1H), 1.29 – 1.20 (m, 1H); ¹³C NMR (126 MHz, DMSO-*d*₆) δ 176.5, 175.0, 167.3, 163.1, 155.7, 145.3, 136.5, 133.1, 132.7, 128.4, 128.3, 127.91, 127.86, 127.7, 96.1, 86.7, 83.5, 71.5, 65.9, 54.9, 49.4, 40.8, 34.9.

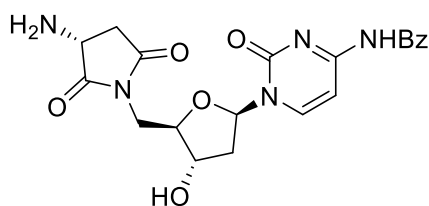
methyl *N*⁴-(((2*R*,3*S*,5*R*)-5-(4-benzamido-2-oxopyrimidin-1(2*H*)-yl)-3-hydroxytetrahydrofuran-2-yl)methyl)-*N*²-((benzyloxy)carbonyl)-*L*-asparaginate (**5.16**)



5.10 (100 mg, 0.303 mmol) was added to the mixture of Z-Asp-OMe (85 mg, 0.303 mmol), EDC (64 mg, 0.333 mmol), and HOBt (49 mg, 0.363 mmol) in DMF (1 mL), and the mixture was stirred overnight. Water was added to the mixture and extracted with EtOAc/MeOH (9:1) four times - a lot of organic solvent was added to extract the formed solid because of solubility issue. The organic phase was dried over anhydrous sodium sulphate and concentrated under reduced pressure. The residue turned into a gel after adding DCM. After concentrating it again, the solid was filtered using water and ether to give a white solid (145mg, 81%). ¹H NMR (500 MHz, DMSO-*d*₆) δ 11.22 (s, 1H), 8.25 – 8.13 (m, 2H),

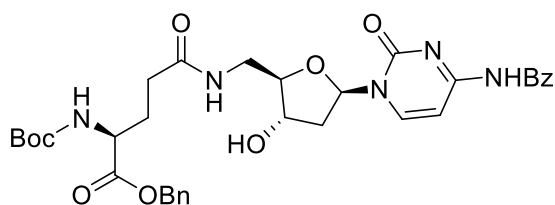
8.00 (d, $J = 7.4$ Hz, 2H), 7.62 (dd, $J = 8.0, 5.7$ Hz, 2H), 7.51 (t, $J = 7.7$ Hz, 2H), 7.42 – 7.26 (m, 5H), 6.11 (t, $J = 6.7$ Hz, 1H), 5.31 (d, $J = 4.2$ Hz, 1H), 5.02 (s, 2H), 4.48 (q, $J = 7.2$ Hz, 1H), 4.17 – 4.11 (m, 1H), 3.91 – 3.85 (m, 1H), 3.61 (s, 2H), 3.38 – 3.32 (m, 1H), 2.66 (dd, $J = 15.3, 6.2$ Hz, 1H), 2.58 – 2.50 (m, 1H), 2.34 – 2.27 (m, 1H), 2.05 (dt, $J = 13.4, 6.6$ Hz, 1H); ^{13}C NMR (126 MHz, DMSO- d_6) δ 172.0, 169.1, 167.3, 163.0, 155.7, 154.4, 145.3, 136.8, 132.7, 128.4, 128.34, 128.30, 127.86, 127.78, 127.65, 96.2, 86.5, 85.8, 71.2, 65.5, 52.0, 50.6, 41.1, 37.0.

N-(1-((2*R*,4*S*,5*R*)-5-(((*R*)-3-amino-2,5-dioxopyrrolidin-1-yl)methyl)-4-hydroxytetrahydrofuran-2-yl)-2-oxo-1,2-dihydropyrimidin-4-yl)benzamide (**5.17**)



The mixture of **5.16** (135 mg, 0.227 mmol) and 10% Pd/C (14 mg) in MeOH/DMF (2:1) (9 mL) was stirred under H₂ gas balloon overnight. The mixture was filtered through Celite[®] pad and washed with MeOH. The filtrate was concentrated under reduced pressure and the residue was purified by flash chromatography on silica eluting with 10% → 20% MeOH in DCM to give a white solid (21 mg, 22%). ^1H NMR (500 MHz, DMSO- d_6) δ 8.28 (d, $J = 7.5$ Hz, 1H), 8.01 (dd, $J = 8.1, 1.4$ Hz, 2H), 7.62 (td, $J = 7.3, 1.5$ Hz, 1H), 7.51 (t, $J = 7.8$ Hz, 2H), 7.36 (d, $J = 7.5$ Hz, 1H), 6.11 (t, $J = 6.6$ Hz, 1H), 5.41 (d, $J = 4.2$ Hz, 1H), 4.22 – 4.16 (m, 1H), 4.05 – 3.98 (m, 1H), 3.77 (dd, $J = 8.7, 5.1$ Hz, 1H), 3.72 – 3.58 (m, 2H), 3.16 (t, $J = 4.0$ Hz, 1H), 2.96 (dd, $J = 17.7, 8.7$ Hz, 1H), 2.39 – 2.27 (m, 2H), 2.20 – 2.12 (m, 1H).

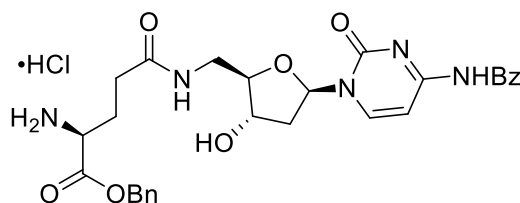
benzyl *N*⁵-(((2*R*,3*S*,5*R*)-5-(4-benzamido-2-oxopyrimidin-1(2*H*)-yl)-3-hydroxytetrahydrofuran-2-yl)methyl)-*N*²-(tert-butoxycarbonyl)-*L*-glutamate (**5.19**)



5.10 (100 mg, 0.303 mmol) was added to the mixture of Boc-Glu-OBzl (102 mg, 0.303 mmol), EDC (64 mg, 0.333 mmol), and HOBt (49 mg, 0.363 mmol) in DMF (1 mL), and the mixture was stirred overnight. Water was added to the mixture and extracted with EtOAc

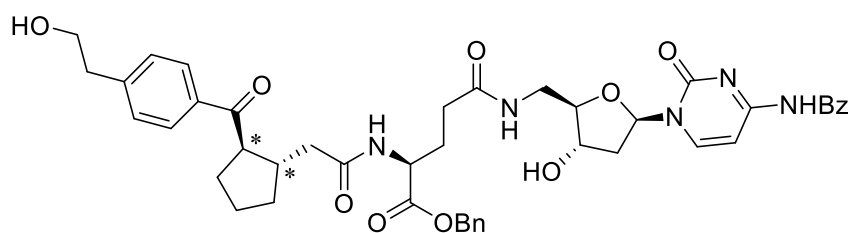
twice. The combined organic phase was washed with brine, saturated aqueous NaHCO₃, and water. The organic phase was dried over anhydrous sodium sulphate and concentrated under reduced pressure. The residue was purified by flash chromatography on silica eluting with 5% → 10% MeOH in DCM to give a white solid (182 mg, 92%). ¹H NMR (500 MHz, DMSO-*d*₆) δ 11.21 (s, 1H), 8.22 (d, *J* = 7.5 Hz, 1H), 8.05 (t, *J* = 5.8 Hz, 1H), 8.00 (dd, *J* = 8.3, 1.3 Hz, 2H), 7.66 – 7.59 (m, 1H), 7.51 (t, *J* = 7.8 Hz, 2H), 7.40 – 7.27 (m, 6H), 6.10 (t, *J* = 6.6 Hz, 1H), 5.31 (d, *J* = 4.2 Hz, 1H), 5.11 (q, *J* = 12.6 Hz, 2H), 4.13 (dq, *J* = 6.8, 3.5 Hz, 1H), 4.04 – 3.97 (m, 1H), 3.89 – 3.84 (m, 1H), 3.40 – 3.25 (m, 2H), 2.30 (ddd, *J* = 13.4, 5.8, 3.2 Hz, 1H), 2.25 – 2.18 (m, 2H), 2.08 – 1.93 (m, 2H), 1.78 (dq, *J* = 15.1, 8.0 Hz, 1H), 1.36 (s, 9H); ¹³C NMR (126 MHz, DMSO-*d*₆) δ 172.3, 171.6, 167.3, 163.0, 155.5, 154.4, 145.2, 136.0, 133.1, 132.7, 128.4, 128.3, 127.9, 127.7, 96.2, 86.5, 85.9, 78.2, 71.2, 65.8, 53.3, 41.0, 31.6, 28.1, 26.5.

benzyl *N*⁵-(((2*R*,3*S*,5*R*)-5-(4-benzamido-2-oxopyrimidin-1(2*H*)-yl)-3-hydroxytetrahydrofuran-2-yl)methyl)-*L*-glutamate hydrogen chloride salt (**5.20**)



To a stirred solution of **5.19** (176 mg, 0.271 mmol) in dioxane (3 mL) under nitrogen gas was added 4N HCl in dioxane (1 mL) dropwise. The reaction mixture was stirred for 4 h, after which time the mixture was concentrated to give a white solid as the HCl salt. This material was used without further purification.

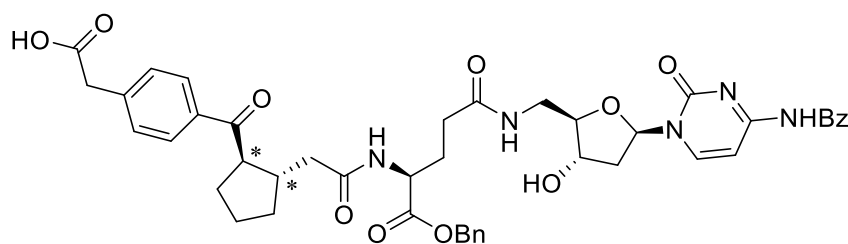
benzyl *N*⁵-(((2*R*,3*S*,5*R*)-5-(4-benzamido-2-oxopyrimidin-1(2*H*)-yl)-3-hydroxytetrahydrofuran-2-yl)methyl)-*N*²-(2-(*trans*-2-(4-(2-hydroxyethyl)benzoyl)cyclopentyl)acetyl)-*L*-glutamate (**5.21**)



* represents relative stereochemical configurations.

5.20 (0.253 mmol) and TEA (124 μ L, 0.887 mmol) were added to the mixture of **4.07** (70 mg, 0.253 mmol), EDC (53 mg, 0.279 mmol), and HOBt (45 mg, 0.334 mmol) in DMF (2 mL), and the mixture was stirred overnight. Water and EtOAc were added to the mixture to form a solid. The mixture was filtered and washed with water and EtOAc to give **5.21** (white solid) as a mixture of diastereomers (169 mg, 82%). ^1H NMR (500 MHz, DMSO- d_6) δ 11.24 (br s, 1H), 8.27 (dd, $J = 9.9, 7.4$ Hz, 1H), 8.18 (d, $J = 7.5$ Hz, 1H), 8.09 – 8.03 (m, 1H), 8.00 (d, $J = 7.7$ Hz, 2H), 7.85 (dd, $J = 8.3, 3.5$ Hz, 2H), 7.61 (t, $J = 7.5$ Hz, 1H), 7.50 (t, $J = 7.6$ Hz, 2H), 7.33 (h, $J = 5.2, 4.2$ Hz, 8H), 6.11 (t, $J = 6.6$ Hz, 1H), 5.31 (s, 1H), 5.13 – 5.03 (m, 2H), 4.66 (s, 1H), 4.22 (dq, $J = 14.4, 7.6$ Hz, 1H), 4.12 (s, 1H), 3.85 (s, 1H), 3.67 – 3.59 (m, 2H), 3.59 – 3.51 (m, 1H), 3.30 (s, 2H), 2.77 (t, $J = 6.8$ Hz, 2H), 2.63 – 2.53 (m, 1H), 2.29 (ddd, $J = 13.5, 6.0, 3.3$ Hz, 1H), 2.24 – 2.08 (m, 4H), 2.08 – 1.90 (m, 3H), 1.86 – 1.71 (m, 2H), 1.69 – 1.48 (m, 3H), 1.33 (dq, $J = 14.8, 7.7$ Hz, 1H); ^{13}C NMR (126 MHz, DMSO- d_6) δ 201.56, 201.50, 171.82, 171.77, 171.60, 171.50, 171.47, 145.32, 145.30, 135.91, 134.59, 134.56, 132.53, 129.17, 129.14, 128.45, 128.42, 128.34, 128.22, 128.21, 127.99, 127.93, 127.73, 127.67, 126.57, 126.37, 96.51, 86.42, 85.82, 71.23, 65.80, 61.58, 51.75, 51.67, 50.83, 50.73, 41.00, 38.84, 31.58, 31.50, 30.44, 30.28, 26.67, 26.61, 24.28, 24.20.

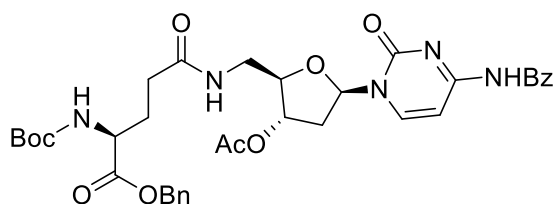
Attempted synthesis of 2-(4-(*trans*-2-(2-(((*S*)-5-(((2*R*,3*S*,5*R*)-5-(4-benzamido-2-oxopyrimidin-1(2*H*)-yl)-3-hydroxytetrahydrofuran-2-yl)methyl)amino)-1-(benzyloxy)-1,5-dioxopentan-2-yl)amino)-2-oxoethyl)cyclopentane-1-carbonyl)phenyl)acetic acid (**5.22**)



* represents relative stereochemical configurations.

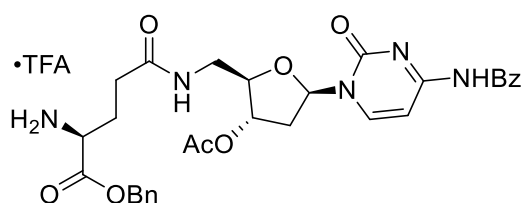
To the mixture of **5.21** (100 mg, 0.124 mmol) in MeCN/H₂O (1:1) (10 mL) were added TEMPO (3 mg, 0.022 mmol) and PhI(OAc)₂ (88 mg, 0.272 mmol) and the resulting white suspension was stirred for 2 days. Solvent was evaporated to give a white solid. ^1H NMR indicated a mixture of starting material **5.21** and reagents.

benzyl *N*⁵-(((2*R*,3*S*,5*R*)-3-acetoxy-5-(4-benzamido-2-oxopyrimidin-1(2*H*)-yl)tetrahydrofuran-2-yl)methyl)-*N*²-(tert-butoxycarbonyl)-*L*-glutamate (**5.23**)



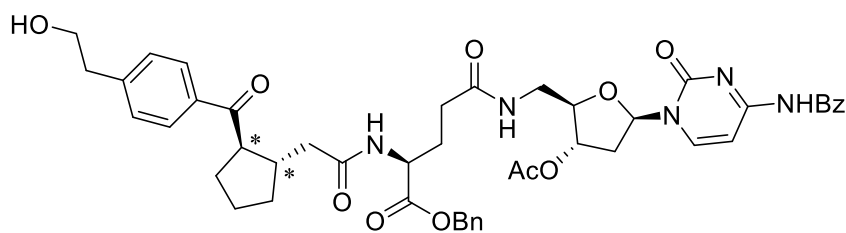
To a suspension of **5.19** (200 mg, 0.308 mmol), DMAP (2 mg, 0.018 mmol) and TEA (102 μ L, 0.730 mmol) in MeCN (5 mL) was added acetic anhydride (30 μ L, 0.320 mmol). The suspension was stirred at ambient temperature overnight. Since TLC indicated starting material **5.19** left, acetic anhydride (30 μ L, 0.320 mmol) was added more. After 2 h, the mixture was concentrated under reduced pressure. The residue was purified by flash chromatography on silica eluting with 5% MeOH in DCM to give a white solid (206 mg, 97%). ^1H NMR (500 MHz, DMSO- d_6) δ 11.27 (br s, 1H), 8.23 (d, $J = 7.5$ Hz, 1H), 8.09 (t, $J = 6.0$ Hz, 1H), 8.03 – 7.98 (m, 2H), 7.65 – 7.60 (m, 1H), 7.51 (t, $J = 7.8$ Hz, 2H), 7.41 – 7.25 (m, 5H), 6.08 (dd, $J = 8.0, 5.8$ Hz, 1H), 5.18 – 5.05 (m, 3H), 4.08 (td, $J = 5.9, 2.4$ Hz, 1H), 4.04 – 3.97 (m, 1H), 3.45 – 3.34 (m, 2H), 2.46 (ddd, $J = 14.3, 5.8, 2.1$ Hz, 1H), 2.33 – 2.17 (m, 3H), 2.06 (s, 3H), 2.01 – 1.92 (m, 1H), 1.84 – 1.73 (m, 1H), 1.35 (s, 9H); ^{13}C NMR (126 MHz, DMSO- d_6) δ 172.2, 171.8, 169.9, 163.1, 155.5, 145.2, 136.0, 133.1, 132.7, 128.43, 128.41, 128.34, 128.32, 128.0, 127.9, 127.6, 96.4, 86.6, 83.2, 78.2, 74.9, 65.8, 53.3, 40.6, 36.9, 31.5, 28.1, 26.4, 20.8.

benzyl N^5 -(((2*R*,3*S*,5*R*)-3-acetoxy-5-(4-benzamido-2-oxopyrimidin-1(2*H*)-yl)tetrahydrofuran-2-yl)methyl)-*L*-glutamate trifluoroacetic acid salt (**5.24**)



A solution of **5.23** (1.50 g, 2.24 mmol) in DCM (3.3 mL) was cooled with ice-bath and TFA (0.33 mL) was added. The reaction proceeded without bath for 4 h, then was quenched by evaporation of the organic solvent and by removing the excess of TFA under high vacuum. This material was used without further purification.

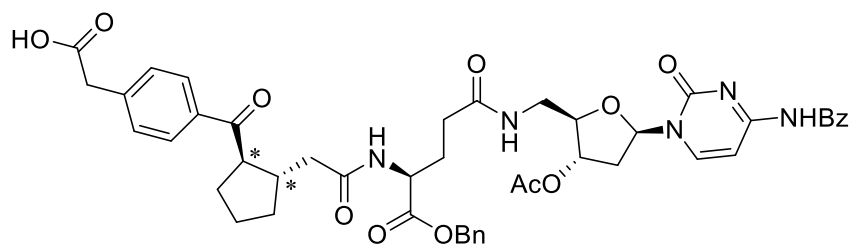
benzyl N^5 -(((2*R*,3*S*,5*R*)-3-acetoxy-5-(4-benzamido-2-oxopyrimidin-1(2*H*)-yl)tetrahydrofuran-2-yl)methyl)- N^2 -(2-(*trans*-2-(4-(2-hydroxyethyl)benzoyl)cyclopentyl)acetyl)-*L*-glutamate (**5.25**)



* represents relative stereochemical configurations.

To a solution of **4.07** (88 mg, 0.318 mmol) and HOBt (47 mg, 0.347 mmol) in DMF (2 mL) were added EDC (61 mg, 0.318 mmol) and a solution of **5.24** (199 mg, 0.289 mmol) in DMF (2 mL) and TEA (155 μ L, 1.113 mmol). The reaction mixture was stirred at ambient temperature overnight, then diluted with EtOAc. The organic phase was washed with water once and saturated aqueous NaHCO₃ twice. The organic phase was dried over anhydrous sodium sulphate and concentrated under reduced pressure. The residue was purified by flash chromatography on silica eluting with 5% MeOH in DCM to give **5.25** (white solid) as a mixture of diastereomers (161 mg, 65 %). ¹H NMR (500 MHz, DMSO-*d*₆) δ 11.25 (br s, 1H), 8.30 – 8.20 (m, 2H), 8.09 (td, *J* = 6.1, 2.8 Hz, 1H), 8.03 – 7.98 (m, 2H), 7.88 – 7.83 (m, 2H), 7.62 (t, *J* = 7.4 Hz, 1H), 7.54 – 7.48 (m, 2H), 7.42 – 7.26 (m, 7H), 6.08 (t, *J* = 6.9 Hz, 1H), 5.15 (td, *J* = 4.7, 2.1 Hz, 1H), 5.11 – 5.02 (m, 2H), 4.66 (t, *J* = 5.2 Hz, 1H), 4.27 – 4.17 (m, 1H), 4.12 – 4.04 (m, 1H), 3.66 – 3.59 (m, 2H), 3.59 – 3.51 (m, 1H), 3.43 – 3.34 (m, 2H), 2.77 (t, *J* = 6.8 Hz, 2H), 2.63 – 2.54 (m, 1H), 2.49 – 2.42 (m, 1H), 2.29 (dt, *J* = 14.3, 7.0 Hz, 1H), 2.24 – 2.09 (m, 3H), 2.06 (d, *J* = 1.4 Hz, 3H), 2.03 – 1.90 (m, 2H), 1.86 – 1.71 (m, 1H), 1.70 – 1.48 (m, 3H), 1.33 (dq, *J* = 11.8, 7.6 Hz, 1H); ¹³C NMR (126 MHz, DMSO-*d*₆) δ 201.55, 201.50, 171.82, 171.76, 171.71, 171.69, 171.58, 169.87, 145.33, 145.31, 135.91, 134.59, 134.57, 133.08, 132.73, 129.16, 128.41, 128.33, 128.24, 128.19, 127.94, 127.73, 127.66, 96.36, 86.72, 86.63, 83.21, 83.17, 74.97, 74.87, 65.82, 65.81, 61.59, 51.73, 51.65, 50.79, 40.65, 38.85, 36.93, 31.57, 31.50, 30.43, 30.29, 26.58, 24.27, 24.20, 20.78, 20.73.

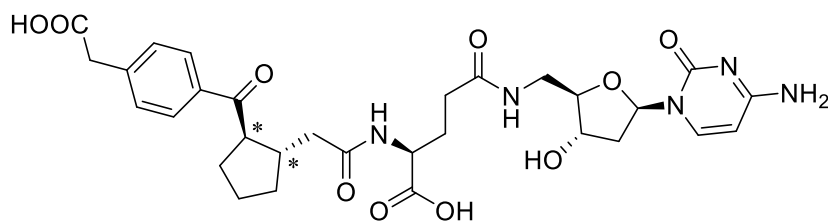
2-(4-(*trans*-2-(2-(((*S*)-5-(((2*R*,3*S*,5*R*)-3-acetoxy-5-(4-benzamido-2-oxopyrimidin-1(2*H*)-yl)tetrahydrofuran-2-yl)methyl)amino)-1-(benzyloxy)-1,5-dioxopentan-2-yl)amino)-2-oxoethyl)cyclopentane-1-carbonyl)phenyl)acetic acid (**5.26**)



* represents relative stereochemical configurations.

A solution of **5.25** (94 mg, 0.11 mmol) in acetone (2 mL) was treated with Jones reagent (0.16 mL of a 2.7 M solution, prepared via standard method) slowly dropwise at 0°C for 10 min. The resulting reaction mixture was stirred at 0°C for 1 h and then was quenched with isopropanol. The mixture was filtered with a pad of Celite® and the pad of Celite® was washed with EtOAc. The combined organic phase was washed with brine and water, dried over anhydrous sodium sulphate, and concentrated under reduced pressure. The residue was purified by flash chromatography on silica eluting with 10% MeOH in DCM to give **5.26** (white solid) as a mixture of diastereomers (64 mg, 67%). ¹H NMR (500 MHz, DMSO-*d*₆) δ 11.28 (br s, 1H), 8.30 – 8.20 (m, 2H), 8.09 (td, *J* = 6.0, 2.6 Hz, 1H), 8.03 – 7.97 (m, 2H), 7.88 (dd, *J* = 8.1, 4.7 Hz, 2H), 7.62 (t, *J* = 7.4 Hz, 1H), 7.54 – 7.48 (m, 2H), 7.42 – 7.26 (m, 7H), 6.08 (dd, *J* = 8.0, 5.8 Hz, 1H), 5.15 (dq, *J* = 5.0, 2.3 Hz, 1H), 5.12 – 5.01 (m, 2H), 4.27 – 4.17 (m, 1H), 4.10 – 4.05 (m, 1H), 3.65 (s, 2H), 3.60 – 3.52 (m, 1H), 3.44 – 3.35 (m, 2H), 2.65 – 2.54 (m, 1H), 2.48 – 2.42 (m, 1H), 2.29 (ddd, *J* = 14.3, 8.2, 6.2 Hz, 1H), 2.24 – 2.09 (m, 4H), 2.05 (d, *J* = 1.5 Hz, 3H), 2.03 – 1.89 (m, 2H), 1.86 – 1.71 (m, 2H), 1.69 – 1.48 (m, 3H), 1.33 (dq, *J* = 12.0, 7.6 Hz, 1H); ¹³C NMR (126 MHz, DMSO-*d*₆) δ 201.58, 201.53, 172.10, 171.82, 171.77, 171.72, 171.70, 171.58, 169.88, 163.12, 154.20, 145.21, 140.39, 135.92, 135.12, 135.09, 133.14, 132.73, 129.73, 129.70, 128.43, 128.42, 128.33, 128.26, 128.25, 127.94, 127.73, 127.67, 96.40, 86.65, 83.19, 74.92, 65.82, 51.72, 51.64, 50.92, 50.83, 40.65, 40.57, 39.25, 36.92, 31.57, 31.50, 30.43, 30.27, 26.62, 26.55, 24.27, 24.19, 20.76.

*N*⁵-(((2*R*,3*S*,5*R*)-5-(4-amino-2-oxopyrimidin-1(2*H*)-yl)-3-hydroxytetrahydrofuran-2-yl)methyl)-*N*²-(2-(*trans*-2-(4-(carboxymethyl)benzoyl)cyclopentyl)acetyl)-*L*-glutamine (**5.05**)



* represents relative stereochemical configurations.

To a mixture of **5.26** (60 mg, 0.069 mmol) in THF:MeOH:H₂O (3:1:1) (2 mL) was added LiOH (7 mg, 0.3 mmol) and the mixture was stirred for 17 hours. The resulting mixture was acidified with 1 M HCl to pH = 4 and concentrated under reduced pressure. The residue was purified by flash chromatography on C18-reversed phase silica gel eluting with 15% water in MeCN to give **5.05** (white solid) as a mixture of diastereomers (14 mg, 32%). ¹H NMR (500 MHz, DMSO-*d*₆) δ 12.44 (br s, 2H), 8.16 – 7.97 (m, 2H), 7.96 – 7.85 (m, 2H), 7.61 (dd, *J* = 7.5, 1.5 Hz, 1H), 7.40 (dd, *J* = 8.3, 2.7 Hz, 2H), 6.11 (t, *J* = 6.8 Hz, 1H), 5.72 (d, *J* = 7.5 Hz, 1H), 4.15 – 3.94 (m, 3H), 3.80 – 3.70 (m, 2H), 3.67 (s, 2H), 3.64 – 3.55 (m, 1H), 3.24 – 3.15 (m, 2H), 2.68 – 2.56 (m, 1H), 2.30 – 1.99 (m, 5H), 1.98 – 1.50 (m, 5H), 1.44 – 1.29 (m, 1H); ¹³C NMR (126 MHz, DMSO-*d*₆) δ 201.68, 201.64, 173.42, 173.38, 172.09, 171.62, 171.59, 171.45, 165.20, 154.66, 141.32, 140.29, 140.26, 135.17, 135.13, 129.74, 128.32, 128.30, 94.15, 85.16, 84.99, 71.34, 51.57, 51.49, 50.88, 50.82, 41.11, 40.99, 40.51, 39.26, 31.84, 31.75, 31.65, 31.61, 30.50, 30.32, 30.18, 27.00, 26.94, 24.35, 24.25; HRMS calcd for C₃₀H₃₇N₅O₁₀ [M + H]⁺ 628.2613, found 628.2614.

6.6 References for Chapter Six

1. Soares da Costa, T. P.; Tieu, W.; Yap, M. Y.; Pardini, N. R.; Polyak, S. W.; Sejer Pedersen, D.; Morona, R.; Turnidge, J. D.; Wallace, J. C.; Wilce, M. C.; Booker, G. W.; Abell, A. D., Selective inhibition of biotin protein ligase from *Staphylococcus aureus*. *J Biol Chem* **2012**, *287* (21), 17823-32.
2. Ju, Y.; Kumar, D.; Varma, R. S., Revisiting nucleophilic substitution reactions: microwave-assisted synthesis of azides, thiocyanates, and sulfones in an aqueous medium. *J. Org. Chem.* **2006**, *71* (17), 6697-700.
3. Pardin, C.; Roy, I.; Lubell, W. D.; Keillor, J. W., Reversible and competitive cinnamoyl triazole inhibitors of tissue transglutaminase. *Chem. Biol. Drug Des.* **2008**, *72* (3), 189-96.
4. Malkoch, M.; Schleicher, K.; Drockenmuller, E.; Hawker, C. J.; Russell, T. P.; Wu, P.; Fokin, V. V., Structurally Diverse Dendritic Libraries: A Highly Efficient Functionalization Approach Using Click Chemistry. *Macromolecules* **2005**, *38* (9), 3663-3678.
5. Soares da Costa, T. P.; Tieu, W.; Yap, M. Y.; Zvarec, O.; Bell, J. M.; Turnidge, J. D.; Wallace, J. C.; Booker, G. W.; Wilce, M. C.; Abell, A. D.; Polyak, S. W., Biotin analogues with antibacterial activity are potent inhibitors of biotin protein ligase. *ACS Med. Chem. Lett.* **2012**, *3* (6), 509-14.
6. Simonin, J.; Vernekar, S. K. V.; Thompson, A. J.; Hothersall, J. D.; Connolly, C. N.; Lummis, S. C. R.; Lochner, M., High-affinity fluorescent ligands for the 5-HT₃ receptor. *Bioorg. Med. Chem. Lett.* **2012**, *22* (2), 1151-1155.
7. Winum, J. Y.; Toupet, L.; Barragan, V.; Dewynter, G.; Montero, J. L., N-(tert-butoxycarbonyl)-N-[4-(dimethylazanumylidene)-1,4-dihydropyridin-1-ylsulfonyl] azanide: A new sulfamoylating agent. Structure and reactivity toward amines (vol 3, pg 2243, 2001). *Org. Lett.* **2001**, *3* (18), 2939-2939.
8. Muhammad, N.; Sadia, N.; Zhu, C. C.; Luo, C.; Guo, Z. J.; Wang, X. Y., Biotin-tagged platinum(IV) complexes as targeted cytostatic agents against breast cancer cells. *Chem. Commun.* **2017**, *53* (72), 9971-9974.
9. Neustadt, B. R., Facile Preparation of N-(Sulfonyl)Carbamates. *Tetrahedron Lett.* **1994**, *35* (3), 379-380.

-
10. Goswami, S.; Dey, S., Directed molecular recognition: design and synthesis of neutral receptors for biotin to bind both its functional groups. *J. Org. Chem.* **2006**, *71* (19), 7280-7.
 11. Tieu, W.; da Costa, T. P. S.; Yap, M. Y.; Keeling, K. L.; Wilce, M. C. J.; Wallace, J. C.; Booker, G. W.; Polyak, S. W.; Abell, A. D., Optimising in situ click chemistry: the screening and identification of biotin protein ligase inhibitors. *Chem. Sci.* **2013**, *4* (9), 3533-3537.
 12. Rode, A. B.; Son, S. J.; Hong, I. S., An Efficient One-pot N-Acylation of Deoxy- and Ribo-cytidine Using Carboxylic Acids Activated in situ with 2-Chloro-4,6-dimethoxy-1,3,5-triazine. *Bull. Korean Chem. Soc.* **2010**, *31* (7), 2061-2064.